Conditional Source-Term Estimation Evaluations for Partially-Premixed Flames

Nikola Šekularac

Exeter College

University of Oxford

A thesis submitted for the degree of

Doctor of Philosophy

Trinity 2022

Acknowledgement

I would like to thank my supervisor Prof. Martin Davy for allowing me to study at Oxford and guiding me through this DPhil. His patient supervision and extensive technical insights were invaluable to this work.

My special thanks and deepest gratitude goes to my good friend Dr. Xiaohang (Leo) Fang, who shared his broad scope of knowledge in combustion modelling, taught me and provided daily guidance on the different milestones of this project.

Along with Prof. Martin Davy, I would also like to acknowledge Prof. Richard Stone, Prof. Felix Leach, Prof. Benjamin Williams and Dr. Nick Papaioannou for enrolling me into this excellent research group and providing moral support during this journey.

I wish also to express my thanks to Prof. Kendal Bushe for giving me the opportunity to work with him and providing the motivation to pursue some of the work presented throughout this thesis.

I am very grateful to be part of the Thermal Propulsion Systems Research Group and to work along side Mr. Sam Baker, Ms. Ruixuan Zhu, Mr. Varun Shankar, Dr. Abdullah Bajwa, Mr. Tejo Jehart, Mr. Sam White, Mr. Qichi He, Dr. Hannah Rana, Dr. Priyav Shah, Dr. Li Shen and Dr. Kharthik Chakravarthy who were available to answer all my questions and created an enjoyable workplace.

I want to extend my gratitude to the Jaguar Land Rover team, Dr. Tom Lockyer, Dr. Lyn McWilliam, John Geddes and Efe Tunç for providing important support, without whom this project would not have been possible. I would like to thank Dr. Rickard Solsjö from Siemens PLM Software for all the support provided during this project and particularly with STAR-CCM+.

Moreover, I would like to particularly thank my previous professors, Prof. Philippe Guibert, Prof. Daniel Gaffie, Prof. Alexis Matynia and Prof. Guillaume Legros from Sorbonne University, who all enabled me to pursue my studies towards this DPhil with a strong background in thermodynamics, combustion and especially combustion modelling.

Most importantly, I would like to underline the unconditional support of my family, Nataša, Radomir, Severine, Boban, Loic and Dimitrije, but also my friends Bogdan, Marko, Dharish, Erman, Gauthier, Sacha, Diane, Leonard, Ahmed, Leo, Ula, Nikos, Efimia, Leo, Liz, and the *Air Montenegro* fellowship.

Last but not least, I wish to express special thanks to my sister, Andrea, for her moral support, her encouragement and her endless love.

Abstract

Partially-premixed flames, characterised by both premixed and non-premixed flame structures, have been identified to be of particular importance within most practical combustion-powered devices. However, as most existing combustion models assume a single flame structure, the present understanding of partially-premixed flames under lean mixture conditions and high turbulence intensity is still limited, and further research is needed to better represent these processes numerically.

A detailed overview of different approaches used in combustion modelling for simultaneously capturing premixed and non-premixed flames, classified as either geometrical models (relying on the laminar burning velocity) or statistical models (relying on the probability density function), is presented. A new study validating for the first time a previously developed empirical laminar burning velocity correlation from Oxford for iso-octane/ethanol fuel blends is carried out. A complementary analysis involving simplified three-dimensional spark-ignition engine simulations is also performed using the new Oxford correlation coupled with ECFM-3Z within a Reynolds-Averaged Navier-Stokes (RANS) turbulence framework. Here, the importance attributed to the laminar burning velocity in the closure of the mean chemical source-term is found to decrease the range of applicability of geometrical models significantly, motivating the use of statistical modelling.

Conditional source-term estimation (CSE) is a statistical combustion model that invokes the conditional moment closure (CMC) hypothesis to approximate the mean chemical source-term in an averaged transport equation. An inversion process estimates the conditional scalar field. Previous CSE studies have shown that this model could successfully predict

the characteristics of both premixed and non-premixed flames, regardless of the combustion regime. However, limited work has been undertaken to assess the modelling capabilities of CSE to account for partially-premixed structures.

To investigate further, a previously developed CSE model coupled with the flamelet generated manifold (FGM) is applied to study the Engine Combustion Network (ECN) diesel "Spray A" case within a RANS framework. The proposed combustion model accounts for detailed chemistry and turbulence-chemistry interaction effects, essential for capturing the strong coupling between fluid dynamics and chemical kinetics. It is found that the CSE-FGM approach successfully demonstrates the capability of realistically predicting diesel-fueled transient spray combustion. However, there are slight discrepancies with experimental ignition delay times and flame lift-off lengths under low-temperature conditions within this approach due to the inclusion of a single control scalar based on mixture fraction.

Adopting doubly CSE (DCSE) and, as such, two conditioning variables relying on mixture fraction and progress variable provides far greater modelling capabilities compared to the conventional CSE. However, while a generalised mixture fraction definition has been provided and well accepted by the community, various progress variable definitions have been adopted over the years for different applications. This study focuses on the effect of progress variable selection on the conditional fluctuations obtained with one-condition conditional averages and doubly conditional averages from two of the most well-known burners. Among the four progress variables tested, it is found that the definition attributed to the progress variable within a doubly conditional moment closure approach has no particular importance in the closure of the chemical source-term. The results obtained with principal component analysis promote the use of a progress variable definition based on temperature for chemistry tabulation techniques, considering that species diffusivity is often simplified by assuming unity Lewis numbers. Lastly, this work also suggests that DCSE will likely be needed for capturing partially-premixed flames, combustion under high levels of turbulence intensity (where the inclusion of turbulence-chemistry interaction is compulsory), and reactive flows encountered in practical combustion systems.

Contents

List of Figures

List of Tables

List of Abbreviations

AMR . . . . . Adaptive mesh refinement

ASOI . . . . . After start of injection

BML . . . . . Bray–Moss–Libby

CAD . . . . . Crank-angle degrees

CDF . . . . . Counter-flow diffusion flame

CFD . . . . . Computational fluid dynamics

CI . . . . . Compression ignition

CMC . . . . . Conditional moment closure

CPU . . . . . Central processing unit

CSE . . . . . Conditional source-term estimation

DNN . . . . . Deep neural network

DNS . . . . . Direct Numerical Simulation

ECFM-3Z . . . . . Three zones extended coherent flame model

ECN . . . . . Engine Combustion Network

EGR . . . . . Exhaust gas recirculation

FGM . . . . . Flamelet generated manifold

FPV . . . . . Flamelet/progress variable

FSD . . . . . Flame surface density

ICE . . . . . Internal combustion engine

IDT . . . . . Ignition delay time

ILDM . . . . . Intrinsic low-dimensional manifolds

LBV . . . . . Laminar burning velocity

LES . . . . . Large Eddy Simulation

LOL . . . . . Lift-off length

MFB . . . . . Mass fraction burned

MFGM . . . . . Multidimensional flamelet generated manifold

MILD . . . . . Moderate or intense low-oxygen dilution

MRFGM . . . . . Multi-regime flamelet generated manifold

PCA . . . . . Principal component analysis

PC . . . . . Principal components

PDF . . . . . Probability density function

PM . . . . . Particular matters

RANS . . . . . Reynolds-Averaged Navier-Stokes

SI . . . . . Spark-ignition

SSPF . . . . . Steady-stretchless premixed flame

TCI . . . . . Turbulence-chemistry interaction

TDC . . . . . Top dead centre

TGLDM . . . . . Trajectory generated low-dimensional manifolds

UHC . . . . . Unburned hydrocarbons

WSR . . . . . Well-stirred reactor

δ_{ij} . . . . . Kronecker delta operator

ε . . . . . Turbulent kinetic energy dissipation rate

η . . . . . Mixture fraction sampling space variable

λ . . . . . Thermal conductivity

ξ . . . . . Progress variable sampling space variable

μ . . . . . Dynamic viscosity

μ_t . . . . . Turbulent dynamic viscosity

ρ . . . . . Density

Σ . . . . . Flame surface density scalar

σ_{ij} . . . . . Stress tensor

τ_{ij} . . . . . Viscous stress tensor

ϕ . . . . . Equivalence ratio

χ . . . . . Scalar dissipation rate

$\dot{\omega}_k$ . . . . . Chemical source-term

$\dot{\omega}_T$ . . . . . Heat release

a . . . . . Strain rate

c . . . . . Progress variable

c_p . . . . . Specific heat

D . . . . . Molecular diffusion coefficient

D_a . . . . . Damköhler number

F . . . . . Global forces

h_s . . . . . Sensible enthalpy

K . . . . . Stretch rate

k . . . . . Turbulent kinetic energy

K_a . . . . . Karlovitz number

Le . . . . . Lewis number

P . . . . . Pressure

Pr . . . . . Prandtl number

Re . . . . . Reynolds number

Sc . . . . . Schmidt number

S_T . . . . . Turbulent flame speed

S_u . . . . . Laminar burning velocity

T . . . . . Temperature

Z . . . . . Mixture fraction

Chapter 1

Introduction

When Wisdom comes, her first lesson is: "There is no such thing as knowledge, there are only aperçus of the Infinite Deity."
Practical knowledge is a different thing; that is real and serviceable, but it is never complete. Therefore to systematise and codify it is necessary but fatal.

–Sri Aurobindo

Contents

1.1 Motivations

Five major sources share the global primary energy consumption: oil, coal, natural gas, nuclear energy and renewables, the latter which include hydropower, wind, solar, bioenergy, geothermal, wave and tidal [35]. Despite a moderate increase in renewables, the global energy mix is still dominated by coal, oil, and gas. In 2019, approximately 85% of the global energy came from burning fossil fuels, i.e. combustion [35]. Combustion can take various forms, from building a fire to heating water and eating, to more complex systems such as engines, which are widely used in different industrial applications such as transportation of both passengers and goods.

Interestingly, the trends observed in the global energy mix are not expected to significantly

change in the next 100 years. While renewables are anticipated to be the fastest-growing class of energy with an average of 6.4% increase per year by 2035 [36], it is nearly impossible to completely shift the world energy mix toward renewables due to the intrinsic drawbacks of each system (e.g. climate intermittence) coupled with governmental legislation. Additionally, global energy demand continues to increase at an average of 1.5% a year to 2035 [37], numbers that are expected to rapidly grow, especially in China, India, and, to a certain extent, in the African continent. Transport demand is expected to grow worldwide in the coming years as the global population increases, incomes rise, and more people can afford vehicles, trains and flights. The International Energy Agency expects global transport to double, vehicle ownership rates to increase by 60%, and demand for passenger and freight aviation to triple by 2070 [38]. Facing that, while the part of renewables should be continuously extended, the share associated with combustion will also have to be increased, in particular those involving oil and gas, as coal is believed to be withdrawn by 2040 in line with the international coal-exit calendar [39].

Combustion of fossil fuels is synonymous with greenhouse gas emissions (in particular CO_2) and pollutant formation which has a direct impact on health – major include particulate matter (PM), unburned hydrocarbons (UHC), carbon monoxide (CO) and nitrogen oxides (NO_x). One solution adopted in the automotive sector is to remove unwanted post-combustion species from the exhaust gases via after-treatment systems (e.g. gasoline's three-way catalytic converters). In recent years, electrification has become a useful technology to reduce regulated tailpipe emissions. Battery electric vehicles could reach a 50% global market share by 2040 with the current adoption rate [40], numbers that are expected to increase in the European Union, as it has mandated that new thermal engines will be banned from 2035. While the electrification (e.g. batteries or fuel cells) of the automotive fleet can be seen as a viable solution to reduce the vehicle's footprint (assuming that electricity is produced from low-carbon sources), using batteries to power aeroplanes or cargo ships still present a number of technical challenges that are yet to be addressed, suggesting that combustion will still be a major contributor for years to come in the various market segments, in particular the transport sector.

Facing that, a complementary means of reducing emissions is through control of the combustion process, i.e. reducing pollutant formation at the source. Pollutant formation is largely governed by the state of the charge (mixture composition and homogeneity) and the engine's operating condition (speed and load, which in turn affect pressure, temperature, bulk airflow and turbulence levels). Emission levels are particularly sensitive to equivalence ratio conditions ϕ. A schematic representation is shown in Figure 1.1.

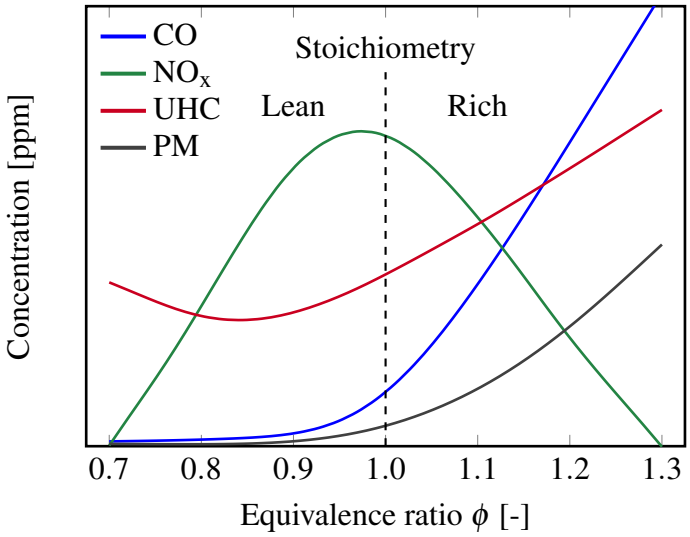

Figure 1.1: Schematic representation of the level of emissions from a spark-ignition (SI) or Otto cycle engine as a function of the mixture condition. Adapted from [1].

Carbon monoxide is mainly produced in rich conditions, i.e. $\phi > 1$, where incomplete combustion occurs due to high fuel concentration levels. As the mixture becomes leaner, leading to an excess of air, CO emissions are improved due to lower combustion temperatures [41] and through the oxidation of carbon monoxide into CO_2. Emissions associated with PM, which include soot particles among so many others, are essentially produced in rich conditions. Soot formation follows a 5-step process: decomposition of the hydrocarbon fuel, nucleation of carbon particles in the flame, growth of soot nuclei, agglomeration of particles, and finally, soot oxidation [1]. Soot concentrations are decreased through the excess of air with lean equivalence ratios, promoting the oxidation of soot particles. Similarly to carbon monoxide, UHC are predominantly produced under rich mixtures due to the excess of fuel, leading to incomplete combustion. Under lean conditions, UHC emissions

are improved due to the excess of air until the reactivity of the mixture reduces, which increases pollutants associated with unburned hydrocarbons [1, 41]. Nitrogen oxide formations rely on complex reactions, described by the Zeldovich mechanism [42]:

$$N_2 + O \longleftrightarrow NO + N \tag{1.1}$$

$$N + O_2 \longleftrightarrow NO + O \tag{1.2}$$

$$N + OH \longleftrightarrow NO + H \tag{1.3}$$

Chemical kinetics have shown that NO_x emissions are highly sensitive to temperatures where important adiabatic flame temperatures are associated with high concentration levels of nitrogen oxides [43]. As high flame temperatures are promoted in slightly rich mixtures [41], this would imply there is a peak of NO_x emissions under $\phi > 1$. Nevertheless, nitrogen oxides, and more particularly NO formations, also need oxygen in the mixture, which declines the peak of emissions to slightly lower equivalence ratio conditions than stoichiometry. As the flame temperature decreases with lean mixtures, NO_x emissions are improved.

Lean operation can, within reason, be a promising control strategy for optimising systems relying on combustion by increasing efficiency, reducing pollutants and minimising CO_2 emissions and consequently controlling global warming [44, 45]. However, maximising these benefits is not an easy task due to the complex coupling of physical and chemical phenomena occurring. Ultra-lean combustion, defined within this thesis by equivalence ratio conditions of $\phi \leq 0.6$, is known to be characterised by low reaction rates with moderate heat releases and an important sensitivity to mixing. As the lean-limit for burning is approached, the reactivity decreases and chemical reactivity cannot be sustained. Consequently, combustion becomes intermittent, with flame extinctions and re-ignitions within the flow field [46]. Extinction is also enhanced under flame quenching, where a flame front is submitted to external perturbations like heat losses or aerodynamic stretch which are sufficiently strong to decrease the reaction rate through the flame front to a negligible value, or in some cases, completely suppress the combustion process [47].

Controlling such flames remains challenging as they are highly susceptible to any perturbation within a given system, suggesting that further research on lean mixtures under engine conditions is needed to accurately assess the potentiality of such technology.

1.1.1 Partially-Premixed Flames

Various numerical and experimental studies [48, 49, 50, 51] have shown that partially-premixed flames, characterised by both premixed and non-premixed flame structures, are prevalent in ultra-lean combustion, real propulsion systems (e.g. aircraft gas turbines) and, more generally, in inhomogeneous mixtures [52, 53, 54]. For instance, combustion occurring in diesel engines combines simultaneous characteristics of auto-ignition, premixing, and diffusion in this specific order [55].

The theory behind partially-premixed flames can be better understood through the case study of a tribrachial flame, more commonly known as a triple flame. A schematic representation of such flame structure is shown in Figure 1.2 where Z denotes the mixture fraction, defined by Bilger [56] as:

$$Z = \frac{2\frac{Y_C - Y_{C,2}}{M_C} + \frac{1}{2}\frac{Y_H - Y_{H,2}}{M_H} - \frac{Y_O - Y_{O,2}}{M_O}}{2\frac{Y_{C,1} - Y_{C,2}}{M_C} + \frac{1}{2}\frac{Y_{H,1} - Y_{H,2}}{M_H} - \frac{Y_{O,1} - Y_{O,2}}{M_O}} \tag{1.4}$$

where the mass fraction of the element is denoted by Y_k, M_k is the element molar mass $\big($Carbon (C), Hydrogen (H) and Oxygen (O)$\big)$ and subscripts 1 and 2 denoting, respectively, the initial composition in the fuel and oxidiser streams.

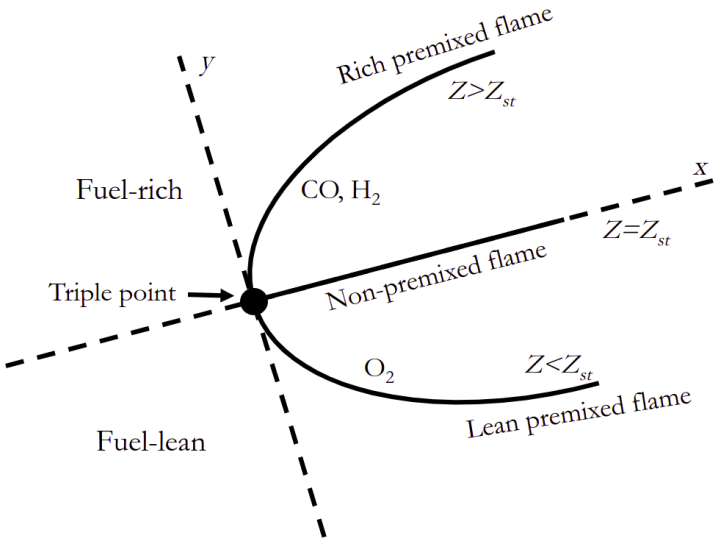

Figure 1.2: Schematic representation of a triple flame. Z_{st} corresponds to the stoichiometric mixture fraction. Adapted from [2].

The mixture fraction determines the local equivalence ratio and, thereby, the value of the

mass burning rate. Since premixed flame speeds reach the maximum for near stoichiometric conditions [5], a flame in a partially-premixed field propagates preferentially along surfaces of the mixture fraction of maximum burning velocity (in practice, a near stoichiometric value). On the fuel-lean side, a lean premixed flame front is seen, while a rich premixed flame front is established on the fuel-rich side. Both of these flame fronts propagate with a lower burning velocity than the leading edge of the flame, called the triple point. Behind the partially-premixed flame front, two streams, one containing radicals and/or unburned intermediates such as CO, and the other unburned oxidant, come together and burn as a diffusion flame.

The triple flame is a complex phenomenon of particular importance under most practical combustion scenarios. However, most existing combustion models assume a single structure of flame [57], i.e. premixed or non-premixed. These single flame architecture models are unable to effectively capture the underlying physics occurring in ultra-lean combustion and current real engines. As the industry seeks to realise the potential benefits of lean operation, it is clear that considerable research is needed, both experimentally and numerically, in order to develop a better understanding of partially-premixed flames and the physical mechanisms describing the interaction between the turbulent flow field and the chemical kinetics.

1.2 Objectives

Increasing computational power has made numerical modelling more popular over the past few years. Advanced numerical models are able to describe many complex phenomena occurring in combustion engines. However, the present understanding of partially-premixed flames in ultra-lean combustion operation is still limited, and further investigation is needed to better represent these processes numerically.

Current combustion models are not adequate to fully describe partially-premixed flames due to the inclusion of a single flame architecture, i.e. premixed or non-premixed. Additionally, only a few models have been found to incorporate turbulence-chemistry interaction (TCI) effects, essential for capturing finite-rate phenomena (e.g. extinction). Therefore, the proposed research will investigate the applicability of a novel chemical source-term closure model in a computational fluid dynamics (CFD) code, facilitating the use of detailed chemistry and temporal resolution while considering both flame structures. The ability to include detailed chemistry forms the basis for quantitative pollutant formation predictions, although pollutant predictions are outside the current project scope. The performance and validity of a previously developed model are tested via a turbulent reactive spray configuration under diesel engine relevant conditions. The set of validation data comprises liquid and gas phase spray penetration, ignition delay, lift-off length and various temperature contours. With respect to the physical mechanisms describing the interaction between the turbulent flow field and the chemistry, this study seeks to develop a deeper understanding and identification of the governing parameters and processes in the proposed modelling approach relating to turbulence-chemistry interaction. The retained model is improved by adopting a reverse-engineering practice using point-based measurements of various species mass fractions and temperature from two of the most well-known burners. This thesis provides an in-depth analysis of the different improvement steps needed for the selected combustion model to account for partially-premixed flame behaviours under lean mixture conditions and high turbulence intensity, as encountered in real engines.

1.3 Thesis Overview

A brief overview of this thesis is provided in this section. This thesis consists of eight chapters that cover the numerical methods for turbulent reacting flow modelling (Chapter 2), the discussion around partially-premixed flame modelling (Chapter 3), the development of a previously established empirical laminar burning velocity (LBV) correlation for ultra-lean combustion modelling (Chapter 4), the theory behind the conditional source-term estimation (CSE) model (Chapter 5), the application of a previously developed combustion modelling approach based on CSE (Chapter 6) along with the evaluation of the conditional space for the definition of the progress variable (Chapter 7). Each chapter begins with a short introduction and brief discussion of current literature.

More specifically, Chapters 2 and 3 summarise the numerical methods that describe turbulent reacting flows involving partially-premixed flame structures. Chapter 2 focuses on the governing equations for single-phase flows, while Chapter 3 gives a detailed overview of different approaches used in combustion modelling for capturing simultaneously premixed and non-premixed flames, classified as either flame topology models or probability density function-based models.

Chapter 4 focuses on validating a previously developed empirical laminar burning velocity correlation, which aims to investigate the feasibility/applicability of topologically-based models for simulating partially-premixed flame structures under ultra-lean mixture conditions. The content in this chapter presents the first application of this "Oxford" LBV correlation to iso-octane/ethanol fuel blends by means of a mixing rule approach. A complementary study around three-dimensional spark-ignition (SI) engine simulations is also carried out using the new Oxford correlation. Simulations are performed within a Reynolds-Averaged Navier-Stokes (RANS) framework using the commercial CFD solver STAR-CCM+. The simulation results obtained with the well-known Metghalchi & Keck correlation are included.

Chapter 5 presents an in-depth description of the CSE model's underlying physical and mathematical principles. The inclusion of TCI within CSE is investigated through a robust

literature review undertaken to account for the most recent advances made within the field. Particular attention is brought to chemistry tabulation techniques.

Chapter 6 assesses the modelling capabilities of a previously developed CSE-FGM approach applied to a complex hydrocarbon fuel, n-dodecane, under Engine Combustion Network's (ECN) "Spray A" conditions. Detailed chemistry is included in tabulated form using the flamelet generated manifold methodology. The results obtained with the well-stirred reactor model are also included. Simulations are performed within a RANS framework using the commercially-available CFD solver CONVERGE. The performance of the concerned model in predicting the most relevant reacting spray characteristics compared to the ECN experimental database is presented through the ignition delay time, the flame lift-off length, and both the Favre-averaged conditional mass fraction of reactive species and temperature.

Chapter 7 investigates the feasibility of CSE to model flows at conditions found in practical systems. As CSE relies on a single control variable to describe the thermo-chemical state-space, the scalar selected for characterising premixing effects needs further research to appropriately quantify the underlying chemistry occurring. The analysis is undertaken using experimental measurements taken from two well-known burners. Both burners exhibit flow conditions relevant to the topic tackled within this thesis. A discussion around the applicability of CSE for modelling reactive flows operating under lean conditions and high turbulence intensity is presented.

Chapter 8 summarises the main conclusions from the work presented in the thesis. It also provides suggestions for future work that could extend the scope of this thesis.

1.4 List of Publications

The content presented in Chapter 4 has been peer-reviewed and published in the following:

- N. Sekularac, X. Fang, V. Shankar, S.J. Baker, F.C.P. Leach and M. H. Davy, "Development of a Laminar Burning Velocity Empirical Correlation for Combustion of iso-octane/ethanol Blends in Air," *Fuel*, 307 (2022), Article 121880

The content of Chapter 6 contains the results of two peer-reviewed and published papers in the following:

- X. Fang, R. Ismail, N. Sekularac and M. H. Davy, "On the Prediction of Spray A End of Injection Phenomenon Using Conditional Source-Term Estimation," in *WCX SAE World Congress Experience*, SAE International, apr 2020.

- X. Fang, N. Sekularac and M.H. Davy, "Parametric Studies of a Novel Combustion Modelling Approach for Low Temperature Diesel Spray Simulation," *Proceedings of the ASME 2020 Internal Combustion Engine Division Fall Technical Conference*, vol. ASME 2020 Internal Combustion Engine Division Fall Technical Conference, 11 2020. V001T06A005.

The content presented in Chapter 7 has been submitted to Combustion Theory and Modelling:

- N. Sekularac, X. Fang, W. K. Bushe and M. H. Davy, "Conditional Space Evaluation of Progress Variable Definitions for Cambridge/Sandia Swirl Flames," *Combustion Theory and Modelling*, 2022

Other work planned for submission:

- N. Sekularac, X. Fang, W. K. Bushe and M. H. Davy, "Conditional Space Evaluation of Progress Variable Definitions for Sandia/TUD Jet Flames," *Combustion and Flame*, 2023

Chapter 2

Background

Classical thermodynamics ... is the only physical theory of universal content which I am convinced ... will never be overthrown.

–Albert Einstein

Contents

2.1 Overview

In this chapter, a brief background introduction for turbulent reacting flow modelling will be provided. The basic physical principles that provide the foundation for numerical simulation of fluid dynamics in combustion systems and which are relevant for the research conducted in this thesis are presented. Turbulent reacting modelling requires a comprehensive understanding of: (i) turbulence and its mechanisms, and (ii) the underlying chemistry taking place. Up to this date, the use of CFD models to predict reactive flows found in real engines still present a number of challenges where the flow encountered can be compressible, multi-phase, multi-scale, unsteady and three-dimensional. In Section 2.2, the governing equations for fundamental fluid dynamics and thermodynamics are outlined, followed

by some of the most used turbulence modelling strategies adopted for RANS simulations in Section 2.3. Numerical approaches for combustion modelling will be elaborated in a more detailed way in the following chapter.

2.2 Instantaneous Balance Equations

The instantaneous form of partial differential equations for a single-phase Newtonian fluid with non-constant density are given according to [5]. The basic set of balance equations comprises the classical Navier-Stokes, species, and energy transport equations.

Mass:

$$\frac{\partial \rho}{\partial t} + \frac{\partial}{\partial x_j}(\rho u_j) = 0 \tag{2.1}$$

Momentum ($i = 1,2,3$):

$$\frac{\partial \rho u_i}{\partial t} + \frac{\partial}{\partial x_j}(\rho u_j u_i) = \frac{\partial}{\partial x_j}\sigma_{ij} + F_i \tag{2.2}$$

where F_i denotes a body force and σ_{ij} is the stress tensor defined below as:

$$\sigma_{ij} = -p\delta_{ij} + \tau_{ij} \tag{2.3}$$

where p, δ_{ij} and τ_{ij} are, respectively, the hydrostatic pressure, the Kronecker delta operator and the viscous stress tensor. Equation 2.2 can then be rewritten as follows:

$$\frac{\partial \rho u_i}{\partial t} + \frac{\partial}{\partial x_j}(\rho u_j u_i) = -\frac{\partial p}{\partial x_i} + \frac{\partial \tau_{ij}}{\partial x_j} + F_i \tag{2.4}$$

such that τ_{ij} for a Newtonian fluid is defined as:

$$\tau_{ij} = -\mu \frac{2}{3}\frac{\partial u_k}{\partial x_k}\delta_{ij} + \mu\left(\frac{\partial u_i}{\partial x_j} + \frac{\partial u_j}{\partial x_i}\right) \tag{2.5}$$

where μ is the dynamic viscosity.

Energy via sensible enthalpy:

$$\frac{\partial \rho h_s}{\partial t} + \frac{\partial}{\partial x_j}(\rho u_j h_s) = \dot{\omega}_T + \frac{Dp}{Dt} - \frac{\partial q_j}{\partial x_j} + \tau_{ij}\frac{\partial u_j}{\partial x_i} \tag{2.6}$$

where q_j and $\dot{\omega}_T$ are, respectively, the enthalpy diffusive flux and the heat release due to combustion. By using Fourier's law, q_j can be described as follows:

$$q_j = -\lambda \frac{\partial T}{\partial x_j} + \rho \sum_{k=1}^{N} v_{k,j} Y_k h_{s,k} \tag{2.7}$$

where λ is the thermal conductivity and $v_{k,j}$ the j-component of the diffusion velocity v_k of species k, used again below for the species transport equation.

Species (for N species, $k = 1, ..., N$):

$$\frac{\partial \rho Y_k}{\partial t} + \frac{\partial}{\partial x_j}\left(\rho V_j^{(k)} Y_k\right) = \dot{\omega}_k \tag{2.8}$$

where $V_j^{(k)}$ is the instantaneous speed of the species k which can be decomposed into a velocity component (independent of k) and a specific diffusion velocity, u_j and $v_{k,j}$, respectively. Thus, Equation 2.8 can be rewritten to have as follows:

$$\frac{\partial \rho Y_k}{\partial t} + \frac{\partial}{\partial x_j}(\rho u_j Y_k) = -\frac{\partial}{\partial x_j}\left(v_{k,j} Y_k\right) + \dot{\omega}_k \tag{2.9}$$

where $\dot{\omega}_k$ is the chemical source-term of species k. As such, the heat release $\dot{\omega}_T$ from Equation 2.6 can be defined as:

$$\dot{\omega}_T = -\sum_{k=1}^{N} \Delta h_{f,k}^0 \dot{\omega}_k \tag{2.10}$$

where $\Delta h_{f,k}^0$ is the enthalpy of formation of species k at standard temperature conditions.

Before elaborating on the development and explanation of the species and energy equations, turbulence from a theoretical aspect needs to be introduced along with the various techniques to model it.

2.3 Turbulence Modelling

Most practical flows that we encounter are turbulent. Defined as an irreversible stochastic phenomenon in which instabilities and eddy structures influence the behaviour of the average flow, turbulence is not a property of a fluid. Promoting exchanges of masses, momentums, species and energy, the non-linear convection term of the Navier-Stokes equation is at the origin of triggering and developing turbulence in a flow.

Considered as an ensemble of eddies associated with characteristic scales evolving in the flow, turbulence is comparable to a diffusion mechanism, thus introducing a turbulent viscosity μ_t, also known as the Boussinesq approximation [58, 59]. Subject to significant

velocity gradients, the eddies distort, change, and stretch into smaller ones. This phenomenon, known as the Kolmogorov cascade, does not occur indefinitely. Indeed, a limit of eddies' sizes exists, below where the turbulence process is extinguished; the smallest eddies are dissipated under the effects of viscosity. Figure 2.1 presents this cascade through the turbulent kinetic energy spectrum $E(\kappa)$.

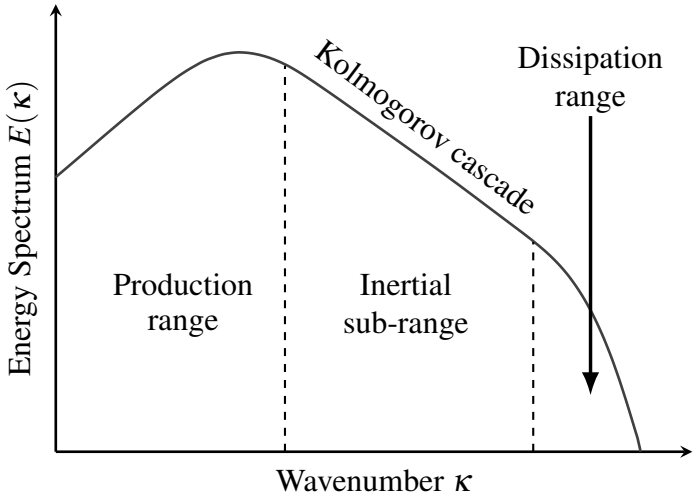

Figure 2.1: Graphical representation of the turbulent kinetic energy spectrum plotted as a function of wave numbers (log-log diagram). Adapted from [3].

Three different areas can be distinguished within Figure 2.1:

- Production range: this range contains the integral length scale eddies that interact with the mean flow extracting energy from it.
- Inertial sub-range: the cascade process is engaged as it transports energy from large eddies to smaller ones towards the dissipation area. Eddies in this region are independent of both the production range and the dissipation range, and the flow of energy through this range is expressed by Kolmogorov's $-\frac{5}{3}$ law:

$$E(\kappa) = Constant \cdot \varepsilon^{2/3} \kappa^{-5/3} \tag{2.11}$$

  where ε is the turbulent dissipation rate.
- Dissipation range: eddies are dissipated under the effects of viscosity, shutting down the turbulence process.

The existence of turbulence (or not) results from the competition between inertial forces, initialised by turbulence, and viscous forces. Turbulent flows can be modelled through three major methods, each associated with different scales: Direct Numerical Simulation (DNS), Large Eddy Simulation (LES) and Reynolds-Averaged Navier-Stokes (RANS) simulation.

2.3.1 Direct Numerical Simulations

Developed in the last forty years, thanks to the development of high-performance computers, Direct Numerical Simulation has changed the analysis of turbulent combustion. DNS has offered a new way to investigate flame/turbulence interactions, and significant progress has been achieved both for models and for fundamentals of turbulent combustion. In DNS, the full instantaneous Navier-Stokes equations described in Section 2.2 are solved without any model for turbulent motions: all turbulence scales are explicitly determined and their effects on combustion are captured. DNS predicts all-time temperature variations exactly like a high-resolution sensor would measure them in an experiment. A complete numerical simulation of the three-dimensional (3-D) balance equations describing a reactive flow and including differential diffusion, realistic thermodynamics and complex chemistry has brought DNS to levels of precision never reached before. Although these studies have shown great progress in understanding the fundamental physics behind turbulent combustion processes, DNS methods are still limited, in terms of parameter range and geometry, to academic situations. For example, a DNS of a 3-D turbulent flame at atmospheric pressure typically requires 1 to 2 million grid points with a computational box corresponding to physical size of $5 \times 5 \times 5$ mm^3 [5]. For these reasons, DNS is found to be impractical to solve most flows in engineering applications.

2.3.2 Large Eddy Simulations

Large Eddy Simulation aims at explicitly computing the largest structures of the flow field, typically larger than the computational mesh size, whereas the effects of the smallest ones are modelled. The underlying idea behind LES is that most large-scale flow structures in turbulent flows are geometry dependent, whereas small-scale structures generally exhibit

universal properties. While DNS fields correspond to raw data, LES fields are obtained through spatial filtering. In LES, turbulent properties are filtered (usually denoted by G) either in spectral space, where resolved components greater than a given cut-off frequency are limited (cut-off filter), or in physical space, where a weighted average is calculated in a given volume (box or Gaussian filter). LES techniques have been widely adopted for reacting flows since the increase of computational power. Significant progress has been made in the past few years. In 2020, the first 360-degree Large Eddy Simulation of a full turbofan engine (DGEN-380) was performed from the fan, to the compressor stages, and to the combustion chamber [60, 61]. LES contained around two billion cells on these three instances, carried out with the AVBP code of CERFACS. The CPU cost is large but still within reach, performing around one fan turn every five days.

2.3.3 Reynolds-Averaged Navier-Stokes Simulations

Reynolds-Averaged Navier-Stokes (RANS) simulation has historically been the first possible approach to model turbulence because the computation of the instantaneous flow field in a turbulent flame was impossible. In RANS, only mean flow fields are resolved, and no turbulent motion is explicitly captured. RANS is extensively used in current engineering practice because it is less demanding in terms of resources. However, its validity is limited by the closure models describing turbulence and combustion, discussed below.

Balance equations for the mean quantities in RANS simulations are obtained by averaging the instantaneous equations (cf. Equations 2.1, 2.4, 2.6 and 2.9). This averaging procedure introduces unclosed terms that have to be modelled using turbulent combustion models. Each quantity Φ is split into a mean $\overline{\Phi}$ and a fluctuation from the mean Φ' as follows:

$$\Phi = \overline{\Phi} + \Phi' \quad \text{and} \quad \overline{\Phi'} = 0 \tag{2.12}$$

This classical Reynolds averaging technique is widely used in non-reacting incompressible flows [5, 62, 63, 64]. If we apply this method to the mass balance equation, we have:

$$\frac{\partial \overline{\rho}}{\partial t} + \frac{\partial}{\partial x_j}\left(\overline{\rho u_j} + \overline{\rho' u'_j}\right) = 0 \tag{2.13}$$

The above equation introduces an unclosed quantity $\overline{\rho' u_j'}$ known as the density-velocity correlation whose closure adds another level of complexity. To avoid this difficulty when handling CFD, mass-weighted averages, also called Favre averages [65], are preferred. Also adapted to compressible flows, Favre proposes a new average weighted method by using density such that:

$$\Phi = \widetilde{\Phi} + \Phi'' \tag{2.14}$$

$$\widetilde{\Phi} = \frac{\overline{\rho\Phi}}{\overline{\rho}} \quad \text{and} \quad \widetilde{\Phi''} = \frac{\overline{\rho\left(\Phi - \widetilde{\Phi}\right)}}{\overline{\rho}} = 0 \tag{2.15}$$

Using the above formalism, the instantaneous conservation formulas become:

Mass:

$$\frac{\partial \overline{\rho}}{\partial t} + \frac{\partial}{\partial x_j}\left(\overline{\rho}\widetilde{u}_j\right) = 0 \tag{2.16}$$

Momentum ($i = 1,2,3$):

$$\frac{\partial \overline{\rho}\widetilde{u}_i}{\partial t} + \frac{\partial}{\partial x_j}\left(\overline{\rho}\widetilde{u}_j\widetilde{u}_i\right) = -\frac{\partial \overline{p}}{\partial x_i} + \frac{\partial}{\partial x_j}\left(\overline{\tau}_{ij} - \overline{\rho u_i'' u_j''}\right) + \overline{F_i} \tag{2.17}$$

Energy via sensible enthalpy:

$$\begin{aligned}\frac{\partial \overline{\rho}\widetilde{h}_s}{\partial t} + \frac{\partial}{\partial x_j}\left(\overline{\rho}\widetilde{u}_j\widetilde{h}_s\right) = \overline{\dot{\omega}}_T + \frac{\overline{Dp}}{Dt} + \left[\overline{\lambda\frac{\partial T}{\partial x_j}} - \overline{\rho}\widetilde{u_j'' h_s''}\right]_{,j} \\ - \left[\overline{\rho\sum_{k=1}^{N} v_{k,j} Y_k h_{s,k}}\right]_{,j} + \overline{\tau_{ij}\frac{\partial u_j}{\partial x_i}}\end{aligned} \tag{2.18}$$

Some quantities from the above equation can be rewritten as follows:

$$\frac{\overline{Dp}}{Dt} = \frac{\partial \overline{p}}{\partial t} + \overline{u_j\frac{\partial p}{\partial x_j}} = \frac{\partial \overline{p}}{\partial t} + \widetilde{u}_j\frac{\partial \overline{p}}{\partial x_j} + \cancel{\overline{u_j''\frac{\partial p}{\partial x_j}}} \tag{2.19}$$

such that the last term of Equation 2.19 can be neglected.

Species (for N species, $k = 1,...,N$):

$$\frac{\partial \overline{\rho}\widetilde{Y}_k}{\partial t} + \frac{\partial}{\partial x_j}\left(\overline{\rho}\widetilde{u}_j\widetilde{Y}_k\right) = -\frac{\partial}{\partial x_j}\left(\overline{v_{k,j}Y_k} + \widetilde{\overline{\rho}u_j''Y_k''}\right) + \overline{\dot{\omega}}_k \tag{2.20}$$

As a result of the averaging procedure, a number of additional quantities have been introduced into the above equations. Referred to as unclosed terms, turbulent combustion modelling proposes closures for these unknowns:

- The enthalpy and species turbulent fluxes $\overline{\rho}\widetilde{u_j''h_s''}$ and $\overline{\rho}\widetilde{u_j''Y_k''}$, respectively, can be approximated via the gradient diffusion hypothesis as:

$$\overline{\rho}\widetilde{u_j''h_s''} = -\frac{\mu_t}{Sc_{kt}}\frac{\partial\widetilde{h}_s}{\partial x_j} \qquad \overline{\rho}\widetilde{u_j''Y_k''} = -\frac{\mu_t}{Sc_{kt}}\frac{\partial\widetilde{Y}_k}{\partial x_j} \tag{2.21}$$

  where μ_t and Sc_{kt} are, respectively, the turbulent viscosity which is determined via the turbulence model and the turbulent Schmidt number for species k. Nevertheless, this assumption may be wrong in some premixed turbulent flames where counter-gradient turbulent transport (i.e., in an opposite direction compared to the one predicted from Equation 2.21) may be observed in flames with weak turbulence [5, 64].

- The laminar diffusive fluxes for species and sensible enthalpy are generally neglected compared to turbulent transport, assuming a sufficiently large turbulence level, i.e. $Re \gg 1$. The averaged laminar diffusive flux for species can be modelled as follows:

$$\overline{v_{k,j}Y_k} = -\overline{\rho}\overline{D_k}\frac{\partial\widetilde{Y}_k}{\partial x_j} \tag{2.22}$$

  where $\overline{D}_k$ is the mean species molecular diffusion coefficient $\left(D_k = \frac{\lambda}{\rho c_p Le_k}\right.$ where c_p is the specific heat and Le_k is the species k Lewis number$\left.\right)$. The averaged laminar diffusive flux for sensible enthalpy is often given as follows:

$$\overline{q_j} = -\overline{\lambda\frac{\partial T}{\partial x_j}} + \overline{\rho\sum_{k=1}^{N} v_{k,j}Y_k h_{s,k}} = \overline{\lambda}\frac{\partial\widetilde{T}}{\partial x_j} + \overline{\rho\sum_{k=1}^{N} v_{k,j}Y_k h_{s,k}} \tag{2.23}$$

- The closure of the chemical reaction rate $\overline{\dot{\omega}}_k$ is one of the main objectives of turbulent combustion modelling. The main modelling approaches will be described in a more detailed way in Chapter 3.

One last quantity from the momentum equation (cf. Equation 2.17) called Reynolds' tensor $\left(\overline{\rho u_i'' u_j''}\right)$ needs a closure mechanism. In RANS approximations, the entire energy spectrum is modelled, and its various closure methodologies can be broken down into models that adopt the Boussinesq assumption and those that do not. Boussinesq proposed that the Reynolds tensor is a function of the mean velocity gradients and the turbulent viscosity μ_t,

thus giving as follows:

$$\overline{\rho u_i'' u_j''} = \overline{\rho}\widetilde{u_i'' u_j''} = -\mu_t\left(\frac{\partial \widetilde{u}_i}{\partial x_j} + \frac{\partial \widetilde{u}_j}{\partial x_i} - \frac{2}{3}\delta_{ij}\frac{\partial \widetilde{u}_k}{\partial x_k}\right) + \frac{2}{3}\overline{\rho}k \tag{2.24}$$

where k is the turbulent kinetic energy defined as:

$$k = \frac{1}{2}\sum_{k=1}^{3}\widetilde{u_k'' u_k''} \tag{2.25}$$

Adopting this assumption leaves only the turbulent viscosity μ_t as the unknown of this problem. Four main approaches have been proposed to evaluate this quantity presented below:

- Zero-equation model: proposed by Prandtl [66], this approach suggests to link turbulent viscosity to the velocity gradient via an algebraic expression as:

  $$\mu_t = \overline{\rho} l_m^2 |\widetilde{S}| \tag{2.26}$$

  where $\widetilde{S}$ and l_m^2 are, respectively, the mean stress tensor and the mixing length (to be given by the user).

- One-equation model: this formulation, also called the Prandtl-Kolmogorov model, incorporates a closure of the balance equation for the turbulent kinetic energy k, hence giving the turbulent viscosity formula as:

  $$\mu_t = \overline{\rho} C_\chi l_{pk}\sqrt{k} \tag{2.27}$$

  where C_χ is a model constant and l_{pk} is a characteristic length to be given. The two models presented above require empirical relations for l_m and l_{pk}.

- Reynolds Stress Model: avoiding the use of the Boussinesq assumption by solving transport equations for each component of the Reynolds tensor, this model solves the equation [3]:

  $$\frac{\partial \overline{\rho}\widetilde{u_i'' u_j''}}{\partial t} + \frac{\partial}{\partial x_k}\left(\overline{\rho}\widetilde{u}_k\widetilde{u_i'' u_j''}\right) = D_{ij} + P_{ij} + R_{ij} + \Omega_{ij} - \varepsilon_{ij} \tag{2.28}$$

where D_{kij}, P_{ij}, R_{ij}, Ω_{ij} and ε_{ij} are, respectively, the molecular and turbulent diffusion, the stress production, the pressure-strain, production by system rotation, and the dissipation rate. Some of the above terms (i.e. turbulent diffusion, pressure-strain, and dissipation rate) have to be modelled for closing the equation.

- Two-equation model (e.g. k-ε): First introduced by Jones & Launder [67], the turbulent viscosity is estimated as:

$$\mu_t = \overline{\rho} C_\mu \frac{k^2}{\varepsilon} \tag{2.29}$$

where k and the turbulent kinetic energy dissipation rate ε are described by closure of two balance equations given by:

$$\begin{aligned} \underbrace{\frac{\partial \overline{\rho} k}{\partial t}}_{\text{Unsteady evolution}} + \underbrace{\frac{\partial}{\partial x_j}\left(\overline{\rho}\widetilde{u}_j k\right)}_{\text{Flow convection}} = & \underbrace{\frac{\partial}{\partial x_j}\left[\left(\mu + \frac{\mu_t}{\sigma_k}\right)\frac{\partial k}{\partial x_j}\right]}_{\text{Molecular and turbulent diffusion}} \\ & - \underbrace{\overline{\rho}\varepsilon}_{\text{Viscous dissipation}} \\ & - \underbrace{\overline{\rho}\widetilde{u_i'' u_j''}\frac{\partial \widetilde{u}_j}{\partial x_i}}_{\text{Turbulent kinetic energy production}} \end{aligned} \tag{2.30}$$

$$\frac{\partial \overline{\rho}\varepsilon}{\partial t} + \frac{\partial}{\partial x_j}\left(\overline{\rho}\widetilde{u}_j \varepsilon\right) = \frac{\partial}{\partial x_j}\left[\left(\mu + \frac{\mu_t}{\sigma_\varepsilon}\right)\frac{\partial \varepsilon}{\partial x_j}\right] - \overline{\rho} C_{\varepsilon 2}\frac{\varepsilon^2}{k} - C_{\varepsilon 1}\frac{\varepsilon}{k}\overline{\rho}\widetilde{u_i'' u_j''}\frac{\partial \widetilde{u}_j}{\partial x_i} \tag{2.31}$$

where the Reynolds tensor $\overline{\rho}\widetilde{u_i'' u_j''}$ is determined using the Boussinesq expression (cf. Equation 2.24). According to [5], the constants are typically:

$$C_\mu = 0.09 \quad ; \quad \sigma_k = 1.0 \quad ; \quad \sigma_\varepsilon = 1.3 \quad ; \quad C_{\varepsilon 1} = 1.44 \quad \text{and} \quad C_{\varepsilon 2} = 1.92 \tag{2.32}$$

The remaining unclosed term, the mean chemical source-term (cf. Equation 2.20), will be presented in a more elaborated way in the following section, with a particular emphasis given to the various closure techniques.

Chapter 3

Combustion Modelling for Partially-Premixed Flames

In nature nothing is created, nothing is lost, everything changes.

–Antoine-Laurent de Lavoisier

Contents

3.1 Overview

Combustion is a complicated phenomenon that involves chemical, time and length scale interactions. As combustion processes are difficult to capture from an analytical point of view, numerical analyses have been extensively used since the exponential increase in computing power. The closure of the mean chemical source-term $\overline{\omega}_k$ remains one of the

greatest challenges in combustion modelling due to its high non-linearity and sensitivity to truncation. Furthermore, the inclusion of partially-premixed flames in the closure of the mean reaction rate still presents significant problems to the combustion community due to the difficulties of simultaneously accounting for premixed and non-premixed flame structures. This chapter considers various combustion modelling approaches adopted for partially-premixed flames. Section 3.2 presents a detailed review of the chemical source-term, followed by some of the most common flame topology models adopted for partially-premixed flames in Section 3.3. Probability density function models are depicted in Section 3.4, followed by the conditional moment closure approach in Section 3.5.

3.2 Chemical Source-Term

A combustion process involving N species through M reactions may be written in the general form, also known as Penner notation, defined below as:

$$\sum_{k=1}^{N} \nu'_{kj} \mathscr{L}_k \Leftrightarrow \sum_{k=1}^{N} \nu''_{kj} \mathscr{L}_k \qquad j = 1, ..., M \tag{3.1}$$

where $\mathscr{L}_k$, ν'_{kj} and ν''_{kj} are, respectively, a symbol for species k and the molar stoichiometric coefficients of species k in reaction j for reactants and products. For mass conservation:

$$\sum_{k=1}^{N} \nu'_{kj} W_k = \sum_{k=1}^{N} \nu''_{kj} W_k \quad \text{or} \quad \sum_{k=1}^{N} \nu_{kj} W_k = 0 \qquad j = 1, ..., M \tag{3.2}$$

such that W_k is the molar weight of species k and ν_{kj} is defined below as:

$$\nu_{kj} = \nu''_{kj} - \nu'_{kj} \tag{3.3}$$

Thus, we can introduce the definition of the reaction rate $\dot{\omega}_k$ from Equation 2.9 as:

$$\sum_{k=1}^{N} \dot{\omega}_k = \sum_{j=1}^{I} \left(Q_j \sum_{k=1}^{N} W_k \nu_{kj} \right) = 0 \tag{3.4}$$

where Q_j is known as the progress rate of reaction j such that:

$$Q_j = k_{fj} \prod_{k=1}^{N} \left(\frac{\rho Y_k}{W_k} \right)^{\nu'_{kj}} - k_{bj} \prod_{k=1}^{N} \left(\frac{\rho Y_k}{W_k} \right)^{\nu''_{kj}} \tag{3.5}$$

and where the rate constants k_{fj} and k_{bj} are modelled via the empirical Arrhenius law as:

$$k_{fj} = A_{fj} T^{\beta_j} \exp\left(- \frac{E_j}{RT} \right) = A_{fj} T^{\beta_j} \exp\left(- \frac{T_{aj}}{T} \right) \quad \text{such that} \quad E_j = R T_{aj} \tag{3.6}$$

where A_{fj} and β_j are the pre-exponential rate constants, R as the gas constant and E_j as the activation energy, thus making T_{aj} the activation temperature. The backward rates k_{bj} are computed from the forward rates through the equilibrium constants as:

$$k_{bj} = \frac{k_{fj}}{\left(\frac{P_a}{RT}\right)^{\sum_{k=1}^{N} \nu_{kj}} \exp\left(\frac{\Delta S_j^0}{R} - \frac{\Delta H_j^0}{RT} \right)} \tag{3.7}$$

P_a is the atmospheric pressure fixed at 10^5 Pascal while ΔS_j^0 and ΔH_j^0 are, respectively, entropy and enthalpy changes for reaction j under standard conditions.

A direct approach to evaluate mean reaction rates is considered in this section. Based on a series expansion developed by Poinsot & Veynante [5], this formalism illustrates the difficulties arising from the non-linear character of chemical sources.

Considering a simple irreversible reaction between fuel and oxidiser, F and O, respectively:

$$F + sO \rightarrow (1+s)P \tag{3.8}$$

where s denotes the mass stoichiometric ratio defined as $s = (Y_O/Y_F)_{st}$. Poinsot & Veynante proposed that the mean reaction rate can be evaluated as a function of the mean mass fractions, density and temperature through a Taylor expansion of the temperature fluctuations [5]:

$$\exp\left(- \frac{T_A}{T} \right) = \exp\left(- \frac{T_A}{\widetilde{T}} \right) \left(1 + \sum_{n=1}^{+\infty} P_n \frac{T''}{\widetilde{T}^n} \right) \tag{3.9}$$

$$T^b = \widetilde{T}^b \left(1 + \sum_{n=1}^{+\infty} Q_n \frac{T''}{\widetilde{T}^n} \right) \tag{3.10}$$

where P_n and Q_n are given by:

$$P_n = \sum_{k=1}^{n} (-1)^{n-k} \frac{(n-1)!}{(n-k)![(k-1)!]^2 k} \left(\frac{T_A}{\widetilde{T}} \right)^k \tag{3.11}$$

$$Q_n = \frac{(b-1)(b-2)...(b-n)}{n!} \tag{3.12}$$

The fuel mean reaction rate $\overline{\dot{\omega}}_F$ then becomes:

$$\begin{aligned}\overline{\dot{\omega}}_F = &-A\overline{\rho}^2\widetilde{T}^b\widetilde{Y}_F\widetilde{Y}_O\exp\left(-\frac{T_A}{\widetilde{T}}\right)\\ &\times\left[1+\frac{\widetilde{Y_F''Y_O''}}{\widetilde{Y}_F\widetilde{Y}_O}+(P_1+Q_1)\left(\frac{\widetilde{Y_F''T''}}{\widetilde{Y}_F\widetilde{T}}+\frac{\widetilde{Y_O''T''}}{\widetilde{Y}_O\widetilde{T}}\right)\right.\\ &\left.+(P_2+Q_2+P_1Q_1)\left(\frac{\widetilde{Y_F''T''^2}}{\widetilde{Y}_F\widetilde{T}^2}+\frac{\widetilde{Y_O''T''^2}}{\widetilde{Y}_O\widetilde{T}^2}\right)+...\right]\end{aligned} \tag{3.13}$$

Equation 3.13 leads to various difficulties. New covariance terms are introduced that need to be closed using algebraic or transport expressions. Because of non-linearities, large truncation errors are introduced, implying poor approximation. Furthermore, this same equation is valid only for a single irreversible reaction step. As such, this type of direct closure is avoided in turbulent combustion modelling involving multi-step chemical schemes. Methodologies for turbulent combustion modelling are generally grouped into two main categories: infinitely fast chemistry and finite rate chemistry, each which corresponds to the chemical/turbulent time scales for which they are applicable. Several combustion modelling approaches that might serve as a basis for future partially-premixed flame model development, classified as either geometrical or statistical methods, are presented below.

3.3 Flame Topology Methods

In this section, a description of the different flame topologically-based models is presented. The general theory of each approach is discussed in detail. A robust literature review is undertaken to account for the most recent advances made within the field.

3.3.1 Flame Surface Density

The flame surface density (FSD) model describes the mean reaction rate $\overline{\dot{\omega}}_k$ in term of flame surface area, i.e. as the product of the flame surface density Σ and the local consumption/reaction rate per unit of flame area $\overline{\dot{\Omega}}_k$, such that:

$$\overline{\dot{\omega}}_k = \overline{\dot{\Omega}}_k\Sigma \tag{3.14}$$

Defined as the available flame surface area per unit volume (unit: m^2/m^3), the flame surface density accounts for the flame's stretching, wrinkling, and distortion due to turbulence. The quantity Σ measures the reaction zone convolutions, implying that a high flame surface density corresponds to a high turbulence reaction rate. This model's main advantage relies on separating the chemistry effects, accounted by $\overline{\dot{\Omega}}_k$, from the turbulence features described by the flame surface density. Following this, a common approach to computing $\dot{\Omega}_k$ is to use one-dimensional (1-D) laminar flame codes coupled with complex chemistry. The corresponding results are stored in flamelet libraries where the consumption/reaction rate per unit flame area is tabulated as a function of a limited set of scalars (e.g. temperature, equivalence ratio, and/or scalar dissipation rate). The quantity $\dot{\Omega}_k$ is calculated as:

$$\dot{\Omega}_k = \rho Y_k S_u \tag{3.15}$$

where S_u denotes the laminar burning velocity (LBV). The flame surface density Σ can be determined using a simple algebraic expression based on the flamelet crossing frequency [68] or fractal theories [69]. The second method consists of solving a transport equation for Σ. An exact balance equation for the flame surface density was derived by Pope [70], Trouvé & Poinsot [71] and Vervisch *et al.* [72]. However, the Σ equation is unclosed and requires modelling for the turbulent flux of the flame surface along with strain rate and curvature effects. A closed transport equation was proposed in [5]. A generalised form of the flame surface density was introduced by Boger *et al.* [73] defined as $\Sigma_{\text{gen}} = \overline{|\nabla c|}$, where c is the progress variable. The generalised flame surface density can be used irrespective of the combustion regime as long as unclosed quantities can be modelled. Vervisch *et al.* derived in [74] a transport equation for Σ_{gen}, written as:

$$\frac{\partial \Sigma_{\text{gen}}}{\partial t} + \nabla(\overline{U})_s \Sigma_{\text{gen}} = (\overline{\rho S_d})_s \Sigma_{\text{gen}} \tag{3.16}$$

where $()_s$ denotes the surface-averaging such that $(\overline{\Phi})_s = \overline{\Phi|\nabla c|}/\Sigma_{\text{gen}}$ [75] with Φ denoting any quantity describing the flow or thermo-chemical conditions. The surface-averaged displacement speed $(\overline{\rho S_d})_s$ can be approximated following Bray & Libby's work [76] as $(\overline{\rho S_d})_s \approx \rho^u S_u$, where ρ^u is the unburned density. Ma *et al.* [77] have made an in-depth

review of the various closure models available for Σ_{gen}.

The flame surface density model is often used for the study of premixed flame structures [75, 78, 79, 80]. Despite the limited number of works tackling partially-premixed flame simulations with FSD, Cavallo Marincola *et al.* [81] and Fiorina *et al.* [82] have investigated the use of a generalised flame surface density for the modelling of stratified flames in an LES context. In addition to solving a transport equation for the mixture fraction, a balance equation for the progress variable was solved to account for the mixture stratification effects, where the laminar flame speed was modelled using the mixture fraction to take into consideration the local mixing conditions such that $S_u = S_u(\widetilde{Z})$. The predicted results are in good agreement with the experimental trends. Nevertheless, the sub-grid turbulent fluctuations of Z and c and their correlation, which can be significant when a relatively large LES grid size is used, are ignored in this modelling approach.

For clarity purposes, a brief description regarding the progress variable c introduced previously is given here. Defined as a reduced quantity that goes from zero in fresh gases to one in burned gases, c is perhaps the most used scalar in turbulent combustion modelling to describe premixed flame structures. The temperature or the mass fraction of a major combustion product (e.g. H_2O or CO_2) have both been widely used to define c. A more detailed description is reviewed in Chapter 7.

3.3.2 Three Zones Extended Coherent Flame Model

The three zones extended coherent flame model, more commonly referred to as the ECFM-3Z model, was first proposed by Colin & Benkenida [4]. The ECFM-3Z formulation accounts for both premixed and non-premixed flame structures, suggesting that partially-premixed effects can be captured. Premixed flames are modelled using the unburned/burned states of the conventional extended coherent flame model (ECFM) [83], with the latter being an improved version of the coherent flame model (CFM) proposed by Marble & Broadwell [84]. For calculating the premixed chemical source terms, all three models rely on Equation 3.14 (i.e. a flame surface density approach). Colin *et al.* [83] have developed

a transport equation for Σ in ECFM-3Z characterised by production and destruction terms, which is:

$$\frac{\partial \Sigma}{\partial t} + \frac{\partial \widetilde{u}_j \Sigma}{\partial x_j} = \frac{\partial}{\partial x_j}\left[\left(\frac{\mu_t}{Sc_t} + \frac{\mu}{Sc}\right)\frac{\partial \Sigma/\overline{\rho}}{\partial x_j}\right] + (\mathrm{P}_1 + \mathrm{P}_2 + \mathrm{P}_3)\Sigma - \mathrm{D} + \mathrm{P}_k \tag{3.17}$$

where P_1 is the flame production by turbulent stretch, P_2 is the production by the mean flow dilatation, and P_k as the source-term applied during ignition period by a spark-plug model. The last terms, P_3 and D are defined as:

$$\mathrm{P}_3 = \frac{2}{3} S_u \frac{1-\widetilde{c}}{\widetilde{c}} \Sigma \quad \text{and} \quad \mathrm{D} = S_u \frac{\Sigma^2}{1-\overline{c}} \tag{3.18}$$

The quantity P_3 models the effects of the flame thermal expansion and curvature while D is a destruction term due to consumption, preventing an infinite growth of the flame area. Veynante & Vervisch [64] have extensively compared source and consumption terms in the flame surface density balance equations. Like the flame surface density model, the LBV plays a fundamental role in the Σ transport equation through Equation 3.18, being the main chemical parameter appearing in the balance Equation 3.17. Equation 3.14 highlights the importance of burning velocities within this model, used for the closure of the chemical source-term.

Non-premixed combustion, known to be mainly mixing-driven, is added by splitting each unburned/burned region into three zones: a pure fuel zone F, a pure air plus possible EGR zone A, and a mixed zone M as illustrated in Figure 3.1. The ECFM-3Z model assumes that combustion can only occur in the mixing regions, i.e. M_u and M_b, which correspond to premixed and non-premixed combustion. A mixing model quantifies the mass flux from zones A and F towards zone M. The mixing rate of the fuel is assumed to be proportional to the turbulent time scale τ_m provided by the turbulence model, here being $\tau_m = k/\varepsilon\beta_m$ with β_m a constant set to unity.

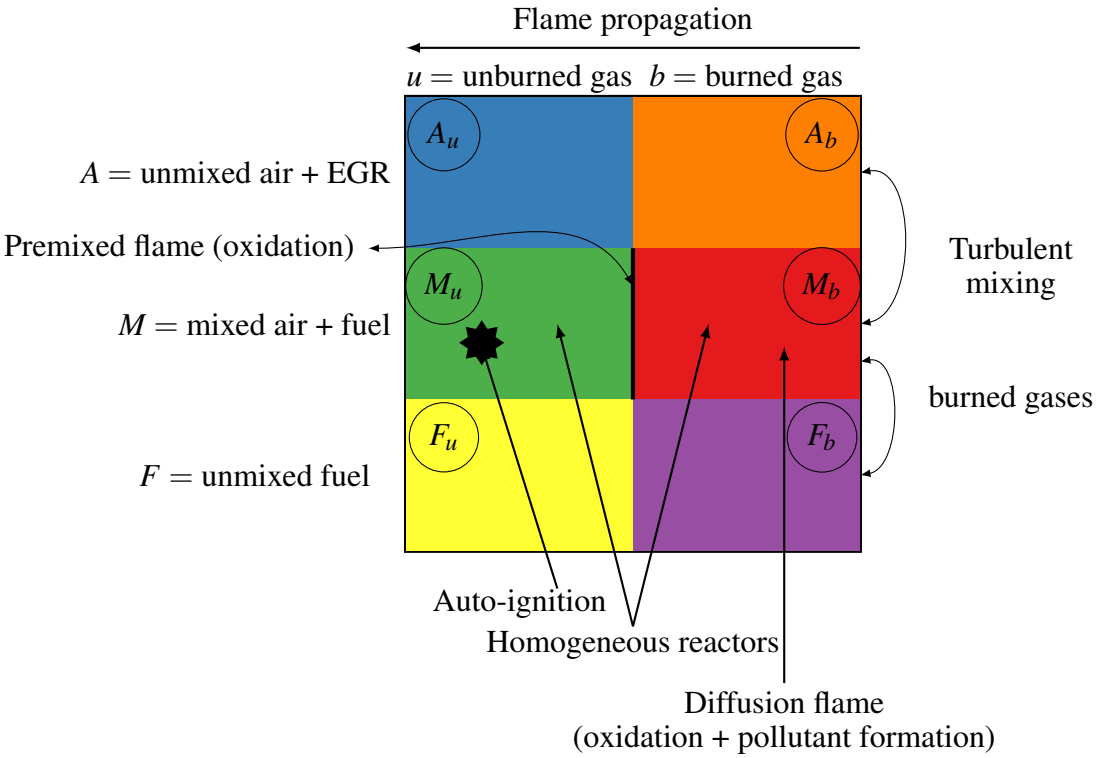

Figure 3.1: ECFM-3Z schematic adapted from [4].

By considering the burned mixing zone M_b to be perfectly mixed, the combustion process is assumed to be entirely controlled by chemistry. Hence, by introducing an approach based on a chemical time scale τ_c, the non-premixed chemical source-term can be computed as follows:

$$\overline{\dot{\omega}}_F^b = -\frac{\overline{\rho}\widetilde{Y}_F^b}{\tau_c} \quad \text{with} \quad \tau_c = Ae^{\frac{T_a}{\widetilde{T}^b}} \tag{3.19}$$

with $A = 2.10^{-6}$ and $T_a = 6000$ K given in [4]. In the case of mixture heterogeneities within the combustion chamber, the mixture can have rich local equivalence ratios leading to incomplete oxidation of the fuel. ECFM-3Z assumes that any part of the fuel present in M_u that is not fully consumed by the premixed sub-model is moved towards the M_b region where it will be post-oxidised via a non-premixed flame. This phenomenon is taken into consideration through a third chemical source-term, defined as:

$$\overline{\dot{\omega}}_F^{u\to b} = -\overline{\dot{\omega}}_F^u(1 - \frac{\phi_{crit}}{\overline{\phi}}) \tag{3.20}$$

where $\overline{\phi}$ is the Reynolds-averaged local equivalence ratio and ϕ_{crit} is the critical equivalence

ratio defined as $\phi_{\text{crit}} = \frac{2}{x}\left(x + \frac{y}{4}\right)$, where x and y denote the number of carbon and hydrogen atoms, respectively. ECFM-3Z has the capability, along with the premixed and non-premixed combustion processes, to include auto-ignition, therefore leading to a full combustion methodology for in-cylinder internal combustion engine (ICE) simulations with the prediction of the three main ignition events encountered in ICEs. Typically, auto-ignition is modelled using tabulated kinetics [85] whereby ignition delay values are computed before the CFD calculation.

The ECFM-3Z model has often been used for in-cylinder ICE simulations with overall satisfactory modelling capabilities, particularly for predicting global quantities such as pressure, temperature and mass fuel burning rates. Mobasheri [86] tested the ECFM-3Z against a high-speed direct injection diesel engine. The results show good agreement in comparison with experimental data. The in-cylinder pressure traces, as well as NO_x and soot formation trends, are well reproduced by the model. Recently, Pulga *et al.* [87] and Najar *et al.* [88] have respectively used the ECFM-3Z model for SI and compression-ignition (CI) engine simulations. In both studies, the combustion model's predictions agree with experimental trends.

Despite low-priced computational costs, the ECFM-3Z model does not include turbulence-chemistry interaction effects for the closure of the chemical source terms. Furthermore, ECFM-3Z does not allow species transport, as is typically the case for detailed chemistry simulations [89, 90, 91] due to its assumption of chemical species reaching equilibrium. Additionally, "ignition" of the model can only be undertaken during the premixed phase. Hence, the model assumes that a diffusion flame cannot exist without a premixed one. Moreover, Equations 3.14-3.15 and 3.17-3.18 highlight the premixed model's dependence on the laminar burning velocity to close terms within the FSD transport equation and the chemical source-term. As such, an accurate description of combustion phenomena using ECFM-3Z relies, to a certain extent, on an accurate approximation of the LBV scalar for which a number of challenges need to be addressed. There will be emphasised in Chapter 4.

3.3.3 *G*-Equation/Level-set Approach

The *G*-Equation model, also known as the Level-set approach, was first proposed for corrugated flamelets and later extended to thin reaction zone regimes for premixed flame combustion [52]. Based on the use of a scalar field variable G, whose definition is completely arbitrary [52, 92], the flame front is defined to be at the surface $G(x,t) = G_0$. In this geometrical description, the model considers the kinematics of the flame front propagation and describes the flame as an interface between fresh reactants ($G < G_0$) and burned gases ($G > G_0$). It avoids complications associated with counter-gradient diffusion, and since G is non-reacting, there is no need for a source-term closure. The transport equation for the mean G reviewed in [92, 93] can be written as:

$$\overline{\rho}\frac{\partial \widetilde{G}}{\partial t} + \overline{\rho}\widetilde{u}_j\frac{\partial \widetilde{G}}{\partial x_j} = \overline{\rho}S_T\left|\frac{\partial \widetilde{G}}{\partial x_j}\right| - \overline{\rho}D_t\widetilde{\upsilon}\left|\frac{\partial \widetilde{G}}{\partial x_j}\right| \tag{3.21}$$

where S_T is the turbulent flame speed and requires a closure model, for which many approaches are proposed and reviewed by Poinsot & Veynante [5] and Peters [52]. The quantity $\widetilde{\upsilon}$ describes the mean curvature as $\widetilde{\upsilon} = -\nabla\frac{\nabla G}{|\nabla G|}$ while D_t is the turbulent diffusivity given by μ_t/Sc_t [94]. The thermo-chemical state of the mixture can be parameterised by a distance $x_n = (G - G_0)/|\nabla G_0|$ to the G_0 surface. Together with a presumed probability density function (PDF) for G, the mean quantities can be obtained.

Within a partially-premixed framework, a limited number of studies have been undertaken using the Level-set approach. Müller *et al.* [95] proposed to determine flame propagation and lift-off heights in turbulent methane jet flames. A RANS formulation of S_T to combine the *G*-Equation for the propagating flame surface with the non-premixed structure is proposed through mixture fraction Z. The turbulent flame speed can then be computed as follows [95]:

$$S_T = \Bigg[\underbrace{S_L^0(Z_{st}) + b_2\left[S_L^0(Z_{st})u'\right]^{1/2} + b_1u'}_{\text{Premixed}}\Bigg]\Bigg[\underbrace{P(Z_{st})(\Delta Z)_{S_L^0}}_{\text{Partially-premixed}}\Bigg]\Bigg[\underbrace{1 - a\frac{\overline{\chi}_Z}{\chi_Z^q}}_{\text{Quenching}}\Bigg] \tag{3.22}$$

where a, b_1 and b_2 are model parameters and u' is the turbulent fluctuation. The mixture fraction dissipation rate χ_Z is a measure of the mixture fraction gradients and species fluxes

towards the flame, defined below as.

$$\chi_Z = 2D_Z \frac{\partial Z}{\partial x_j} \frac{\partial Z}{\partial x_j} \tag{3.23}$$

where D_Z is the molecular diffusivity of the mixture fraction. The above formalism proposed in [95] was extended by Chen *et al.* [96] for the study of lifted turbulent methane-air and propane-air jet flames with a variety of fuel exit velocities and nozzle diameters. The mean turbulent burning velocity was computed using the local mixture fraction and the local Damköhler number (D_a) definition proposed by Peters [97], but also by including an integral across the partially-premixed flame brush with a presumed PDF for the mixture fraction. In both studies, the simulation results predicted lift-off heights that are in good agreement with experimental data. Recent studies [98, 99, 100, 101] have shown the satisfactory modelling capabilities of the Level-set approach for SI engine configurations. Nevertheless, like the flame surface density model and ECFM-3Z, the *G*-Equation has an important dependency on the flame speed scalar and particularly the turbulent flame speed which remains still today an important field of study within the community as it is not a well-defined quantity and no universal model is available [5].

3.3.4 Flamelet Modelling

The flamelet model was first introduced in 1975 by Williams [102] for non-premixed flames where a turbulent diffusion flame consists of an ensemble of stretched laminar flamelets. This model assumes that chemical time scales are shorter than characteristic turbulence scales such that the reaction zone can be seen as an infinitely thin interface. Accordingly, the turbulent reaction zone is viewed as a collection of laminar flame elements (flamelets) embedded in the turbulent stream, not affecting the inner flame structure, which remains close to a laminar flame. The flame structure is considered locally one-dimensional, depending only on time and the coordinate normal to the flame front. A coordinate system attached to the iso-surface of the mixture fraction Z was first proposed by Peters [103, 104]. Following a transformation from the spatial-temporal space to a mixture fraction-temporal space, the complete flamelet equations can be derived, as done in [105, 106]. Under certain

assumptions (no differential diffusion, no Z-derivative of the heat capacity, and no radiating heat losses), the simplified flamelet equations can be found as:

$$\rho \frac{\partial Y_k}{\partial t} = \frac{\rho \chi}{2Le_k} \frac{\partial^2 Y_k}{\partial Z^2} + \dot{\omega}_k \tag{3.24}$$

$$\rho \frac{\partial T}{\partial t} = \frac{\rho \chi}{2} \frac{\partial^2 T}{\partial Z^2} + \dot{\omega}_T \tag{3.25}$$

where χ is defined according to Equation 3.23. Thermo-chemical properties characterising the flame structure can be computed such that species mass fractions and temperatures can be found as:

$$T = T(Z,t) \quad \text{and} \quad Y_k = Y_k(Z,t) \tag{3.26}$$

While this is not explicit in the present notation, the two scalars T and Y_k are parametrised by χ. The scalar dissipation rate has the dimension of inverse time (analogous to strain). It measures the Z-gradients and the molecular fluxes of species towards the flame. Consequently, the flame structure is given by the set of functions $T(Z,\chi_{st})$ and $Y_k(Z,\chi_{st})$. All thermo-chemical properties may be computed independently of the turbulent code and stored in so-called flamelet libraries. The mean species mass fractions and temperatures are then obtained from:

$$\overline{\rho}\widetilde{Y}_k = \int_0^1 \int_0^\infty \rho Y_k(Z,\chi_{st}) \widetilde{P}(Z,\chi_{st}) d\chi_{st} dZ \tag{3.27}$$

$$\overline{\rho}\widetilde{T} = \int_0^1 \int_0^\infty \rho T(Z,\chi_{st}) \widetilde{P}(Z,\chi_{st}) d\chi_{st} dZ \tag{3.28}$$

where $\widetilde{P}(Z,\chi_{st})$ is the mass-weighted joint-PDF of Z and χ_{st}. This is the starting point for various modelling efforts, with different choices of flamelet models, and assumptions in the modelling of the joint-PDF.

A common approach adopted for modelling partially-premixed flames is to use the flamelet/ progress variable model (FPV) [107, 108]. The FPV approach has been developed to incorporate flame dynamic effects into the steady flamelet model (cf. Equations 3.24-3.25 without the temporal term). In this approach, a chemistry tabulation is used based on the solutions of the steady flamelet equations. However, instead of a parameterisation with the scalar dissipation rate commonly used in steady flamelet models, a reactive scalar is

used, which is assumed to be independent of Z. A reaction progress variable c is often selected [109, 110] to identify each flamelet in the library. The FPV model describes all thermo-chemical states by a two-dimensional manifold. Assuming the shape of the joint-PDF function is presumed [111], mean species mass fractions and temperatures can be retrieved from:

$$\overline{\rho}\widetilde{Y}_k = \int_0^1 \int_0^1 \rho Y_k(Z,c)\widetilde{P}(Z,c)dZdc \tag{3.29}$$

$$\overline{\rho}\widetilde{T} = \int_0^1 \int_0^1 \rho T(Z,c)\widetilde{P}(Z,c)dZdc \tag{3.30}$$

where $\widetilde{P}(Z,c)$ is the mass-weighted joint-PDF of Z and c. Multiple studies [112, 113, 114, 115, 116] reported in the literature have shown that the FPV approach can accurately predict the experimental trends in a variety of turbulent reacting systems. Recently, Sun *et al.* [117] used an unsteady configuration of FPV to model a diesel spray combustion relevant to modern CI engines. The mixture fraction, the progress variable, and the local stoichiometric scalar dissipation rate serve as controlling variables for the three-dimensional table. Across all downstream locations of the jet, very good results were obtained.

3.4 Probability Density Function

The PDF $P(\Psi^*;\vec{x},t)$ or $P(\Psi^*)$ quantifies the probability of finding, for a given location, $\vec{x}$ and time t, a variable Ψ (temperature, mass fraction, velocity, etc.) within the range $[\Psi^* - \Delta\Psi/2, \Psi^* + \Delta\Psi/2]$. These methods go back to the early work of Toor [118] and have been widely used in RANS simulations [119]. The PDF is established by obeying the following relations:

$$\int_\Psi \overline{P}(\Psi^*)d\Psi^* = 1 \tag{3.31}$$

$$\overline{\Psi} = \int_\Psi \Psi^* \overline{P}(\Psi^*)d\Psi^* \tag{3.32}$$

$$\overline{\Psi'^2} = \int_\Psi (\Psi^* - \overline{\Psi})^2 \overline{P}(\Psi^*)d\Psi^* \tag{3.33}$$

where Ψ^* is the sample space variable of Ψ. Furthermore, a mass-weighted PDF $\widetilde{P}$ is also introduced as $\overline{\rho}\widetilde{P}(\Psi) = \rho P(\Psi)$. Any Favre-averaged quantity $\widetilde{\Phi}$ may then be expressed as:

$$\overline{\rho}\widetilde{\Phi} = \overline{\rho\Phi} = \int_\Psi \rho(\Psi^*)\Phi(\Psi^*)\widetilde{P}(\Psi^*)d\Psi^* = \overline{\rho}\int_\Psi \Phi(\Psi^*)\widetilde{P}(\Psi^*)d\Psi^* \tag{3.34}$$

For more than one variable, a joint probability density function can be applied such that $P(\Psi_1^*,...,\Psi_N^*)$. Any mean quantity $\overline{\Phi}$ can then be obtained as:

$$\overline{\Phi} = \int_{\Psi_1,...,\Psi_N} \Phi(\Psi_1^*,...,\Psi_N^*)\overline{P}(\Psi_1^*,...,\Psi_N^*)d\Psi_1^*...d\Psi_N^* \tag{3.35}$$

or, in terms of Favre averaging:

$$\widetilde{\Phi} = \int_{\Psi_1,...,\Psi_N} \Phi(\Psi_1^*,...,\Psi_N^*)\widetilde{P}(\Psi_1^*,...,\Psi_N^*)d\Psi_1^*...d\Psi_N^* \tag{3.36}$$

They offer the advantage that all the single-point statistical information pertaining to the desired field is embedded within the PDF. The challenge here is to define the PDF, which changes at every point in the flow field. Two main paths have been proposed [119, 120]: transported PDF and presumed PDF.

3.4.1 Transported PDF

First introduced by Pope [119], the balance equation for the PDF, based on the Navier-Stokes equations, is written as follows:

$$\begin{aligned}\underbrace{\overline{\rho}\frac{\partial \widetilde{P}}{\partial t}}_{\text{Unsteady evolution}} + \underbrace{\frac{\partial}{\partial x_j}\left(\overline{\rho}\widetilde{u}_j\widetilde{P}\right)}_{\text{Flow convection}} = &- \underbrace{\frac{\partial}{\partial x_j}\left[\overline{\rho}\overline{(u_j''|Y=\Psi^*)}\widetilde{P}\right]}_{\text{Turbulent convection}} \\ &- \underbrace{\overline{\rho}\sum_{k=1}^{N}\frac{\partial}{\partial \Psi_k^*}\left[\overline{\left(\frac{1}{\rho}\frac{\partial}{\partial x_j}\left(\rho D\frac{\partial Y_k}{\partial x_j}\right)|Y=\Psi^*\right)}\widetilde{P}\right]}_{\text{Molecular diffusion}} \\ &- \underbrace{\overline{\rho}\sum_{k=1}^{N}\frac{\partial}{\partial \Psi_k^*}\left(\frac{1}{\rho}\dot{\omega}_k(\Psi_1^*,\Psi_2^*,...,\Psi_N^*)\widetilde{P}\right)}_{\text{Chemical reaction}}\end{aligned} \tag{3.37}$$

where the first three terms correspond, respectively, to the unsteady evolution, the convection due to the mean flow field and convection due to the turbulent motions. They describe the PDF evolution in physical space. Due to mixing and combustion, the last two terms correspond to molecular diffusion and chemical reaction, thus describing the PDF evolution in composition space, i.e. Ψ_i^*. The terms on the right-hand side are closed, as is the chemical reaction quantity, knowing that it depends only on chemical variables and does not require any modelling. Hence, the transported PDF is able to handle any complex chemical

scheme. Nonetheless, the molecular diffusion term is unclosed and difficult to model due to $\overline{\Phi|Y=\Psi^*}$, which corresponds to a conditional averaging of the quantity Φ for the sampling values Ψ_k^*. Lastly, these PDF balance equations are generally solved by Monte-Carlo methods where the chemical composition is described by using stochastic "fluid particles" [5], making this method time-consuming for industrial applications.

3.4.2 Presumed PDF

A possible approach established by Williams [121] is to suppose the shape of the PDF by closing two additional balance equations for the first two moments (mean and variance) of the progress variable c for premixed flames and the mixture fraction Z for non-premixed structures. The most popular and practical PDF for diffusion flames is the so-called β-function [122, 123, 124], illustrated in Figure 3.2 and written as:

$$\widetilde{P}(Z^*) = \frac{1}{B(a,b)}(Z^*)^{a-1}(1-Z^*)^{b-1} = \frac{\Gamma(a+b)}{\Gamma(a)\Gamma(b)}(Z^*)^{a-1}(1-Z^*)^{b-1} \tag{3.38}$$

where $B(a,b)$ is the normalisation factor given by:

$$B(a,b) = \int_0^1 (Z^+)^{a-1}(1-Z^+)^{b-1}dZ^+ \tag{3.39}$$

and the Γ function defined as:

$$\Gamma(x) = \int_0^{+\infty} e^{-t}t^{x-1}dt \tag{3.40}$$

which is usually tabulated. The PDF parameters a and b are expressed as follows:

$$a = \widetilde{Z}\left[\frac{\widetilde{Z}(1-\widetilde{Z})}{\widetilde{Z''^2}} - 1\right] \quad ; \quad b = \frac{a}{\widetilde{Z}} - a \tag{3.41}$$

The β-PDF has been acknowledged by the combustion modelling community to well approximate the statistical distribution of the mixture fraction used for describing the mixing effects of non-premixed flames [125, 126, 127].

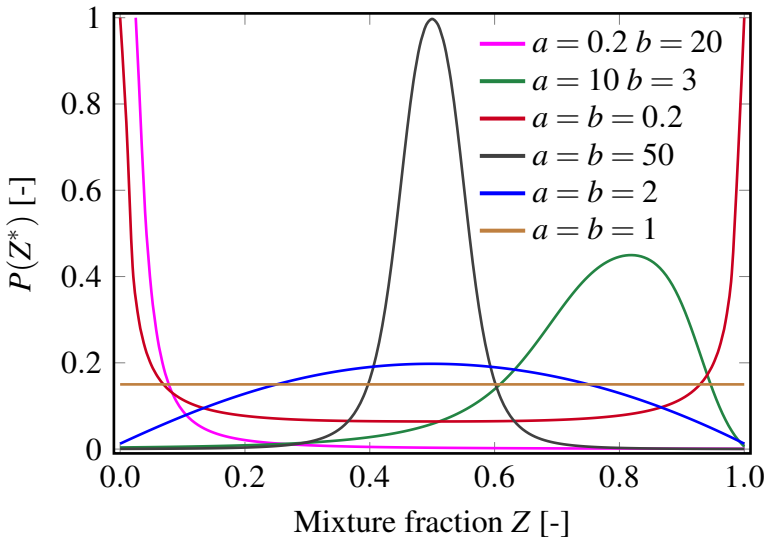

Figure 3.2: Examples of mixture fraction β-PDF shapes for various values of parameters a and b. Adapted from [5].

While the β-PDF method has been very successful in modelling non-premixed flames, the straightforward application of such a function to estimate the source-term in the c transport equation of premixed flames can yield inaccurate results. Previous studies conducted by Bray *et al.* [128] suggested that the β-PDF is not appropriate near the thin flame limit. Recently, Pfitzner [129] showed that for small c variances, the β-PDF results are reasonable, while for large variances of c, the β-function strongly over-predicts the reaction rate of the progress variable $\dot{\omega}_c$, particularly for flames with large activation energy. In classical Bray–Moss–Libby (BML) theory [68, 130], the PDF is expressed as a sum of fresh, fully burned and burning gases contributions, with the latter often assumed to have values near zero. Since the chemical source-term $\dot{\omega}_c$ vanishes at $c = 0$ and $c = 1$, its mean cannot be evaluated from $P_{\mathrm{BML}}(c)$ with the burning gas contributions set to zero. Presumed premixed flame PDFs derived from numerically generated 1-D laminar flame profiles have been proposed in [128, 131, 132, 133]. The authors invoked empirical cutoffs near $c = 0$ and $c = 1$ to avoid numerical divergence of their integrals when calculating the normalisation condition of the PDF along with the mean and variance of the progress variable. Despite providing acceptable results, as the premixed PDF is generated from laminar flame codes and thus was derived under the "flamelets" assumption, the validity of the proposed c-PDF might be

erroneous at high turbulence intensity. Therefore, a new presumed PDF approach is needed to give reasonably accurate results while possibly being applied to various premixed flame regimes. Pfitzner & Klein [134] recently extended the premixed laminar flamelet-PDF in the case of large Karlovitz (K_a) number flames. The probability density function for simulations of premixed turbulent combustion is:

$$P(c^*) = P_{1\mathrm{D}}(c^*)I(c^*)\Xi(c^*) \tag{3.42}$$

where $I(c^*)$ and $\Xi(c^*)$ are, respectively, the correction factor accounting for the flame thickening (e.g. due to strain) and the geometrical flame wrinkling effects. The term $P_{1\mathrm{D}}$ denotes the laminar flamelet-PDF calculated from 1D laminar flame code, formulated as:

$$P_{1\mathrm{D}}(c^*) = \frac{1}{N}\frac{1}{dc/d\Lambda}H(c^* - c^-)H(c^+ - c^*) \tag{3.43}$$

where $H(x)$ is the Heaviside function, $c^- = c(\Lambda^-)$ and $c^+ = c(\Lambda^+)$, with Λ^- and Λ^+ denoting the left and right boundaries of the LES filter interval, respectively. Pfitzner introduced in [129] a correlation for approximating c^- and c^+. The quantity N is a normalisation factor such that $N = \Delta_\Lambda$, with $\Delta_\Lambda = (\rho_u S_u c_p/\lambda)\Delta_x$, where Δ_x denotes the LES filter size. The denominator term $dc/d\Lambda$ is written as:

$$dc/d\Lambda = a \cdot c[1 - (c/C)^m] \tag{3.44}$$

where a and C are two coefficients set to unity when strain effects are ignored (accounted for by I and Ξ). The power exponent m is expressed as follows:

$$m = \frac{4}{5}(\alpha + \beta) - 1 \tag{3.45}$$

with $\alpha = (T^b - T^u)/T^b$ and $\beta = \alpha T^a/T^b$.

3.5 Conditional Moment Closure

The conditional moment closure (CMC) was first proposed by Klimenko [135] and Bilger [136]. Both authors independently derived the model with Bilger making an in-depth comparison in [137]. CMC assumes that fluctuations in scalar quantities such as species and

temperature can be associated with the fluctuations of one or several selected scalars. In non-premixed combustion, this principal scalar is often the mixture fraction Z [94], while for premixed flames, the variable chosen is usually the progress variable c [138]. The CMC model calculates conditional moments at a fixed location within the flow field using modelled transport equations for the conditional moments of the reactive scalars with no assumptions on the small-scale structure of reaction zones or on the relative time scale of chemistry and turbulence. Only the set of CMC equations in a non-premixed framework will be presented for clarity purposes. The means of species mass fraction Y_k and temperature T, conditioned on the mixture fraction, can be written as:

$$Q_k(x,t,\eta) = \langle Y_k(x,t)|Z(x,t)=\eta\rangle \tag{3.46}$$

$$Q_T(x,t,\eta) = \langle T(x,t)|Z(x,t)=\eta\rangle \tag{3.47}$$

where $\langle\Phi\rangle$ denotes the ensemble average of the quantity Φ while η denotes the sampling space variable of mixture fraction. Following the decomposition strategy proposed by Bilger [137], mean quantities can be decomposed as (note that only mean species mass fraction is shown here):

$$Y_k(x,t) = Q_k(x,t,\eta) + Y_k''(x,t) \tag{3.48}$$

Similar to the Reynolds averaging concept, here the conditional mean Q_k is treated as a non-fluctuating quantity. By applying this concept to Favre-averaged species (cf. Equation 2.20) and enthalpy (cf. Equation 2.18), the derived CMC transport equation for Q_k is:

$$\underbrace{\frac{\partial Q_k}{\partial t}}_{\text{Unsteady evolution}} + \underbrace{\langle u_j|\eta\rangle\frac{\partial Q_k}{\partial x_j}}_{\text{Convection}} - \underbrace{\langle \chi_Z|\eta\rangle\frac{\partial^2 Q_k}{\partial \eta^2}}_{\text{Molecular mixing}} + \underbrace{\frac{1}{\overline{\rho}\widetilde{P}(\eta)}\frac{\partial}{\partial x_j}\Big[\langle \rho u_j'' Y_k''|\eta\rangle \widetilde{P}(\eta)\Big]}_{\text{Diffusion}} = \underbrace{\langle \dot{\omega}_k|\eta\rangle}_{\text{Chemical source}} \tag{3.49}$$

Unlike the flamelet model, the CMC model has no constraint regarding the flame propagation type, which allows it to accommodate more practical cases. The derived CMC

transport equation for Q_T is given by:

$$\begin{aligned}\frac{\partial Q_T}{\partial t}+\langle u_j|\eta\rangle\frac{\partial Q_T}{\partial x_j} =&\langle\chi_Z|\eta\rangle\frac{\partial^2 Q_T}{\partial\eta^2}\\ &-\frac{1}{\overline{\rho}\widetilde{P}(\eta)}\frac{\partial}{\partial x_j}\Big[\langle\rho u_j'' T''|\eta\rangle\widetilde{P}(\eta)\Big]\\ &+\langle\chi_Z|\eta\rangle\frac{\partial Q_T}{\partial\eta}\left[\frac{1}{\langle c_p|\eta\rangle}\left(\frac{\partial\langle c_p|\eta\rangle}{\partial\eta}+\sum_{k=1}^{N}c_{p,k}\frac{\partial Q_T}{\partial\eta}\right)\right]\\ &+\frac{\langle\omega_H|\eta\rangle}{\langle\rho|\eta\rangle\langle c_p|\eta\rangle}\\ &+\frac{1}{\langle c_p|\eta\rangle}\left\langle\frac{1}{\rho}\frac{\partial P}{\partial t}|\eta\right\rangle\end{aligned}\tag{3.50}$$

Solving these equations (for non-premixed flames) will provide the conditional mass fractions of all species and temperatures for all locations and times in the flow field. In the case of premixed flames, the mean variable is conditioned on the progress variable c through the sample space variable ξ. For premixed flame structures, Klimenko *et al.* [139] and Bilger [140] have respectively derived the CMC transport equations for the mean species mass fraction and the conditional enthalpy, which can be used to recover temperature. Assuming small fluctuations of mean reaction rate around its conditional averages, the chemical source-term can be closed using first-order closure:

$$\langle\dot{\omega}_k|\eta\rangle\approx\dot{\omega}_k\big(\langle Y_k|\eta\rangle,\langle T|\eta\rangle,\langle\rho|\eta\rangle\big)\tag{3.51}$$

where $\langle T|\eta\rangle$ is the conditional temperature, $\langle Y_k|\eta\rangle$ and $\langle\rho|\eta\rangle$ are the conditional mass fractions of species k and the conditional density, respectively. For non-premixed flames, the unconditional mean chemical source-term is thus computed knowing the PDF of the mixture fraction:

$$\overline{\dot{\omega}}_k=\int_0^1\langle\dot{\omega}_k|\eta\rangle\overline{P}(\eta)d\eta\tag{3.52}$$

A number of methods have been proposed in [94, 139, 141] to close the conditional turbulent fluxes $\langle u_j''\Phi''|\eta\rangle$, the conditional scalar dissipation $\langle\chi_Z|\eta\rangle$, the conditional velocity $\langle u_j|\eta\rangle$ and the conditional heat release $\langle\omega_H|\eta\rangle$.

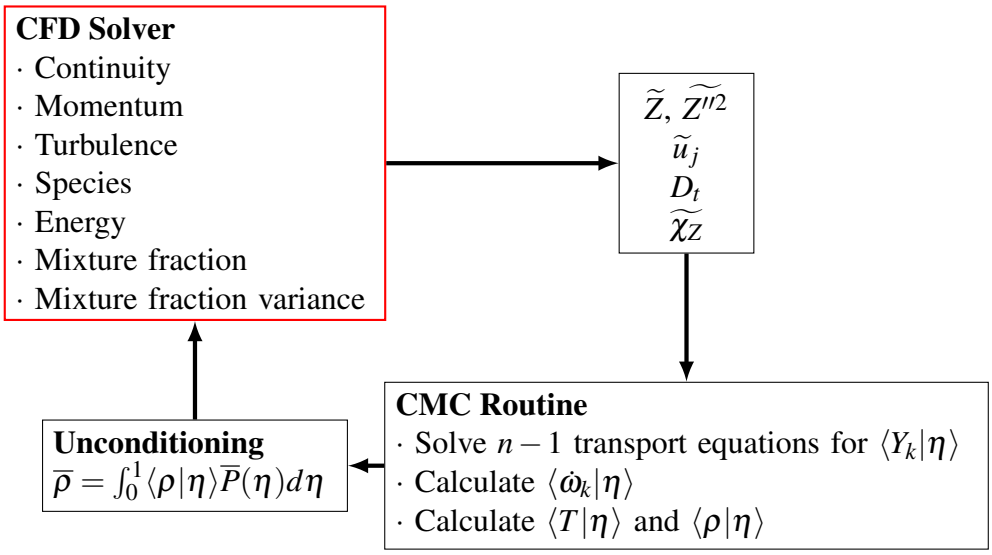

Figure 3.3: Typical CMC routine structure for diffusion flames.

First-order CMC methods using a single conditioning variable have been tested for a variety of premixed flames [142, 143, 144] and non-premixed flames [145, 146, 147, 148]. A general routine structure of CMC used for non-premixed flames is illustrated in Figure 3.3. For partially-premixed flames, Kronenburg *et al.* [149] have managed to couple LES with a conservative formulation of the conditional moment closure for the computation of a turbulent dimethyl-ether jet flame. The mixture fraction Z is selected as the single conditioning variable. A high CMC resolution provides excellent agreement with experiments throughout the flame, and the results demonstrate CMC's capability to accurately predict TCI effects in partially-premixed flames with different detailed chemical mechanisms. An improvement of the previous methodology for partially-premixing has also been proposed using Z and c as two conditioning scalars, known as doubly CMC (DCMC) [139]. Various studies have investigated the modelling capabilities of DCMC to account for partially-premixing [150, 151, 152, 153]. The predicted scalars are well aligned with the experimental trends. However, at high turbulence intensity, promoting extinction and re-ignition phenomena, DCMC along with second-order closure methods have been found to not fully resolve the problem [154].

Unlike the transported PDF method, the computational expense and numerical challenges are much more reduced since the CMC equations are conditioned on the mixture fraction

and/or the progress variable; thus, the dimensionality is lowered. Nevertheless, CMC models are still computationally expensive, not only due to the modelling of unclosed terms in the transport equations (cf. Equations 3.49-3.50) but also due to the additional dimension in the CMC equations introduced by a second conditional variable. Indeed, when partially-premixing is modelled, the CMC approach can not be easily extended to a doubly conditioned formulation as additional unclosed terms appear which require closure [94]. For the reasons quoted previously, it is expected that within an ultra-lean combustion scenario, exposed to moderate or severe turbulence intensity, DCMC might not be adapted to account for extinction and re-ignition pockets.

3.6 Summary

The simulation of turbulent reacting flows presents a number of challenges associated, among so many others, to the strong coupling between fluid dynamics and chemical kinetics. Depending on the studied case, and thus the combustion characteristics taking place (i.e. the choice of fuel, structures of flames, length and time scales), different combustion models can be used to tackle the problem. However, within the scope of this thesis, which tackles partially-premixed flames under ultra-lean conditions, most existing models can be categorised into two main types: either topologically-based (i.e. flamelet models and the G-Equation) or PDFs. Despite not relying on any flame structure assumptions and K_a-D_a numbers, quite a few issues are yet to be addressed with PDF-based models, such as accurately predicting the shape of the joint-PDF, for instance. On the contrary, geometrical models have shown great potential for practical applications due to their simplicity, low computational cost and reasonably good accuracy. Although these models have mainly been used in the literature for a broad range of flame configurations, their modelling capabilities to account for partially-premixed structures are still limited to the inclusion of a single structure of flame. Over the years, researchers have extended some of the available models to account for partially-premixing by adding a second control variable to describe either the mixing effects in diffusion flames or the propagation of the premixed flame front.

As the topologically-based models introduced in this chapter rely on the laminar burning velocity scalar (and the turbulent burning velocity in the case of the *G*-Equation model), the next chapter will investigate the feasibility/applicability of geometrical analysis models for simulating flames operating under ultra-lean mixture conditions by validating a previously developed empirical laminar burning velocity correlation.

Chapter 4

Development of a Laminar Burning Velocity Empirical Correlation for Combustion of iso-octane/ethanol Blends in Air

It can scarcely be denied that the fundamental phenomena which first led mankind into chemical inquiries are those of combustion.

–William Crookes

Contents

The content in this chapter is a result of the collaborative efforts of the author, Dr. X. H. Fang, V. Shankar, S. J. Baker, Prof. F. C. P. Leach and Prof. M. H. Davy. The author is responsible for all studies presented. The corresponding author is Dr. Fang. The content in this chapter has been published in the peer-reviewed journal Fuel [155].

4.1 Overview

This chapter investigates the feasibility of using flame topologically-based models relying on the LBV scalar for predicting combustion under lean mixture conditions. The proposed "Oxford" laminar burning velocity correlation is extensively validated to assess its applicability in CFD applications.

The content in this chapter presents the first application of the LBV correlation of Hinton and co-workers [33] to iso-octane/ethanol fuel blends by means of a mixing rule approach. Firstly, an in-depth validation of this "Oxford" correlation for pure iso-octane and ethanol is undertaken against various experimental LBV measurements and different 1-D kinetics models. A wide range of equivalence ratios, pressures and temperatures are examined. Subsequently, various mixing rule strategies are investigated and compared over a fixed set of temperature and pressure conditions for 25%, 50% and 75% ethanol by volume. The performance of the Oxford correlation/mixing rule approach for iso-octane/ethanol blends is assessed against various experimental LBV measurements available within the literature and against chemistry mechanism simulations. Previously unpublished burning velocity data at higher pressures from the experimental measurements of Varea *et al.* [25] and Broustail *et al.* [14] are gathered. Similarly, LBV data for stoichiometric iso-octane/ethanol (50% vol/vol) mixtures at elevated temperatures (380 K and 450 K) and pressures (1, 2 and 4 bar) collected by Hinton during his doctoral studies [26] are included. A complementary study is also carried out presenting the first application of the Oxford LBV correlation for for a simplified single-cylinder spark-ignition engine simulations.

4.2 Generalities

One of the fundamental properties of a premixed flame is its laminar burning velocity. Defined as the velocity of an unstretched adiabatic one-dimensional flame propagating towards the unburned gas, the LBV is known to be strongly dependent on the mixture conditions, i.e. pressure, temperature and equivalence ratio. Rallis & Garforth [156] have proposed the following equation for the LBV:

$$S_u = S_s - S_g \tag{4.1}$$

where S_s and S_g are respectively the unstretched laminar flame speed and the unburned gas velocity immediately ahead of the flame front (cf. Figure 4.1). The LBV has been shown to be of great importance in spark-ignition engine modelling, as its correlation with burn duration influences the power output and efficiency [32, 157].

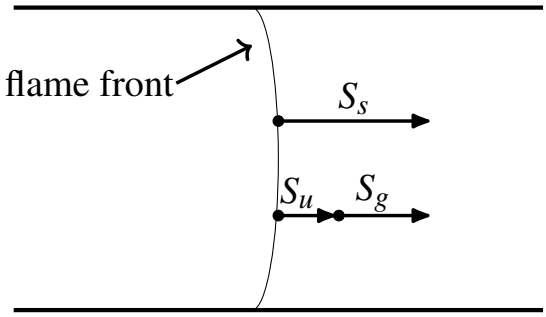

Figure 4.1: Schematic representation of the laminar burning velocity.

Laminar burning velocities can be obtained following two approaches:

- Empirical correlations given by experimental measurements for which Egolfopoulos *et al.* [158] have present an in-depth review of the various advances and challenges.
- Numerical analysis undertaken through 1D simulation codes along with detailed reaction mechanisms as described by Konnov *et al.* [159].

A wide range of combustion models (including the previously presented topologically-based models) that are in common use rely on the LBV to close chemical source terms,

emphasising its essential role in the description of combustion phenomena such as pollutant formation, flame propagation, flame stabilisation or extinction [159, 160].

However, LBV data are at times contradictory and require careful analysis before use. Konnov *et al.* [159] suggested that differences observed between correlations are mainly due to the inherent characteristics of the different experimental methods, which can affect the flame structure. Egolfopoulos *et al.* [158] also noted that LBV data obtained from experimental studies typically correspond to lower pressure and temperature conditions than those encountered in modern internal combustion engines. Additionally, to the best of the authors' knowledge, burning velocities have not been extensively studied at equivalence ratio conditions below 0.6, particularly for liquid fuels at high pressure and temperature conditions [46, 161]. This has led to the use of LBV data derived from 1-D simulations. For example, Benajes *et al.* [162] performed simulations under unsteady RANS (URANS) for passive pre-chamber ignition concept in a turbocharged single-cylinder port fuel injection SI engine at ultra-lean operating conditions with $\phi = 0.5$ using ECFM. Laminar flame speeds were calculated via 1-D simulations using a primary reference fuel (PRF) chemistry mechanism [163]. Combustion could not be achieved in the simulations for equivalence ratios of $\phi \leq 0.5$ as the pre-chamber's burning rates were substantially decreased due to low predicted burning velocities.

There are two points worthy of note here: First, the study by Benajes and co-workers' provides how critical it is to have accurate LBV data at the edge of the operating envelope. Second, the accuracy of the 1-D simulation results for LBV data in the ultra-lean region is unknown. The numerical approach will yield a physically correct result – however, as there are no existing validation data, the accuracy of any particular 1-D scheme and chemical mechanism in predicting the LBV can not be proven. The collection of LBV data for nominally liquid hydrocarbon fuels under lean and ultra-lean conditions and at engine relevant temperatures and pressures remains a pressing need for the combustion modelling community, while simultaneously presenting a substantial technical challenge to experimentalists worldwide.

Biofuels have increasingly gained attention as a feasible solution for more sustainable in-

ternal combustion engines [45]. Ethanol is the most widely used biofuel in SI engines due to its relatively mature production infrastructure compared to other alcohol-based biofuels such as methanol or n-butanol [164]. The addition of ethanol to gasoline has been recognised as a promising strategy to reduce emissions of unburned hydrocarbons, nitric oxides, soot particles, and carbon monoxide [165, 166, 167]. In comparison with gasoline, ethanol is more resistant to knock, enabling the use of an increased compression ratio which yields a higher thermal efficiency in SI engines [168, 169]. However, to fully realise these benefits, the fundamental combustion performance of ethanol needs to be well understood, especially at engine relevant conditions, both to evaluate the potential performance of the fuel, but also to provide input parameters for models used in technological development.

Various studies reported in the literature provide experimentally derived LBV correlations of gasoline surrogate fuels such as iso-octane, for example, the Gülder correlation [170], or the Metghalchi & Keck correlation [171]. The Metghalchi & Keck correlation has not been extended to pure ethanol or iso-octane/ethanol blends, thus limiting its use for the study of gasoline/alcohol fuels. Gülder's LBV correlation does extend to iso-octane/ethanol blends but only up to 20% of ethanol by liquid volume [172]. Del Pecchia *et al.* [173] have extended a previously developed correlation [174] to include different gasoline/ethanol blends using data from a 1-D detailed chemical kinetics model. Although the results of this study were in good agreement with the chemical mechanisms used for validation, at higher proportions of ethanol blending, the interactions between the ethanol and gasoline surrogate sub-chemistries are not well characterised, creating a potential source of error [175, 176]. It is also worth noting that alcohols have a structure with many potential isomeric fuel radicals for a given carbon chain length, which increase the number of reaction paths, implying larger and more complex mechanisms, with long calculation times as a result [177, 178].

Since the collection of LBV data under engine-relevant conditions of temperature and pressure and the subsequent development of a useful LBV correlation represents a significant challenge for any fuel, it is practically difficult to develop dedicated correlations for every fuel blend of interest. Accordingly, mixing strategies have gained interest in the engine community over the past few years as a promising method for determining the burning

velocities of a blend from the LBV of its components. An in-depth review of the mixing rules for gasoline/alcohol blends, which are expected to be non-linear in the fuel blend composition [23, 179], is provided by Sileghem *et al.* [23].

4.3 The Oxford LBV Correlation

The general form of the Oxford LBV correlation was first established by Marshall *et al.* [32] who used a constant volume vessel and a multi-zone model [180] to investigate the effects of combustion residuals on the LBV of various liquid fuels (including iso-octane and ethanol) under a range of high pressures and temperatures (Table 4.1). Pressure rise methods were adopted to determine burning velocities, where a Schlieren system is used to detect cellularity. A 12 term correlation is provided by Marshall *et al.*'s work, where 30,000 data points from 150 experiments were included. Following the work from Marshall & co-workers, a 14 term correlation was developed by Hinton *et al.* [33] where a second-order dependence on equivalence ratio was included in the exponents of temperature and pressure.

Table 4.1: Iso-octane/air and ethanol/air measurement ranges given respectively by Marshall *et al.* [32] and Hinton *et al.* [33].

Fuels	Iso-octane		Ethanol	
Parameters	Min	Max	Min	Max
Temperature [K]	310	450	380	450
Pressure [bar]	0.5	4	0.5	4
Equivalence ratio [-]	0.7	1.4	0.7	1.4
Residual mole fractions [-]	0	0.3	0	0

The second-order dependence enables a more reliable representation of the burning velocity's reliance on temperature, which is of great importance in engine modelling, where knowledge of behaviour at elevated conditions of temperature and pressure is vital. More importantly, whereas Marshall *et al.*'s work did not successfully determine the unstretched burning velocities, Hinton's study employed a linear extrapolation to zero stretch to account for stretch effects. Reconciliation of two different methods for determining LBV (flame front imaging and pressure rise) was also demonstrated for the first time during Hinton's

study, providing strong cross-validation and robust foundation to the Oxford correlation. The final correlation is characterised by 14 coefficient terms, defined as follows:

$$S_u = \Big[S_{u,0} + S_{u,1}(\phi-1) + S_{u,2}(\phi-1)^2 + S_{u,3}(\phi-1)^3 + S_{u,4}(\phi-1)^4\Big] \times T^{\alpha} \times P^{\beta} \times \Big[1 - \mu_1 x_r^{(\mu_2+(\phi-1)\mu_3)}\Big] \tag{4.2}$$

with,

$$\alpha = \alpha_0 + \alpha_1(\phi-1) + \alpha_2(\phi-1)^2 \tag{4.3}$$

$$\beta = \beta_0 + \beta_1(\phi-1) + \beta_2(\phi-1)^2 \tag{4.4}$$

$$P = \frac{P_u}{1.0} \quad T = \frac{T_u}{298} \tag{4.5}$$

where x_r is the mole fraction of the residual gases. Further information regarding the experimental setup can be found in Marshall's and Hinton's work [32, 33], which detail the various instruments and setups used during their respective studies. The Oxford LBV correlation coefficients for neat iso-octane and ethanol are given in Table 4.2.

Note: (i) the LBV correlation for pure ethanol has not been extended to include the residual mole fraction and, (ii) for stoichiometric mixtures, a modified correlation is adopted where only three coefficient terms are needed.

Table 4.2: Coefficient values to calculate burning velocities for Equation 4.2, valid for both fuels within the range of $340 \leq T_u \leq 640$ K, $0.7 \leq P_u \leq 6$ bar and $0.7 \leq \phi \leq 1.3$.

Fuels	$S_{u,0}$	$S_{u,1}$	$S_{u,2}$	$S_{u,3}$	$S_{u,4}$	α_0	α_1
Iso-octane	28.48	13.11	-80.05	56.59	57.73	1.889	-0.08456
Ethanol	35.616	21.159	-130.38	-38.952	79.839	1.9195	-0.2463
	α_2	β_0	β_1	β_2	μ_1	μ_2	μ_3
Iso-octane	0	-0.1997	0.1074	0	2.081	0.8283	0.02103
Ethanol	2.3624	-0.2596	0.21003	-0.30893	1.4380	1.4111	0.20056

4.4 Comparison of Mixing Rules

The Oxford correlation, in its initial form, is designed for single fuel components. To extend the use of the Oxford correlation for fuel blends, a mixing rule is required. Simple mixing rules based on mole, mass or energy-fraction are commonly used by the community.

These may be generalised as follows [181]:

$$S_{u,blend} = \sum_{k=1}^{n=2} \alpha_k S_{u,k} \tag{4.6}$$

where $S_{u,k}$ is the LBV of the neat fuel, and α_k is the blending method adopted for the mixing rule.

For the mixing rule of this type investigated in this work, which is based on energy-fraction, α_k is defined by:

$$\alpha_k = \frac{\Delta h^0_{f,k} x_k}{\sum_{k=1}^{n=2} \Delta h^0_{f,k} x_k} \tag{4.7}$$

where x_k is the mole fraction of the fuel component k within the binary blend, such that $x_1 + x_2 = 1$. The energy-fraction mixing law is chosen over the mass and mole fraction approaches as various studies [23, 182, 183, 184] have documented large sources of errors introduced by mass/mole fraction based mixing rules.

The second mixing strategy examined herein is derived from Le Châtelier's [185] work on predicting lean flammability limits of fuel blends, where blend burning velocity is given by:

$$S_{u,blend} = \frac{1}{\sum_{k=1}^{n=2} \frac{x_k}{S_{u,k}}} \tag{4.8}$$

Sileghem *et al.* [23] proposed a modified version of this rule whereby the mole fraction, x_k, in Equation 4.8 is replaced with the energy-fraction, α_k, of Equation 4.7. The modified Le Châtelier mixing rule has been tested for various gasoline/alcohol blends (including iso-octane/ethanol) with a noticeable improvement compared to the conventional Le Châtelier rule [182, 186, 187].

More complex mixing models exist for estimating a blend's burning velocity, such as the one proposed by Hirasawa *et al.* [179] or Ji & Egolfopoulos [188], which can potentially obtain a higher degree of accuracy on $S_{u,blend}$ predictions [15]. However, such models are typically based on non-linear expressions and require more information for the inputs, such as the adiabatic flame temperature of the binary blend as well as each compound. In order to adapt these forms of mixing rules, the adiabatic flame temperature of each pure fuel is

considered identical, leading to the third mixing law considered in this study:

$$S_{u,blend} = exp\left(\sum_{k=1}^{n=2} Y_k S_{u,k}\right) \tag{4.9}$$

where Y_k is the fuel mass fraction in the binary blend.

Note that Baloo *et al.* [157] have successfully used Equation 4.9 with LBV correlations for the individual fuels for predicting the burning velocities of various iso-octane/methane fuel concentrations.

4.5 Modelling Details

For all experimental conditions investigated, corresponding LBV values were computed using CONVERGE CFD software, where details of the computational setup can be found in the manual [189]. Conservation equations to govern steady, quasi-1-D flame propagation at constant pressure are determined using an implicit finite-difference approach in conjunction with the time-reliant and steady-state schemes. Flame location in the domain follows a coordinate system, wherein the temperature specified at a point fixes the flame position. The laminar burning velocity is an eigenvalue and is computed as part of the solution of the governing equations. The computational procedure commences with the reduction of non-linear governing equations to algebraic equations using a finite difference scheme. Convergence of algebraic equations is taken care of by the damped Newton's approach. Multi-component transport formulation describes molecular diffusion.

Three reduced chemical mechanisms are considered in this work (see Table 4.3). The first is based on the work of Wu *et al.* [11] where three different reduction techniques were employed under a wide range of temperature, pressure and equivalence ratio conditions relevant to modern ICEs. For mixtures of toluene primary reference fuel (TPRF) surrogates and ethanol, experimental data on ignition delay times of an n-heptane/iso-octane/toluene/ethanol blend (10.2%/37.8%/12%/40% by liquid volume) suggested by Cancino *et al.* [190] was employed. Experimental measurements on burning velocities of an ETPRF blend with 15% of ethanol by volume fraction from Dirrenberger *et al.* [6] was included. The skeletal mechanism was shown to be reasonably accurate for both ignition

delay times and burning velocities with regards to experimental data and the results calculated by the detailed kinetics model of the Lawrence Livermore National Laboratory (LLNL) [191].

The second chemical mechanism is a highly reduced four-component (toluene/n-heptane/iso-octane/ethanol) gasoline surrogate kinetics mechanism developed by Li *et al.* [12]. The model was validated against various experimental data (ignition delays and laminar burning velocities) for different ethanol concentrations. The ETPRF mechanism has also been coupled with CFD models to simulate measurements taken from a compression ignition engine (pressure and temperature traces). The results obtained with n-heptane/iso-octane/toluene/ethanol mixtures (20%/44.3%/27.5%/8.2% by liquid volume) suggested that the model can qualitatively predict the experimental trends.

The final chemical mechanism is a kinetics model of TPRFs for the oxidation of gasoline surrogates, characterised by 159 species and 734 reactions. Developed by Andrae & Kovács [13], the main oxidation pathways of the mechanism were validated against ignition delay experiments, pressurised flow reactor data, combustion timing in a HCCI engine, and laminar burning velocities. This mechanism by Andrae *et al.* has been extensively validated against a blend of iso-octane, toluene, and n-heptane (42.9/43.4/13.7% mole) suggested by Dirrenberger *et al.* [6], as a model for a commercial gasoline (Ref. IFPEN: TAE7000).

Table 4.3: Summary of various reaction mechanisms used in the present work.

Authors	Fuels	Species-Reactions	Origin
Wu *et al.* [11]	ETPRF	165-839	[191]
Li *et al.* [12]	ETPRF	59-270	[192]
Andrae *et al.* [13]	TPRF	159-734	[193, 194, 195]

4.6 Results & Discussion

4.6.1 Pure Component Results

Figures 4.2 and 4.3 highlight the effect of equivalence ratio, ambient temperature and pressure on burning velocities for both iso-octane and ethanol, respectively. In each case, the results from the Oxford correlation results are plotted alongside the most relevant experi-

mental data found within the literature and the results of the applicable kinetics simulations.

Table 4.4: Summary of various experimental measurements used in the present work for neat iso-octane (O) and ethanol (E), and iso-octane/ethanol blends (OE) with SEF: spherically expanding flame, HF: heat flux and EHDC: externally heated diverging channel.

Year	Authors	Method	Fuel	T_u [K]	P_u [bar]	ϕ [-]	Ref.
2011	Broustail *et al.*	SEF	E, OE	393	1	0.8–1.4	[24]
2011	van Lipzig *et al.*	HF	OE	298–338	1	0.6–1.15	[196]
2012	Galmiche *et al.*	SEF	O	323-473	1-10	0.6–1.6	[7]
2013	Broustail *et al.*	SEF	E, OE	423	1-10	0.7–1.4	[14]
2013	Varea *et al.*	SEF	OE	373	1-10	0.7–1.5	[25]
2014	Dirrenberger *et al.*	HF	O, E	298–398	1	0.7–1.4	[6]
2014	Knorsch *et al.*	HF	E	348–423	1	0.7–1.6	[16]
2014	Sileghem *et al.*	HF	E, OE	298–358	1	0.7–1.5	[15]
2015	Aghsaee *et al.*	SEF	E	318-473	1-5	0.7–1.5	[17]
2015	Rau *et al.*	HF	OE	298-373	1	0.7–1.4	[197]
2018	Katoch *et al.*	EHDC	E	350–620	1	0.7–1.3	[18]
2019	Meng *et al.*	SEF	O, E	298–450	1-4	0.7–1.4	[8]
2019	Kim *et al.*	SEF	E	428	1	0.7–1.5	[19]
2020	Kim *et al.*	SEF	E	373, 428	2, 10	0.7–1.5	[20]
2020	Han *et al.*	HF	O	298–358	1	0.7–1.6	[9]
2021	Kumar *et al.*	EHDC	O	300–640	1	0.7–1.4	[10]
2021	Wang *et al.*	HF	E	298–448	1	0.7–1.6	[21]

Note that throughout this thesis, the experimental data are represented by data markers, the kinetic model data with dashed lines, and the Oxford correlation with a solid line. Table 4.4 details the range of all referenced experimental data and experimental setup used for the data collection.

Analysis of the effects of high pressure and temperature conditions on LBV of neat fuels in this work is restricted to stoichiometric mixture conditions as most of the literature data are limited to a narrow range of ϕ due to the early onset of the flame wrinkling on the

rich side. Note also that, in many cases, correlation values will be an extrapolation beyond the range of fitted data given by Table 4.1. The general trends shown by the correlation in Figures 4.2-4.3 are consistent with the literature. Iso-octane presents slower-burning velocities compared with ethanol, while ethanol is seen to be more strongly affected by increases in temperature and pressure than iso-octane as indicated by Dirrenberger *et al.* [6] and van Lipzig *et al.* [196].

Comparison of neat iso-octane/air LBVs were made with the literature experimental data given by Dirrenberger *et al.* [6] and Han *et al.* [9] obtained using the heat flux method; by Galmiche *et al.* [7] and Meng *et al.* [8] who applied the spherical flame method, and by most recently Kumar *et al.* [10] who used the divergent channel method. A close match is found between the Oxford correlation results and the experimental data of Han *et al.* [9]. A small deviation is seen for richer conditions at lower temperatures. One of the reasons for this could lie in the use of a linear extrapolation for the constant pressure analysis of flame speed. Some scatter is seen in the experimental data. Although, as noted by Galmiche *et al.* [7], some differences are to be expected due to the different experimental setup and methodologies for data post-processing. Nevertheless, at stoichiometric conditions, where most of the current study's experimental data lies, the correlation is fully consistent with the available experimental data even at higher temperature and pressure where the correlation is extrapolated. Note that further information regarding the strength and challenges of each LBV instrument used in the quoted measurements is presented by Egolfopoulos *et al.* [158] and Konnov *et al.* [159].

Figure 4.2(a)-(c) also show the burning velocities of iso-octane/air mixtures obtained with the three chemical mechanisms introduced previously. At atmospheric pressure conditions, all kinetics models accurately follow the experimental trends throughout the entire set of measurements, including at higher unburned temperatures. This is particularly the case for the two ETPRF mechanisms, which closely match the experimental data of Kumar *et al.* [10] under stoichiometric conditions.

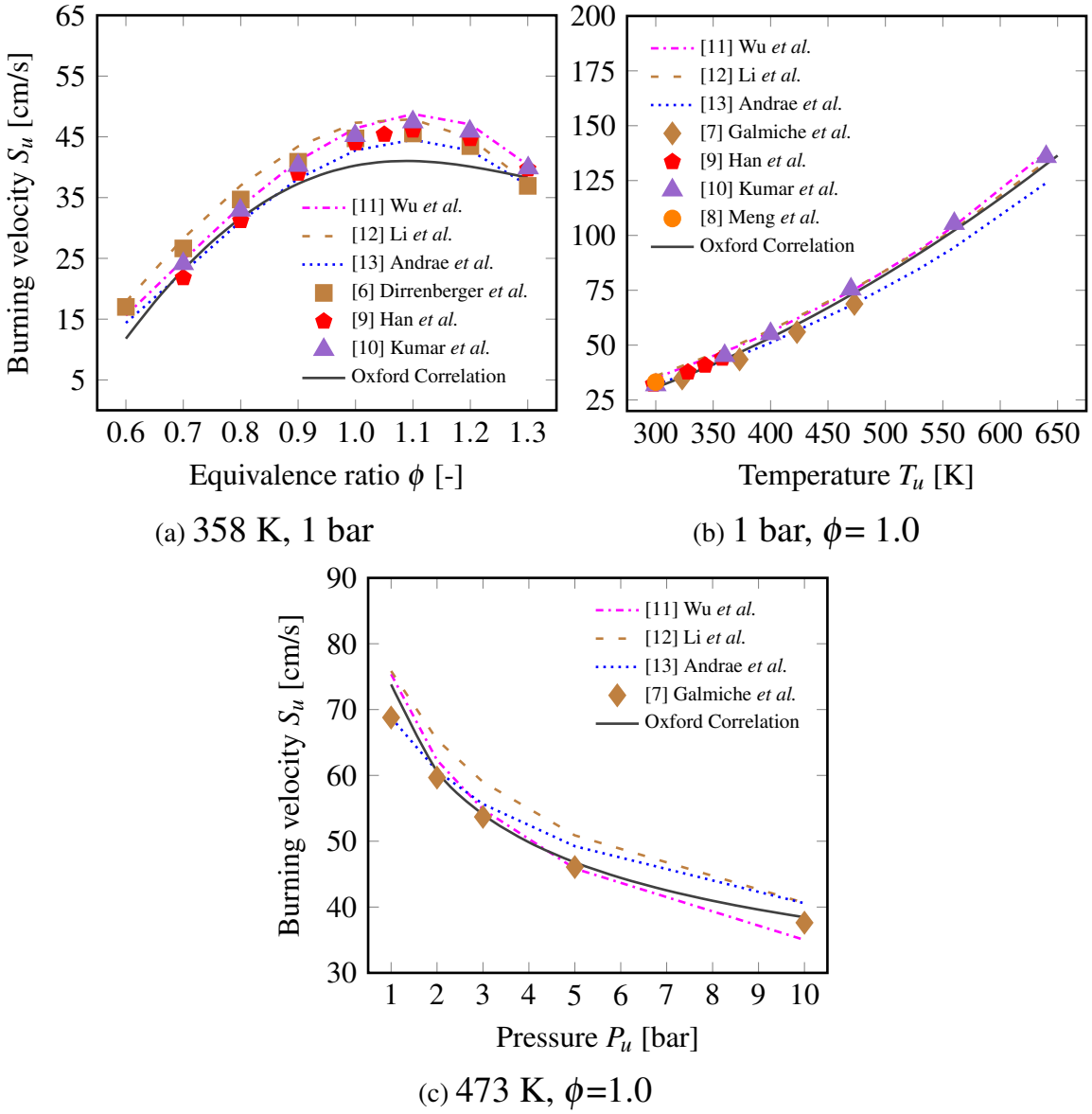

(a) 358 K, 1 bar

(b) 1 bar, ϕ= 1.0

(c) 473 K, ϕ=1.0

Figure 4.2: Comparison of Oxford (solid line) correlation for iso-octane/air ((a),(b),(c)) with experiments (markers) [6, 7, 8, 9, 10] and chemical kinetics simulations (dashed lines) [11, 12, 13]. The residual mole fraction x_r is fixed at zero.

The LBVs estimated by Andrae & Kovács' reaction model seem to under-predict the experimental trends suggested by Kumar & co-authors but is in good agreement with the measurements of Galmiche *et al.* [7]. This is consistent with the observations of Konnov *et al.* [159], suggesting that LBV values obtained with the EHDC method used by Kumar & co-workers reduces the effective flame area and thus increases the burning velocity by 7%. At higher pressures (cf. Figure 4.2(c)), a small deviation from the experimental data

can be seen for LBVs calculated with Andrae *et al.* [13] and Li *et al.* [12]. The model proposed by Wu *et al.* [11] is able to follow the trends accurately.

Comparison of neat ethanol/air LBVs were made with the experimental measurements given by: Sileghem *et al.* [15], Dirrenberger *et al.* [6] and Wang *et al.* [21] using the heat flux method; by Broustail *et al.* [24] and Aghsaee *et al.* [17] using the spherical flame method, and by Katoch *et al.* [18] using the divergent channel method. The current study is best matched with Aghsaee *et al.*'s [17] most recent work on the pyrolysis and oxidation of ethanol mixtures at high temperature. Interestingly, Aghsaee & co-workers used the same experimental technique (spherical flame) as was employed in the present work to collect the data from which the correlation was derived. The flame speed data from Sileghem *et al.* [15] and Dirrenberger *et al.* [6], who both used the heat flux method, are notably higher than those of Aghsaee in the ϕ range of 0.9-1.1. Aghsaee & co-workers suggested that the observed differences in the experimental data could be attributed to errors within the heat flux (misreading of thermocouples and condensation in the fuel pipe). Additional comments from Aghsaee's work also highlight experimental errors in their own study, originating mainly from the error in determining the radius from the images and the limited number of images used, and was estimated to be around 1.5% at 1 bar and between 2% and 8% at 5 bar. Therefore, it is reasonable to say that the LBV from the study and correlation extrapolated LBV agrees well with the experimental data, especially at higher pressures.

Figure 4.3(a)-(c) also shows that LBVs of ethanol/air mixtures calculated with the ETPRF mechanisms of Wu *et al.* [11] and Li *et al.* [12]. Both models match the experimental trends well with regard to the set of experimental data considered herein. However, there are some minor differences. Under $\phi = 1.0$ and $P_u = 1$ bar conditions, the mechanism proposed by Li *et al.* [12] seems to better capture the trends predicted by the Oxford correlation and the measurements taken by Katoch *et al.* [18], as opposed to Wu's mechanism where a small inconsistency is observed at higher temperature conditions. Like the pure iso-octane case, Figure 4.3(c) illustrates LBVs estimated with both mechanisms under stoichiometric mixtures and various pressure conditions.

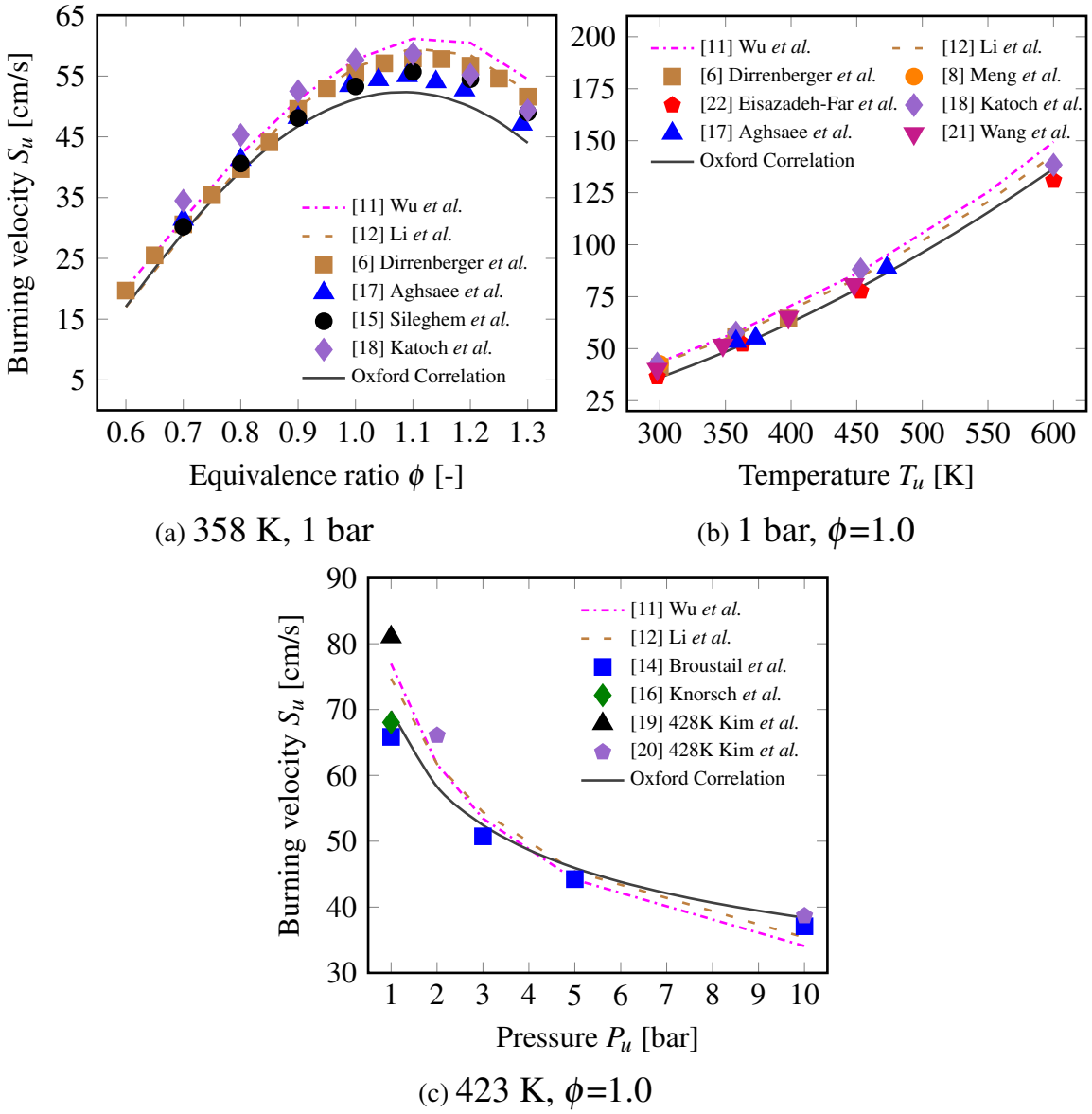

(a) 358 K, 1 bar

(b) 1 bar, ϕ=1.0

(c) 423 K, ϕ=1.0

Figure 4.3: Comparison of Oxford (solid line) correlation for ethanol/air ((a),(b),(c)) with experiments (markers) [8, 14, 15, 16, 17, 18, 19, 20, 21, 22] and chemical kinetics simulations (dashed lines) [11, 12]. The residual mole fraction x_r is fixed at zero.

At higher pressures, both models are able to accurately replicate the LBV data given by Broustail *et al.* [14] and Kim *et al.* [20]. At atmospheric pressure, both kinetics models over-predict the LBV measurements of Knorsch *et al.* [16] and Broustail & co-authors. Note that a similar trend can be seen for the pure iso-octane case. Wu *et al.* [11] have noticed a similar behaviour for their kinetics mechanism. The detailed model from LLNL used for constructing the skeletal mechanism was over-predicting the LBV values of TPRF

and ETPRF blends at atmospheric pressure and stoichiometric conditions. Results obtained with Li *et al.*'s [12] mechanism are in good agreement with the trends published by the authors.

4.6.2 Mixing Rule Results

Figure 4.4 shows the burning velocities of iso-octane/ethanol-air mixtures predicted by the Oxford correlation with: the conventional energy-fraction mixing rule (cf. Equation 4.6), the modified Le Châtelier formula based on energy-fraction (cf. Equation 4.7-4.8), and the simplified Hirasawa *et al.* mixing law (cf. Equation 4.9). The burning velocities are shown as a function of ethanol concentration for lean, stoichiometric, and rich conditions (Figures 4.4(a)-(c), respectively) at a fixed fresh gas temperature and pressure condition of 358 K and 1 bar. Experimental results from Sileghem *et al.* [15] and Han *et al.* [9] are also shown. As expected, the addition of ethanol enhances the burning velocity of the fuel blend. Regardless of the mixing strategy used, the Oxford correlation's results are seen to be in reasonable agreement with the experimental data across the full range of conditions examined. The agreement is good across almost all of the ethanol concentration range under lean conditions $\big($Figure 4.4(a)$\big)$. Under stoichiometric and fuel-rich conditions (Figures 4.4(b) and (c), respectively) there is a clear deviation from the experimental data towards the two extremes of ethanol concentration.

Perhaps the most significant finding from the results shown in Figure 4.4, is that all three mixing strategies considered in this work yield very similar values of LBV for all blend and mixture conditions tested, in agreement with the works of Sileghem *et al.* [23, 15]. The energy-fraction based mixing rule seems to result in slightly higher LBV values than the two other mixing strategies, while the simplified Hirasawa *et al.* rule yields the lowest LBV values.

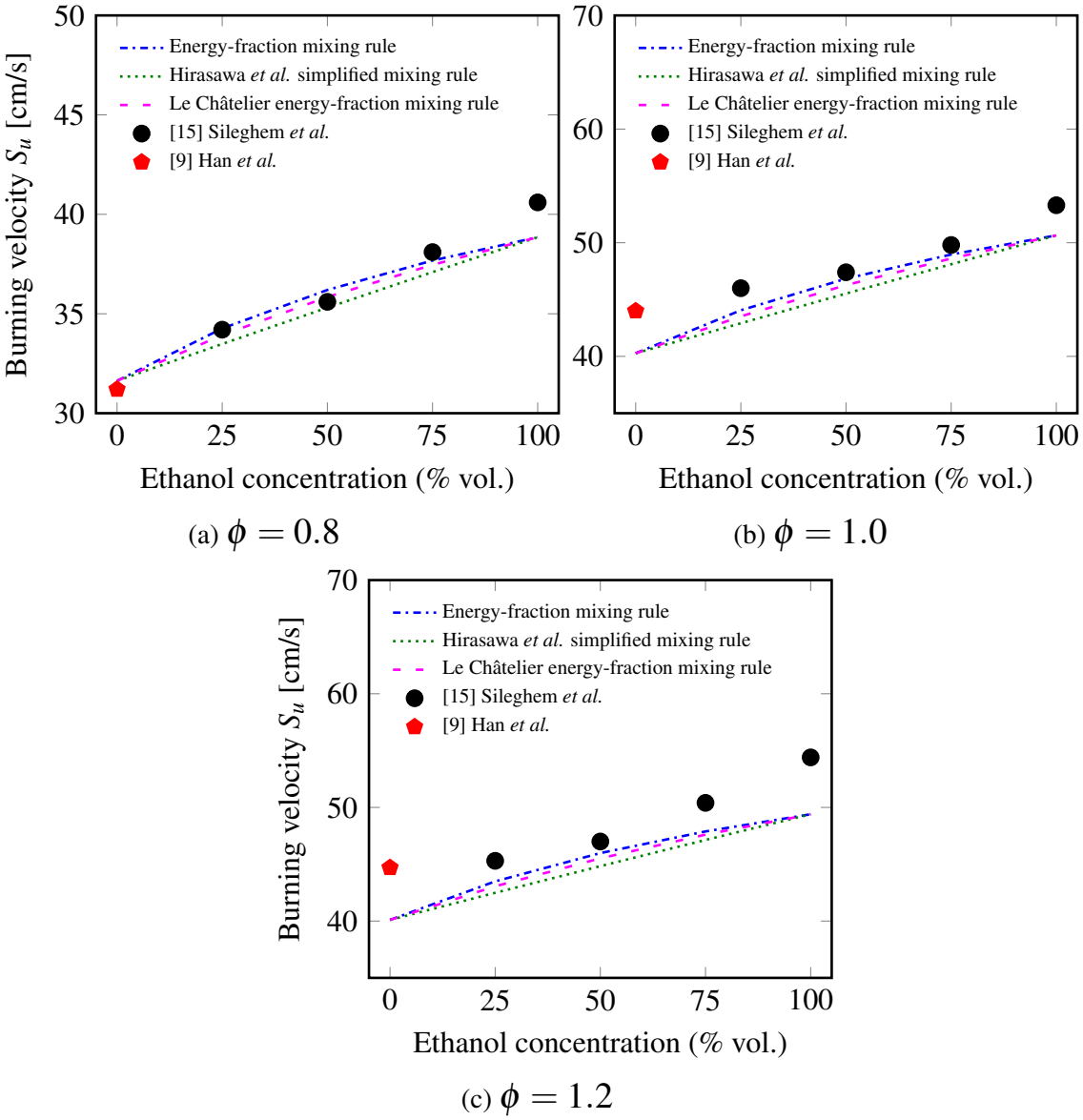

Figure 4.4: Comparison of Oxford (dotted lines) mixing strategies results for iso-octane/ethanol-air mixtures, as a function of ethanol concentration at $T_u = 358$ K and $P_u = 1$ bar. Experimental data (markers) from Sileghem *et al.* [23] and Han *et al.* [9] are also included for neat and blended fuels. The residual mole fraction x_r is fixed to zero.

Sileghem *et al.* [15] have previously shown the modified Le Châtelier rule to outperform the energy fraction mixing rule when applied to iso-octane/ethanol blends. Accordingly, the modified Le Châtelier mixing rule was applied throughout the remainder of this study.

4.6.3 Iso-octane/Ethanol Blend Results

Figure 4.5 illustrates the laminar burning velocities obtained with the Oxford correlation/modified Le Châtelier rule for fixed temperature and pressure conditions of 393 K and 1 bar.

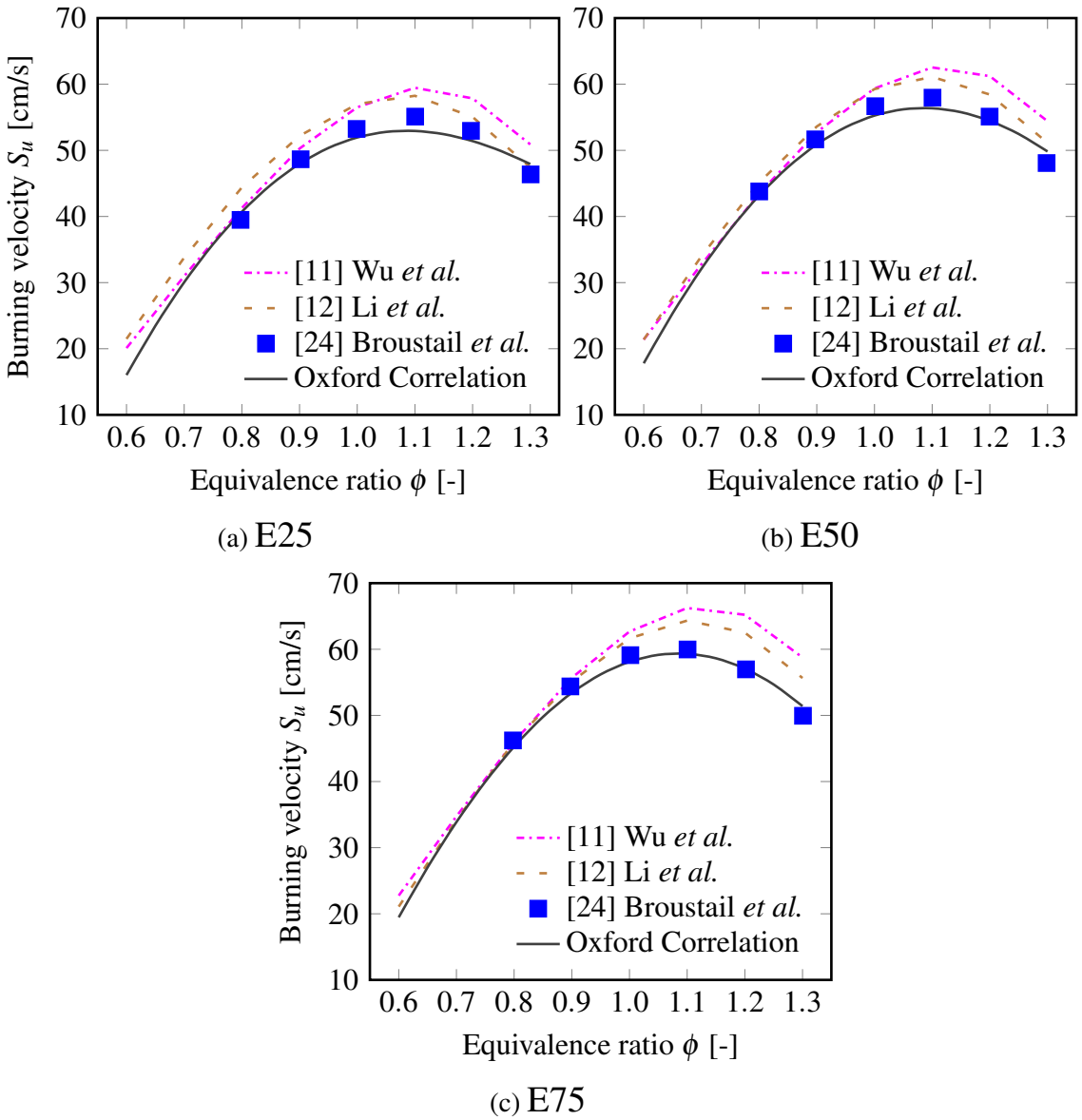

Figure 4.5: Comparison of Oxford (solid line) correlation for iso-octane/ethanol-air mixtures obtained with Le Châtelier's mixing rule based on energy-fraction, for (a) E25, (b) E50 and (c) E75, at $T_u = 393$ K and $P_u = 1$, with experiments (markers) [24] and chemical kinetics simulations (dashed lines) [11, 12]. The residual mole fraction x_r is fixed at zero.

The results are seen to be in excellent agreement against the set of experimental data given

by Broustail *et al.* [24], throughout all ethanol concentrations and mixture conditions. Overall, both chemical mechanisms demonstrate the ability to follow the measurements accurately, particularly in lean regions. However, at stoichiometric and rich mixtures, the simulated LBVs deviate from the trends given by the experimental data. This tendency is highlighted as the proportion of ethanol within the blend increases, visible in Figure 4.5(c) and in the case of pure ethanol $\big($Figure 4.3(c)$\big)$. This behaviour could be due to an inadequate description of the ethanol rich oxidation chemistry, as suggested by Sarathy *et al.* [192] or a difference between the predicted and measured values of the temperature exponent associated to neat ethanol [159], which is expected to become worse at higher mixture temperatures as depicted in Figure 4.7.

Prior results have established the validity of the Oxford correlation at atmospheric pressure and various unburned temperatures. However, it has not yet been validated under higher pressure conditions. To this end, Figures 4.6 and 4.7 compares the LBVs computed from the Oxford correlation/modified Le Châtelier mixing rule with previously unpublished experimental data from the Complexe de Recherche Interprofessionnel en Aérothermochimie (CORIA) and the Laboratoire Pluridisciplinaire de Recherche en Ingénierie des Systèmes, Mécanique, Énergétique (PRISME), collected during the studies of Varea *et al.* [25] and Broustail *et al.* [14] respectively, at elevated pressure conditions (max 10 bar) for various concentrations of ethanol. Only stoichiometric mixture LBV results are included as for both studies, their maximum equivalence ratio achievable at higher pressures was constrained by the safe operating pressure limit of their respective combustion vessels.

Figure 4.6 compare the LBV values from the Oxford correlation and kinetics simulations against experimental data acquired from the CORIA group at 373 K. Burning velocities calculated with the modified Le Châtelier mixing law and chemical mechanisms can accurately replicate the experimental trends, for all tested concentrations. It is worth mentioning that Varea *et al.*'s measurements for E50 deviate from the expected trends at pressures above 7 bar, highlighted by higher LBV values. One reason could be that LBV measurements were affected by cellularity, likely to occur at higher pressures and equivalence ratios greater or equal than stoichiometry [25]. The Oxford correlation seems to deviate less from

the experimental data than the kinetics model of Wu *et al.*, both within and outside the range of validity of the Oxford correlation.

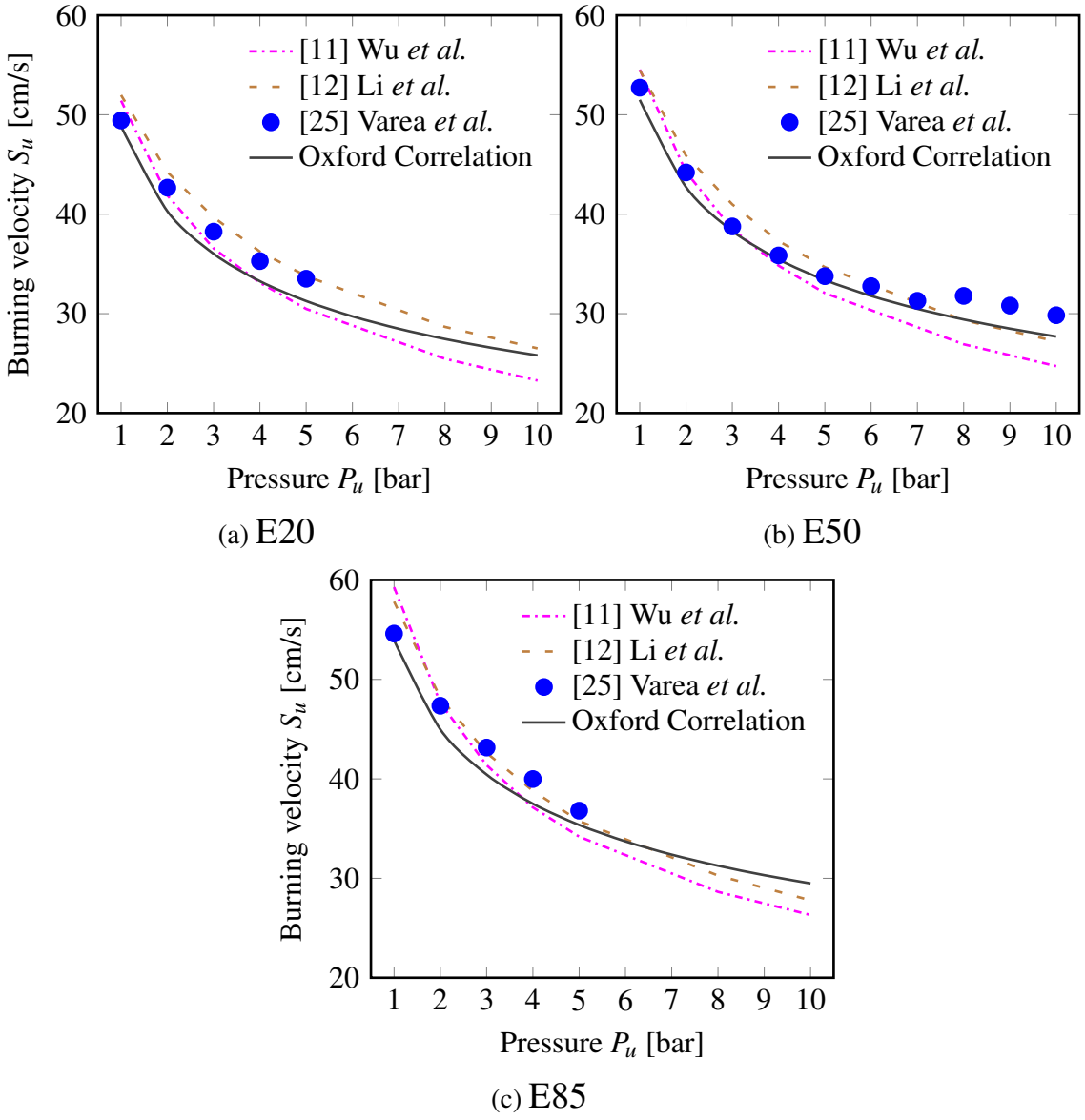

Figure 4.6: Comparison of Oxford (solid line) correlation for stoichiometric iso-octane/ethanol-air mixtures obtained with Le Châtelier's mixing rule based on energy-fraction, with measurements (markers) acquired from Varea *et al.* [25] $\big($(a),(b),(c)$\big)$. The temperature is 373 K with pressure conditions up to 10 bar and $\phi = 1.0$. Chemical kinetics simulations (dashed lines) [11, 12] are also presented. The residual mole fraction x_r is fixed at zero.

Note that the burning velocities estimated by the mechanism from Li & co-workers are in good agreement with the set of measurements presented, especially for pressure condi-

tions below 6 bar. This is in good agreement with the trends previously depicted at lower atmospheric pressures.

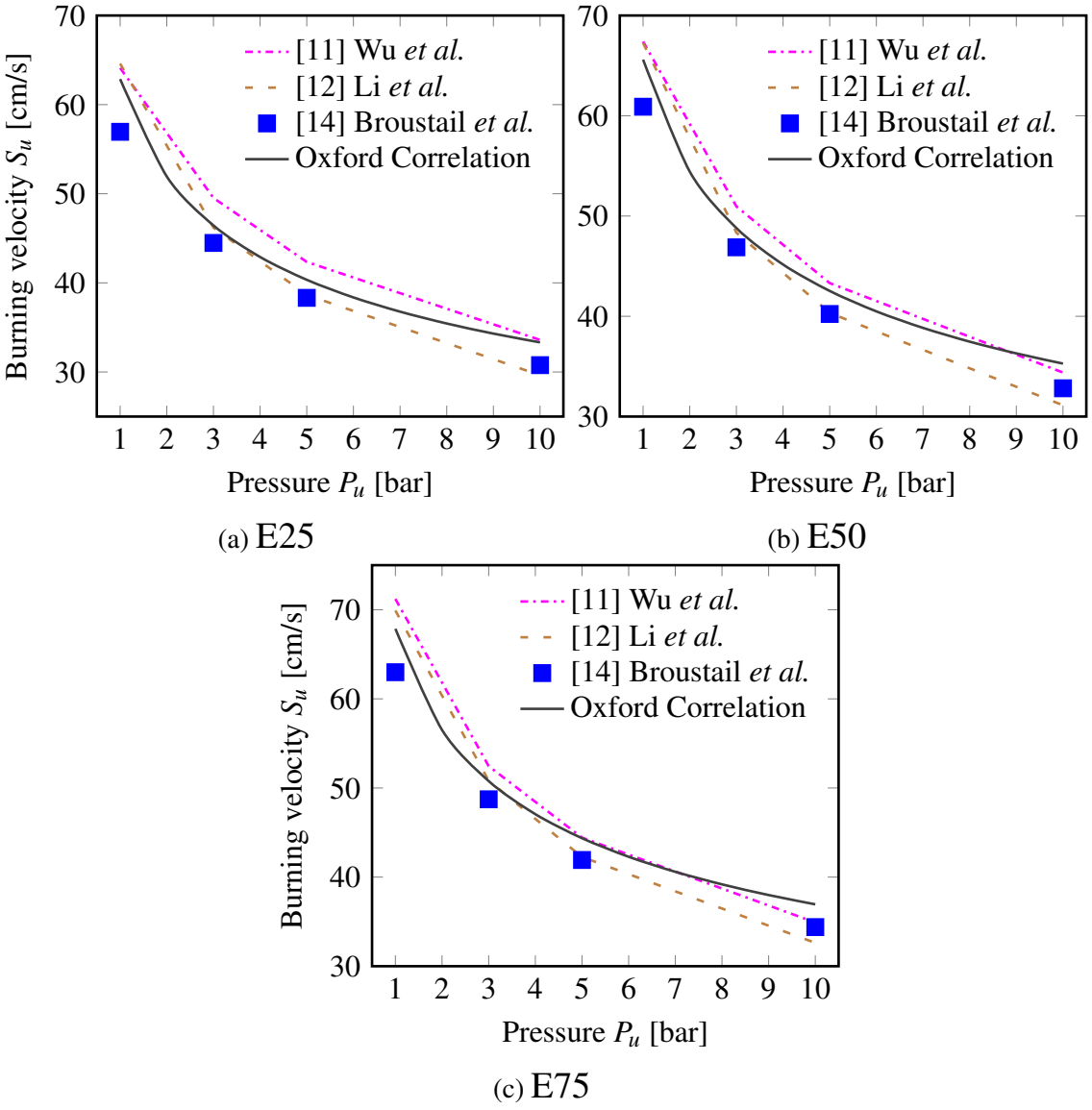

Figure 4.7: Comparison of Oxford (solid line) correlation for stoichiometric iso-octane/ethanol-air mixtures obtained with Le Châtelier's mixing rule based on energy-fraction, with measurements (markers) acquired from Broustail *et al.* [14] ((a),(b),(c)). The temperature is 423 K with pressure conditions up to 10 bar and $\phi = 1.0$. Chemical kinetics simulations (dashed lines) [11, 12] are also presented. The residual mole fraction x_r is fixed at zero.

The reaction mechanism of Wu *et al.* under-predicts burning velocities for all concentrations of ethanol. Zhang *et al.* [169] noticed a similar behaviour for their ETPRF mechanism

and attributed the effects to uncertainties in the transport properties of gasoline-ethanol blends.

Figures 4.7 illustrate the LBV values obtained with the Oxford correlation and kinetics simulations against experimental data shared by the PRISME group at fixed temperature conditions of 423 K. Overall, the Oxford correlation performs satisfactorily – even in the extrapolated region beyond 6 bar. Typically, the correlation is seen to provide closer agreement with the experimental data than the results given by Wu's mechanism, which struggles to replicate the experimental trends for pressure conditions between 1 and 5 bar, particularly at lower concentrations of ethanol. However, better agreement with the experimental data is given by the chemical mechanism developed by Li & co-authors.

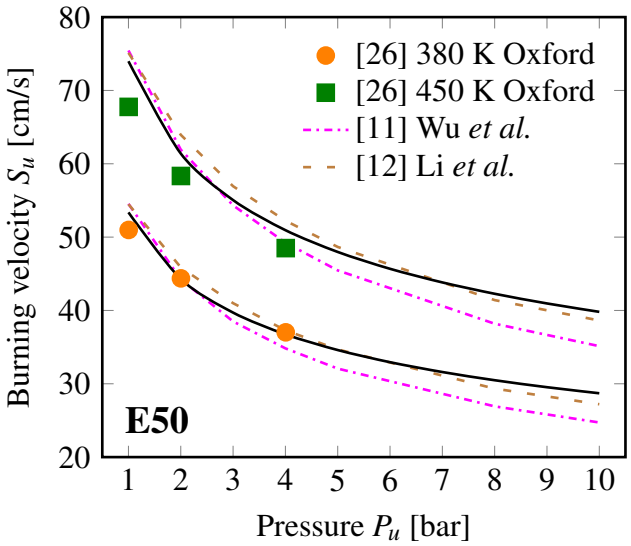

Figure 4.8: Comparison of Oxford (solid line) correlation for stoichiometric iso-octane/ethanol-air mixtures (50/50 vol/vol) obtained with Le Châtelier's mixing rule based on energy-fraction, with measurements (markers) from the Oxford group [26]. The temperatures are respectively fixed at 380 K (orange) and 450 K (green) with pressure conditions up to 4 bar. Chemical kinetics simulations (dashed lines) [11, 12] are also presented. The residual mole fraction x_r is fixed at zero.

Figure 4.8 provides further confirmation as to the accuracy of the Oxford correlation-modified Le Châtelier mixing rule approach. Supplementary LBV measurements conducted for a 50% v/v blend of ethanol in iso-octane undertaken by Hinton during his doctoral studies [26] are included. The given set of data has not been previously published in

Hinton & co-authors' work [33, 198]. Two sets of temperature data are presented, i.e. 380 K and 450 K at 1, 2 and 4 bar. Burning velocities estimated by both ETPRF mechanisms are also added. The empirical correlation agrees well with the experimental data, particularly for temperatures fixed at 380 K.

The results obtained in the above work are a significant first step in extending the capabilities of the Oxford LBV correlation in the context of gasoline/alcohol fuels, providing motivation and a pathway for applications to engine simulations. The content of this chapter continues with the assessment of the proposed Oxford correlation for in-cylinder engine simulations. It should be noted that the results presented hereafter are not part of the published content presented above.

4.7 Application of the Oxford LBV Correlation and ECFM-3Z for Combustion Engine Simulations

The ECFM-3Z model is possibly one of the most adopted combustion tools for in-cylinder SI engine simulations. Various studies reported in the literature provide experimental LBV correlations, of which the previously introduced Metghalchi & Keck correlation [171] (subsequently referred to simply as M&K) is perhaps the most widely used by the engine community for in-cylinder simulations. Despite an extensive range of validity for pressure and temperature conditions, various studies [174, 199, 200] have reported that the M&K correlation can be erroneous for modern engine simulations with lean and ultra-lean mixture conditions, i.e. $\phi \leq 0.7$ $\big($according to D'Adamo *et al.*[201]$\big)$ being particularly problematic. The present section demonstrates the first CFD application of the new "Oxford" correlation under lean conditions. The correlation is used with the ECFM-3Z model, operating within a Reynolds-Averaged Navier-Stokes framework to perform simulations for a simplified single-cylinder spark-ignition engine. The engine simulation results obtained with the newly implemented correlation are compared to the one using the M&K correlation under three lean equivalence ratio conditions.

4.7.1 Oxford Correlation vs. Metghalchi & Keck Correlation

Figure 4.9 gives an brief overview of the performance of the Oxford correlation compared to three experimental datasets [10, 27, 28], chemical kinetics simulations [13, 29] and the M&K correlation for iso-octane/air under high pressure and/or temperature conditions.

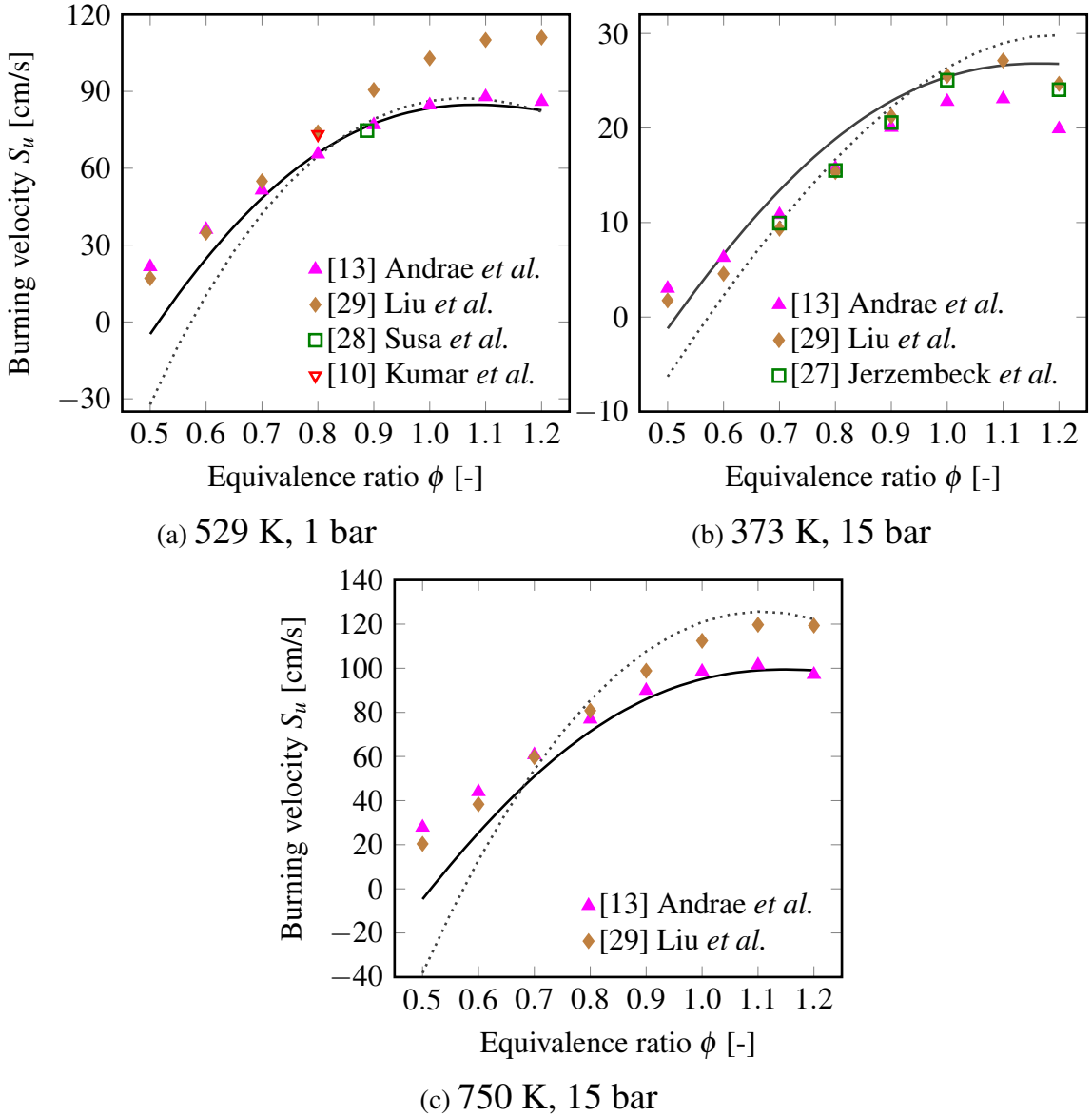

(a) 529 K, 1 bar

(b) 373 K, 15 bar

(c) 750 K, 15 bar

Figure 4.9: Comparison of both Oxford (smooth line) and M&K (dotted line) correlations for iso-octane/air with experiments (hollow marks) [10, 27, 28] and chemical kinetics simulations (filled marks) [13, 29] results at (a) $T_u = 529$ K, $P_u = 1$ bar, (b) $T_u = 373$ K, $P_u = 15$ bar and (c) $T_u = 750$ K, $P_u = 15$ bar. The residual mole fraction x_r is fixed at zero.

A very limited set of data for LBV variations is available in the literature at higher tem-

peratures and pressures. Therefore, investigation of the two different correlations is predominantly undertaken against two chemical kinetics models, Andrae *et al.* mechanism [13] used in the previous study (cf. Figure 4.2), and Liu *et al.* mechanism [29] of TPRF consisting of 56 species and 168 reactions. For equivalence ratios $\phi > 1$, the M&K correlation yields significantly higher flame speeds than the Oxford correlation and chemical kinetics simulations at elevated pressures $\big($although the results are similar in Figure 4.9(a)$\big)$. A slight under-prediction of Oxford correlation is seen compared with simulations at high pressure and temperature conditions before combustion onset. Nevertheless, compared with available experimental studies and chemical kinetics simulations, it is evident that Oxford presents a better match across the range of conditions considered, in particular for engine-like conditions illustrated in Figure 4.9(c). Although no experimental data is available for equivalence ratios lower than 0.7, Oxford's correlation is seen to follow the LBV predicted by the Andrae *et al.* mechanism [13] reasonably well under ultra-lean conditions out to an equivalence ratio of $\phi \approx 0.6$. In contrast, the M&K correlation yields a significantly lower LBV, going negative at $\phi \approx 0.6$, which makes its use in lean combustion simulations problematic. It is clear that the Oxford correlation offers the potential for extending the lean limit of combustion simulations beyond that of the M&K correlation. Therefore, the following sections examine the effects of this in simplified 3D engine simulations.

4.7.2 Computational Setup

Simulations of a generic four-valve single-cylinder SI engine operating at a constant 3600 rpm were conducted for a wide range of lean equivalence ratio conditions. Details of the simulated engine geometry, valve timings, equivalence ratios and spark timings are given in Table 4.5. The selected ignition timings are based on the studies undertaken by Benajes *et al.* [162] and Zembi *et al.* [202]. The simplified engine uses no fuel injector; instead, an ideal homogeneous fuel-air mixture is added in the combustion chamber via the inlet port. This is in order to keep the focus of the study on the qualitative LBV performance rather than the specifics of an engine setup.

Table 4.5: Engine data and operating conditions.

Bore	79.9 mm
Stroke	80.0 mm
Compression ratio	8.658
Engine speed	3600 RPM
Intake valve opening	358 CAD bTDC
Intake valve closing	145 CAD bTDC
Exhaust valve opening	136 CAD aTDC
Exhaust valve closing	352 CAD aTDC
Fuel	iso-octane
Top dead centre (TDC)	0 CAD
Equivalence ratio	0.8, 0.7, 0.6
Spark timing	20, 27, 40 CAD bTDC
Injection	no injector

The ECFM-3Z RANS modelling routines along with the spark-ignition sub-model are built-in capabilities of the commercial CFD solver, STAR-CCM+ [203], used in this study. The unsteady Pressure Implicit with Splitting of Operators (PISO) algorithm [204] was used to solve the transport equations. Turbulence was modelled using the well-known k-ε model [67], with coefficients computed by Launder & Sharma [205]. Some additional terms were added to the turbulence model to account for buoyancy and compressibility effects. The computational domain for RANS is set with the piston moving in the z-direction. The wall boundaries were set as non-slip walls and fixed at a temperature of 500 K. STAR-CCM+ automatically determines the initial gas composition in the intake port, the exhaust port, and the cylinder based on the fuel-air mixture and the exhaust gas recirculation composition provided by the user. The cylinder and the ports were initialised via tabular data that describe the temperature and absolute pressure values as functions of crank angle. The boundary conditions are specified in a similar format. For the valve motion, tables were imported that describe the valve lifts as functions of crank angle. These tabulated conditions are all provided in the STAR-CCM+ documentation [203].

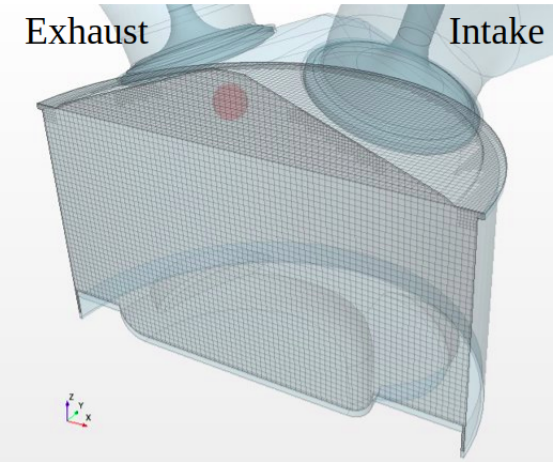

Figure 4.10: Cylinder's y and z computational domains. The red sphere illustrates the position of the ignitor.

To reflect the play resulting from loose connections between the rocker arm and the valve stem, a global parameter for the valve lash is defined within STAR-CCM+ and set to 0.5 mm. Simulations were performed using automatic time step controls, which adjust the time step size based on preset valve lift thresholds. In general, an analysis is run over multiple engine cycles to reduce initial conditions' effect on the final results. For computational cost purposes, the simulations were setup to start at 60 CAD before the beginning of the single cycle on which results were processed. A half engine model was built to reduce the cell count and the computational time. The volume mesh is extended with orthogonal extruded cells at the inlet and outlet boundaries to prevent reversed flow and aid solution convergence. For this study, the base grid was fixed at 1 mm, with the smallest grid scale of 0.5 mm. The y and z section views of the computational domain can be seen in Figure 4.10.

4.7.3 Results & Discussion

The following section presents the performances of the group's correlation in comparison against the M&K correlation. The laminar burning velocity fields of both correlations are presented in Figure 4.11 for the three equivalence ratio conditions ($\phi = 0.8, 0.7,$ and 0.6) at their respective spark timings (20, 27 and 40 CAD bTDC).

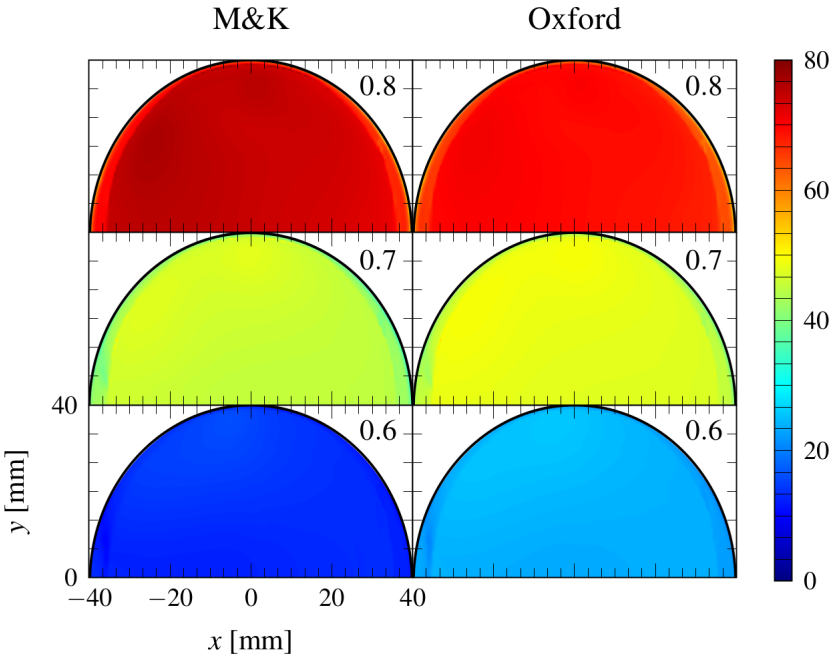

Figure 4.11: Comparison of instantaneous laminar burning velocity fields in cylinder's *xy*-plane for various equivalence ratio conditions shown on the top right of each image, taken at their respective spark timings. The colourbar on the right corresponds to the LBV colourmap in cm/s.

It should be noted that these simulations consider the ideal case of a homogeneous mixture. The cylinder's *xy*-plane is taken to be at the piston's TDC timing, as represented in Figure 4.10. At equivalence ratios equal to 0.8, the M&K correlation predicts slightly higher values of LBV compared to the Oxford correlation. The results for $\phi = 0.7$ follow the opposite trend, with the M&K correlation giving scarcely lower values of LBV than the Oxford correlation. For $\phi = 0.6$, a substantial difference can be seen, where the M&K correlation promotes lower values of LBV, by a factor of approximately 1.6, compared to values obtained with the group's (Oxford) correlation. The present results indicate that a crossing point between the two empirical correlations occurs under engine-like conditions further into leaner mixtures, i.e. $\phi \approx 0.7$.

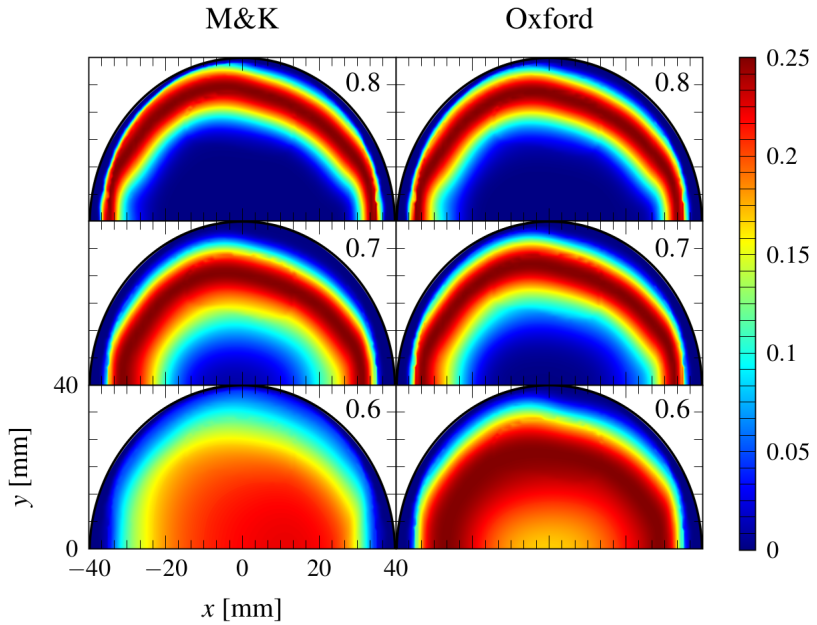

Figure 4.12: Comparison of instantaneous $c(1-c)$ fields at 20 CAD aTDC in cylinder's *xy*-plane for various equivalence ratio conditions shown on the top right of each image. The colourbar on the right corresponds to $c(1-c)$ colourmap.

The position of the flame for both correlations is illustrated in Figure 4.12 at 20 CAD aTDC. The current combustion model ECFM-3Z does not include the capabilities to track the flame front via the radical OH (due to its assumption of chemical species reaching equilibrium). Given that, the use of the flame front brush thickness quantity [206], defined as $c(1-c)$, seems to be a judicious choice as a marker for flame position as per Fontanesi *et al.* [207] (Smallwood *et al.* [206] had previously suggested that the probability of presence of the flame front varies linearly with $c(1-c)$). The results are in good agreement with the LBV fields shown in the above Figure 4.11, with the Oxford correlation predicting faster propagation of the flame than the M&K correlation for equivalence ratios equal to 0.7 and 0.6. It is worth noticing that as mixture conditions get leaner and the flame speed decreases, the flame front brush thickness range, and hence the flame thickness, increases. This is consistent with the general theory of premixed flames [5, 64]. Note that the simulation results for the case of the M&K correlation at $\phi = 0.6$ do not show a clear reaction flame front marked by $c(1-c)$; i.e. the ECFM-3Z model does not predict an obviously

propagating flame when the M&K correlation is used at this ultra-lean equivalence ratio.

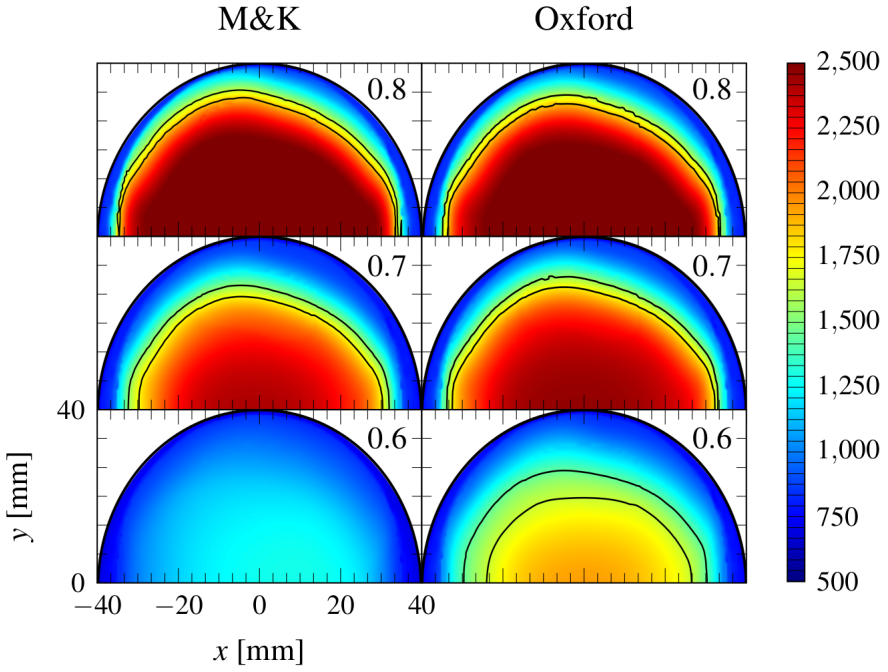

Figure 4.13: Comparison of instantaneous temperature fields at 20 CAD aTDC in cylinder's *xy*-plane for various equivalence ratio conditions shown on the top right of each image. The black lines are the flame fronts given by the model. The colourbar on the right corresponds to the temperature colourmap in kelvin.

A similar trend is seen in Figure 4.13, which shows the instantaneous temperature fields at 20 CAD aTDC for both correlations. The flame front position suggested by the $c(1-c)$ model is represented by the black lines in the images. The temperature of burned gases is associated with the flame front's propagation and, thus, the LBV. As expected from the faster flame propagation shown in Figure 4.12, the use of the Oxford correlation promotes higher burned gas temperatures in the $\phi = 0.7$ and $\phi = 0.6$ equivalence ratio cases.

The nitric oxide (NO) fields of the two correlations at 20 CAD aTDC are illustrated in Figure 4.14. The predicted trends are obtained with the Nitrogen Oxide Relaxation Approach (NORA) model introduced by Vervisch *et al.* [208] and are available within STAR-CCM+. The NORA model is based on the tabulation of three species' equilibrium values obtained from detailed chemistry calculations, i.e. NO, NO_2 and N_2O.

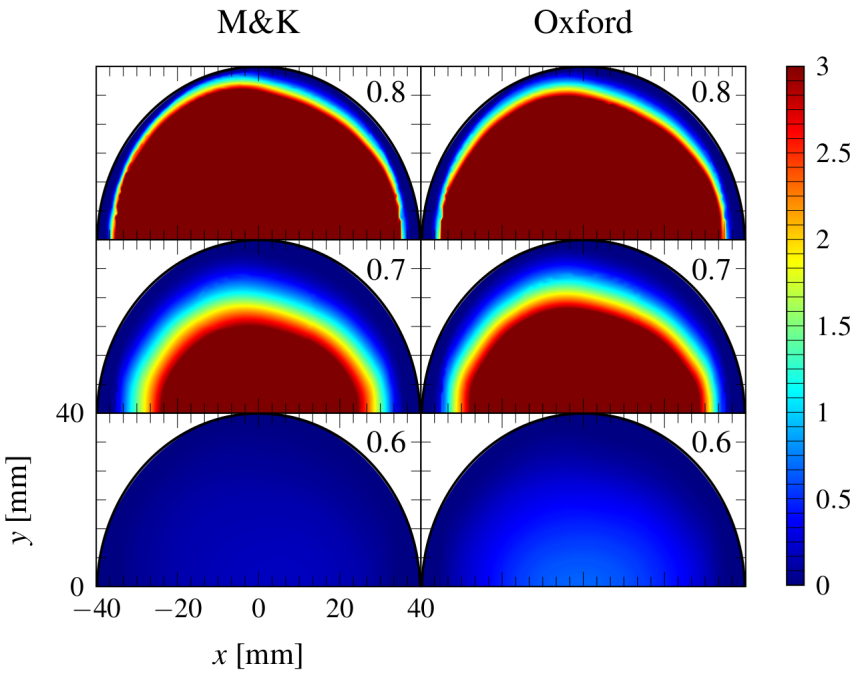

Figure 4.14: Comparison of instantaneous NO fields at 20 CAD aTDC in cylinder's *xy*-plane for various equivalence ratio conditions shown on the top right of each image. The colourbar on the right corresponds to the NO.10^{-4} colourmap.

The results are found to be consistent with the temperature fields previously introduced in the above Figure 4.13. At equivalence ratios equal to 0.6, the use of M&K's correlation promotes NO levels close to zero, which is in good agreement with the cylinder's temperature fields. Indeed, the temperatures for this particular case are under the commonly cited threshold of 2000 K, above which NO_x emissions are formed [41, 43, 209].

The 10%, 50% and 90% mass fraction burned (MFB) timings for both correlations at all three equivalence ratios are presented in Figure 4.15. The MFB is calculated as:

$$x_b = \frac{Y_{u,F} - Y_F}{Y_{u,F}} \tag{4.10}$$

As expected, there is a general trend of retarding 50% and 90% MFB values with decreasing equivalence ratio. The results underline the influence of the low predicted flame speeds of the M&K correlation under ultra-lean mixtures, where 90% MFB is not achieved at $\phi = 0.6$, suggesting incomplete combustion under these conditions.

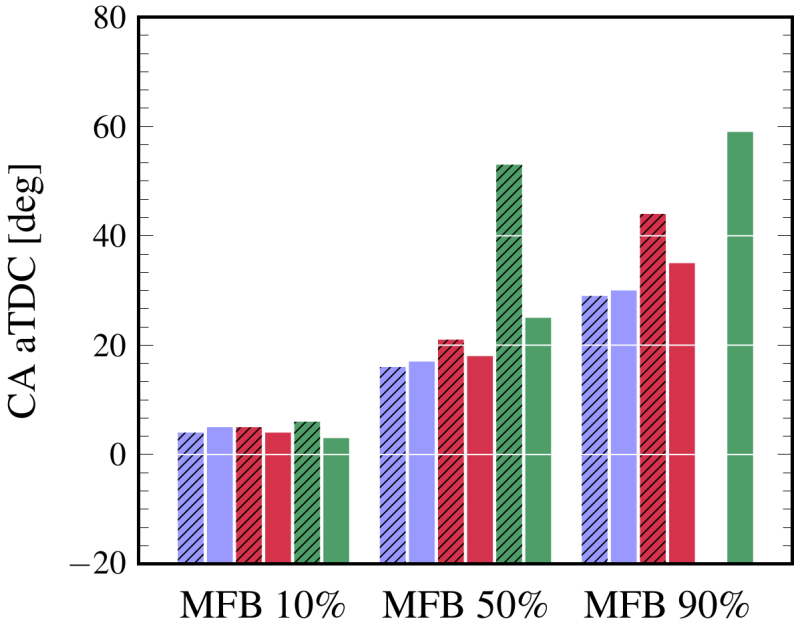

Figure 4.15: Comparison of both Oxford (solid) and M&K (strips) correlations' mass fraction burned at $\phi = 0.8$ (blue), $\phi = 0.7$ (red) and $\phi = 0.6$ (green). M&K's MFB 90% for $\phi = 0.6$ is not illustrated due to incomplete combustion.

Figure 4.16 provides more insight on the combustion process predicted by the ECFM-3Z model along with both correlations at an equivalence ratio of $\phi = 0.6$. The predicted LBV and MFB histories throughout the combustion event at a global equivalence ratio of $\phi = 0.6$ are detailed in Figure 4.16**(a)**, while Figure 4.16**(b)** provides a snapshot of the predicted distribution of the local equivalence ratio and progress variable in the central tumble plane at 59 CAD aTDC – corresponding to the 90% MFB timing obtained with the Oxford LBV model correlation. It is worth mentioning that the instantaneous LBV values presented in Figure 4.16**(a)** are averaged values calculated over the *xy*-plane. At 160 CAD aTDC, the peak of MFB is reached for results promoted by the M&K correlation equal to 0.85. This timing corresponds to 24 CAD after the exhaust valve opens, suggesting the influence of M&K's under-prediction on burning velocities at lean engine operating conditions. Both MFBs well-capture the impact of LBVs on fuel consumption, with lower velocities promoted by M&K compared to Oxford over the entire considered history time.

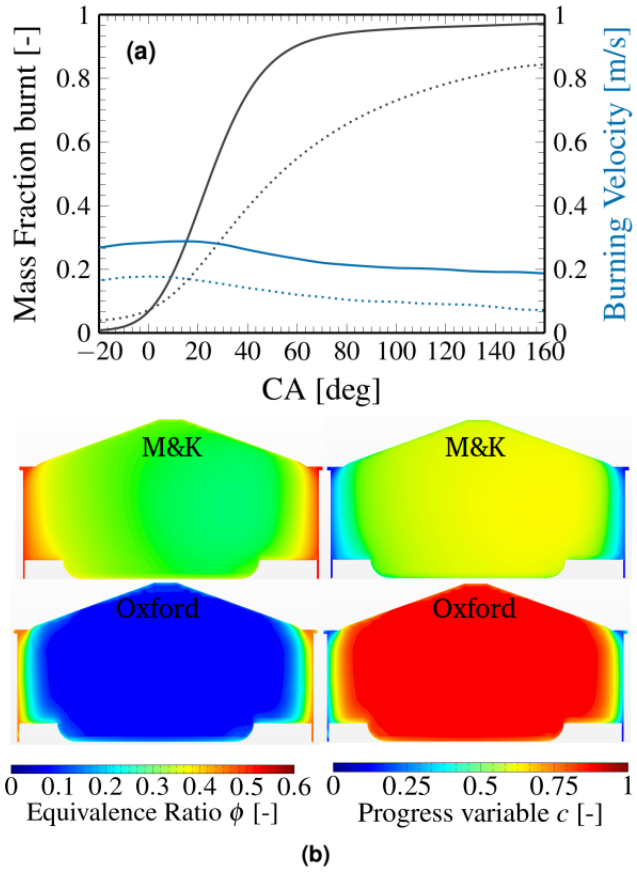

Figure 4.16: Comparison of Oxford (solid) and M&K (dotted) correlation effects on ECFM-3Z model results at $\phi = 0.6$ **(a)** MFB (black) and LBV (blue) predictions (average in the *xy*-plane). **(b)** Predicted equivalence ratio (left) and progress variable (right) distributions in cylinder's central tumble plane fields at 59 CAD aTDC.

The effects of both correlations within ECFM-3Z simulations of lean, homogeneous, and SI engine operation can further be considered via the predicted cylinder pressures, temperatures and heat release rates (HRR), respectively illustrated in Figures 4.17, 4.18 and 4.19. The in-cylinder pressure traces for both correlations under the three lean equivalence ratio conditions are shown in Figure 4.17 along with a motored case that has been added for illustrative purposes. The faster LBVs given by the Oxford correlation for $\phi = 0.7$ and $\phi = 0.6$ conditions are associated with higher peak pressures, temperatures, and burn rates compared to the M&K correlation. The substantially lower LBV of the M&K correlation at equivalence ratios equal to 0.6 suggests that the predicted MFB does not reach 90% within

the time-frame of the simulation – in fact, it is predicted to reach less than 80% MFB by the time the exhaust valve opens (136 CAD aTDC).

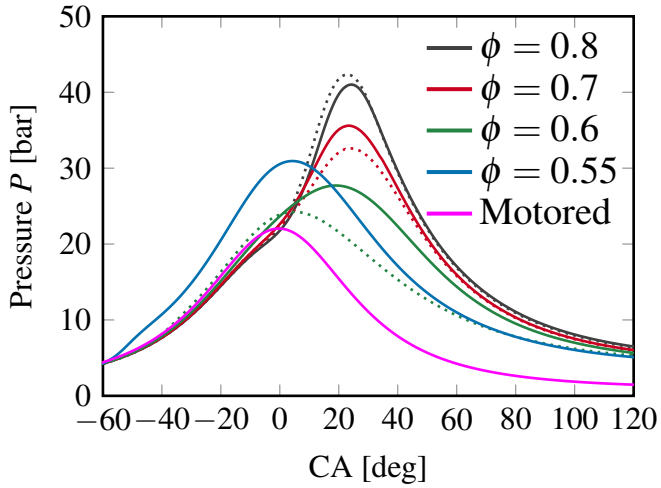

Figure 4.17: Comparison of both Oxford (smooth lines) and M&K (dotted lines) correlations' in-cylinder pressure traces at various equivalence ratio conditions.

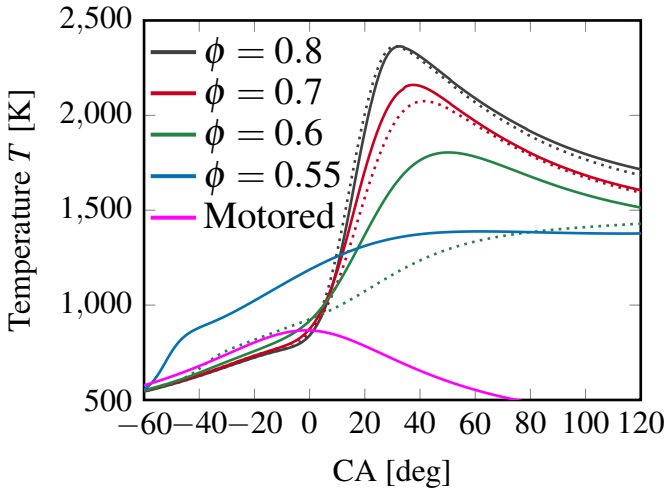

Figure 4.18: Comparison of both Oxford (smooth lines) and M&K (dotted lines) correlations' in-cylinder temperature traces at various equivalence ratio conditions.

The corresponding progress variable field at 59 CAD aTDC (cf. Figure 4.16**(b)**), along with the slowly increasing in-cylinder temperature trace shown in Figure 4.18 and the predicted heat release trace shown in Figure 4.19, emphasise the slow partial burn characteristic of the M&K correlation under ultra-lean conditions. Comparing the performance of two LBV

correlations within the ECFM-3Z model at an equivalence ratio of $\phi = 0.6$, it is clear that the use of the Oxford correlation results in "conventional" pressure, temperature, and heat release profiles as might be expected from the combustion of a lean homogeneous mixture [201, 210, 211].

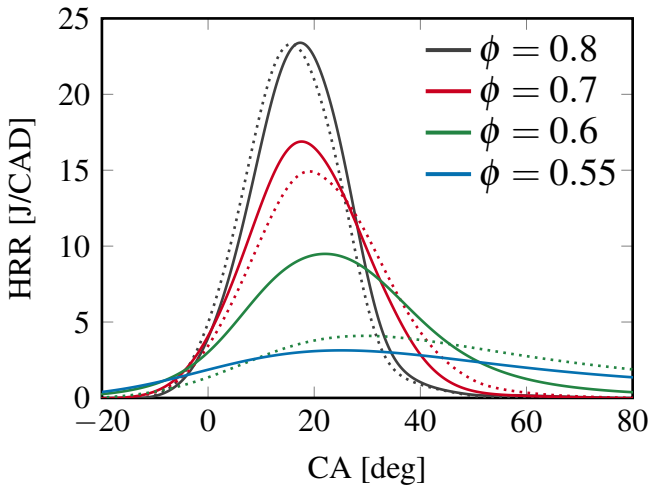

Figure 4.19: Comparison of both Oxford (smooth lines) and M&K (dotted lines) correlations' in-cylinder HRR traces at various equivalence ratio conditions.

In comparison, the temperature and heat release profiles obtained with the M&K correlation differ from these norms promoted by the slow partial burn. This leads one to believe that the ECFM-3Z predictions through the Oxford correlation would predict $\phi = 0.6$ to be a potentially viable operating condition, whereas the use of the M&K correlation would suggest otherwise. Within this study, an additional case for $\phi = 0.55$ with a spark timing set to 65 CAD bTDC has been included in Figures 4.17, 4.18 and 4.19 to show the lean-limit of Oxford's correlation. Further leaner conditions cause the Oxford LBV correlation to give negative values which lead to non-physical simulation results. The pressure trace at $\phi = 0.55$ follows the expected trend despite the early peak achieved at TDC. Due to significantly lower LBV values, the temperature and HRR profiles are prolonged and occur further in the expansion stroke, highlighted by lower peak values. As no experimental measurements are available in the literature, the simulation results of $\phi = 0.55$ cannot be validated, leading to uncertainty with the obtained data.

4.8 Summary

In this study, an empirical laminar burning velocity correlation was tested for the first time for combustion of iso-octane/ethanol mixtures selected to mimic gasoline-alcohol behaviours in air. An in-depth validation for both neat fuels was undertaken using various measurements available in the literature and three kinetics mechanisms. Overall, it was shown that the Oxford correlation accurately captures the burning velocity behaviours of iso-octane/air and ethanol/air mixtures, both within and outside the correlation's previous validity range.

Estimation of the LBVs of blends was achieved by comparing three mixing law strategies over a fixed set of temperature and pressure conditions. The modified Le Châtelier mixing rule based on energy-fraction was found to match the LBV measurements considered, which is in agreement with previous findings in the literature.

The assessment of the Oxford correlation for iso-octane/ethanol blends was undertaken both with experimental data and LBV results from two reaction mechanisms. Comparisons were undertaken between the Oxford correlation and previously unpublished experimental LBVs at higher pressures ($P_u \leq 10$ bar) undertaken by Varea *et al.* (CORIA) and Broustail *et al.* (PRISME). Novel experimental measurements from the Oxford group at elevated temperatures (380 K and 450 K) and pressures (1, 2 and 4 bar) were also included. Within its validity range, the Oxford correlation gave very good results compared to the kinetics models for the entire set of unburned temperature and pressure conditions and ethanol concentrations.

A complementary study around three-dimensional SI engine simulations was also performed using the new Oxford correlation coupled with ECFM-3Z within a RANS turbulence framework. The simulation results obtained with the well-known Metghalchi & Keck correlation were included. The simulations were carried out in the commercial code STAR-CCM+ and compared under three lean equivalence ratios. The results showed that the higher LBVs given by the Oxford correlation led to more practical combustion behaviour, especially in the ultra-lean conditions of $\phi = 0.6$. Use of the group's correlation

with the ECFM-3Z model effectively extended the "lean-limit" of combustion simulations, below which yielded negative LBV values and unfeasible simulation results. The lean-limit was given as $\phi = 0.55$ in this case.

However, there are three points worth noting here regarding the LBV and, consequently, the applicability of geometrically-based models relying on LBVs:

- The equivalence ratio conditions at which LBV data points have been measured have not been extended to ultra-lean mixture conditions.
- Up to this date, the experimental data of laminar burning velocities correspond to pressure and temperature conditions far lower than those found in real engines. Hence, the accuracy of any empirical LBV correlation or chemistry mechanism to compute flame speeds is unknown and can lead to biased simulation results.

Additionally, while the "flamelets" assumption is arguably true for many flames, at high turbulence intensity where the chemical and turbulence length scales are of the same orders of magnitude, this assumption might not be applicable as the Kolmogorov scales can become comparable or even smaller than the reaction zone, thus penetrating the inner layer of the flame [212]. The applicability of the flame surface density, ECFM-3Z, FPV and, more generally, flamelet models is consequently restricted to flows operating at $K_a < 1$. In similar ways, the G-Equation model's dependence on the turbulent flame speed introduces additional complexities as no accurate and generalised definition is available.

The numerical approach proposed for ultra-lean combustion simulations involving partially-premixed flames using topologically-based models can thus lead to potentially misleading results, in particular for flows encountered in real engines. Therefore, a new combustion model with the same extension to higher orders such as CMC, having no constraint on flame propagation types and being more computationally efficient, might be more attractive. One suitable candidate is the conditional source-term estimation or, more commonly, CSE. Less computationally expensive and following the same first-order hypothesis as CMC for the closure of the chemical source terms, CSE can be reasonably extended to doubly CSE

(DCSE) to account for partially-premixing, as opposed to DCMC, which introduces far greater implementation complexities.

Chapter 5

Conditional Source-Term Estimation

Thermodynamics is a funny subject. The first time you go through it, you don't understand it at all. The second time you go through it, you think you understand it, except for one or two small points. The third time you go through it, you know you don't understand it, but by that time you are so used to it, it doesn't bother you any more.

–Arnold Sommerfeld

Contents

5.1 Overview

This chapter presents the physical and mathematical principles used to build the foundation of the conditional source-term estimation (CSE) model. CSE is a combustion model that relies on the first-order hypothesis invoked in CMC. A detailed description of the CSE formulation will be presented in Section 5.2. The inclusion of detailed chemistry in combustion models is often associated with long computational times. Over the past few years, various techniques which enable incorporating complex chemistry have been developed to reduce computational costs. Section 5.3 details the theoretical aspects of some of the most

adopted chemistry tabulation methods found in the literature. A possible extension on how the latter can be coupled with CSE is included.

5.2 Generalities

Conditional source-term estimation was first proposed by Bushe & Steiner [213]. Following the same first-order hypothesis as CMC for closing chemical source terms, and therefore neglecting the spatial conditional fluctuations, the mean conditional chemical source-term for species k is obtained according to Equation 3.51. For a non-premixed case, the unconditional mean chemical source-term is obtained by integrating the conditional value over the averaged PDF of the mixture fraction, as follows:

$$\overline{\dot{\omega}}_k(\vec{x},t) = \int_0^1 \langle \dot{\omega}_k|\eta\rangle(\eta,\vec{x},t)\overline{P}(\eta,\vec{x},t)d\eta \tag{5.1}$$

The conventional CMC approach is based on solving transport equations for conditional scalars. Such transport equations contain several unclosed terms that require substantially greater computational time to solve compared to the CSE approach. In CSE, the conditionally averaged scalars are obtained by inverting the following integral equation (a Fredholm integral equation of the first kind):

$$\widetilde{Y}_k(\vec{x},t) = \int_0^1 \overline{Y_k|\eta}(\eta,\vec{x},t)\widetilde{P}(\eta,\vec{x},t)d\eta \tag{5.2}$$

where $\vec{x}$, t and $\widetilde{Y}_k$ are, respectively, the spatial coordinate, time, and the Favre-averaged mass fraction of the k^{th} species. CSE makes the assumption of spatial homogeneity for conditional means [213], also commonly taken in the CMC combustion model to reduce the computational cost of the simulation [214]. Hence, localised cells – referred to as an ensemble – may be selected in the flow field with statistical homogeneity in conditional averages, enabling Equation 5.2 to be rewritten as below:

$$\widetilde{Y}_k(\vec{x}_j,t) = \int_0^1 \langle Y_k|\eta\rangle(\eta,\vec{x}_j,t)\widetilde{P}(\eta,\vec{x}_j,t)d\eta \qquad x_j \in D \tag{5.3}$$

where x_j is the spatial coordinate of the j^{th} point in the ensemble D. $\widetilde{Y}_k(\vec{x}_j,t)$ in the above equation is determined via transport equations while $\langle Y_k|\eta\rangle(\eta,\vec{x}_j,t)$ is the unknown value

of this problem. This equation must be solved at every time step in the reacting flow solver to provide the conditional averages which enable Equation 3.51 to obtain the conditional chemical source terms. As mentioned previously, Equation 5.3 is a Fredholm integral equation with $\widetilde{P}(\eta,\vec{x}_j,t)$ as the kernel [215]. Hence, it can be rewritten as a numerical expression, i.e. in discrete form, as:

$$\vec{b} = \mathbf{A}\vec{\alpha} \tag{5.4}$$

where $\vec{b}$ is the unconditional Favre-averaged mass fraction of species k at position $\vec{x}_j$ $\left(\text{i.e. } \widetilde{Y}_k(\vec{x}_j,t)\right)$, while $\vec{\alpha}$ is the conditional mean in the j^{th} bin $\left(\text{i.e. } \overline{Y_k|\eta}(\eta,\vec{x}_j,t)\right)$. On the other hand, $\mathbf{A}$ is an $N \times M$ matrix with $N > M$ of the integrated PDF over some interval of the mixture fraction or progress variable, where N is the number of points in each ensemble and M is the number of bins in mixture fraction or progress variable space. $\mathbf{A}$ can be computed as:

$$A_{ij} = \int_0^1 \widetilde{P}(\eta_i,\vec{x}_j,t)d\eta \tag{5.5}$$

The solution of Equation 5.4, i.e. $\vec{\alpha} = \mathbf{A}^{-1}\vec{b}$, is sensitive to any perturbations in the system which makes it an ill-posed problem [216]. Different methods have been applied to resolve this issue. Bushe & Steiner [213] introduced an approach minimising the residual of Equation 5.3 and the conditional averages' derivatives with respect to mixture fractions. Tikhonov proposed a regularisation approach based on an *a priori* knowledge of the solution, which was later introduced by Grout *et al.* [217]. One way to implement this approach is to solve the following least-squares problem to obtain the solution of Equation 5.4:

$$\vec{\alpha} = \text{argmin}\left\| \begin{bmatrix} A \\ \zeta I \end{bmatrix} \vec{\alpha} - \begin{bmatrix} \vec{b} \\ \zeta\vec{\alpha}^0 \end{bmatrix} \right\|_2^2 \tag{5.6}$$

where $\|\cdot\|_2$ denotes the L2 norm of a vector, I is the identity matrix, ζ is the regularisation parameter and $\vec{\alpha}^0$ is the prior knowledge of the solution which may take any initial value (as the solution will be independent of it). Keep in mind that ζ is evaluated based on the characteristics of the inversion problem and, according to [217], can be defined as follows:

$$\zeta = \frac{Tr(A^T A)}{Tr(I)} \tag{5.7}$$

where Tr is the trace of the matrix. A typical routine structure adopted for non-premixed flame simulations using CSE is illustrated in Figure 5.1.

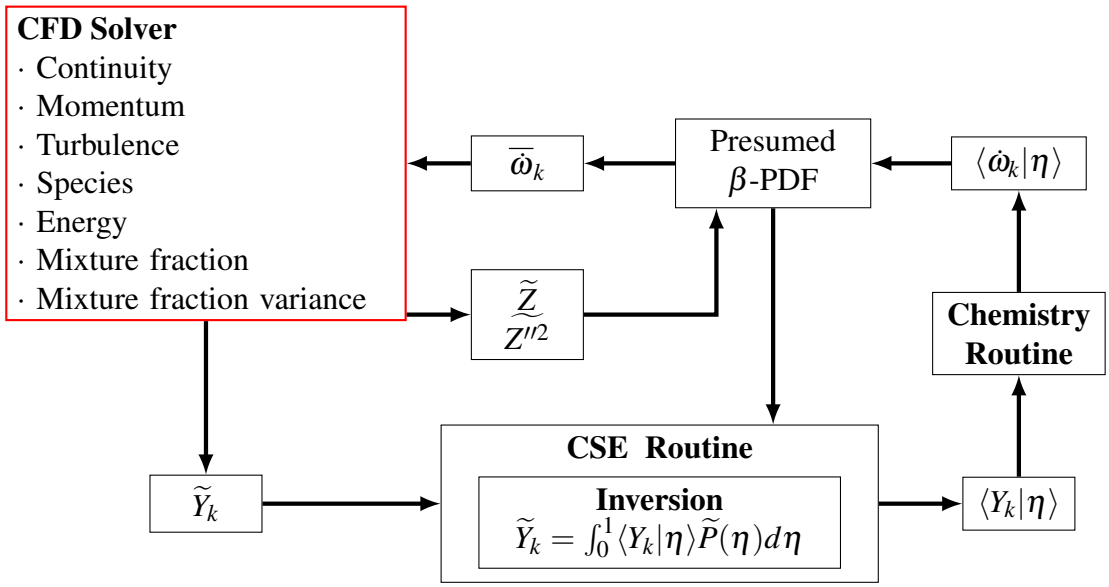

Figure 5.1: Typical CSE routine structure for a non-premixed flame.

5.3 Chemistry Tabulation

Incorporating detailed chemistry into any combustion model is a challenging task, particularly for "real", i.e. liquid hydrocarbon, fuels (e.g. iso-octane or n-dodecane). Combustion mechanisms for fuels are characterised by hundreds of species and thousands of reactions – each requiring the solution of the related transport equations – therefore drastically increasing the computational time. Within the CSE framework, inverting the species for these fuels would be computationally prohibitive as the inversion would have to be carried out at every time step in the reacting flow solver. Therefore, a reduced chemistry model would be preferred so that a limited number of scalars can represent the detailed chemistry. The most common models used for chemistry reduction include the Partial Equilibrium Approximation (PEA) method [218] and the Quasi-Steady-State Approximation (QSSA) [219]. In these methods, the species and equations selected to describe the reduced chemical mechanism are derived individually for each mechanism. Other methods based on the two previous ones have been derived, such as the so-called Rate-Controlled Constrained Equilibrium

(RCCE) method [220]. Here, a subset of chemical kinetics involving the major species is employed to drive the integration, while a set of algebraic equations derived from the minimisation of the free energy (but pertaining only to the minor species) are used to close the ordinary differential equation (ODE) system [221]. Several new techniques based on chemistry tabulation have been developed over the past years and are reviewed within this thesis. Among many others, these include Intrisic Low-Dimensional Manifolds (ILDM), Trajectory Generated Low-Dimensional Manifolds (TGLDM) and methods derived from flamelets.

5.3.1 Intrisic Low-Dimensional Manifolds (ILDM)

First introduced by Maas & Pope [222] as a chemistry reduction mechanism, the Intrinsic low-dimensional manifold (ILDM) model identifies fast and slow species by eigenvalue (which are, in fact, the inverse of the characteristic chemical time scales) analysis of the Jacobian of the reaction source terms. After the fast processes are completed, the main idea behind ILDM is that reaction systems converge onto a lower-dimensional manifold in which reactions proceed only according to longer time scales. Consequently, the chemical system may be described by a reduced set of variables in the composition space. This reduced set may contain a progress variable and/or mixture fraction which measures the evolution of the reaction and describes the mixing, respectively. A look-up table is then built with entries corresponding to the variables of the reduced set and searched using multi-linear interpolations. The ILDM formalism is based on a strong mathematical foundation and provides very good results for high temperatures close to equilibrium values. Unfortunately, low temperature regions are not well described [5]. In fact, these regions are not covered by ILDM and are usually determined only by linear interpolations. Gicquel *et al.* [223] have introduced the Flame Prolongation of ILDM (FPI) by applying the flamelet assumption to extend the manifold generated by ILDM. FPI recovers the ILDM results for high temperatures and provides better results in low-temperature regions. Fiorina *et al.* [224] tested a new version of FPI on a laminar partially-premixed case involving natural gas and air. The model was found to give a good estimation of all the flame fea-

tures, such as flame stabilisation (driven by heat losses), flame structure, and the profile of major and minor species. Embouazza *et al.* [225] used FPI to model the European TOPDEC burner. The results and the flame structure agree with the experimental database. The required CPU time is tremendously reduced compared to detailed chemistry. However, ILDM has been found to have limited applicability when complex hydrocarbon fuels such as iso-octane and n-dodecane are used.

5.3.2 Trajectory Generated Low-Dimensional Manifolds (TGLDM)

First proposed by Pope & Maas [226] as an alternative to ILDM, TGLDM is based on the fact that fast processes with short time scales approach a quasi-steady state rapidly. As such, they can be decoupled from slow processes to reduce the total dimensionality of the reaction system. TGLDM takes this advantage by computing the manifold along reaction trajectories associated with slow time scales so that the construction of the manifold is significantly simpler compared to ILDM. In this chemistry reduction method, the trajectories are determined by solving the governing ODEs, and unlike the ILDM method, this method guarantees that the manifold is inertial, i.e. invariant, meaning that the reaction rate vector at any point along the manifold is locally tangential to the trajectory [227]. The mass fractions of H_2O and CO_2 are often selected to parameterise TGLDM as they have relatively long formation time scales and are associated with significantly different branches of the oxidation chemistry of a given fuel. The proposed model has been successfully implemented into combustion models such as CSE to study different combustion problems. A typical routine structure adopted for non-premixed flame simulations with CSE-TGLDM is illustrated in Figure 5.2. Wang *et al.* [228] modelled the Sandia/TUD jet Flame D [229] within an LES framework by coupling CSE and TGLDM. Compared to experimental data, the non-premixed turbulent combustion model provided good predictions of all species and temperatures. This study also demonstrated that good predictions of NO using CSE-TGLDM were possible by solving a transport equation and interpolating the conditional source-term from the TGLDM table. Salehi *et al.* [214] tested the first application of CSE for a premixed flame. The CSE-TGLDM combustion model is used in a RANS code to

simulate a turbulent premixed Bunsen burner. The results showed that this model could reasonably predict the mean velocity and temperature field.

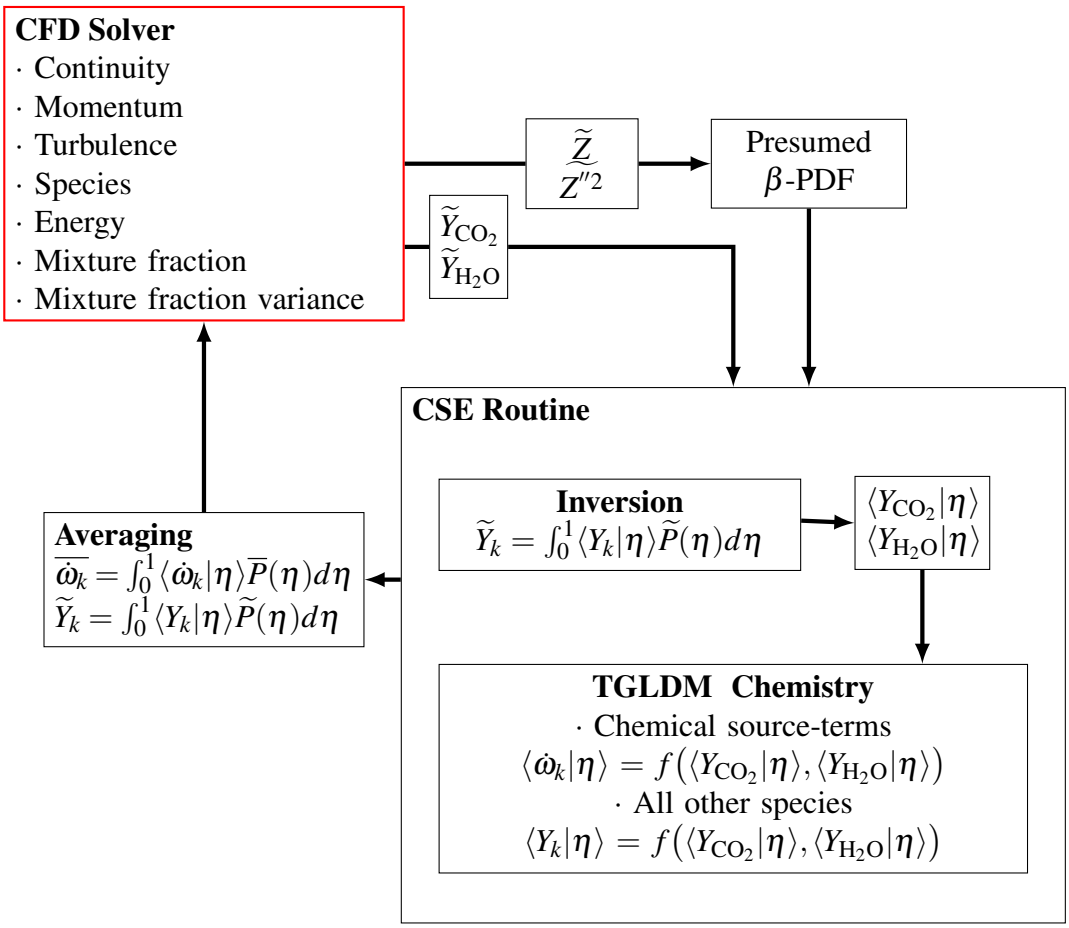

Figure 5.2: Typical CSE routine structure for a methane-air non-premixed flame using TGLDM.

Labahn *et al.* [230] studied species and temperature profiles in a Moderate or intense low-oxygen dilution (MILD) furnace using a non-adiabatic CSE formulation coupled with TGLDM. The study indicates that species concentrations and temperatures present within this combustion system can be well captured. Recently, Hussien & Devaud [231] have used both CSE and DCSE to model partially-premixed turbulent ethanol spray flames. Chemistry tabulation was obtained through TGLDM parametrised by Y_{H_2O} and Y_{CO_2}. The simulation results of both models were in good agreement against the experimental data, with better predictions obtained with DCSE. However, few deviations from the experiments were observed, possibly attributed to the joint-PDF assumption or to the difficulties

TGLDM faces with heavier carbon fuels such as ethanol. Further studies [90] have shown that the conventional TGLDM might not be suitable for heavy fuels such as diesel and gasoline surrogates.

5.3.3 Flamelet Generated Manifold (FGM)

Proposed by van Oijen & de Goey [232], the flamelet generated manifold (FGM) was first developed as a combustion model. Originating from flamelet concepts, it treats a multi-dimensional flame as an ensemble of 1-D flames, enabling it to build a low-dimensional manifold tabulating reaction rates and species mass fractions as a function of a limited set of coordinates. Depending on the combustion application, a flame configuration must be selected to adequately represent the chemical processes taking place in the flame of interest. The diffusion nature of the combustion is best represented by the counter-flow diffusion flame (CDF), illustrated in Figure 5.3.

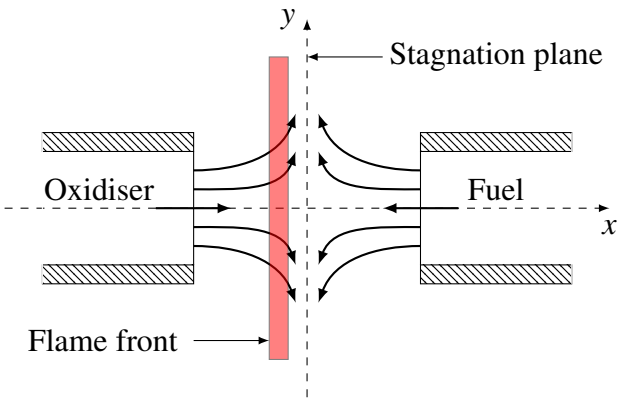

Figure 5.3: Schematic of laminar non-premixed CDF.

The oxidiser and fuel streams are opposed to each other, forming a reaction zone perpendicular to the flows. Straining of the flame is achieved by either increasing the flow velocities or reducing the distance between the two streams. An unstrained flame will depart from chemical equilibrium with increasing strain until it quenches. Following Stahl & Warnatz's 1-D governing equations [233], CDF formulas are given as:

$$\frac{\partial \rho}{\partial t} + \frac{\partial \rho u}{\partial x} = -\rho K \tag{5.8}$$

$$\frac{\partial \rho h}{\partial t} + \frac{\partial \rho u h}{\partial x} = \frac{\partial}{\partial x}\left(\rho D \frac{\partial h}{\partial x}\right) - \rho K h \tag{5.9}$$

$$\frac{\partial \rho Y_k}{\partial t} + \frac{\partial \rho u Y_k}{\partial x} = \frac{\partial}{\partial x}\left(\rho D \frac{\partial Y_k}{\partial x}\right) + \dot{\omega}_k - \rho K Y_k \quad k \in [1, N-1] \tag{5.10}$$

$$\frac{\partial \rho K}{\partial t} + \frac{\partial \rho u K}{\partial x} = \frac{\partial}{\partial x}\left(\mu \frac{\partial K}{\partial x}\right) + \rho_{ox} a^2 - \rho K^2 \tag{5.11}$$

where D assumes a unity Lewis number and K is the stretch rate which accounts for the y-component of flow and its effect on the flame. Moreover, K is a function of x and t, and varies by the prescribed strain rate a at the oxidiser boundary:

$$K(x,t) = \frac{\partial u_y}{\partial y} \tag{5.12}$$

$$K(x \to \infty) = a \quad \text{and} \quad K(x \to -\infty) = a\sqrt{\frac{\rho(x \to -\infty)}{\rho(x \to \infty)}} \tag{5.13}$$

Dirichlet boundary conditions for Y_k and h are imposed in both the oxidiser and fuel stream:

$$Y_k(x \to -\infty) = Y_{k,f} \quad \text{and} \quad h(x \to -\infty) = h_f \tag{5.14}$$

$$Y_k(x \to \infty) = Y_{k,ox} \quad \text{and} \quad h(x \to \infty) = h_{ox} \tag{5.15}$$

Premixed flames are best schematised by the free propagating steady-stretchless premixed flame (cf. Figure 5.4) also known as SSPF.

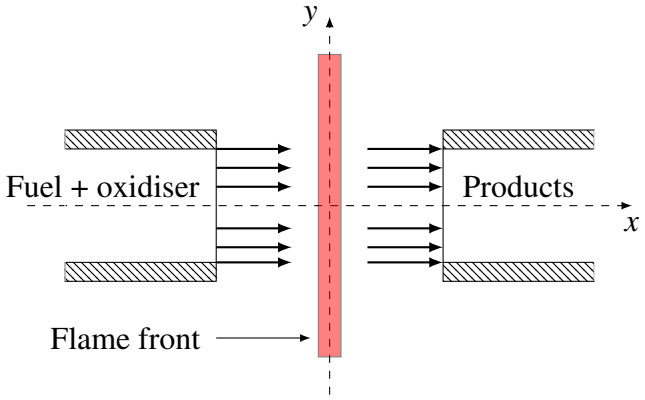

Figure 5.4: Schematic of laminar SSPF.

The fuel and oxidiser streams are premixed before the combustion process is established. Following Ramaeker [234] and the previous CDF 1-D equations, the governing formulas

for an SSPF are as follows:

$$\frac{\partial}{\partial x}(\rho u) = 0 \tag{5.16}$$

$$\rho \frac{\partial u Y_k}{\partial x} = \frac{\partial}{\partial x}\left(\frac{\lambda}{Le_k c_p}\frac{\partial Y_k}{\partial x}\right) + \dot{\omega}_k \tag{5.17}$$

$$\rho \frac{\partial u h}{\partial x} = \frac{\partial}{\partial x}\left[\frac{\lambda}{c_p}\frac{\partial h}{\partial x} + \frac{\lambda}{c_p}\sum_{k=1}^{I}\left(\frac{1}{Le_k} - 1\right)h_k \frac{\partial Y_k}{\partial x}\right] \tag{5.18}$$

It can be easily seen that this system of equations is equal to the CDF formulas of Equations 5.8-5.11, but without the stretch K and the time t. It should be noted that van Oijen *et al.* [235] have proposed a new set of flamelet equations for premixed flames to account for stretch and curvature effects, referred to as strongly stretched flamelet equations (SSFE). Dirichlet boundary conditions for Y_k and h are imposed at the unburned side, leading to:

$$Y_k(x \to -\infty) = Y_{k,-\infty} \quad \text{and} \quad h(x \to -\infty) = h_{-\infty} \tag{5.19}$$

which, for a given pressure, composition, and temperature of fuel and oxidiser, can be described as a function of the flame stoichiometry ϕ only. At the chemical equilibrium side, Neumann (i.e. zero-gradient) boundary conditions for Y_i and h are imposed:

$$\frac{\partial Y_k}{\partial x}(x \to \infty) = 0 \quad \text{and} \quad \frac{\partial h}{\partial x}(x \to \infty) = 0 \tag{5.20}$$

The flamelet generated manifold has been tested over a variety of premixed and non-premixed flame configurations. For partially-premixed cases, Ramaekers *et al.* [236] tested various configurations of premixed and non-premixed FGM with multi-component diffusion and unity Lewis number against the Sandia/TUD flames C-F [229]. All manifolds tested are parameterised on Z and c to account for both flame structures. The CDF FGM predictions of species mass fractions for all four flames are in close agreement with experimental observations. This trend is expected as the main structures describing Sandia flames are diffusion flames. The mass fraction of the radical OH was found in [234] to be much more accurately predicted using the set of premixed flamelet equations. Recently, Zhang *et al.* [237] adopted an LES-FGM formalism to model a non-swirl Cambridge/Sandia turbulent stratified flame [31]. Three 3-D premixed FGM models were adopted, parameterised

on mixture fraction for fuel stratification, enthalpy for heat loss, and progress variable for reaction progress. Different assumptions on unity and non-unity Lewis numbers were tested. With non-unity *Le*, the stretch effects were also examined. Good agreement was found between the simulation and experimental results of the velocity fields, species mass fractions, equivalence ratios and temperatures. Inanc *et al.* [238] recently used a tabulated chemistry approach based on premixed FGM to model a bluff-body stabilised turbulent jet flame burning in a stratified mode of combustion for fuel-lean methane-air mixtures. The simulation results agreed well with the measurements, especially for the RMS values.

Recently, Fang [30] developed a combustion model coupling CSE with FGM to predict diesel spray combustion. The proposed model was the first application of CSE-FGM for heavy-fuel combustion. A single conditioning variable based on mixture fraction was adopted. The simulation results were in very good agreement compared to the experimental measurements of the investigated test case. Further details regarding CSE-FGM's setup and modelling capabilities are discussed in the next chapter.

However, partial premixing of fuel and oxidiser leads to compositionally inhomogeneous mixtures and complex reaction zone structures that can simultaneously exhibit characteristics of both premixed and non-premixed flames [239, 240]. Therefore, a representation of local flame characteristics by pure premixed or non-premixed processes, as done by FGM, may not be sufficient. New FGM-based combustion and chemistry models were introduced in the last decade to address this matter. Two are presented in the following sections.

5.3.3.1 Multidimensional Flamelet Generated Manifold

First proposed by Nguyen *et al.* [241], the multidimensional flamelet generated manifold (MFGM) evolves in five dimensions: two in composition space (i.e. the mixture fraction and the progress variable, enabling one to take into consideration the non-premixed and premixed behaviours, respectively) and three scalar dissipation rates (χ_Z, χ_c and χ_{Zc}). These three scalar dissipation rate parameters represent the mixing time scales and the related flame straining effects. They are also representative of the composition space shape in physical space when the coordinate transformation is applied. The mixture fraction dissipa-

tion rate, approximated through Peters formula [52], is used to quantify large-scale mixing, and its distribution is therefore not expected to depend on chemistry. On the other hand, the progress variable dissipation rate is influenced by both small-scale mixing and chemistry. For small Damköhler numbers, χ_c can be influenced by the mixing scale, whereas in the thin reaction zone where $D_a >> 1$, the progress variable dissipation rate is greater due to ∇c. It is thus essential to find a method that considers the impact of Z on χ_c. By manipulating Peters' formulation, the progress variable dissipation rate can be defined using input variables c and Z. The cross-scalar dissipation rate χ_{Zc} has been a strong field of research over the past few years for turbulent flames [242, 243, 244]. By taking two unit vectors, considered normal to their respective iso-surface (i.e. for the diffusion and the premixed states) it is possible to consider the partially-premixing behaviour of a flame. Indeed, in the case of a curved non-premixed flame, the Z and c gradients are supposed to be aligned such that $n_Z \times n_c \approx \pm 1$. For a premixed flame, the reaction zone (the flame front) is considered perpendicular to iso-Z surfaces, leading to $n_Z \times n_c \approx 0$. Hence, the partially-premixed flame would be promoted in the $-1 < n_Z \times n_c < 1$ interval. Following this, the multidimensional flamelet generated manifold equations for partially-premixing are computed as:

$$\rho \frac{\partial Y_k}{\partial t} + \frac{\partial Y_k}{\partial c}\dot{\omega}_c = \rho \frac{\chi_c}{Le_k}\frac{\partial^2 Y_k}{\partial c^2} + \rho \frac{\chi_Z}{Le_k}\frac{\partial^2 Y_k}{\partial Z^2} + 2\rho \frac{\chi_{Zc}}{Le_k}\frac{\partial^2 Y_k}{\partial Z \partial c} + \dot{\omega}_k \tag{5.21}$$

$$\begin{aligned} \rho \frac{\partial T}{\partial t} + \frac{\partial T}{\partial c}\dot{\omega}_c - \frac{1}{c_p}\left(\frac{\partial c_p}{\partial c} + \sum_{k=1}^{N}\frac{c_{p_k}}{Le_k}\frac{\partial Y_k}{\partial c}\right)\left(\rho \frac{\partial T}{\partial c}\chi_c + \rho \frac{\partial T}{\partial Z}\chi_{Zc}\right) \\ - \frac{1}{c_p}\left(\frac{\partial c_p}{\partial Z} + \sum_{k=1}^{N}\frac{c_{p_k}}{Le_k}\frac{\partial Y_k}{\partial Z}\right)\left(\rho \frac{\partial T}{\partial Z}\chi_Z + \rho \frac{\partial T}{\partial c}\chi_{Zc}\right) \\ = \rho \chi_c \frac{\partial^2 T}{\partial c^2} + \rho \chi_Z \frac{\partial^2 T}{\partial Z^2} + 2\rho \chi_{Zc}\frac{\partial^2 T}{\partial Z \partial c} - \frac{1}{c_p}\sum_{k=1}^{N} h_k \dot{\omega}_k \end{aligned} \tag{5.22}$$

Some important drawbacks are worthy of note: heat release modifies the composition space coordinates and the scalar dissipation rates through mass transport (as in partially-premixed flame fronts, for example) [245, 246]; the current model is missing direct unsteady coupling with the velocity field, which has a direct impact on scalar dissipation rates [247, 248]. Additionally, due to the five dimensions of this method, the size of the lookup table could rapidly become a problem. A potential application of MFGM and CSE can be found in

Figure 5.5.

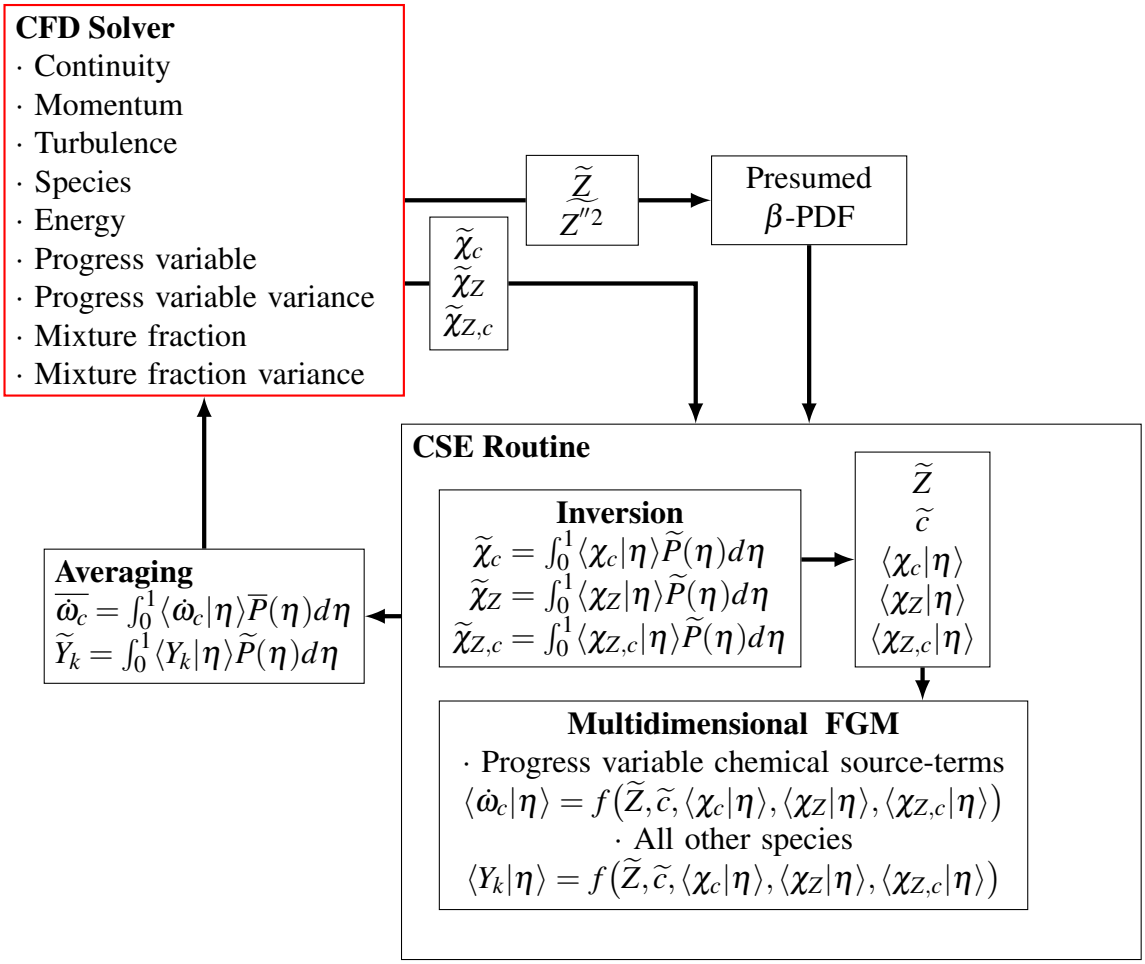

Figure 5.5: CSE-MFGM routine structure.

5.3.3.2 Multi-Regime Flamelet Generated Manifold

Multi-regime flamelet generated manifold (MRFGM) was first proposed by Knudsen & Pitsch [249] with the aim to:

- Distinguish the dominant mode of flame propagation (i.e. premixed or non-premixed) at a specific time and location within the cell.
- Transition between solutions from a single flame structure.

The MRFGM approach considers the balance between reaction and diffusion processes. If the combustion reaction is mainly mixing-driven, the local flame can be considered non-premixed. On the other hand, if the reaction is balanced by transport along vectors of

constant mixture fraction, the local flame can be characterised as premixed-driven.

Two quantities are derived from the flamelet equations, Θ_{P} and Θ_{NP}, enabling the estimation of the contribution of each flame structure on the chemical source-term, with P denoting the premixing and NP the non-premixed structures. Both terms are derived in [250], expressed as:

$$\Theta_{\mathrm{P}} = \rho_u S_u \left(|\nabla c| - \frac{\partial c}{\partial Z} |\nabla Z| \right) - \nabla \left(\rho D \nabla c \right) + \frac{\partial c}{\partial Z} \left(\nabla \left(\rho D \nabla Z \right) \right) + \rho \frac{\chi_Z}{2} \frac{\partial^2 c}{\partial Z^2} \tag{5.23}$$

$$\Theta_{\mathrm{NP}} = \rho \frac{\chi_Z}{2} \frac{\partial^2 c}{\partial Z^2} \tag{5.24}$$

In order to account for diffusive and convective processes within non-reactive areas of the premixed flame, which cancel with one another (i.e. $\Theta_{\mathrm{P}} = 0$) [250], MRFGM defines the premixed quantity Θ_{P} via a maximum function:

$$\Theta_{\mathrm{P}} = \max \left(\Theta_{\mathrm{P}}, \rho_u S_u \left[|\nabla c| - \frac{\partial c}{\partial Z} |\nabla Z| \right] \right) \tag{5.25}$$

such that Θ_{P} is at least as large as the premixed convective flux term. A similar uncertainty can be detected for the diffusion case via Equation 5.24 when Z is not at stoichiometric burning conditions, leading the second derivative to approach zero. Indeed, it is possible to find flow regions that are diffusion-driven but that are subject to only very weak transport in mixture fraction space. Therefore, the current model defines the non-premixed quantity Θ_{NP} via a minimum function:

$$\Theta_{\mathrm{NP}} = -\rho \frac{\chi_Z}{2} \min \left(\frac{\partial^2 c}{\partial Z^2}, \iota \right) \tag{5.26}$$

where ι assures the functionality of the model. The quantity ι should be smaller than the value of the second derivative at the most reactive mixture fraction so that it does not influence the model in reacting flow regions. In reference to [250], ι is set to -1 such that it is less than 1% of the peak magnitude of the second derivatives found in the non-premixed flamelets.

Equations 5.23 and 5.24 do not describe how solutions from different modes should be combined when their relative contributions to the chemical source-term are similar in magnitude. The second goal of MRFGM is to transition between both flame structure solutions.

A weighting coefficient is used to determine the local contribution of each flame propagation, defined below as:

$$\Phi_i(\mathrm{o}, Z, c) = \Phi_i^{\mathrm{NP}}(1-\mathrm{o}) + \Phi_i^{\mathrm{P}}\mathrm{o} \tag{5.27}$$

where Φ_i denotes a random variable such as species mass fractions or chemical source terms. In reference to [251], the weighting coefficient o is defined below as:

$$\mathrm{o} = \frac{\int_V \Theta_{\mathrm{P}} dV}{\max(\int_V \Theta_{\mathrm{P}} dV + \int_V \Theta_{\mathrm{NP}} dV, \lambda)} \tag{5.28}$$

where λ and V are, respectively, a small positive number and the volume of a domain comprised of the neighbouring computational cell in each direction. The term λ is used to ensure that the flame propagation is always well defined. When o approaches 1, $\Theta_{\mathrm{P}} >> \Theta_{\mathrm{NP}}$, and, vice versa, when o approaches 0, $\Theta_{\mathrm{NP}} >> \Theta_{\mathrm{P}}$, enabling the fully premixed and diffusion combustion characteristics to be captured by the model.

Finally, the two Θ variables in a RANS framework are calculated as follows:

$$\overline{\Theta}_{\mathrm{P}} = \rho_u S_T \left(|\nabla \widetilde{c}| - \frac{\partial \widetilde{c}}{\partial Z} |\nabla \widetilde{Z}| \right) - \nabla\left(\overline{\rho} \widetilde{D} \nabla \widetilde{c}\right) + \frac{\partial \widetilde{c}}{\partial Z}\left(\nabla\left(\overline{\rho} \widetilde{D} \nabla \widetilde{Z}\right)\right) + \overline{\rho} \frac{\widetilde{X}_Z}{2} \frac{\partial^2 \widetilde{c}}{\partial Z^2} \tag{5.29}$$

$$\overline{\Theta}_{\mathrm{NP}} = -\overline{\rho} \frac{\widetilde{\chi}_Z}{2} \frac{\partial^2 \widetilde{c}}{\partial Z^2} \tag{5.30}$$

Recently, Hu & Kurose [252] have used the exact same flame index formulation as is in the MRFGM model for simulating partially-premixed acetone spray flames. Within this LES research, the authors managed to present results in good agreement with experiments while capturing the two predominant flame structures and their transitions.

Interaction of the CSE-MRFGM combustion model with the CFD code is illustrated in Figure 5.6 below. Coupling with the CFD solver can be achieved by solving four additional transport equations for the progress variable, mixture fraction, and their variances. The Favre-averaged mixture fraction $\widetilde{Z}$, along with its variance $\widetilde{Z''^2}$, is used to compute the β-PDF, while $\widetilde{c}$ and $\widetilde{c''^2}$ are used in the computation of the laminar flamelet-PDF. The Favre-averaged progress variable $\widetilde{c}$ and mixture fraction $\widetilde{Z}$ are parsed into the CSE routine where, as described earlier, the conditionally averaged progress variable $\langle c|\eta \rangle$ and mixture fraction $\langle Z|\xi \rangle$ are computed via the inversion method.

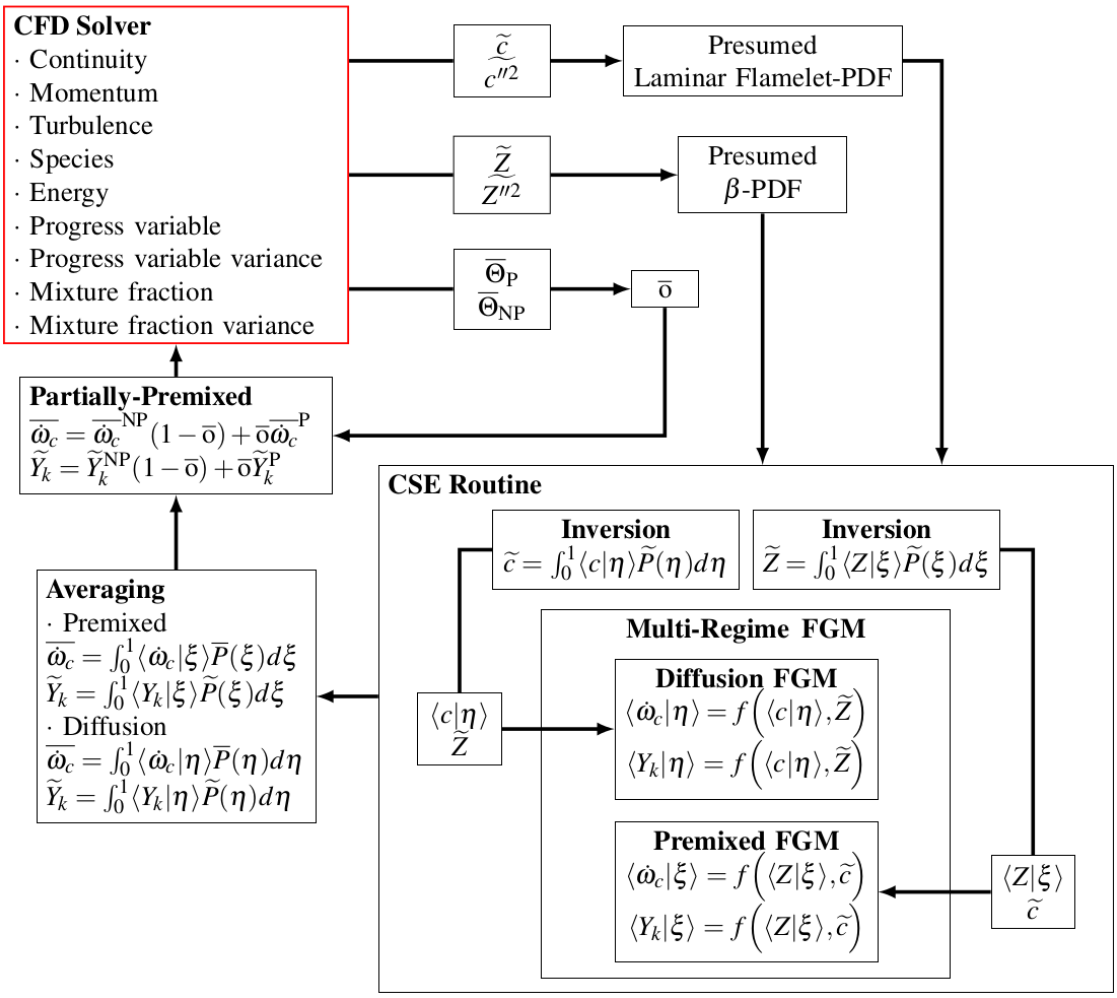

Figure 5.6: CSE-MRFGM routine structure.

The conditionally averaged progress variable is used with the Favre-averaged mixture fraction $\widetilde{Z}$ to lookup the conditionally averaged reaction rate $\langle \dot{\omega}_c|\eta\rangle$ and mass fraction $\langle Y_k|\eta\rangle$ from the diffusion FGM table previously built. Meanwhile, the conditionally averaged mixture fraction together with the Favre-averaged progress variable $\widetilde{c}$ are used to lookup the conditionally averaged reaction rate $\langle \dot{\omega}_c|\xi\rangle$ and mass fraction $\langle Y_k|\xi\rangle$ from the premixed FGM table. These are then integrated, respectively, with the β-PDF and the laminar flamelet-PDF before being weighted by the averaged coefficient $\overline{\mathrm{o}}$ computed by using $\overline{\Theta}_{\mathrm{P}}$ and $\overline{\Theta}_{\mathrm{NP}}$. The final values are then parsed into the CFD solver enabling one to close the loop.

5.4 Summary

Previous studies suggested that CSE-based combustion models can provide results with high levels of accuracy and reduced computational costs. The inclusion of partially-premixed flames using CSE can be achieved by adding a second control variable while preserving the first-order hypothesis. This leads to doubly CSE (DCSE), which has been shown to have far greater modelling capabilities compared to the conventional CSE. However, the inversion process used to calculate the conditional values of the thermodynamic variables (e.g. mass fractions) coupled with the current presumed shapes of the joint-PDFs have been found to be the two most significant sources of error associated with DCSE [253].

Over the past few years, various techniques have been developed to incorporate detailed chemistry in CSE to reduce computation times, attributed to the inversion process of species that has to be repeated at each time step. Manifold methods have been a promising tool to account for detailed chemistry while reducing computational costs. Among many others, methods originating from flamelet concepts have shown satisfactory modelling capabilities. However, while restricted to a single flame structure, either premixed or non-premixed, including partially-premixing in this configuration seems unfeasible. The multi-regime flamelet generated manifold (MRFGM) offers the possibility to distinguish premixed and non-premixed pockets within the flow field. The conditional mass fractions, the conditional densities and the conditional temperatures, can be independently pre-calculated for each premixed and diffusion flame before being passed to CSE. While preserving a single conditioning variable in the CSE routine and thus avoiding the difficulties associated with the joint-PDF, CSE-MRFGM incorporates detailed chemistry and turbulence-chemistry interaction effects, essential for capturing finite-rate phenomena.

Among the existing models coupling CSE with chemistry tabulation techniques, the CSE-FGM model developed by Fang [30] during his doctoral studies is utilised to assess the feasibility of accounting for detailed chemistry using FGM as a chemistry manifold. It should be noted that without the premixed routine, CSE-MRFGM reduces to the CSE-FGM model proposed by Fang.

Chapter 6

Assessment of a CSE-FGM Approach for the Simulation of Diesel Spray Flames

From success, you learn absolutely nothing. From failure and setbacks conclusions can be drawn. That goes for your private life as well as your career.

–Niki Lauda

Contents

The content in this chapter is adapted from two previously published papers.
The first article is a result of the collaborative efforts of Dr. X. H. Fang, Dr. R. Ismail, the author, and Prof. M. H. Davy. The author is responsible for data-curation, validation and writing the original draft. The content of this paper has been published and peer-reviewed within the framework of the WCX SAE World Congress Experience [90].
The second article is a result of the collaborative efforts of Dr. X. H. Fang, the author, and Prof. M. H. Davy. Dr. Fang and the author share equal contribution. The author is responsible for the conceptualisation, data-curation, formal analysis and writing the original draft. Dr. Fang is responsible for the investigation, conceptualisation, methodology, formal analysis and writing the original draft. This study has been published in the peer-reviewed Proceedings of the ASME Internal Combustion Engine Division Fall Technical Conference [254].

6.1 Overview

Multiple studies have shown CSE's modelling capabilities in successfully predicting flame characteristics for both premixed and non-premixed flame structures. In this chapter, the primary objective is to evaluate the modelling capabilities of CSE-FGM developed by Fang [30] using a RANS formulation. The assessment of the proposed combustion model will enable one to estimate CSE-FGM's ability to account for detailed chemistry and turbulence-chemistry interaction effects under engine-like conditions. The novel combustion modelling approach is applied to study the Engine Combustion Network (ECN) diesel "Spray A" case. First, the efficacy of the CSE-FGM model is explored with respect to the "Spray A" auto-ignition and flame development characteristics for the baseline conditions and also for parametric variations of ambient temperature and oxygen concentration. The modelling results are compared with the available experimental data and simulations performed using the well-stirred reactor model. This includes a detailed description of the trends followed by the ignition delay, the flame lift-off length, and the analysis of flame spatial contours. The auto-ignition process and the reacting spray structure are also discussed in detail.

6.2 ECN "Spray A"

Within this study, Engine Combustion Network "Spray A" simulations will be investigated and validated against ECN's high-quality and high-fidelity dataset. "Spray A" promotes low-temperature combustion phenomena typically encountered in modern compression ignition engines. As such, the injector specifications are common to current advanced injection systems with high pressures. The ECN database includes different physical properties of diesel sprays, including spray liquid and vapour penetration length as well as ignition delay times (IDT) and flame lift-off length (LOL). Experimental luminosity data is also available for different spray conditions using the diesel fuel surrogate n-dodecane. The measurements of a reacting and non-reacting spray case are included in the database. Both liquid penetration and vapour penetration will be examined to ensure a valid non-reacting spray case setup. A detailed description of the experimental setup and test cell conditions can be found in [34]. For reacting studies, different physical characteristics are validated against the ECN database, including IDT, flame LOL, and temperature luminosity images. All "Spray A" conditions tested within this thesis are listed in Table 6.1.

Table 6.1: ECN "Spray A" experimental nominal test conditions. "Test II" denotes ECN baseline condition.

Test	O_2 [% volume]	T_{amb} [K]	Unchanged
0	0	900	Fuel = $NC_{12}H_{26}$
I	15	800	Fuel mass = 14 [mg]
II	**15**	**900**	$\varnothing_{nozzle}$ = 0.090 [mm]
III	15	1000	ρ_{amb} = 22.8 [kgm^{-3}]
IV	15	1100	T_{fu} = 363 [K]
V	13	900	P_{inj} 150 [MPa]
VI	21	900	

The existence of turbulent regions within the proposed test case, composed of both rich partially-premixed pockets and a non-premixed flame with diffusion effects, makes this spray an ideal test case for assessing the modelling capabilities of CSE-FGM to account for detailed chemistry and TCI effects.

6.3 Combustion Models

This section presents a brief description of the different combustion models used in this study. The CONVERGE-implemented SAGE combustion model will be discussed first, followed by a more detailed description of CSE-FGM.

6.3.1 SAGE

The principal idea behind the well-stirred reactor model is that the mixing in a turbulent field is considered infinitely fast compared to chemistry, and the species within each cell are assumed to be homogeneously distributed. SAGE is a well-stirred reactor combustion model implemented in CONVERGE, where the mean reaction rates for each elementary reaction are directly integrated based on Arrhenius-type correlations. Only first-order moments, i.e. the mean of scalars, are considered in this calculation (cf. Equation 3.13). Given an accurate chemical mechanism and fine resolution, SAGE can be used for different combustion regimes. SAGE has been used in practical engine simulations with favourable results [30]. Despite successful simulations in diesel sprays, studies using the well-stirred reactor assumption can have large errors due to the highly non-linear behaviour of the mean chemical source-term and the lack of TCI within the model. Furthermore, the computational cost for the SAGE model can be greatly increased if detailed chemical kinetics are used.

6.3.2 CSE-FGM

This section depicts the CSE-FGM setup. The CSE routine was structured to account for a unique control variable based on mixture fraction. CSE's mathematical and physical aspects are identical to those provided in Chapter 5. It should be noted that Dr. Fang is responsible for the underlying development of the CSE code and implementation of the combustion model to the CFD solver, the spray sub-models, and the chemistry tabulation using the flamelet generated manifold.

6.3.2.1 Flamelet Generated Manifold

Chemistry tabulation is based on the FGM approach, where 1-D flamelet solutions are pre-computed using detailed chemistry and parametrised using a reduced number of control variables.

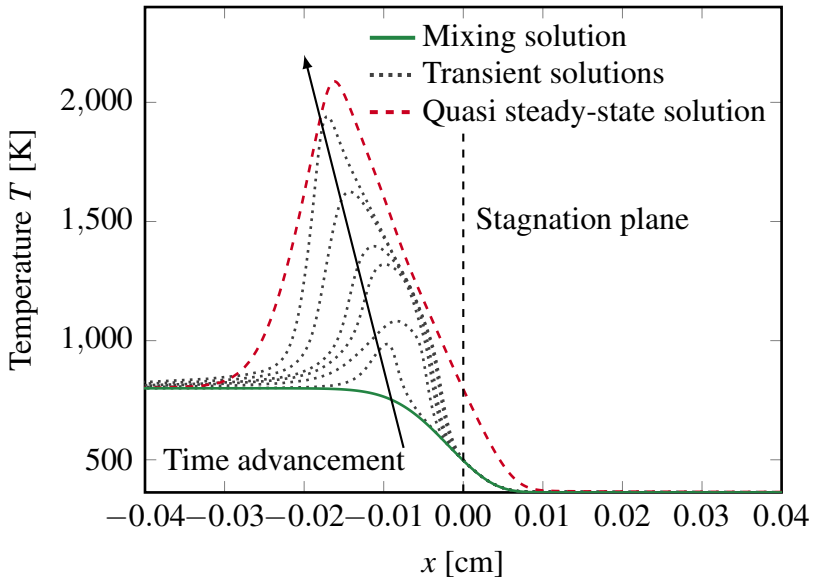

(a) $T_{amb} = 800$ K, $P_{amb} = 5.25$ MPa

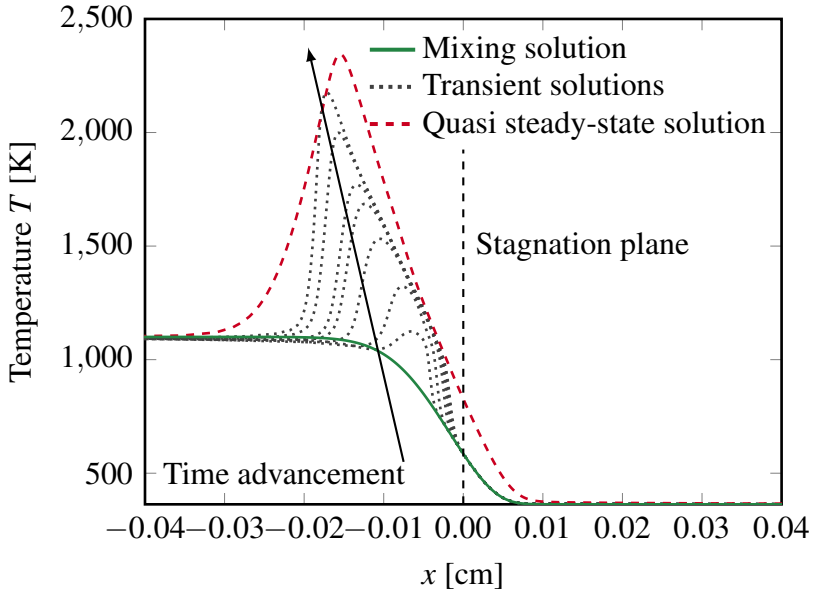

(b) $T_{amb} = 1100$ K, $P_{amb} = 7.3$ MPa

Figure 6.1: Temperature evolution in physical space x and time t for two counter-flow diffusion flames with n-dodecane: $a = 500$ s^{-1}, T$_f$ = 363 K and 15% by volume of O_2.

More details about the underlying physics of FGM have been provided in Chapter 5, Section 5.3.3. Depending on the combustion application, a flame configuration must be selected that adequately represents the chemical processes taking place in the flame of interest. Diesel combustion is predominantly non-premixed and is, therefore, best represented by the counter-flow diffusion flame, illustrated in Figure 5.3. In this work, the CHEM1D code [255] of Eindhoven University of Technology is used to solve one-dimensional CDFs in physical space and time with the possibility to choose different chemical mechanisms. A unity Lewis number is assumed in order to simplify the transport equations (cf. Equations 5.8–5.11). In order to account for the unsteadiness in the spray flame, igniting flamelets are included. For each condition tested, a corresponding manifold is needed for the CSE calculation. Figure 6.1 shows the two different manifolds for a fixed n-dodecane mechanism at a strain rate of 500 s^{-1} from an initially mixed but non-reacting state (green line) at ambient temperatures and pressures of 800 K and 5.25 MPa and 1100 K and 7.3 MPa, respectively. The black lines in the figure illustrate the temporal evolution of the laminar flame before reaching a quasi-steady state (red line). Note that the maximum temperature reached by the quasi-steady state solution increases as a function of the ambient conditions (2100 K and 2400 K, respectively).

6.3.2.2 Parametrisation of FGM

The full composition space of the flamelet solutions is described by $N+2$-dimensional solutions spanned by enthalpy, pressure and N number of species. Through careful consideration, a reduced set (any number or combination) of controlling variables can be used to parameterise the flamelet solutions as long as the full mixture composition is described. Increasing the number of controlling variables will increase accuracy up to $N+2$-dimensions, where eventually the full composition space will be recovered.

As this work will focus on spray combustion applications: fuel-oxidizer mixing, ignition and combustion progression in the diffusion flame are the main physical phenomena of interest. Mixing can be described by the mixture fraction Z using the definition of Bilger. The mixture fraction is a monotonic function of spatial coordinate x which allows direct

mapping of flamelet solutions from physical space to mixture fraction space. Starting from the mixing solution up until chemical equilibrium, any variable that continuously increases or decreases with time can be used to describe ignition and combustion progression. In this work, the reaction progress variable c is defined as a weighted linear combination of certain key species mass fractions that represent each stage of combustion evolution:

$$c = \frac{Y_{CH_2O}}{Y^{eq}_{CH_2O}} + \frac{Y_{CO}}{Y^{eq}_{CO}} + \frac{Y_{CO_2}}{Y^{eq}_{CO_2}} \tag{6.1}$$

To capture ignition, formaldehyde (CH_2O) is included as it is found in high concentrations at the onset of ignition [256]. Major combustion products of CO and CO_2 represent the intermediate and end phases of combustion. In order for each species in the reaction progress variable definition to have a balanced contribution, it is weighted by its equilibrium mass fraction.

The FGM database generated by igniting CDFs is extended further by including solutions of steady flamelets at strain rates varying from the highest non-quenching strain rate down to $a = 1\ s^{-1}$. This covers the entire Z-c space from the mixing line up to chemical equilibrium. All flamelet calculations are carried out assuming constant pressure and conserved enthalpy and, therefore, if variations in any of these quantities occur, additional dimensions will be required in the FGM database in order to account for the influence of these variables on combustion. Figure 6.2 shows the resultant manifolds in mixture fraction and progress variable space for the ambient temperature and pressure pairs of 800 K and 5.25 MPa and 1100 K and 7.3 MPa previously depicted with respect to physical space x and temperature T in Figure 6.1. Figure 6.2 provides significantly greater insights into the nature of the two manifolds. Each of the FGMs is characterised by three well defined reaction zones, as expected. The low progress variable values indicate the early ignition stage, while the intermediate and high values of c promote the intermediate and end of combustion, respectively. The 800 K manifold shows relatively lower source term values in all three regions which correspond to the extended temperature rise in flamelet solutions for this case, illustrated in Figure 6.1(a).

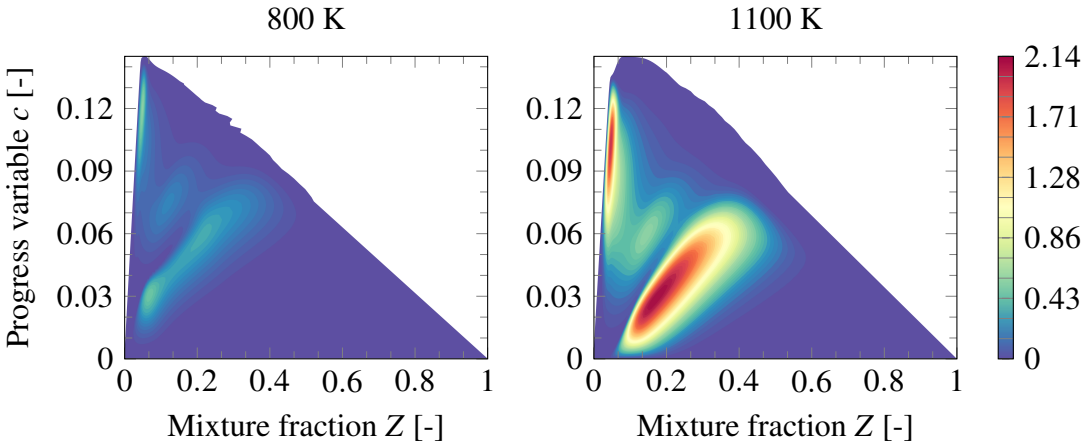

Figure 6.2: Reaction rate of the progress variable for two manifolds with different ambient conditions (left figure: 800 K, 5.25 MPa – right figure: 1100 K, 7.3 MPa). The colourbar on the right corresponds to the colourmap of $\dot{\omega}_c \cdot 10^5$.

The 1100 K manifold is characterised by notably higher chemical source term values during the early stage of combustion which is expected to have a significant impact on ignition timing. The entire solving process of the currently implemented CSE-FGM combustion model can be seen in Figure 6.3. It is worth noting that for each of the conditions tested, a corresponding manifold is needed for the calculation of CSE.

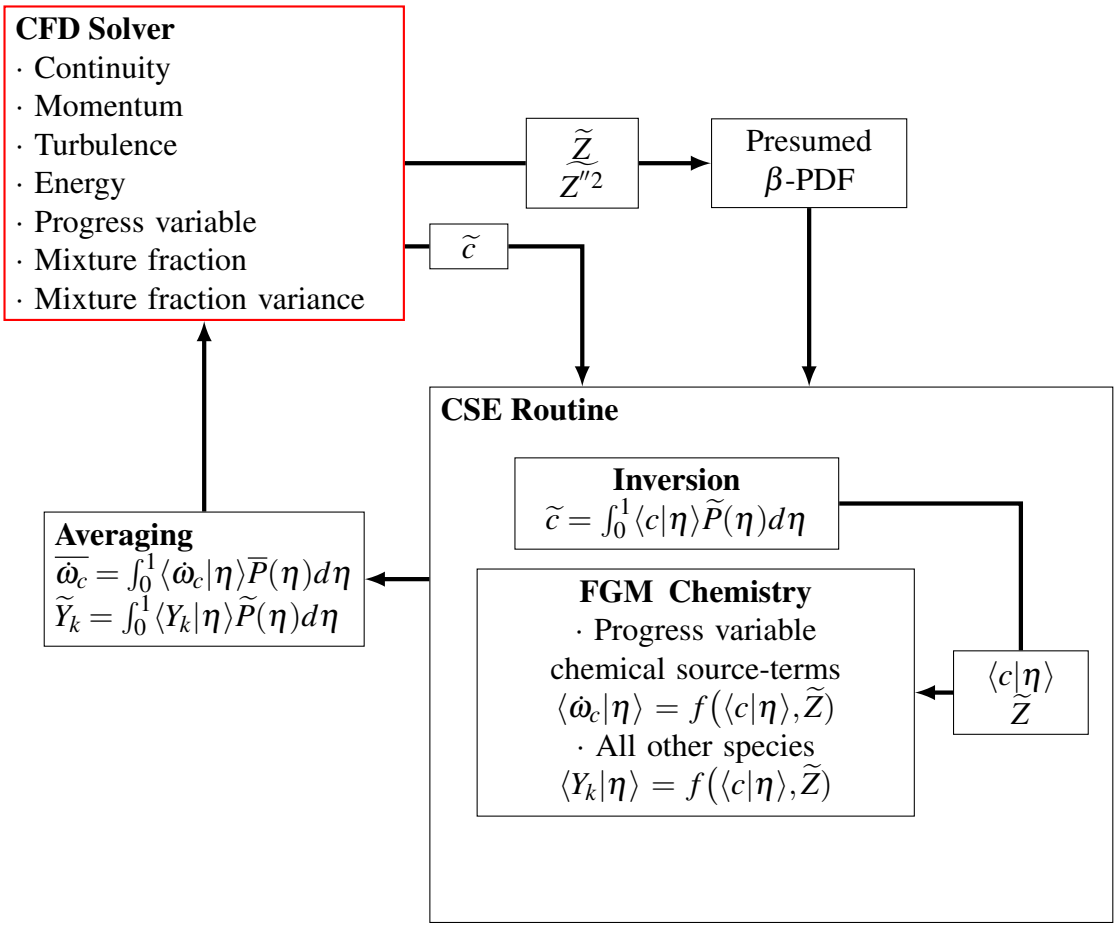

Figure 6.3: CSE-FGM routine structure for ECN diesel "Spray A".

6.4 Computational Setup

A parametric study of the CSE-FGM combustion model was performed under the Reynolds-Averaged Navier-Stokes Simulation framework. Simulations of ECN "Spray A" were made across the full range of ambient conditions listed in Table 6.1, Tests I-VI, and validated against the ECN's high-quality and high-fidelity datasets for both non-reacting and reacting test conditions.

The entire modeling routine was developed in the commercially available CFD solver CONVERGE through user-defined functions [257]. The Pressure Implicit with Splitting of Operators (PISO) method [204] was used to solve the transport equations. All transported variables in CONVERGE are co-located at the centre of the cell. The Rhie-Chow [258] algorithm was used to prevent checker-boarding. Second-order accurate central dif-

ferencing schemes were used for spatial discretisation in all simulations, with fully implicit first-order accurate time integration to maintain stability. A variable time step was used based on the Courant-Friedrichs-Lewy (CFL) condition for convection ($\mathrm{CFL}_u = u\frac{\Delta t}{\Delta x}$), diffusion ($\mathrm{CFL}_\nu = \nu\frac{\Delta t}{\Delta x^2}$) and speed of sound ($\mathrm{CFL}_a = a\frac{\Delta t}{\Delta x}$). Here, Δx is the grid size, Δt is the time step, u is the cell velocity, ν is the dynamic viscosity, and a is the speed of sound. Turbulence was modelled using the RANS k-ε model with modified model constants given in [89].

Table 6.2: Spray simulation discrete phase sub-models.

Sub-models	
Injection	Blob method
Droplet breakup	KH-RT without breakup length
Droplet drag	Dynamic droplet drag
Droplet collisions	No Time Counter
Vaporisation	Frossling correlation
Droplet heat transfer	Ranz-Marshall
Turbulent dispersion	O'Rourke

The well known Lagrangian-Eulerian framework was used to model the liquid phase where all sub-models used are stated in Table 6.2. Details about the spray modelling setup and the relevant sub-models (developed and implemented by Dr. Fang [30]) will not be presented as it is considered to be out of the scope of this study. Further information can be found in [89, 259]. The chemical mechanism chosen for this study is the 54 species, 268 reactions Yao *et al.* [260] mechanism (later referred to as the Yao mechanism). The computational domain for RANS was set to be volumetrically identical to the experimental combustion vessel of the Sandia National Laboratories [261], with the injector positioned centrally and an injection flow being in the axial direction. The walls' boundaries were set as non-slip walls with a fixed temperature of 461 K, as measured in the experiments.

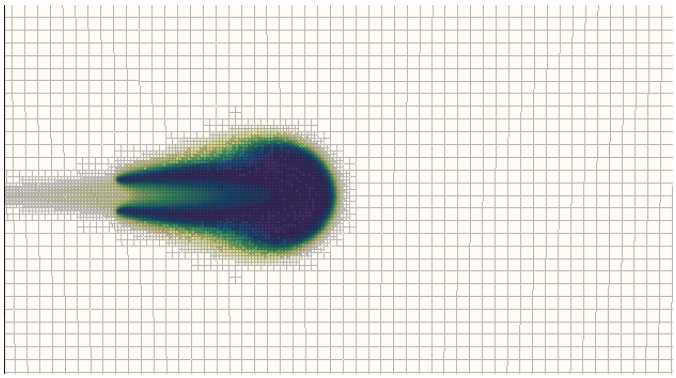

Figure 6.4: Computational domain of ECN "Spray A" showing AMR.

A systematic mesh resolution and grid sensitivity study were previously conducted in [89]. For this study, adaptive mesh refinement (AMR) was used, allowing the base volume of a computational cell to be split into smaller volumes during run time. Based on previous studies, the base grid of this particular case was chosen to be 2 mm, and the smallest grid scale allows via 3 levels of AMR corresponding to 0.25 mm. A near nozzle section view of the computational domain can be seen in Figure 6.4. For the present studies, all simulations are performed locally on workstations with 20 cores at 2.4$\sim$2.5 GHz of clock speed and 64 GB of RAM size.

6.5 Non-Reacting Spray Results

In order to have an accurate reacting spray case, a non-reacting spray is first modelled and compared with the experiment. It should be noted that the author of this thesis is not responsible for the results presented in this section; there were added to provide further evidence to the reacting spray results detailed in Section 6.6. During Fang's doctoral studies [30], the author undertook an in-depth validation of the non-reacting spray case. The outcome of Fang's work (minimum grid size, variable time step, spray sub-model, implementation) has been used within the framework of this study. The test conditions for the non-reacting spray study are listed in Table 6.1 as Test 0. Liquid penetration, vapour penetration and mixture fraction profiles are validated against the experiment. In this study, liquid penetration was defined as the axial location of 95% liquid mass threshold, while the vapour

penetration is defined as the maximum distance from the injector to where the fuel mass fraction is 0.1%. Figure 6.5 shows the liquid and vapour penetration lengths between the simulation and the experiment. The predictions for both criteria are in excellent agreement with the experimental measurements.

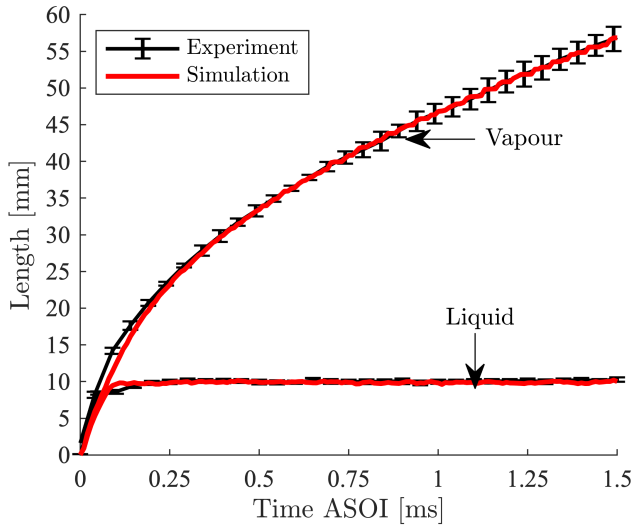

Figure 6.5: Non-reacting liquid and vapour penetration for “Spray A” baseline conditions [30].

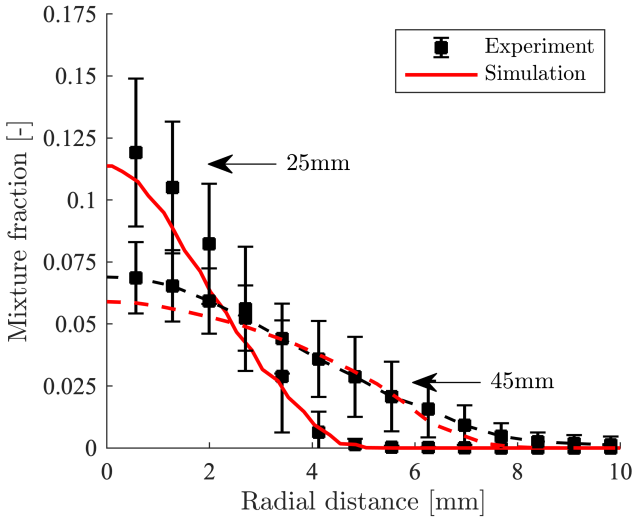

Figure 6.6: Mixture fraction radial profile for non-reacting “Spray A” baseline case at two axial downstream locations [30].

Furthermore, radial mixture fraction profiles at two axial downstream locations are shown in Figure 6.6. Slight underprediction is found near the center of the liquid jet. This is likely due to the size of the computational grid being bigger than the spray droplet size. However, both further downstream along the axial direction and the outer periphery of the spray in the radial direction show good agreement with the experiment.

6.6 Reacting Spray Results

Following the description of the modelling approach, numerical setup and non-reacting sprays results, this section will discuss and validate the CSE-FGM across a wide range of ambient boundary conditions. Simulations results will be discussed in detail. The results are primarily evaluated in terms of the most relevant characteristics of the transient diesel spray, including the auto-ignition event and the quasi-steady flame structure.

6.6.1 Ambient Temperature Sweep

First, the performance of the CSE-FGM combustion model was examined with respect to variations in ambient temperature with all other parameters fixed. The boundary conditions for these tests are given in Table 6.1, i.e. Tests I-IV. Note that a newly tabulated manifold was generated for each of the conditions listed in the table. The CSE-FGM results are compared with the results of simulations made using the same spray model in combination with the CONVERGE well-stirred reactor combustion model (SAGE), and also mean experimental results from the ECN.

Following the ECN simulation guidelines, the ignition delay time is defined as the first time at which the Favre-averaged OH mass fraction reaches 2% of the domain maximum after steady state is established and the lift-off length is given as the distance from the injector nozzle at which the Favre-averaged OH mass fraction reaches 14% of the instantaneous maximum during the steady-state duration. Figure 6.7 illustrates the IDT and LOL of the two combustion models against the mean of the experimental data. Both the CSE-FGM and the WSR models capture the general trends in auto-ignition and lift-off length with temper-

ature. As expected, both the ignition and the lift-off length are increased by lower ambient temperature boundary conditions. In relative terms, the CSE-FGM model shows a significant benefit over the WSR, particularly at the baseline and lower temperature conditions where the WSR model substantially over-predicts.

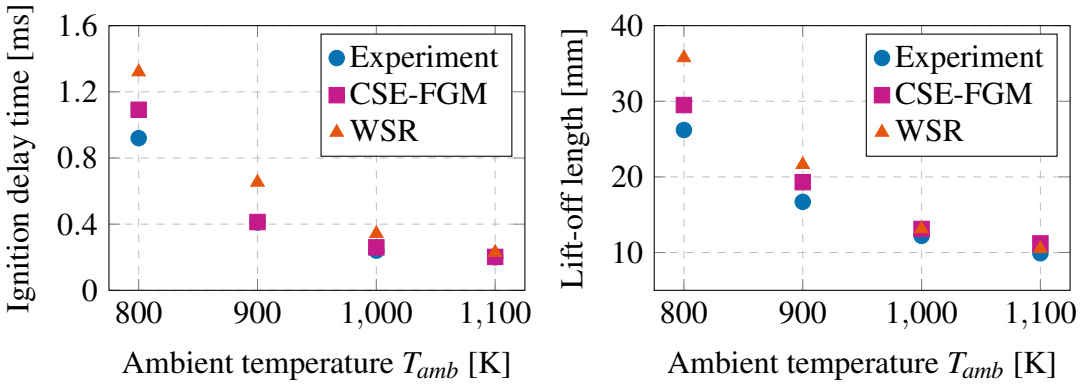

Figure 6.7: Parametric studies of RANS CSE-FGM at different ambient temperature conditions compared against the mean experimental results and well-stirred reactor simulation results for the ignition delay time (left) and the flame lift-off length (right).

This overprediction is attributed to the fact that turbulence chemistry interactions are not included within the WSR model – previous studies have shown the importance of including TCI and sub-grid variance effects in the prediction of low temperature ignition [262, 263]. The local inhomogeneity in mixture fracture space and the flow strain effects are found to promote two-stage combustion in a low temperature transient diesel spray. The inclusion of TCI in the CSE-FGM model therefore allows it to predict ignition significantly better than the WSR model at lower temperatures.

A more detailed ignition behaviour study was conducted through the analysis of temperature - mixture fraction scatters plot at “Spray A” baseline conditions. Figure 6.8 shows the temporal evolution scatter plot of temperature in mixture fraction space around ignition delay time. At 0.19 ms, all the points are clustered around the mixing line. Low-temperature reactions have been initiated at the edge of the spray jet. These reactions first occur in leaner mixtures as these are at the highest temperature in the unburned flow field. Prior to second stage combustion at around 0.40 ms, most points in the figure are clustered in the rich mixture zone. The low-temperature reactions, predominantly initiated by the first-

stage ignition, here coupled with the high scalar dissipation rate in this region, initiate a turbulent cool-flame which transports species and heat release to colder and richer mixtures. This is demonstrated by the shift in conditional temperature, from leaner to richer mixtures. It is worth noting that the current study gives a smooth transition of temperature at different mixture fractions. This is likely due to the "ensemble averaging" process in RANS smoothing out this apparent abrupt transition. At second stage combustion, the combustion event is favouring a mixture fraction of less than 0.15. The temperature continues to rise, and the mean temperature becomes closer to the equilibrium state. At 0.45 ms the highly stratified flow field, formed from high-temperature ignition, initiates turbulent flame propagation from richer to leaner mixtures.

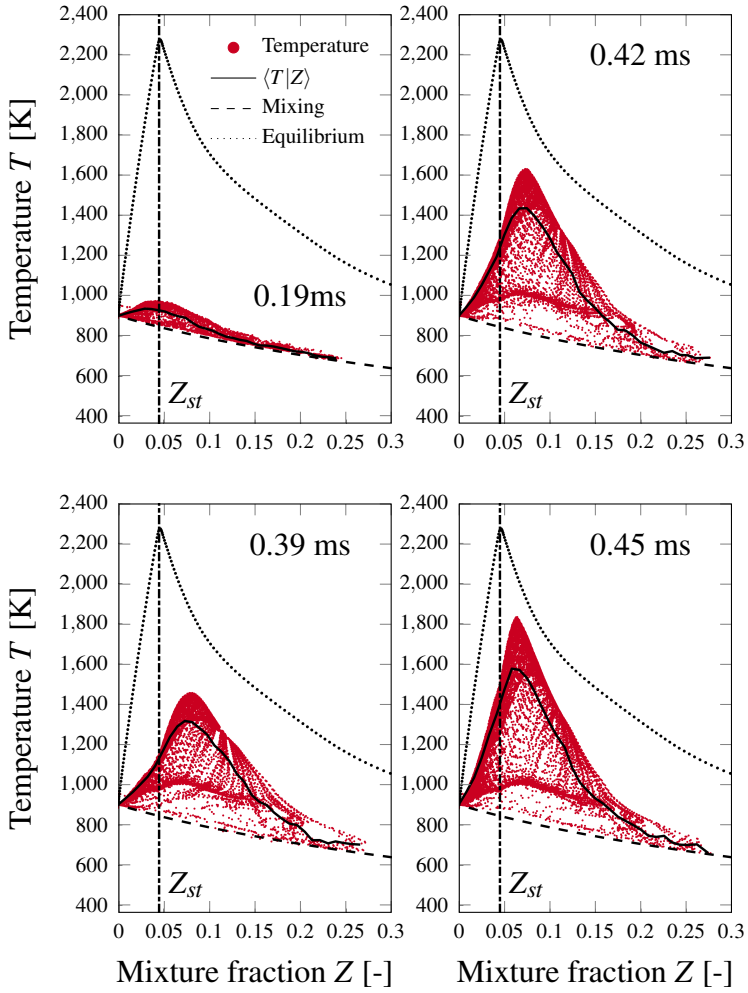

Figure 6.8: Temporal evolution of scatter plot of temperature versus mixture fraction for the 900K "Spray A" baseline conditions.

In order to further study the flame propagation and stabilisation mechanisms, the flame temperature contours and mass fraction distributions of intermediate key species were analysed. Diesel spray flames are typically characterised by two-stage ignition, where studies have found the formation of intermediate species CH_2O to be a strong indication of first stage ignition [262] and the high temperature second stage ignition is visualised by the formation of OH radicals.

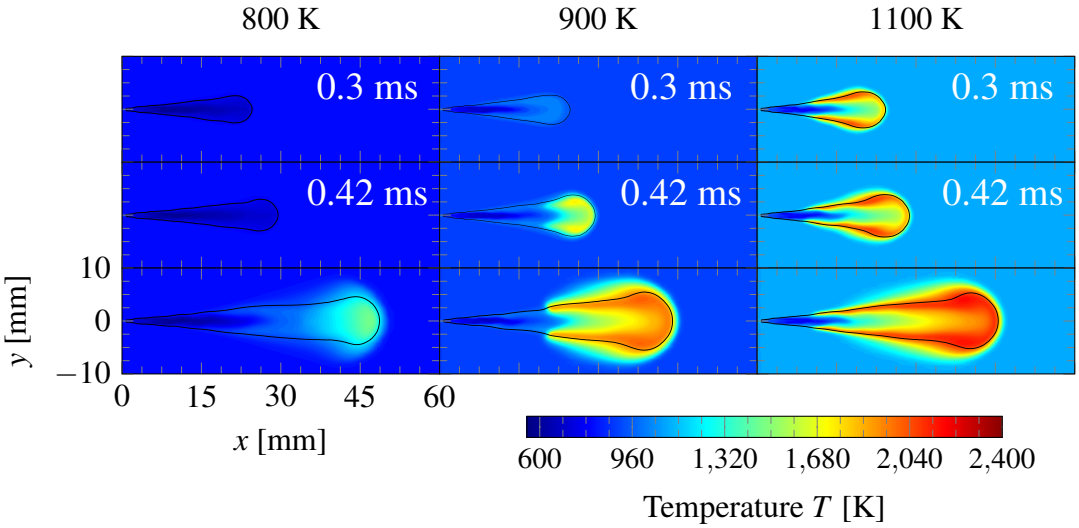

Figure 6.9: Instantaneous temperature fields of RANS simulations for various temperature "Spray A" conditions at 15% of fixed oxygen concentration. The time after start of injection is shown on the top right of each image. The times ASOI of the last line correspond respectively, from the left to the right, to 1.2 ms and 1.0 ms for the last two. The black line is the stoichiometric mixture fraction contour.

Figures 6.9, 6.10 and 6.11, respectively, depict the variation of flame temperature, CH_2O and OH mass fraction contours with changing ambient temperature between 800 K and 1100 K. The black line in the temperature contour represents the isoline of the stoichiometric mixture fraction. Note that due to a comparatively extended ignition delay, the quasi-steady state time selected for the 800 K case in Figure 6.9 is 1.2 ms — as opposed to 1.0 ms for the 900 K and 1100 K cases. Note also that this extended ignition delay is consistent with the earlier discussion of the characteristics of the chemistry manifold, Figure 6.2. The temperature contours in Figure 6.9 show that the shorter ignition delay time at a higher ambient temperature leads to longer jet penetration and a smaller high temperature

combustion spreading angle.

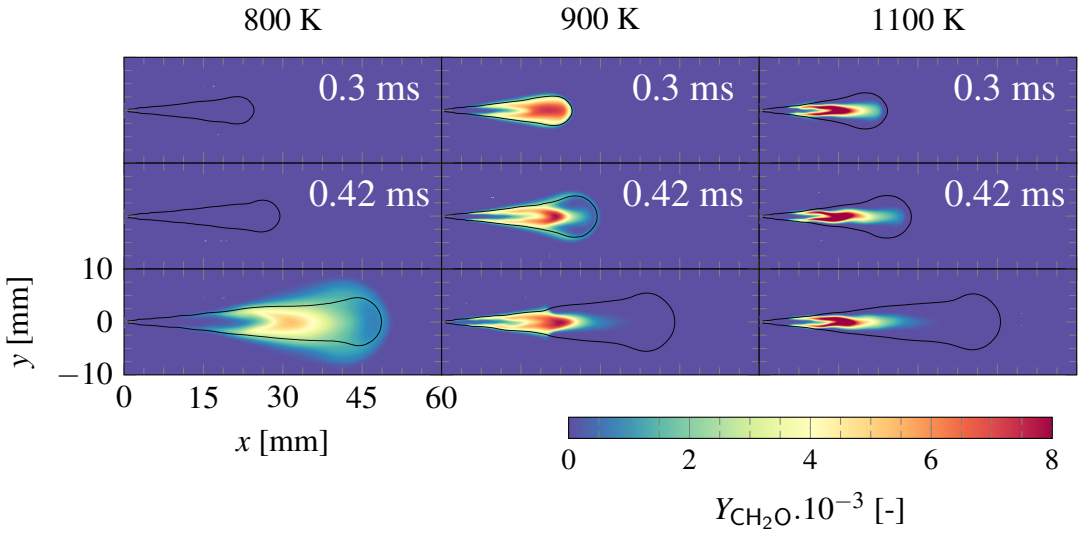

Figure 6.10: Instantaneous CH_2O mass fraction fields of RANS simulations for various temperature "Spray A" conditions at 15% of fixed oxygen concentration. The time after start of injection is shown on the top right of each image. The times ASOI of the last line correspond, from the left to the right, to 1.2 ms and 1.0 ms for the last two, respectively. The black line is the stoichiometric mixture fraction contour.

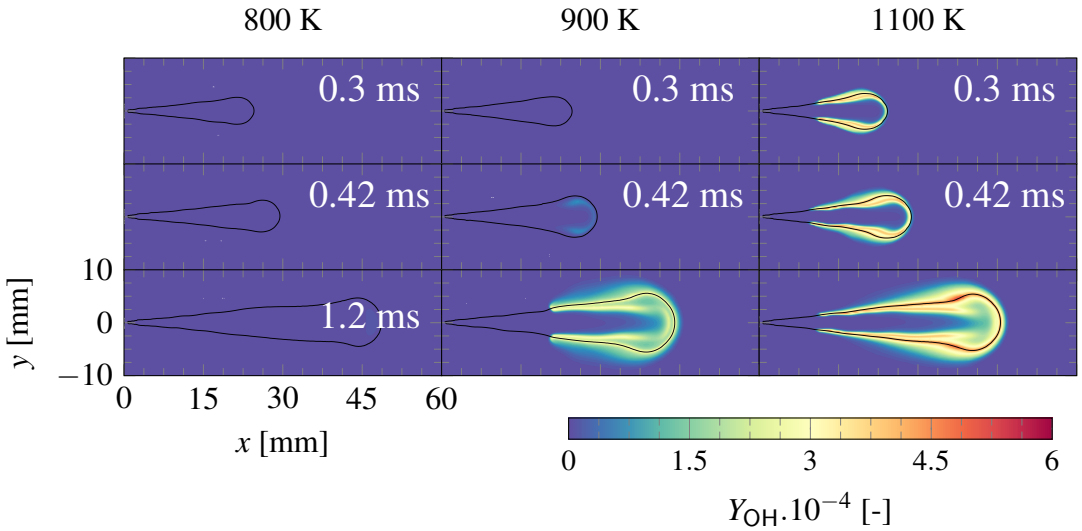

Figure 6.11: Instantaneous OH mass fraction fields of RANS simulations for various temperature "Spray A" conditions at 15% of fixed oxygen concentration. The time after start of injection is shown on the top right of each image with 1.0 ms corresponding to the last cases of the 900 K and 1100 K simulations. The black line is the stoichiometric mixture fraction contour.

The two-stage ignition process is first detailed from the intermediate species, CH_2O, mass fraction contours, Figure 6.10, representing the first stage ignition, also known as the cool flame. Prior to the first stage ignition, the initial CH_2O formation is seen at the periphery of the penetrating jet followed by convection to the jet centre. This is consistent with experimental observations of the characteristics of first stage ignition where heat release is observed at the jet periphery [264]. At the quasi-steady state condition, the highest concentrations of CH_2O are found at the core of the jet (the outer regions having been consumed by high temperature second stage ignition processes). As the ambient temperature is increased, the CH_2O distribution becomes more compact, and the region of maximum CH_2O concentration moves further upstream.

OH is chosen as the indicator of high temperature second stage ignition. The predicted OH mass fraction distributions, Figure 6.11 correspond well with both the temperature and the CH_2O mass fraction contours. A significantly higher OH mass concentration is observed in higher temperature conditions. This is likely linked to the fact that, at lower temperatures conditions, the ignition delay time is prolonged, providing substantially higher mixing in the mixture. With a leaner mixture prior to second stage combustion, both flame temperature and the OH mass fraction are reduced. Overall, the effect of varying ambient temperature on the prediction of diesel spray auto-ignition and thereafter, flame propagation is well captured by the CSE-FGM model.

6.6.2 Oxygen Concentration Sweep

Following the temperature sweep described previously, the performance of the CSE-FGM combustion model was examined with respect to variations in oxygen concentration, keeping all other parameters fixed. The boundary conditions for these tests are given in Table 6.1, Tests II, V and VI refer. Figure 6.12 shows the IDT and LOL simulations results compared to the mean experimental and the WSR model. An increase in oxygen concentration is seen to slightly accelerate the auto-ignition process, whereas the LOL is greatly shortened when oxygen concentration is high.

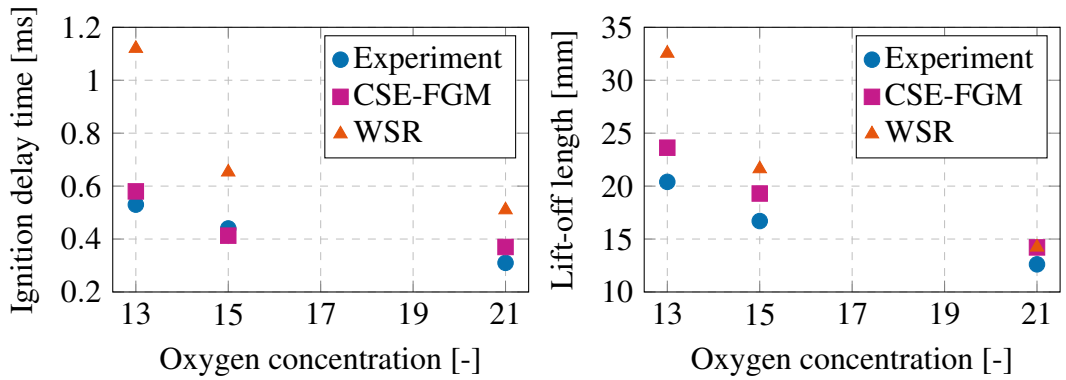

Figure 6.12: RANS CSE-FGM model results at 900 K with various ambient oxygen concentration conditions compared against the mean experimental results and the WSR model results for ignition delay time (left) and flame lift-off length (right).

Figures 6.13, 6.14 and 6.15, respectively, show the temperature, CH_2O and OH mass fraction distributions at 900 K ambient temperature with various oxygen concentrations. The quasi-steady state time for all oxygen concentrations is chosen to be 0.8 ms after the start of the injection. From the CH_2O plots, it is clear that a higher oxygen concentration leads to a faster first stage ignition where intermediate species are consumed earlier for second stage ignition.

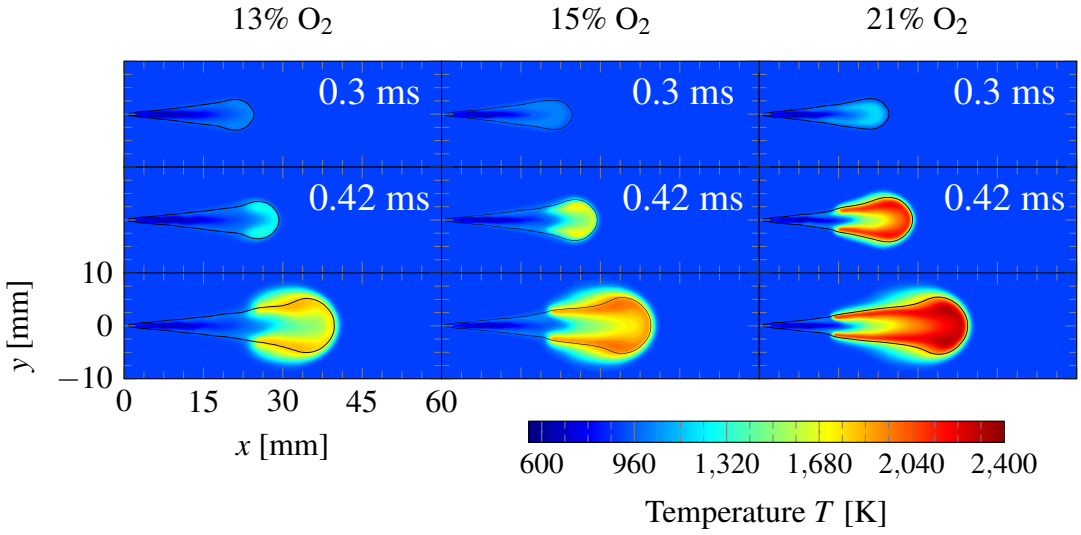

Figure 6.13: Instantaneous temperature fields of RANS simulations at 900 K "Spray A" conditions for various oxygen concentrations. The ASOI time is shown on the top right of each image with the last line corresponding to 0.8 ms. The black line is the stoichiometric mixture fraction contour.

The position of the peak CH_2O concentration is approximately constant at the downstream location of 15 mm at the highest oxygen concentration (21 %). Similar behaviour was observed in previous diesel spray simulations performed using other chemical mechanisms [256]. As shown in Figure 6.13, increasing the ambient oxygen concentration causes the onset of the high temperature reaction zone to be pushed upstream towards the injection nozzle – which is likely caused by the higher reactivity of the mixture when higher oxygen concentration boundary conditions are given.

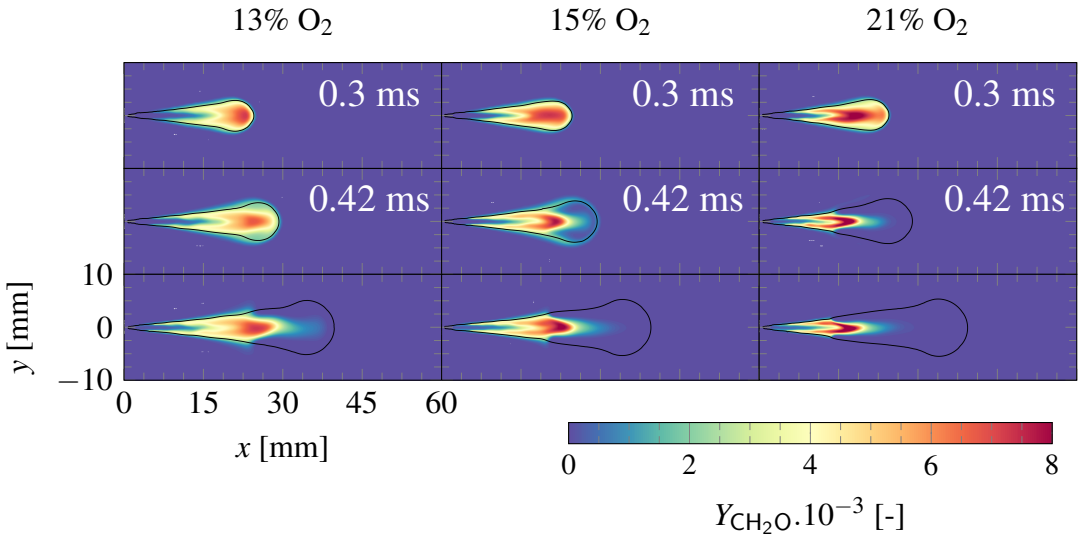

Figure 6.14: Instantaneous CH_2O mass fraction fields of RANS simulations at 900 K "Spray A" conditions for various oxygen concentrations. The time after start of injection is shown on the top right of each image with the last line corresponding to 0.8 ms. The black line is the stoichiometric mixture fraction contour.

An increase of temperature at the tip of the spray is present for all flames in Figure 6.13; however, a clear increase in temperature is observed when oxygen concentration is increased. The variation of reactiveness of the flame can also be seen from the OH mass fraction distribution, Figure 6.15. A significant increase in absolute OH mass fraction is seen at 21 % oxygen conditions where a high concentration of OH shifts to the injector tip, indicating a shorter LOL. It can be seen from these results that the CSE-FGM model is able to capture the subtle impact of changing species concentration on the ignition and flame characteristics.

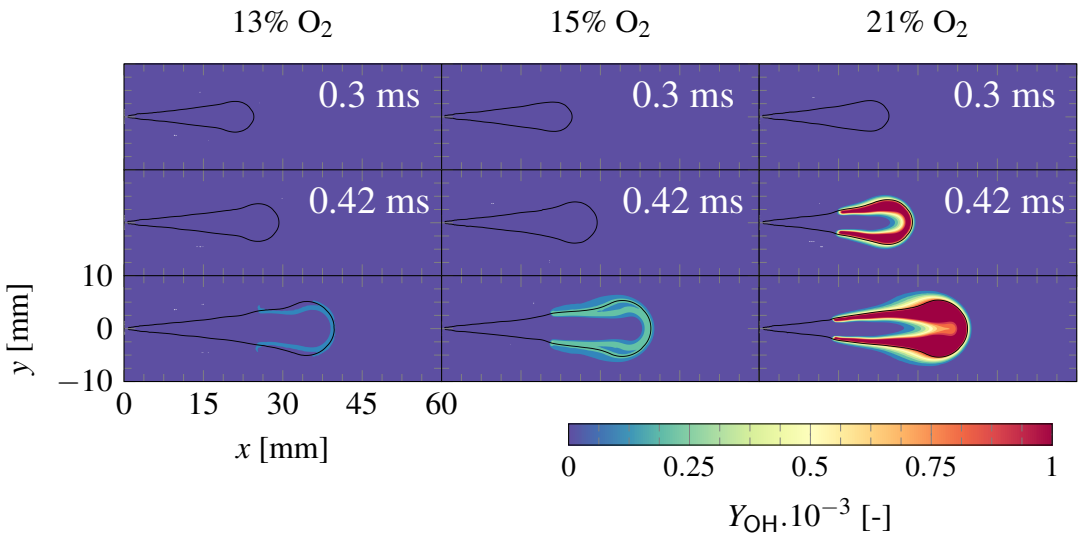

Figure 6.15: Instantaneous OH mass fraction fields of RANS simulations at 900 K "Spray A" conditions for various oxygen concentrations. The time after start of injection is shown on the top right of each image with the last line corresponding to 0.8 ms. The black line is the stoichiometric mixture fraction contour.

6.7 Discussion – CSE-FGM RANS in Context

Previous sections of this work have presented results of an ambient temperature sweep and an oxygen concentration sweep of "Spray A" simulations using CSE-FGM within a RANS framework. In this section, the performance of the CSE-FGM RANS model under baseline conditions (Table 6.1, Test II) is compared with experimental data from the literature [34] and the results of a single CSE-FGM LES realisation from the study of Fang *et al.* [91] at 900 K with two different chemical mechanisms – the Yao mechanism used in the RANS study, and the Luo mechanism (characterised by 106 species and 420 reactions [265]). Further information on the different sub-models (including spray) within a LES framework is depicted in [91]. Table 6.3 details the IDT and LOL results for all simulations. It can be seen that both the RANS and LES simulations are able to capture the combustion metrics to a high degree of accuracy. The IDT predicted by the RANS simulation falls between the LES simulations and is well within the range of the experimental data.

Table 6.3: Ignition delay time and flame lift-off length for ECN "Spray A" baseline condition. Experimental data repeated from [34].

Baseline	Experiment	LES Yao	LES Luo	RANS
IDT [ms]	0.40-0.44	0.408	0.423	0.413
LOL [mm]	15.80-17.90	18.08	22.16	19.31

Similarly, the RANS prediction of LOL falls between the two LES simulations results. In this case, all models slightly over-predict. Previous study has traced the overprediction for the LES simulation with the Luo mechanism to the manifold itself, which gives relatively lower source term values in regions associated with ignition and the intermediate stages of combustion stages [259].

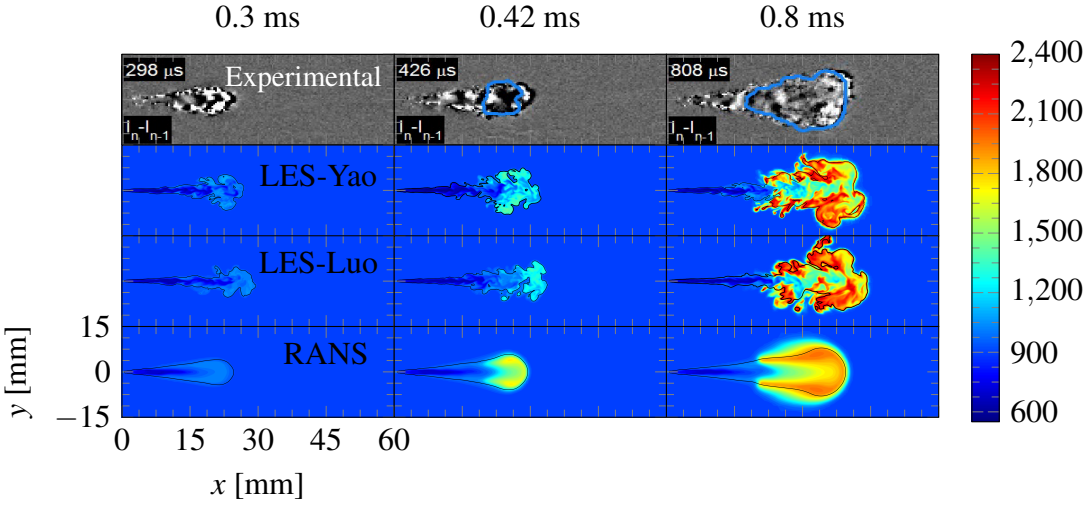

Figure 6.16: Schlieren image (top) and instantaneous temperature fields of LES and RANS simulations at 900 K "Spray A" baseline conditions. The time after start of injection is shown on the top left of each experiments' image. The blue line in the experimental study shows the luminosity border. The black line is the stoichiometric mixture fraction contour. The experimental images are corrected by its background intensity ($I_n - I_{n-1}$). The colourbar on the right corresponds to the temperature colourmap in Kelvin.

The temperature contours of the RANS simulation are plotted against the LES Yao and LES Luo mechanisms and the schlieren experimental images in Figure 6.16. The border of the high-temperature chemiluminescence (blue line) is overlaid on the simultaneously-acquired Schlieren images to help the visualisation of the high temperature reaction. The details of image processing and the experimental setup can be found in [261]. The com-

puted distributions from the RANS and both LES studies show good qualitative agreement with the experiments throughout the evolution of the flame – from ignition to quasi-steady state. As expected, there are significant temperature fluctuations present in the LES results compared to those of RANS simulations at the same time step. Note also that the RANS flame structure is closer to the individual realisation of the flame captured in the experimental data than is the single LES realisation. As discussed in [266], this is also to be expected. For the RANS simulations the Z_{st} line crosses the middle of the high temperature field, which is closer to the jet centerline, overlapping more of the high temperature region compared to LES simulation. In the LES, the Z_{st} line is located at the edge of the flame where high temperature reactions exist. The reason for this is that the LES simulation is a single realisation with spatial averaging, which results in a thin flame due to a very fine mesh. In contrast, RANS is an ensemble averaged simulation which thickens the flame and moves the Z_{st} line to the centre of the flame.

6.8 Summary

Three-dimensional diesel "Spray A" simulations were performed using a newly developed combustion model, CSE-FGM, within a RANS turbulence framework. The model takes the first-moment closure hypothesis from conditional moment closure methods; however, detailed chemistry is incorporated in a tabulated form giving greater flexibility. The simulations were carried out in the commercial code CONVERGE with unsteady flamelet solutions generated from CHEM1D using the 54 species and 268 reactions mechanism of Yao.

A parametric study, which considered a wide range of ambient temperatures and oxygen concentrations, was performed, and the flame auto-ignition and propagation characteristics were detailed. The CSE-FGM RANS model successfully demonstrated the capability of realistically predicting the essential structure of the diesel-fueled transient spray combustion processes. The ignition delay time (IDT) and flame lift-off length (LOL) were accurately predicted over the full range of ambient conditions examined. Analysis of the predicted

temperature fields and intermediate species distributions also demonstrated the ability of the CSE-FGM model to capture the two-stage ignition process present in diesel combustion.

The CSE-FGM RANS model results were also compared with the predictions of a well-stirred reactor model (WSR). It was shown that the CSE-FGM model leads to more accurate results, especially in low-temperature conditions, compared to the WSR model. This was attributed to the CSE-FGM model's inclusion of turbulence chemistry interactions.

Finally, a comparison between the results of the current CSE-FGM RANS study with a previous CSE-FGM LES study [91] under baseline ECN "Spray A" conditions demonstrated the consistency of the combustion model.

The current study demonstrates that the CSE-FGM approach offers a feasible tool for detailed combustion analysis of diesel spray flames over a wide range of engine-relevant conditions. The proposed CSE-FGM model is capable of predicting phenomena relevant to spray configurations with complex chemistry involved and accounting for TCI.

Further improvements can be considered, in particular at low ambient temperatures where the ignition delay times predicted by CSE-FGM were found to slightly deviate from experiments. Under low-temperature conditions, increasing IDT allows the evaporated fuel to partially mix with air, suggesting that a CSE approach which adopts a single scalar based on mixture fraction might not be sufficient to describe the flame characteristics. The inclusion of a second control variable using the progress variable should provide a higher degree of accuracy. This leads to doubly CSE (DCSE) where Z and c should more effectively capture the rich partially-premixed regions and diffusion effects of the studied test case.

However, while the inclusion of the mixture fraction and the progress variable within the closure of the chemical source-term will enable a much more accurate approximation of the mean reaction rate, the choice of the progress variable definition still presents a number of challenges. Depending on the studied system, and possibly the fuel involved, other definitions of c could perhaps be needed to more accurately capture the underlying chemistry taking place. This concern is further discussed in the next chapter.

Statement of Authorship for joint/multi-authored papers for PGR thesis

To appear at the end of each thesis chapter submitted as an article/paper

The statement shall describe the candidate's and co-authors' independent research contributions in the thesis publications. For each publication there should exist a complete statement that is to be filled out and signed by the candidate and supervisor **(only required where there isn't already a statement of contribution within the paper itself).**

Title of Paper	On the Prediction of Spray A End of Injection Phenomenon Using Conditional Source-Term Estimation
Publication Status	☒Published □Accepted for Publication □Submitted for Publication in a manuscript style □Unpublished and unsubmitted work written
Publication Details	X. Fang, R. Ismail, N. Sekularac and M. H. Davy, "On the Prediction of Spray A End of Injection Phenomenon Using Conditional Source-Term Estimation", In *WCX SAE World Congress Experience*, SAE International, 2020, 2020-01-0779.

Student Confirmation

Student Name:	Nikola Sekularac		
Contribution to the Paper	Data curation, Validation, Writing - original draft		
Signature		Date	09/08/2022

Supervisor Confirmation

By signing the Statement of Authorship, you are certifying that the candidate made a substantial contribution to the publication, and that the description described above is accurate.

Supervisor name and title:	Martin Davy		
Supervisor comments:	The above description is accurate. The relevant thesis chapter is appropriately annotated to describe authorship.		
Signature	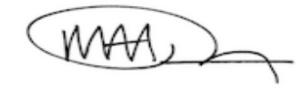	Date	10th August 2022

This completed form should be included in the thesis, at the end of the relevant chapter.

Statement of Authorship for joint/multi-authored papers for PGR thesis

To appear at the end of each thesis chapter submitted as an article/paper

The statement shall describe the candidate's and co-authors' independent research contributions in the thesis publications. For each publication there should exist a complete statement that is to be filled out and signed by the candidate and supervisor **(only required where there isn't already a statement of contribution within the paper itself).**

Title of Paper	Parametric Studies of a Novel Combustion Modelling Approach for Low Temperature Diesel Spray Simulation
Publication Status	☒Published □Accepted for Publication □Submitted for Publication in a manuscript style □Unpublished and unsubmitted work written
Publication Details	X. Fang, N. Sekularac and M. H. Davy, "Parametric Studies of a Novel Combustion Modelling Approach for Low Temperature Diesel Spray Simulation". *Proceedings of the ASME 2020 Internal Combustion Engine Division Fall Technical Conference*, vol. ASME 2020 Internal Combustion Engine Division Fall Technical Conference, 11 2020. V001T06A005.

Student Confirmation

Student Name:	Nikola Sekularac		
Contribution to the Paper	Dr. Fang and Nikola Sekularac share equal contribution. Nikola Sekularac is responsible for the conceptualisation, data-curation, formal analysis and writing - original draft.		
Signature		Date	09/08/2022

Supervisor Confirmation

By signing the Statement of Authorship, you are certifying that the candidate made a substantial contribution to the publication, and that the description described above is accurate.

Supervisor name and title:	Martin Davy, Associate Professor		
Supervisor comments:	The description above is accurate. The corresponding chapter the thesis is appropriately annotated to describe authorship.		
Signature	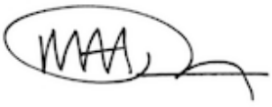	Date	10th August 2022

This completed form should be included in the thesis, at the end of the relevant chapter.

Chapter 7

Conditional Space Evaluation of Progress Variable Definitions

Science knows no country, because knowledge belongs to humanity, and is the torch which illuminates the world. Science is the highest personification of the nation because that nation will remain the first which carries the furthest the works of thought and intelligence.

–Louis Pasteur

Contents

The content in this chapter is a result of the collaborative efforts of the author, Dr. X. H. Fang, Prof. K. W. Bushe and Prof. M. H. Davy. The author is responsible for all studies presented. The corresponding author is Dr. Fang. The content in this chapter has been submitted in the peer-reviewed journal Combustion Theory and Modelling.

7.1 Overview

While the CSE-FGM approach has been shown to predict combustion phenomena relevant to diesel spray flames, adopting DCSE, and as such including a second conditioning variable based on a progress variable, is thought to provide a better description of partially-premixing and the interactions between turbulence and chemistry. While a generalised mixture fraction definition has been provided and well accepted by the community, various progress variable definitions have been adopted over the years for different applications. The current study focuses on the effect of progress variable selection on the conditional fluctuations obtained with one-condition conditional averages and doubly conditional averages of the Cambridge/Sandia swirl burner dataset [31, 267]. Four different progress variable definitions are chosen where all one-point, one-time measurements are included to study conditional fluctuations. The properties and working conditions of the burner and the methodology employed for determining the appropriate progress variable definitions are first introduced. The results are then discussed, and physical insights are provided based on the observations. A complementary study is also carried out with the experimental data of the Sandia/TUD jet flames [229] to provide further evidence to the conclusions drawn with the first test case.

7.2 Generalities

Among different models and studies, local mixture, the degree of progression of the chemical reactions, strain rate, total enthalpy, and residence time are all properties that have been found to be closely related to the chemical rates in a reactive flow field. For non-premixed flames, the mixture fraction is usually retained as the main controlling variable to describe the turbulent mixing effects [64]. For premixed flames, the progress variable is often selected as the primary scalar to describe the rate of progression from the unburned to burned state [5]. It has been shown that the fluctuations found in the species mass fractions and temperature are often correlated with the fluctuations of Z in non-premixed flames and with the fluctuations of c in premixed flames. However, a single scalar variable able to ac-

curately describe the structure of partially-premixed flames and capture regions with high probabilities of local extinction and re-ignition has not yet been found [268, 241]. This has led to different combinations of scalar variables, where often the mixture fraction and the progress variable are simultaneously considered [269]. While mixture fractions are generally incorporated using Bilger's definition, various definitions of the progress variable have been used for different approaches.

For laminar flamelet approaches, progress variables are often chosen as the primary controlling variables to construct a reduced dimension composition space. The temperature and the mass fraction of a major combustion product (e.g., H_2O or CO_2) have been widely used to define c for flamelet models. While suitable for many flames, using a single product mass fraction for larger hydrocarbons may fail to represent the true progress of the chemical reactions. Therefore, more species mass fractions in the form of linear combinations are often incorporated to track the reaction progress in the flow and capture different stages of combustion [89]. Sun *et al.* [117] have investigated the modelling capabilities of the unsteady flamelet/progress variable (UFPV) model in predicting the ECN "Spray A" cases. The progress variable was defined using a combination of major and intermediate species to obtain results across all downstream locations of the jet. While progress variables incorporating more than a single species mass fraction are effectively better performing, two challenges are worth mentioning, of which: (i) the diffusivity of the selected scalars needs to be accounted for in the progress variable transport equation, and (ii) the addition of intermediate species is often in conflict with the monotonicity of c. Studies have tackled the injection of the progress variable by computing weight coefficients using various automated optimisation techniques, e.g. the well-known $\frac{\partial c}{\partial \kappa} > 0$ criterion, where κ often denotes a time or a spatial coordinate [270, 271, 272]. However, most progress variable definitions found in the literature are based on user expertise where the chosen definition can significantly influence the numerical predictions, particularly for fuel-rich/heavy-fuel mixtures [273]. Recently, Gupta *et al.* [274] studied different progress variable definitions for tabulated chemistry through the analysis of premixed methane-air (CH_4/Air) laminar flames. Compared with detailed chemistry, flamelet generated manifold (FGM) results using differ-

ent species mass fraction-based progress variable definitions were shown to give different mass burning rates. Lipatnikov & Sabelnikov [275] also examined the effect of five different progress variable definitions on the flamelet approach predictions of the mean density and the mean mole fractions of various species using DNS data of a premixed hydrogen-air flame. A complementary study was carried out using DNS data of lean hydrogen-air turbulent premixed flames operating under various Karlovitz numbers [276]. Similar findings were obtained, suggesting that the definition of c in flamelet-based models indeed affects the physical modelling while simultaneously impacting numerical errors.

For conditional moment closure models, filtered chemistry is modelled through the separation of model elements which give descriptions for the moments of reactive parameters and model of the distribution function. CMC-based approaches are centred around the hypothesis that fluctuations in reactive scalars are closely correlated with the fluctuations around values of conditioning variables (e.g., mixture fraction and progress variable) [277, 278]. While using CSE-based approaches with a single conditioning variable has been found suitable for non-premixed and premixed flames [91, 90, 254, 269, 279], for partially-premixed or stratified combustion, one conditioning variable is not sufficient. Subsequently, Doubly CSE with mixture fraction and progress variable as conditioning variables have been developed to simulate partially-premixed flames, lifted flames, and spray flames [231, 280, 281]. The CSE and DCSE concepts have also been examined in an a-priori analysis in DNS for high-pressure conditions [282]. The results highlighted that DCSE and double conditioning are likely to be needed for cases closer to real practical combustion applications. Similar to the flamelet approaches, when choosing the conditioning variables for CMC approaches, the mixture fraction definition from Bilger is well accepted by the community, where the choice of progress variable and particularly its effects on conditional variable fluctuations needs more studies. Recently, Bushe [283] and Mousemi & Bushe [284] examined the conditional moment closure hypothesis over the Sandia/TUD, the Sydney Swirl burner, and Cambridge/Sandia stratified swirl burner databases. Their studies suggested two-condition (mixture fraction and progress variable) conditional averages in the Sandia/TUD do not vary in space nor vary with the Reynolds number, whereas, for

Sydney and Cambridge/Sandia swirl burners, a third conditional variable (total enthalpy) might be needed to further reduce the spatial gradients of conditional averages attributed to the heat transfer. For these studies, progress variables based on temperature and mass fraction of CO_2 were used. Perhaps more interestingly, the a-priori studies on single-step high-pressure DNS data from Devaud *et al.* [282] and Bushe *et al.* [253] using CO_2 and temperature-based progress variables suggested the success of DCSE does not depend on a particular choice of the second conditioning variable which significantly increased the capabilities of CSE models. However, further extension of these two studies on the effect of progress variable selections is not possible due to the single-step chemistry nature of the DNS data.

Consequently, two questions around control variables in the context of CMC-based models are worthy of note here - the questions central to this paper:

1. What is the minimum number of scalar variables needed to adequately characterise conditional space for certain flames?

2. Which scalar variables represent the best choices for this, and how do they influence the predictions, in particular for the definition of the progress variable?

Depending on the studied case, Bushe *et al.* [283] also pointed out that the selection and number of control variables must be carefully undertaken to adequately address the effects of turbulence and chemistry. Additionally, the modelling of the joint-PDF gives a substantial challenge to the turbulent combustion modelling community as its shape strongly depends on the selected scalar variables. The validity of the statistical independence assumption used for modelling the presumed joint-PDF was shown to be erroneous, as correlations between conditional variables are important [253].

The present work is motivated by the study of three different groups: Sutherland & Parente's work on principal component analysis-based models [285], Bushe's study on spatial gradients of conditional averages [283], and Gupta *et al.*'s analysis on the impact of the progress variable definition on flamelet generated manifolds [274]. This chapter investigates the two questions posed above with a particular focus on the effect of progress

variable selection on the conditional fluctuations obtained with one-condition conditional averages and doubly conditional averages of the Cambridge/Sandia swirl burner dataset. The results are discussed, and physical insights are provided based on the observations.

7.3 Methodology

7.3.1 Experimental Setup

Experimental measurements of premixed and stratified CH_4/Air flames from the Cambridge/Sandia swirl burner (referred to as SwB) are used in this study. Multiscalar data of nine turbulent flames are examined under: (i) various ratios of stratification, and (ii) various swirl intensity conditions, depicted in Table 7.1.

Table 7.1: Operating conditions for Cambridge/Sandia swirl burner. ϕ_i and ϕ_o denote equivalence ratio of the flow in the inner and outer annuli, respectively. In all cases $\phi_g = 0.75$, $U_i = 8.31$ m/s, $U_o = 18.7$ m/s and $U_{co-flow} = 0.4$ m/s. Conditions highlighted in bold font denote flames under swirling flows.

Flame	Swirl ratio	Stratification factor	ϕ_i	ϕ_o
SwB1	0	1	0.75	0.75
SwB2	**0.25**	**1**	**0.75**	**0.75**
SwB3	**0.33**	**1**	**0.75**	**0.75**
SwB5	0	2	1	0.5
SwB6	**0.25**	**2**	**1**	**0.5**
SwB7	**0.33**	**2**	**1**	**0.5**
SwB9	0	3	1.125	0.375
SwB10	**0.25**	**3**	**1.125**	**0.375**
SwB11	**0.33**	**3**	**1.125**	**0.375**

The burner, shown schematically in Figure 7.1, features a large co-flow of pure filtered air preventing ambient air from entering the reaction zone, and two concentric outer (subscript o) and inner (subscript i) annuli supplying the fuel/air mixture. The annuli's velocities were chosen to maximise the Reynolds numbers in the flows with $Re_i = 5{,}960$ and $Re_o = 11{,}500$. A variable degree of swirl allows the burner to mimic the flow conditions found in many practical systems. The swirl assists flame stabilisation allowing more extreme stratified conditions to be investigated than would otherwise be possible. The stratification factor is defined by the ratio of the equivalence ratio in the inner and outer annuli. The

scalar measurements recorded include temperature and the mole fractions of CO_2, CO, H_2, CH_4, N_2, O_2 and H_2O at different axial and radial positions. A minimum of 300 samples were taken at 60 different radial locations per axial position via Rayleigh and Raman scattering to capture temperature and major species, respectively. Further information on the measurement techniques, the experimental setup and the burner's characteristics can be found in [31, 267]. The existence of turbulent regions within the flames, operating under premixed and/or stratified mixture conditions, with or without swirl, makes this burner an ideal test case for attempting to answer the two questions central to this work.

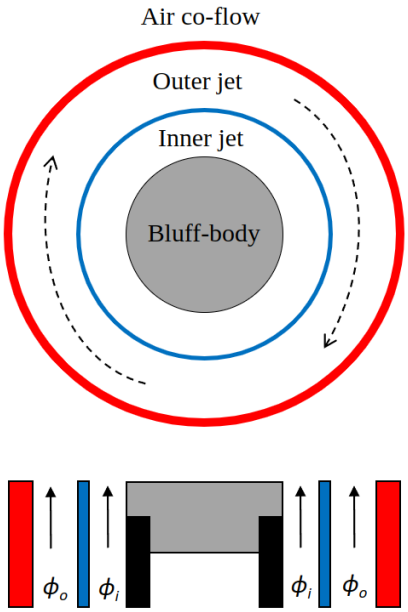

Figure 7.1: Plan view schematic of the exit geometry in the Cambridge/Sandia swirl burner, showing a plan view and a cross section through the burner axis. The curved-dashed arrows in the plan view indicate the direction of swirling flows in the outer annulus. ϕ_i and ϕ_o in the cross section denote the equivalence ratio of the flow in the inner and outer annuli, respectively. Adapted from [31].

7.3.2 Data-Processing

Three datasets have been constructed to investigate the effects of spatial coordinates, swirl flow ratio, and stratification factor on the conditionally-averaged reactive scalars, depicted in Table 7.2. In the first case, the data collected from all nine flames are grouped together to create a general conditional domain for each of the scalars (SwB|all). Here, it is as-

sumed that the conditional averages are independent of spatial coordinate, swirl flow ratio and stratification factor. The second dataset (SwB|Hstratified) combines the measurements of three flames exhibiting varying swirl flow ratio intensities with a single high stratification factor to investigate the dependence of conditional averages on swirl. For the third case, data from 3 flames with different stratification factors and a fixed high swirl flow ratio are grouped to investigate the dependence of conditional averages on stratification (SwB|Hswirl). Grouping the flames in these three distinct datasets, each tackling a specific characteristic of the flow, allows the exploration of the most optimal scalar or combination of scalars needed to sufficiently accurately represent the thermo-chemical state under different conditions.

Table 7.2: Characteristics of the three datasets used for investigating the behaviour of conditional averages.

Case	Flames	Swirl ratio	Stratification factor	Comments
SwB|all	SwB1-11	0-0.33	1-3	All flames grouped
SwB|Hstratified	SwB9-11	0-0.33	3	Fixed stratification
SwB|Hswirl	SwB3,7,11	0.33	1-3	Fixed swirl

The data was first "cleaned" to remove mole fractions displaying negative values associated with experimental uncertainty. All mole fraction measurements were subsequently converted to mass fractions values (note that mass fractions will be used throughout the present study). An artificial exclusion for values of H_2 mass fraction above 0.00025 is adopted and carried out for each flame and database. The mixture fraction Z was calculated for every instantaneous single-point measurement. The definition of Z proposed by Bilger is used to calculate the mixture fraction of all nine flames (cf. Equation 1.4). Mixture fractions of zero and unity are respectively assigned to pure air and the richest entry of the flow through all of the cases with an equivalence ratio of 1.125. For the considered sets of flames, the stoichiometric mixture fraction lies at $Z_{st} = 0.9$, with a lower flammability limit located at $Z = 0.575$ [154]. To investigate the role of control variables in conditional spaces, four of the most common combustion progress variable c used by the community

are considered in this study, defined as

$$c_k = \frac{\Phi_k - \Phi_{k,min}}{\Phi_{k,max} - \Phi_{k,min}} \tag{7.1}$$

where Φ_1 denotes the temperature, while Φ_2, Φ_3 and Φ_4 are the mass fractions of CO_2, $CO + CO_2$ and $CO + H_2 + H_2O + CO_2$, respectively (cf. Table 7.3). The local maximum is determined using a function that returns the upper peak envelopes of the scalar k selected to define c. The envelope is computed using spline interpolation over local maxima separated by 2,500 samples, for which a parametric study was performed to find the optimal number of samples. The local minimum values have been fixed to zero and to 290 K for the species-based progress variables and temperature, respectively.

Table 7.3: Summary of the four progress variables investigated in this study using Equation 7.1.

Label	Scalar(s) Φ_k	Mark
c_1	Temperature	▲
c_2	Y_{CO_2}	■
c_3	$Y_{CO_2} + Y_{CO}$	●
c_4	$Y_{CO} + Y_{H_2} + Y_{H_2O} + Y_{CO_2}$	♦

A second condition based on mixture fraction and the four progress variables (i.e., $Z, c_k < 0$ and $Z, c_k > 1$) is applied to take potential outliers from the analysis as these points are considered to be unphysical. After executing all previous steps, each database consists of 5,518,536 point-based measurements for SwB|all, 1,887,496 for SwB|Hstratified and 1,901,113 for SwB|Hswirl.

To examine the conditional space of Cambridge/Sandia flames, the methodology proposed in [283, 154] is followed and applied to all three datasets. The conditional averages are obtained via a discrete process involving binning, dividing each progress variable dimension into 30 bins. For the first moment hypothesis, the conditional fluctuations of species mass fractions and temperature around one-condition (c_1-c_4) conditional average are calculated at each axial location, such that

$$f'_{i,k} = f_i - \langle f | \xi = c_k \rangle (x) \tag{7.2}$$

where i denotes a single-point measurement, $f'_{i,k}$ is the fluctuation of either mass fraction or temperature around one-condition (c_k), f_i is the point measurement of that reactive scalar and $\langle f|\xi\rangle(x)$ is the conditional average of that reactive scalar evaluated by averaging all of the measurements of the chosen dataset at all radial locations together at each downstream distance. Two reasons for investigating how much conditional averages vary in the axial direction are worth mentioning. First, the conditional fluctuations are larger in the axial positions and are spatially independent in the radial direction [286, 283]. That was shown to be particularly true for jet flames, suggesting that within a CSE framework, group of localised cells, referred to as an ensemble, should be divided along the axial direction. Second, Mousemi *et al.* [154] showed for the same burner that the global conditional averages (equivalent to defining a single CSE/DCSE ensemble where all of the reactive control volumes in the domain are included) did not exhibit a particular functional dependence on the flow dynamics and the burner's geometry assuming that three conditioning variables are selected/retained. Suppose that ensembles are split across all axial positions, the number of conditioning scalars needed to accurately represent the chemical state is reduced, where a single control variable could perhaps be sufficient to separate the conditional averages from spatial coordinate, swirl and/or stratification effects. This approach is of particular interest for CMC-based models as it can be seen as a viable alternative to bypass the challenges associated with joint-PDFs defined by a minimum of two scalars.

If the conditional average is a good representation of the local thermo-chemical state, then it is expected that the mean of the conditional fluctuations will be zero. However, the RMS of those fluctuations is clearly not, as shown by Bushe [283] using the Sandia/TUD database and the Sydney swirl burner. Therefore, the square root of the average of the square of conditional fluctuations can be computed, as

$$\mathrm{RMS}_{i,k} = \sqrt{\langle f'^2_{i,k}\rangle} \tag{7.3}$$

The proposed RMS is normalised by the maximum value of the considered reactive scalar. This last step is justified in two ways: (i) to compare the different scalars to one another which the relative magnitude should be comparable, and (ii) the data has been filtered

to eliminate outliers, suggesting that the maximum measured value is unlikely to be the consequence of a major measurement error. The methodology undertaken within this study to determine the definition of the progress variable is summarised in Figure 7.2.

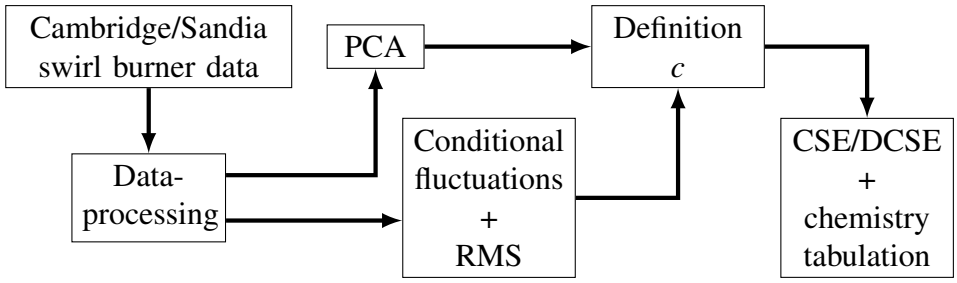

Figure 7.2: Flow chart of the methodology adopted to determine the progress variable definition.

7.3.3 Principal Component Analysis

Over the past decade, low-dimensional manifold representations have been frequently used to mitigate the costs associated with turbulent reacting flows and detailed kinetics [287]. Data-driven analytical tools have seen considerable success in combustion applications for building low-dimensional manifolds while preserving an adequate representation of the thermo-chemical state [288]. Among many others, principal component analysis (PCA) may be employed to find new sets of conditioning variables that have the highest correlations with the reactive scalars to detach the conditional averages from the real domain. PCA parameterises the thermo-chemical state-space using a reduced number of optimal scalars identified in the directions of maximal data variance, principal components (PCs). Projecting the state-space on those PCs gives the PC-scores, and adopting only a subset of those scores as conditioning variables is expected to result in a more accurate representation of the chemical state with smaller discrepancies for the unconditional averages [154]. However, a number of issues are yet to be addressed regarding the applicability of PCA with CMC-based approaches. Suppose more reactive scalars are combined to define a PC, the diffusion term for the selected principal component becomes more complex, and evaluation of the diffusive fluxes for each component is required [289]. Similar to the diffusion problem, the chemical source terms of all scalars used to define the selected PC must

be combined to appropriately describe the principal component's source-term. Moreover, the PCs are often difficult to associate with previously presented control variables, where physical interpretations are not always straightforward depending on the studied case. This raises an additional complexity, in particular with the closure of the chemical source terms, where presuming the shape of the PCs' PDFs is not trivial. Accordingly, rather than adopting PC-scores as controlling variables, here, PCA is utilised as a data-driven technique to identify which definition of c is needed/preferred to accurately describe the flames of interest. Previous studies [290] suggested that one of the first PCs was often found to be highly correlated with Z for non-premixed flames. While this has been thoroughly validated for Sandia/TUD jet flames, to the best of the author's knowledge, premixed flames have not been studied yet with PCA, suggesting that further research is needed.

The mathematical approach to compute the principal components of a given dataset X ($n \times Q$) reduces to an eigenvalue decomposition problem, where rows n represent individual measurements of Q variables. Suppose X has been appropriately standardised (i.e., centred and scaled), PCA projects all Q variables onto a rotated basis obtained from the eigenvalue decomposition of the covariance matrix S ($Q \times Q$) as

$$S = \frac{1}{n-1}\mathrm{X}^{\mathrm{T}}\mathrm{X} = \mathrm{ALA}^{\mathrm{T}} \tag{7.4}$$

where A is the ($Q \times Q$) matrix whose columns are the eigenvectors of S, and L is a ($Q \times Q$) diagonal matrix containing the eigenvalues of S. Following the details of the PCA reduction provided in [285, 291], PC-scores Ψ are obtained as

$$\Psi = \mathrm{XA} \tag{7.5}$$

where Ψ is an ($n \times Q$) matrix. Each column of A describes the weight between the Q variables of X and the corresponding principal component. The dimensionality reduction is undertaken by truncating A, such that only the first q PCs that account for the maximum variance are retained, with $q < Q$. The original dataset X is retrieved as

$$\mathrm{X} \approxeq \mathrm{X_q} = \Psi_{\mathrm{q}}\mathrm{A}_{\mathrm{q}}^{\mathrm{T}} \tag{7.6}$$

where X_q is the approximation of X based on the first q eigenvectors of A, and Ψ_q is the $(n \times q)$ matrix of the principal component scores. Detailed mathematical formulation of PCA is not elaborated here where more details can be found in the literature [292].

Principal component analysis requires high-fidelity datasets to generate the PC-basis and accurately describe the thermo-chemical state-space. The experimental measurements of all three datasets fed to PCA have been cleaned out following the steps presented previously. It should be noted that the mixture fraction and the progress variables have been excluded from the databases before being passed to PCA.

Various studies have tackled the effects of scaling methods on PCA [293, 294]. Scaling has an important outcome on the method's accuracy as it can change the PCA structure by altering the relative importance of various scalars. Auto-scaling, Range scaling, VAST (variable stability) scaling, Level scaling and Pareto scaling are among the most common options used in conjunction with PCA for combustion studies. Range scaling divides each variable by the difference between the minimal and the maximal value, whereas Level scaling adopts the mean values of the variables as the scaling factor. VAST scaling focuses on using the product between the standard deviation and the so-called coefficient of variation, defined as the ratio of the standard deviation and the mean. Pareto scaling was recognised as having a distinct advantage for major species and source terms reconstruction while needing fewer components [295]. Level, VAST, Range and Auto-scaling options were found to provide similar results with often more components needed to achieve the same reconstruction accuracy obtained with Pareto [296]. Therefore, in order to study the scaling effect on the accuracy of the method, the PCA analysis is carried out using two scaling options, assuming that the datasets have been previously centred:

1. Pareto scaling, which adopts the square root of the standard deviation
2. Auto-scaling (AS), which uses the standard deviation as the scaling factor

Previously, Parente & Sutherland [297] found that Auto-scaling is more adapted when an exploratory analysis on the chemical manifold should be performed, whereas Pareto appears more suitable for capturing the principal features of the systems and the behaviour

of the main species. Parente & Sutherland also [297] showed that the square root of the standard deviation enhances the temperature scalar in carrying most of the data variance, and thus, forcing the first principal component to align with temperature. For this reason, the temperature was excluded from the three databases passed on to PCA.

The real utility in PCA comes by founding correlations among the variables defining the state-space. A new coordinate system is identified in the directions of maximal data variance, allowing less important dimensions to be eliminated while maintaining the primary structure of the original data. In order to determine the amount of information captured by each principal component and thus replace the Q elements of X by $q < Q$ principal components, the fraction of total variance accounted by each PC is calculated as

$$t_{q_i} = \frac{\sum_{k=1}^{q_i} l_k}{\sum_{k=1}^{Q} l_k} \tag{7.7}$$

where i and l_k denote a single PC and the variance located on the diagonal of the covariance matrix S, respectively. Since outputs resulting from the two scaling methods have different numerical ranges, their PC-scores have been scaled to the interval $[-1, 1]$.

7.4 Results & Discussion

7.4.1 Principal Component Analysis

The PC analysis was individually performed on all three databases with all radial and axial locations grouped together. Figure 7.3 illustrates the variance accounted by each PC using Equation 7.7. To clarify, figures depicting PCA results do not include the temperature scalar within the analysis. Regardless of the scaling method adopted, a single principal component seems to account for the largest amount of variance present in all three datasets, with $\sim$0.9 using Pareto and $\sim$0.8 with AS. The variance explained by PC1 is in good agreement with the threshold proposed by Parente *et al.* [291]. Their study showed that by accounting for $\sim$0.9 of the total variance, all main species and temperature can be recovered with satisfactory levels of approximation. Consequently, the physical interpretation of all other principal components is omitted in this work, as is it believed to be out of the scope of this study.

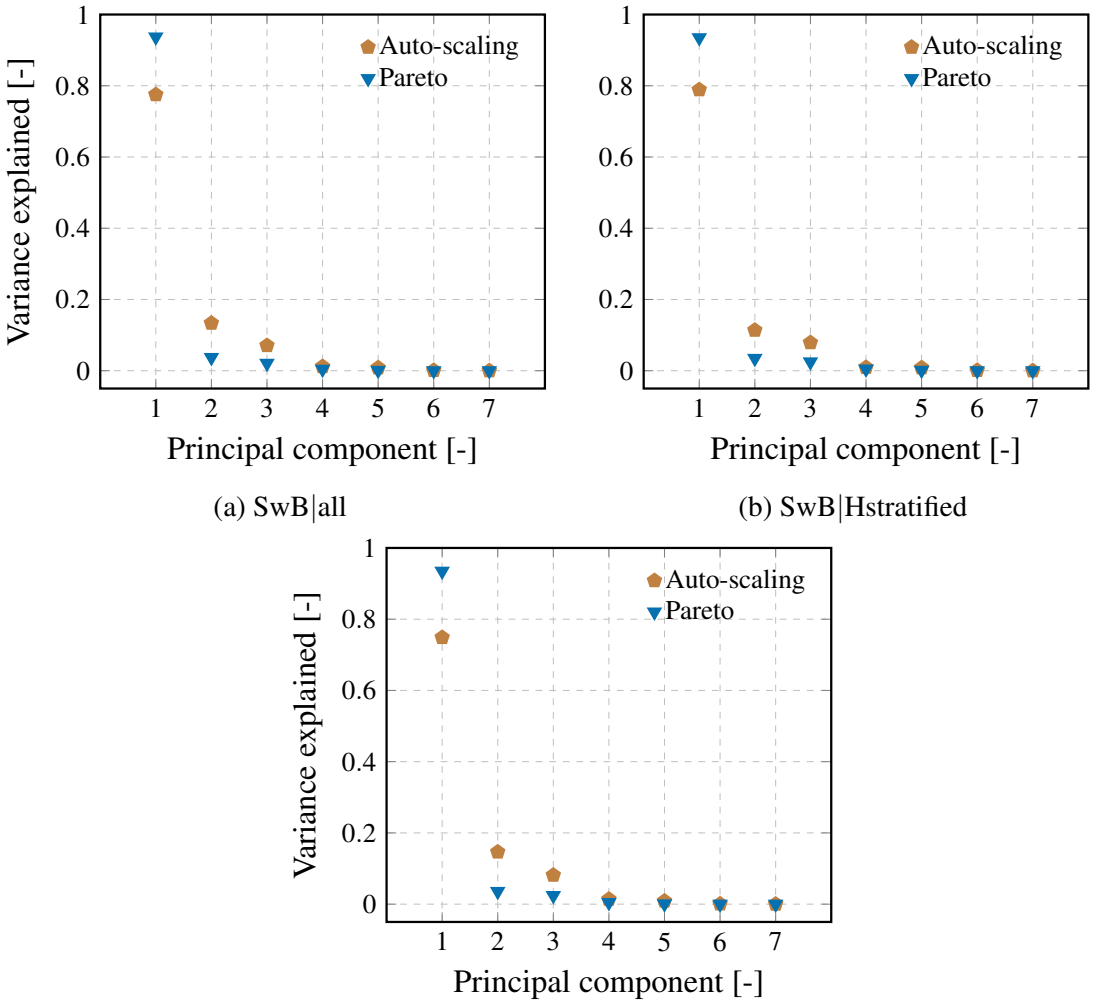

Figure 7.3: Comparison of variance explained with Pareto (triangles) and Auto-scaling (pentagons) for each principal component of (a) SwB|all, (b) SwB|Hstratified and (c) SwB|Hswirl.

In order to determine the underlying structure of PC1, the weights of the original variables characterising the three databases (i.e., matrix A) are presented in Figure 7.4 for both scaling methods. Regardless of the scaling method used, it is interesting to note that PCA is able to automatically distinguish reactants from products, with PC1 being negatively and positively correlated with reactants and combustion products, respectively. Regardless of the dataset, it appears that the mass fractions of CO_2 and O_2 have the most important contributions to PC1-Pareto, and to a larger extent Y_{H_2O}, with coefficients equal to approximately 0.6, 0.65 and 0.35, respectively. This trend is also apparent for PC1-AS, with the latter

having non-negligible weights on intermediate species, as opposed to Pareto, which clearly emphasises main species. This observation agrees with the study undertaken by Parente *et al.* [297] which has shown that the variance accounted for minor species by Auto-scaling is up to ∼20% higher than that explained by the other scaling methods investigated in their work.

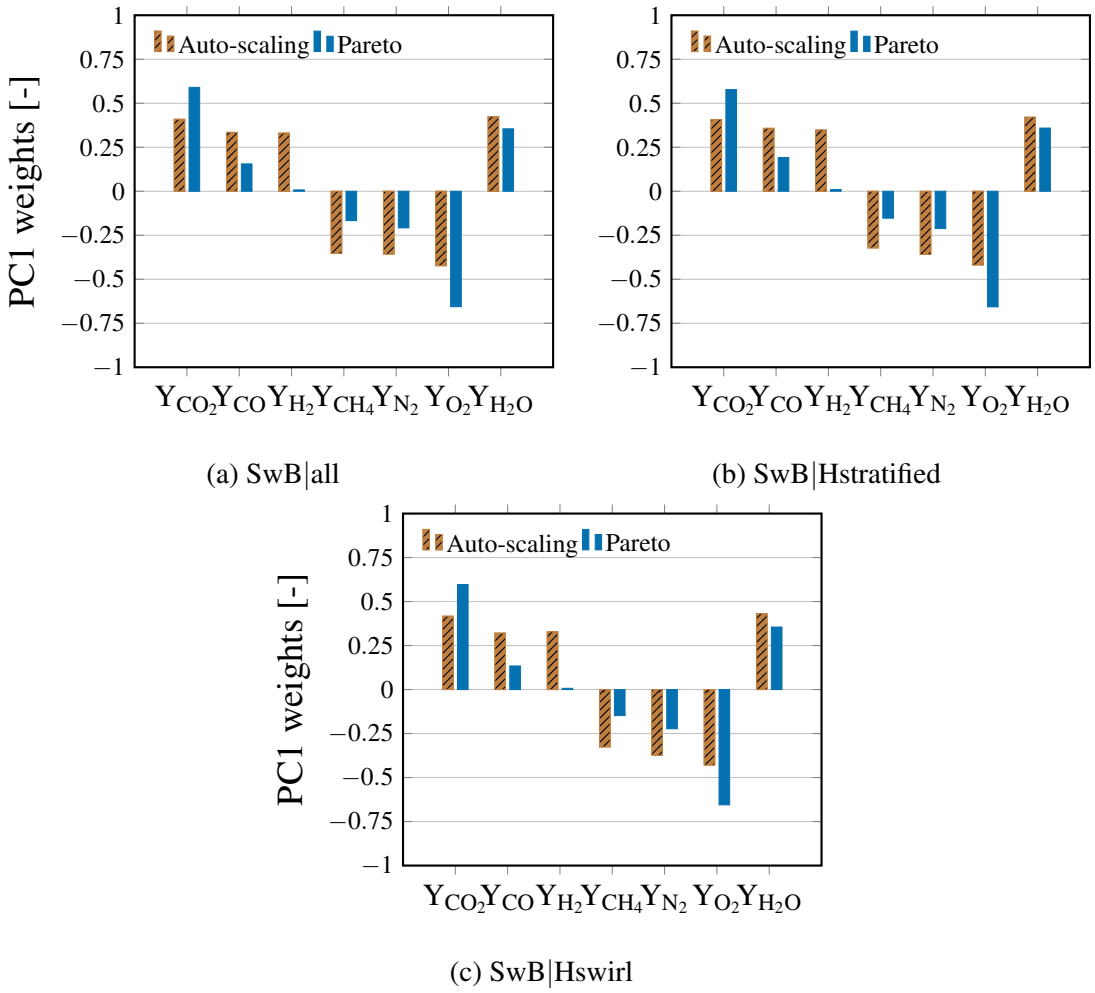

(a) SwB|all

(b) SwB|Hstratified

(c) SwB|Hswirl

Figure 7.4: Comparison of weights obtained with Pareto and Auto-scaling (with strips) for the leading principal component and scalars of (a) SwB|all, (b) SwB|Hstratified and (c) SwB|Hswirl.

Considering the criterion proposed by Ranade & Echekki [298], only coefficients with magnitudes ≥ 0.4 are kept to help identify the more prominent contributors to PC1. As PC1-Pareto, the same three species appear to have dominant weights on PC1-AS, namely the mass fractions of CO_2, O_2 and H_2O, with ∼0.4. It is worth mentioning that all three

scalars are known to behave linearly with temperature, thus suggesting that PC1 is perhaps correlated/aligned with temperature. This trend is illustrated in Figure 7.5, where results of all three datasets considered herein promote a PC1 monotonically increasing with temperature. As expected, this behaviour is clearly accentuated by adopting the Pareto method.

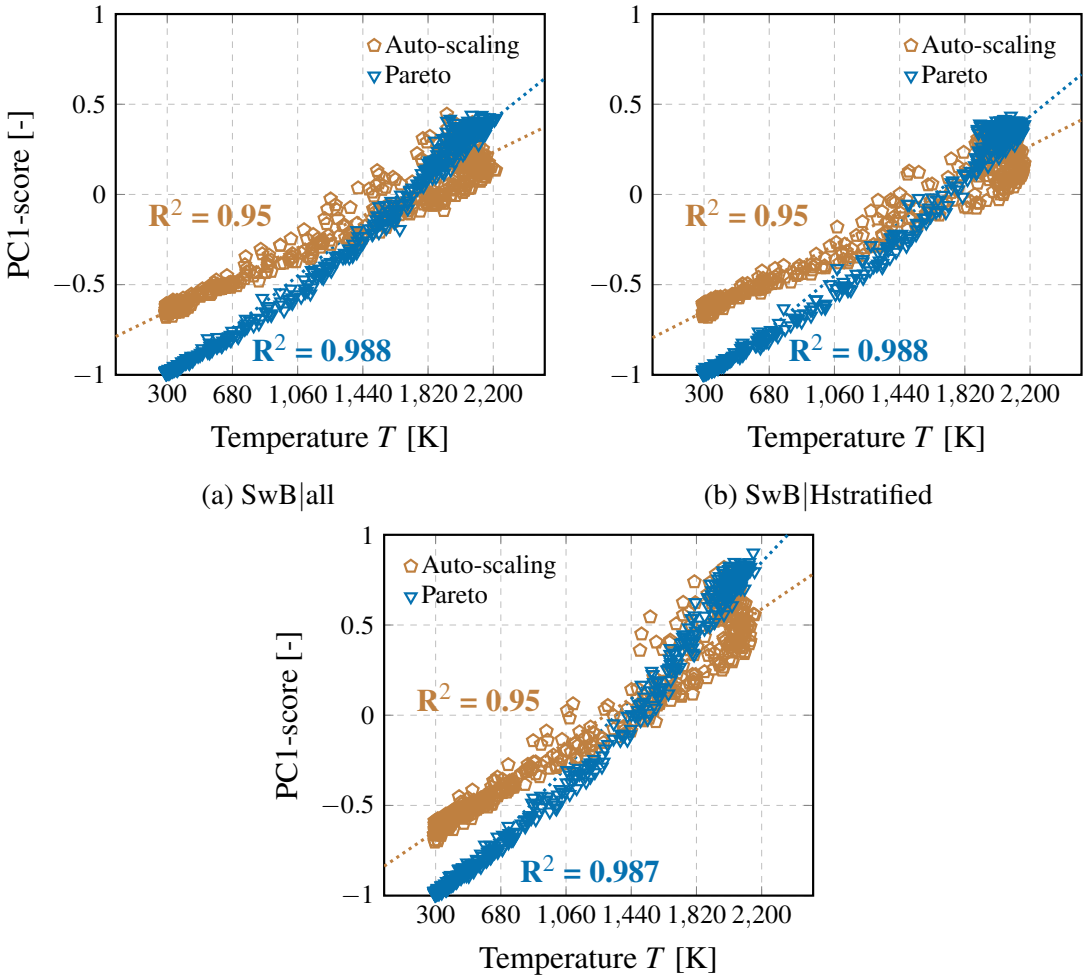

Figure 7.5: Comparison of correlations obtained with Pareto (triangles) and Auto-scaling (pentagons) for the leading principal component with temperature for (a) SwB|all, (b) SwB|Hstratified and (c) SwB|Hswirl. The markers illustrate 500 point-based measurements randomly selected within the flames' and PC1-scores' datasets.

A supplementary analysis was carried out by including temperature in SwB|all and using only Auto-scaling, as PC1-Pareto will be constrained to align with temperature. Figure 7.6 illustrates the dominant contributions to PC1-AS. The temperature scalar and the same

three species mass fractions have the largest weights on PC1, with ∼0.4, suggesting that PC1, regardless of the scaling method adopted, is correlated with temperature.

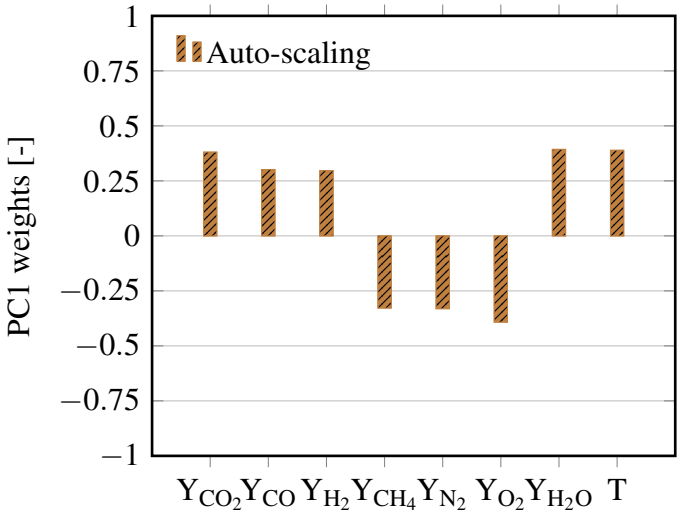

Figure 7.6: Comparison of weights obtained with Auto-scaling (with strips) for the leading principal component and scalars of SwB|all with temperature included. PC1-AS accounts for ∼0.8 of the total variance; $R^2 = 0.97$-AS with temperature.

After identifying the structure of the first principal component, the first-moment conditional fluctuations analysis of all three databases is carried out to investigate which of the proposed progress variables can sufficiently accurately characterise the composition space. As suggested by PCA, particular attention is brought to the temperature-based progress variable c_1.

7.4.2 All Flames (SwB1-11)

Conditional averages of the Q variables describing the SwB|all thermo-chemical state can be calculated and consequently determine the conditional fluctuation associated with each experimental measurement. One-condition conditional averages using one of the four progress variables are investigated and compared to one another in order to determine the most optimal definition of c_k. Figure 7.7 illustrates the conditional fluctuations of temperature and five different species mass fractions. To clarify, throughout the entire document, figures with axial locations account for all data at different radial locations.

Regardless of the progress variable investigated, at all eight downstream locations, conditional fluctuations of the mass fraction of CH_4, CO and H_2 around c_k exhibit an important functional dependence on the physical domain, stratification and/or swirl, visually highlighted by conditional fluctuation points spread far from zero.

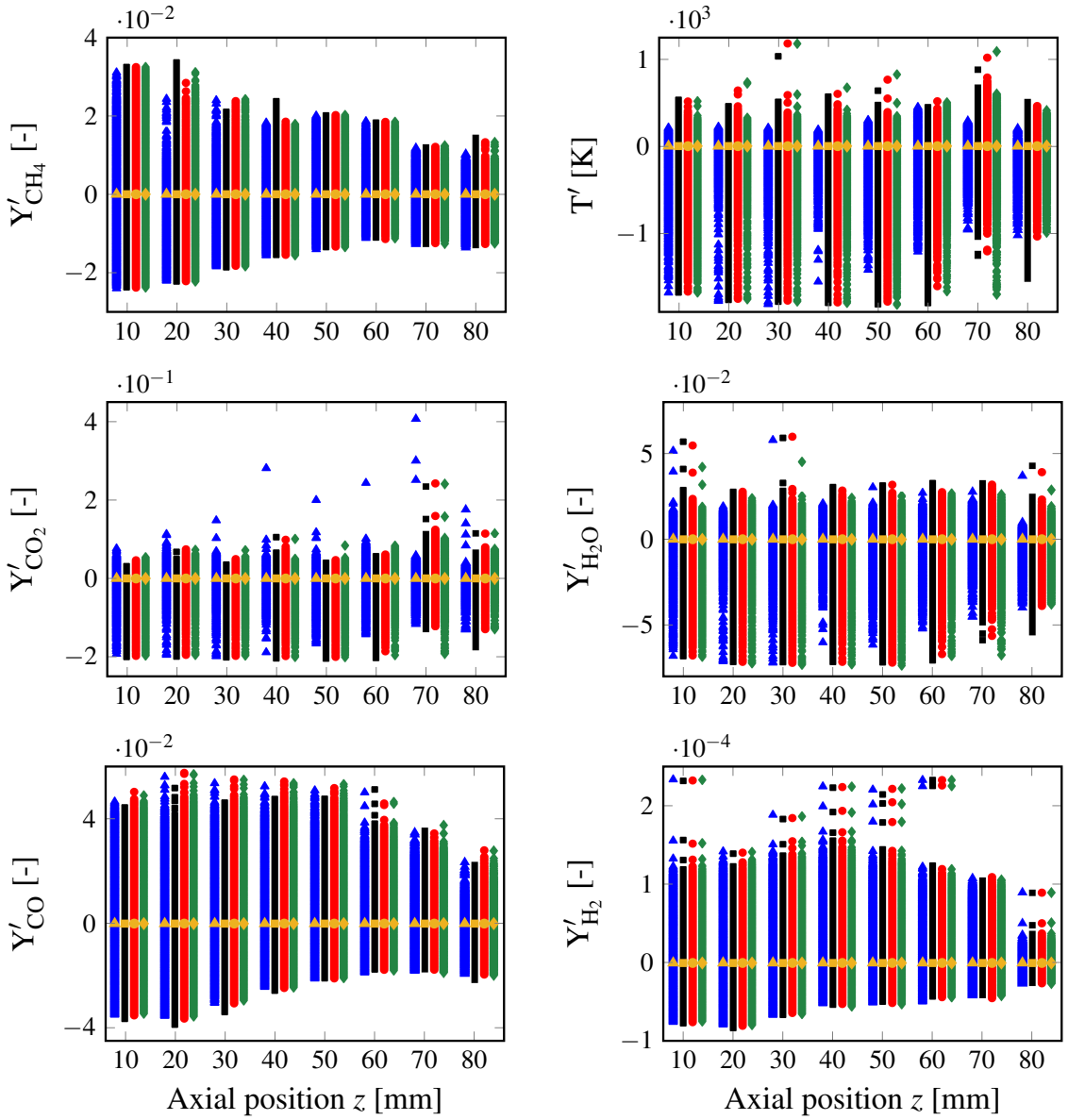

Figure 7.7: Conditional fluctuations of species mass fractions and temperature around the conditional average $\langle f|\xi = c_k\rangle(x)$ for SwB|all database using only c_k as the single conditioning variable and collecting all points at different radii together; the local average of these conditional fluctuations $\langle f'_{i,k}\rangle$ (golden markers) are also shown.

This trend is emphasised near the burner's tip, where the heat exchange with the bluff body might be significant, but also where an important recirculation of the flow is encountered. Due to high swirl, the recirculation zone is extended further downstream, leading to important conditional fluctuations of intermediate species at axial distances corresponding to $z = 40,50$ mm. It is interesting to note that all investigated c_k promote very similar results for the same three previous species. On the contrary, the conditional fluctuations of temperature and mass fractions of CO_2 and H_2O vary in function of the progress variable retained. The conditional fluctuations of Y_{H_2O} around c_1 suggest that a temperature-based progress variable can perhaps more effectively decrease the functional dependence on the physical domain compared to the other c_k. This can be attributed to the fact that the mass fraction of H_2O is closely relevant to temperature. As expected, a similar behaviour can be seen for the conditional fluctuations of T around c_1, and the conditional fluctuations of Y_{CO_2} around c_2.

While local averages of all conditional fluctuations are anchored at zero, and thus, suggesting that all progress variables investigated are doing a good job of characterising the considered dataset, it is nearly impossible to find which definition of c is effectively the best choice to accurately describe the thermo-chemical state-space, and detach it from spatial coordinates, but also swirl and/or stratification effects.

Figure 7.8 enables to distinct the performances of each c_k by analysing each variable's normalised RMS. The normalised RMS of Y'_{CO_2} around c_2 provides the best results due to the inclusion of the CO_2 mass fraction in c_2. As expected, the same trend is observed for the RMS of T' around c_1. It is interesting to note that further downstream the axial position, the RMS of Y'_{CO_2} around c_1 are improved or off the same order of magnitude as the Y_{CO_2}-based progress variable. Additionally, the RMS of Y'_{CH_4} obtained using any c_k are unchanged and remain close to 10%. Assuming that RMS of conditional fluctuations of the order of 10% can be considered as "relatively small" [283], one can suppose that using a single conditioning variable for this database might still give acceptable predictions of the considered reactive scalar for conditional moment closure models.

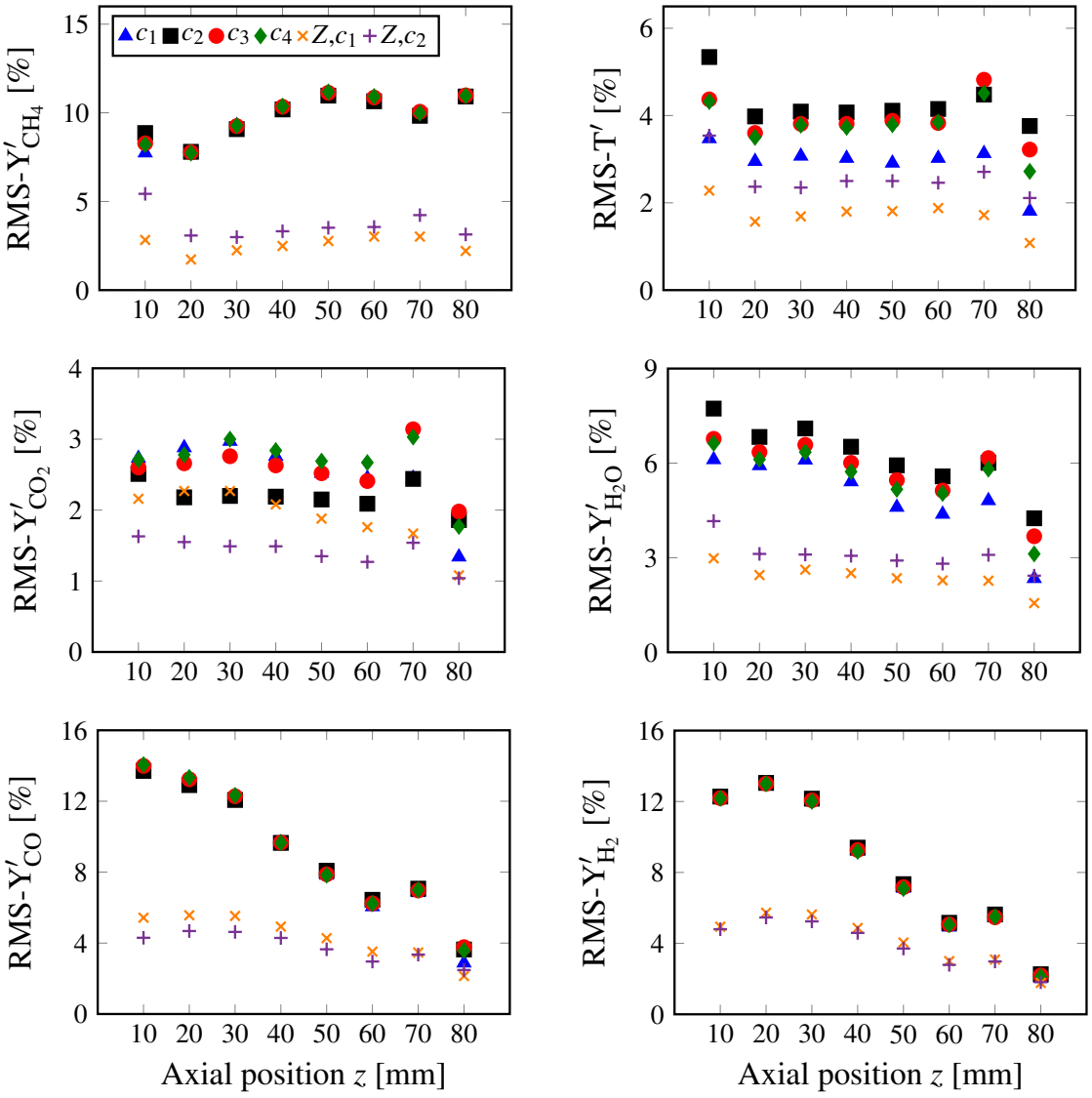

Figure 7.8: Normalised RMS of the conditional fluctuations of temperature and species mass fractions for the SwB|all database around the conditional average $\langle f|\xi = c_k\rangle(x)$ (markers) using c_k as the single conditioning variable, and around the conditional average $\langle f|\eta = Z, \xi = c_1, c_2\rangle(x)$ using the mixture fraction, and the temperature-based progress variable (crosses) or the Y_{CO_2}-based progress variable (plusses), and collecting all points at different radii together.

However, using c_k as a single conditioning variable gives poor results for intermediate species, i.e. CO and H_2, where normalised RMS exceed 10% of the maximum value of that particular scalar in the regions near the burner's tip. This suggests that the conditional averages are different and changing in function of space, stratification and/or swirl. Conse-

quently, conditional fluctuations around two-condition conditional averages using mixture fraction and a temperature-based progress variable (Z, c_1) are considered in this study. Conditional fluctuations around mixture fraction and a Y_{CO_2}-based progress variable (Z, c_2) are also included to provide further insight. Each mixture fraction dimension is divided into 50 bins. It can be deduced that: (i) doubly conditioning is of particular interest for intermediate species, in particular those believed to be highly correlated with Z (e.g., Y_{CO}), and (ii) regardless of the c_k selected, one-condition conditional averages seem to not deviate that much from two conditions (e.g., temperature, carbon dioxide and water). Interestingly, normalised RMS of fluctuations around the one-condition conditional averages of Y_{CO} and Y_{H_2} are nearly as efficient as Z, c_1 and Z, c_2 further downstream the axial direction. The normalised RMS of major species and temperature using the mixture fraction and the temperature-based progress variable are somewhat more effective compared to Z, c_2, excluding, again, the RMS of Y'_{CO_2}. The differences remain minor, suggesting that the choice of a particular progress variable definition does not seem important, as deduced in [282]. However, it is believed that adopting Z and c_1 as the two controlling variables will provide a much more accurate representation of the Cambridge/Sandia flames' chemistry compared to mixture fraction and a species-based progress variable. The underlying assumption here is that diffusion effects play an essential role in describing the chemical states. From this perspective, it is assumed that $c(Y_i)$ would be a poor choice as the diffusion coefficient is often modelled using the unity Lewis number assumption, whereas the reduced temperature progress variable includes the thermal diffusivity by solving the diffusion flux term. Given that, it can be supposed that $c(T)$ is, to a certain extent, more "universal", considering that the production/consumption of certain species is correlated with a given temperature. Recently, Turkeri *et al.* [299] showed through a parametric study that preferential diffusion is less relevant than heat losses for the studied burner, as it was found that the latter are more prevalent to accurately capture the underlying physics, particularly at the inlet of the burner.

The two-condition conditional averages of the temperature and mass fractions of several species around mixture fraction and c_1 are shown in Figure 7.9. The obtained results are

in good agreement with [154], where minor discrepancies are attributed to the different data-processing steps adopted in this study. The contours of conditionally-averaged scalars around Z and a Y_{CO_2}-based progress variable are illustrated in Figure 7.10.

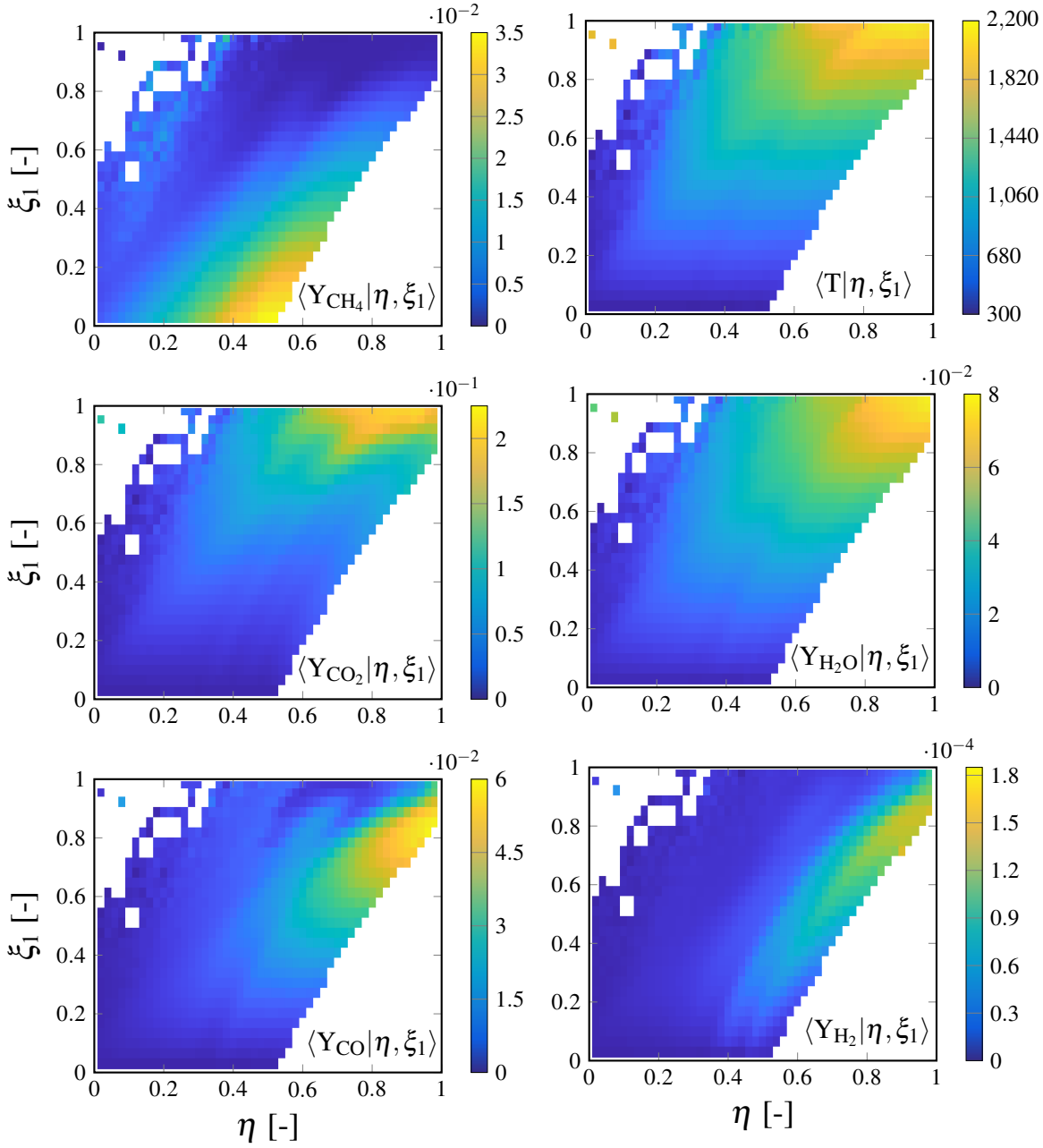

Figure 7.9: Two-condition conditionally averaged reactive scalars from SwB|all using η and ξ_1 as the sampling space variables of mixture fraction and the temperature-based progress variable c_1, respectively, and collecting data at all spatial locations (radial and axial). The temperature colourbar is expressed in Kelvin.

Despite gathering data from all axial and radial locations, one region common to both conditional domains can be identified in which no measurement has been found.

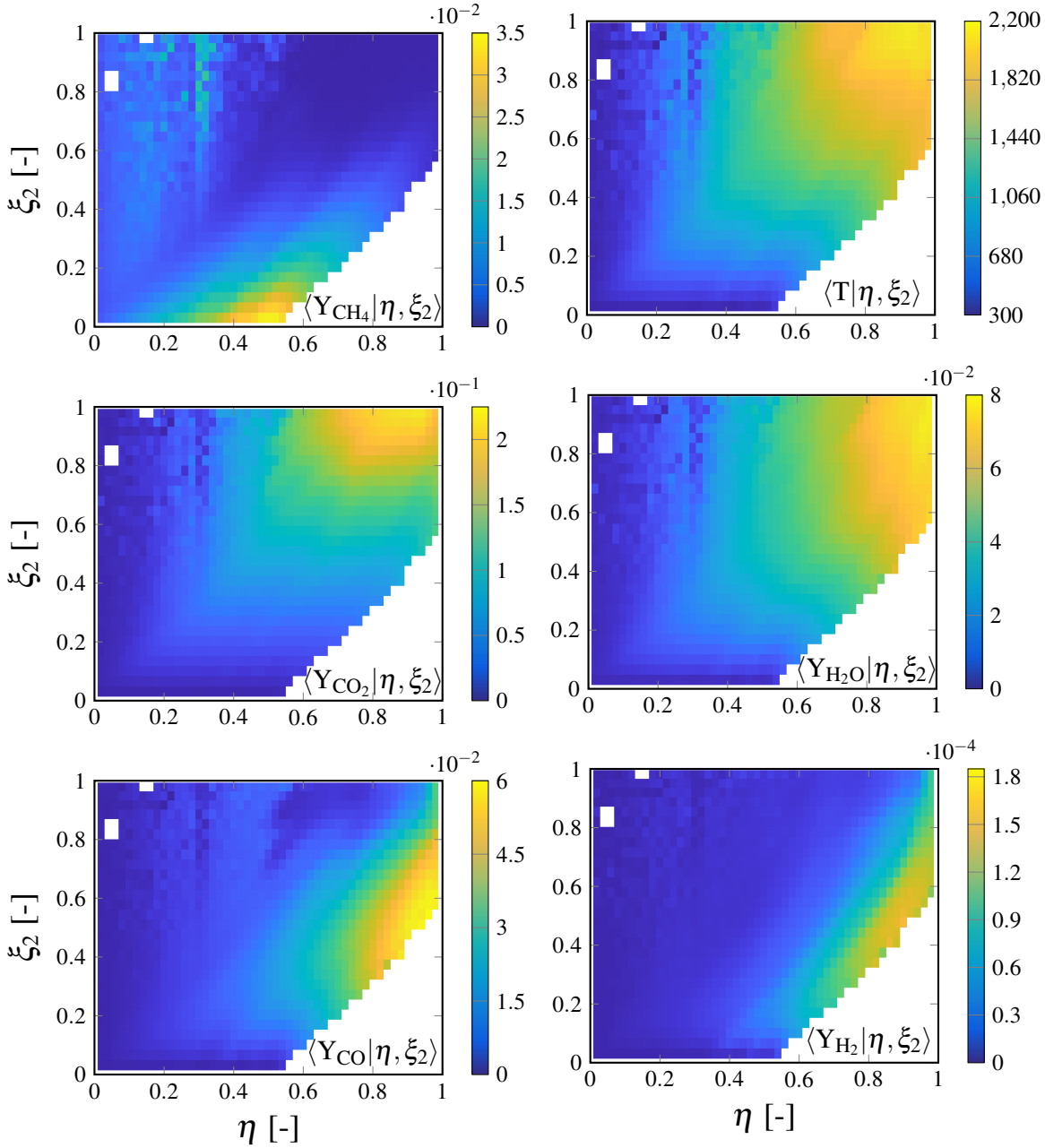

Figure 7.10: Two-condition conditionally averaged reactive scalars from SwB|all using η and ξ_2 as the sampling space variables of mixture fraction and the Y_{CO_2}-based progress variable c_2, respectively, and collecting data at all spatial locations (radial and axial). The temperature colourbar is expressed in Kelvin.

Assuming the mixture fraction lies within the limits of flammability, the empty region sug-

gests that the unburned reactants are becoming unstable and start to react, such that methane is consumed and the progress variable rises. This trend is highlighted in both figures, where the mass fractions of CH_4 peak near the lower flammability limit (i.e., $Z = 0.575$) of the methane-air mixture. It appears that adopting c_1 as a second control variable reduces the complete filling of the η, ξ_1 space, as opposed to selecting a Y_{CO_2}-based progress variable. A second region without measurements is found in the conditional domain using Z and the temperature progress variable. The presence of the top-left region suggests that it is improbable to have a complete reaction with local equivalence ratios well below the lower flammability limit of methane. This behaviour is back-supported by Figure 7.10 where all conditionally-averaged scalars falling within this region are associated with values equal to zero. Interestingly, the conditional domain built using the mixture fraction and c_2 provides a much more complete mapping than Z, c_1, in particular for regions associated with high mixture fractions and progress variable values far from unity. The contours for conditionally-averaged temperature, CO_2 mass fraction and H_2O mass fraction exhibit, as expected, similar behaviours, where their maximum values lie in the vicinity of $Z_{st} = 0.9$ and progress variable of unity.

7.4.3 Fixed High Stratification, Swirl Sweep (SwB9, SwB10, SwB11)

Within this section, the conditional fluctuations of the Q scalars describing SwB|Hstratified around one-condition conditional averages are studied to investigate which progress variable definition can reduce the swirl and spatial dependences, assuming high fixed stratification mixture conditions. The conditional fluctuations of temperature and various species mass fractions, depicted in Figure 7.11, exhibit similar results compared to SwB|all. All studied c_k promote similar behaviours for the conditional fluctuations of Y_{CH_4}, Y_{CO} and Y_{H_2}. This suggests that the progress variable is perhaps not a good choice for describing the variables of interest and that mixture fraction would be a better decision, as the mass fractions of CH_4 and CO are strongly correlated with Z. Moreover, the height of conditional fluctuations (in particular for intermediate species) seems to remain constant throughout all axial positions, as opposed to the trends observed with SwB|all. The local averages of

the presented conditional fluctuations (cf. golden markers in Figure 7.11) are fixed at zero, suggesting that using either of the proposed c_k as a conditioning variable should provide an accurate approximation of the turbulent reaction rate, i.e. a closure utilising only the first term of a Taylor expansion of the reaction rate.

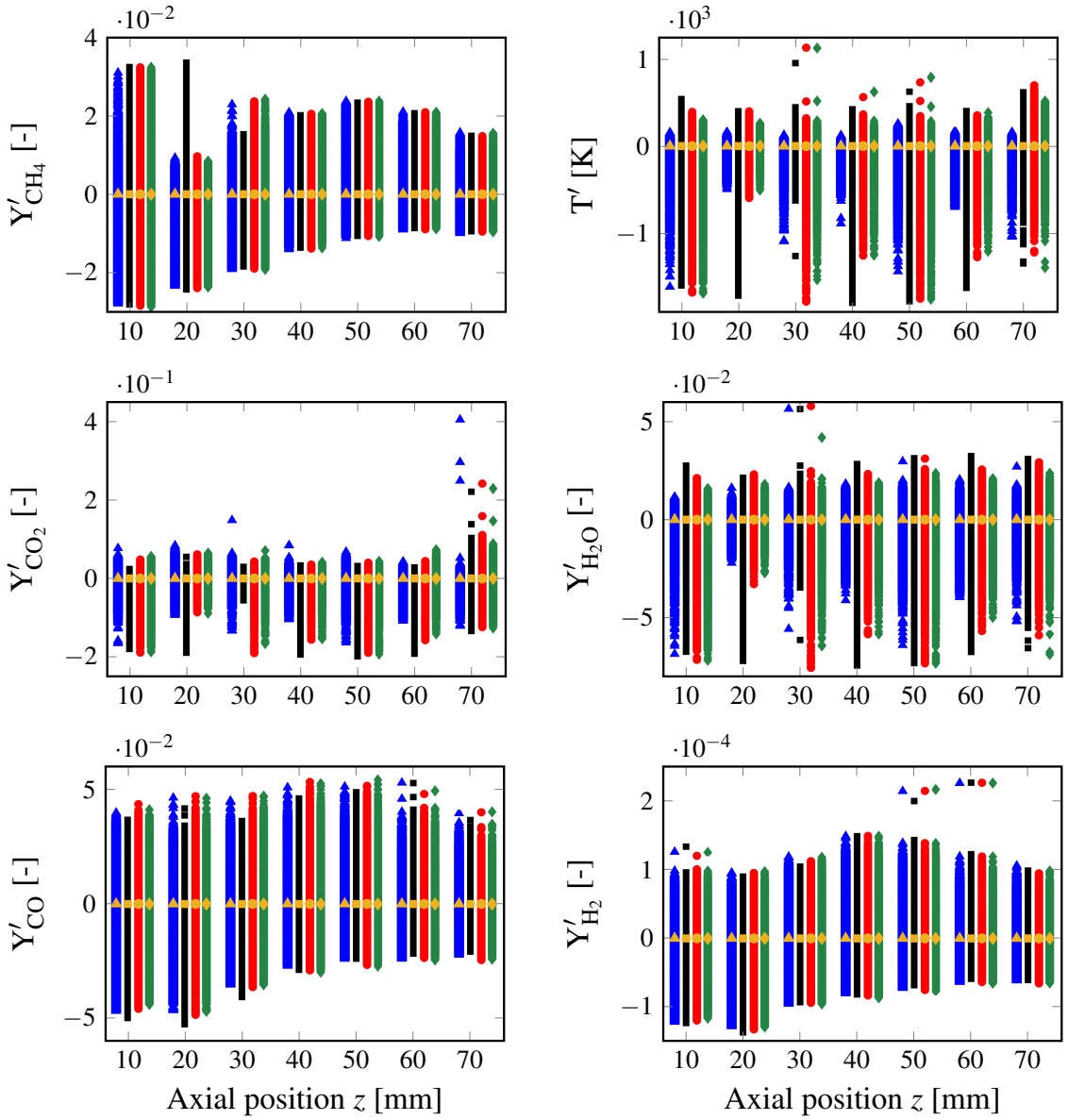

Figure 7.11: Conditional fluctuations of species mass fractions and temperature around the conditional average $\langle f|\xi = c_k\rangle(x)$ for SwB|Hstratified database using only the progress variable as the single conditioning variable and collecting all points at different radii together; the local average of these conditional fluctuations $\langle f'_{i,k}\rangle$ (golden markers) are also shown.

Figure 7.12 provides further insights. The normalised RMS of all variables investigated for the considered database around one-condition (i.e., using c_k) exhibit similar results as seen with SwB|all.

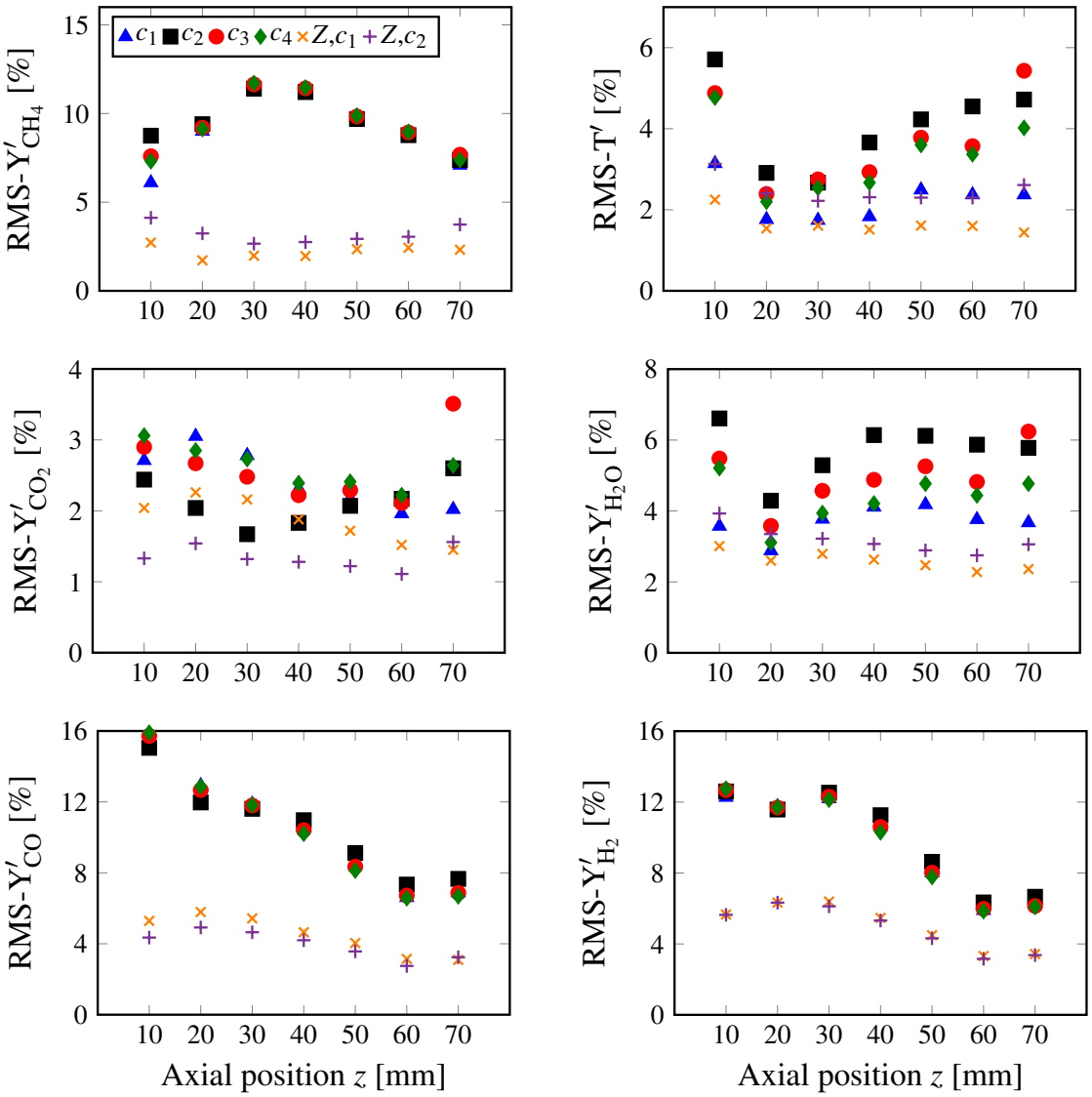

Figure 7.12: Normalised RMS of the conditional fluctuations of temperature and species mass fractions for the SwB|Hstratified database around the conditional average $\langle f|\xi = c_k\rangle(x)$ (markers) using c_k as the single conditioning variable, and around the conditional average $\langle f|\eta = Z, \xi = c_1, c_2\rangle(x)$ using the mixture fraction, and the temperature-based progress variable (crosses) or the Y_{CO_2}-based progress variable (plusses), and collecting all points at different radii together.

As expected, the RMS obtained using a single control variable have much higher swirl

dependence at the inlet of the burner than two-condition conditional averages, in particular for methane, CO and H_2 mass fractions, emphasised by normalised RMS values above 10%. Further downstream the axial direction (i.e., $z = 60, 70$ mm), the normalised RMS are nearly of the same order of magnitude as both combinations of doubly conditioning, suggesting that adding the mixture fraction as a second control variable does not significantly affect the fit. For the same species, the definition attributed to the progress variable seems irrelevant. The differences are more straightforward for major species and temperature, where all c_k provide very good results. Based on these results, the temperature-based progress variable seems to be the most optimal choice, followed by c_4 and c_3, and with the Y_{CO_2}-based progress variable being the worse among the tested reaction variables. These findings are consistent with recent results computed by analysing methane-air [300] and hydrogen-air [275] premixed flames. The normalised RMS around two-condition conditional averages are unchanged compared to the trends observed with the first database. The definition attributed to the progress variable as a second control scalar seems irrelevant for this case. Once again, two-condition conditional averages are sufficient to describe the considered database and detach it from swirl and space. This suggests that a DCSE calculation of these flames (including SwB|all) using both mixture fraction and progress variable as conditioning variables might be successful.

The contours of conditionally-averaged reactive scalars are included. The conditional averages of temperature and several species mass fractions around the mixture fraction and the temperature-based progress variable are shown in Figure 7.13. Figure 7.14 presents the conditional averages of the same scalars using Z and c_2. Similar conclusions drawn for SwB|all can be applied to the considered dataset. Regions with no available measurements are much more accentuated in both conditional domains, attributed to the exclusion of data from 6 flames that do not exhibit the desired characteristics of the current database. Regardless of the second control variable adopted, the conditional averaged scalars vary moderately throughout the two databases assessed, suggesting that the underlying physics and chemistry remain quasi-unchanged in the conditional domains.

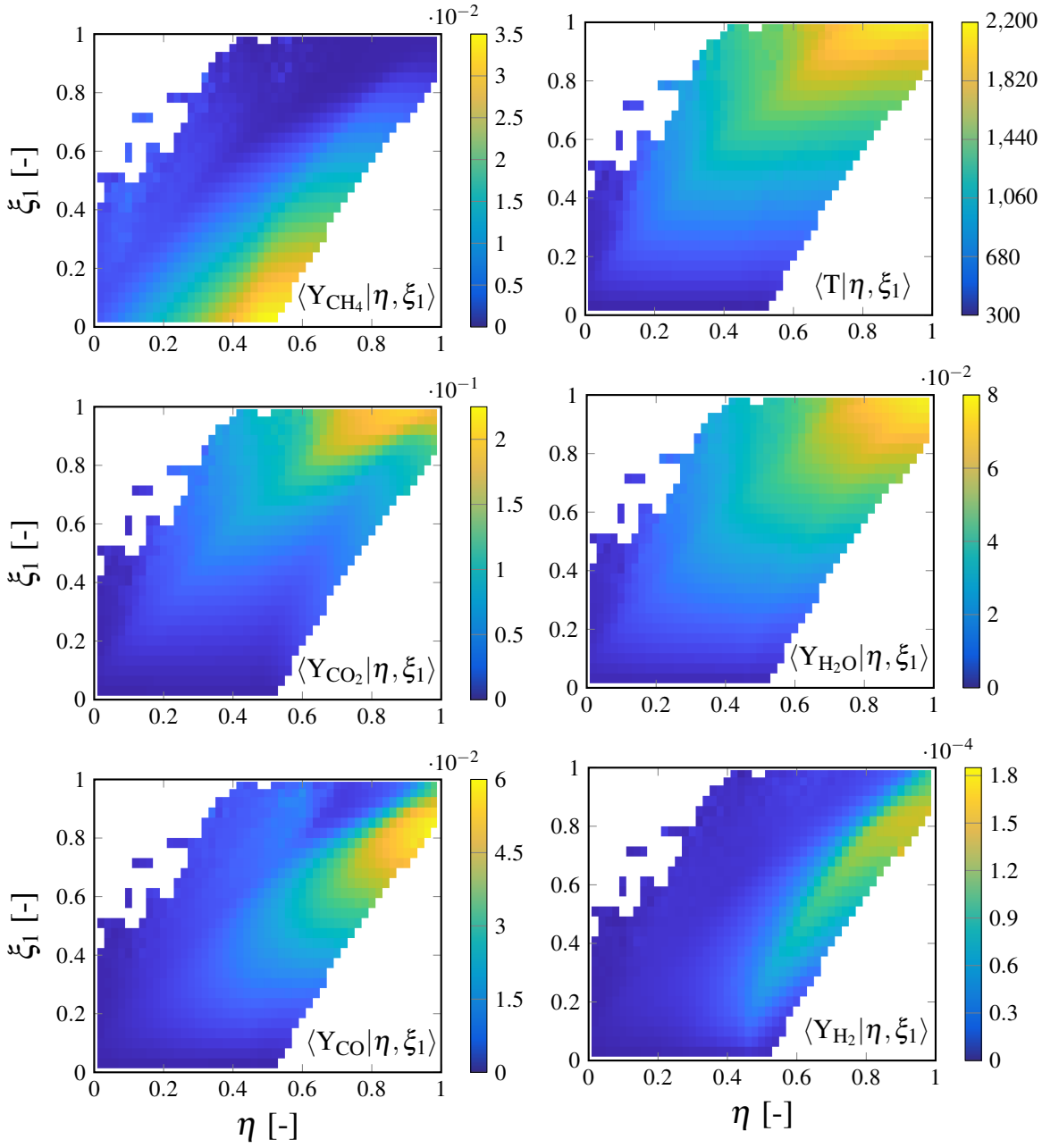

Figure 7.13: Two-condition conditionally averaged reactive scalars from SwB|Hstratified using η and ξ_1 as the sampling space variables of mixture fraction and the temperature-based progress variable c_1, respectively, and collecting data at all spatial locations (radial and axial). The temperature colourbar is expressed in Kelvin.

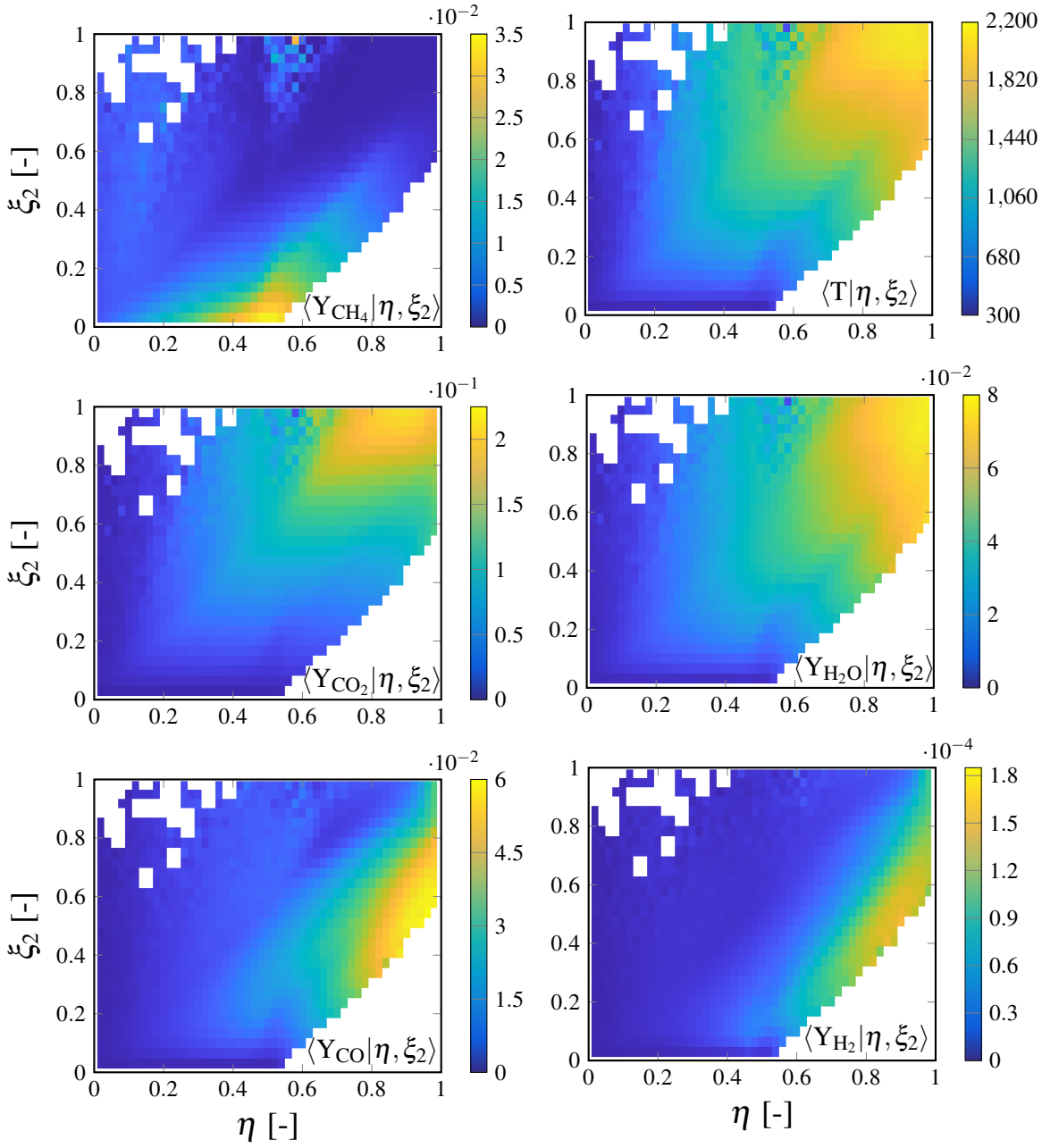

Figure 7.14: Two-condition conditionally averaged reactive scalars from SwB|Hstratified using η and ξ_2 as the sampling space variables of mixture fraction and the Y_{CO_2}-based progress variable c_2, respectively, and collecting data at all spatial locations (radial and axial). The temperature colourbar is expressed in Kelvin.

7.4.4 Fixed High Swirl, Stratification Sweep (SwB3, SwB7, SwB11)

The conditional fluctuations around one-condition conditional averages of the variables describing the SwB|Hswirl database are studied to investigate the most optimal choice of

progress variable definition to cancel stratification and spatial dependences, assuming high fixed swirl intensity. The conditional fluctuations of the scalars previously investigated are shown in Figure 7.15.

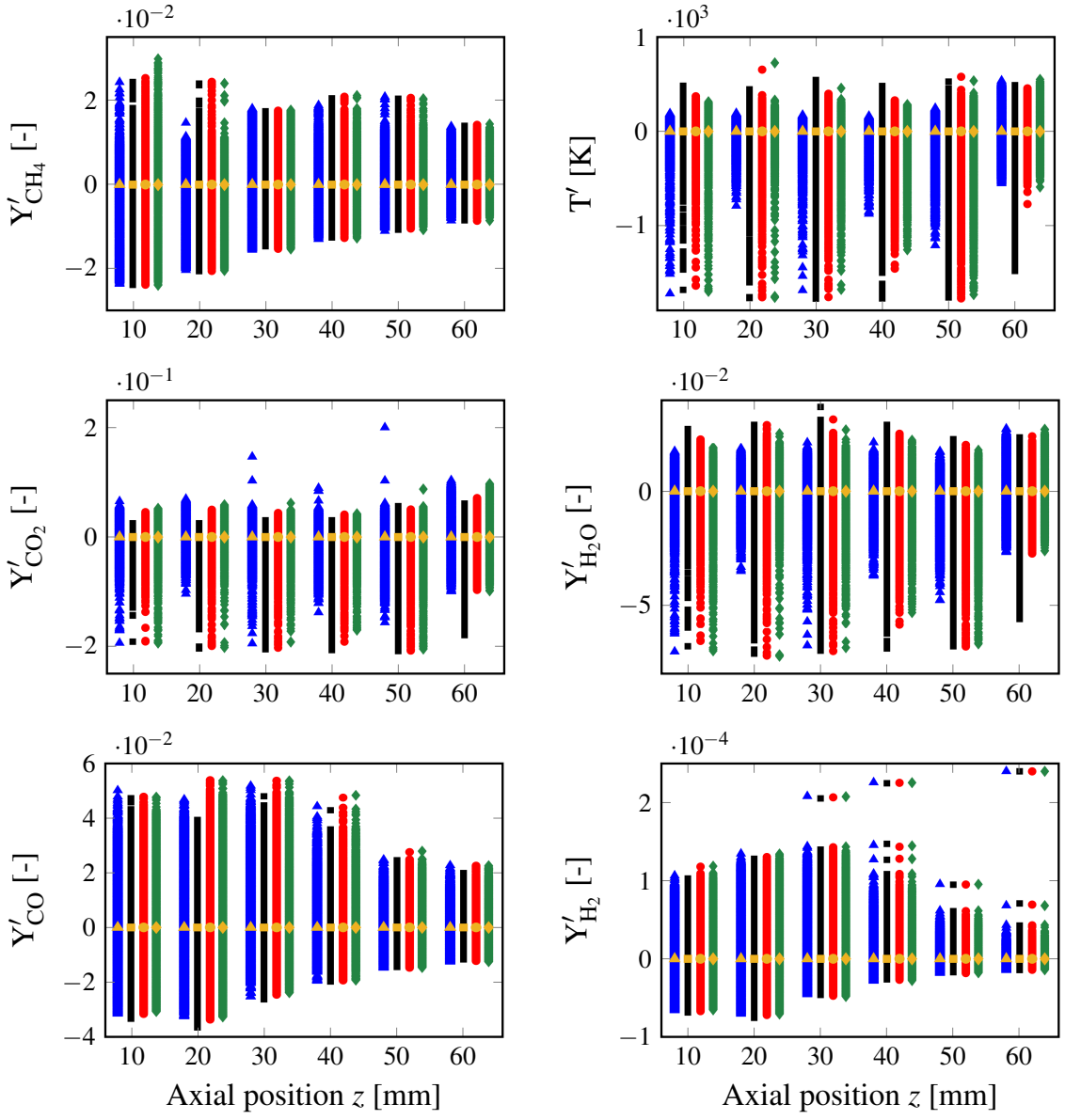

Figure 7.15: Conditional fluctuations of species mass fractions and temperature around the conditional average $\langle f|\xi = c_k\rangle(x)$ for SwB|Hswirl database using only the progress variable as the single conditioning variable and collecting all points at different radii together; the local average of these conditional fluctuations $\langle f'_{i,k}\rangle$ (golden markers) are also shown.

Similar to SwB|all and SwB|Hstratified, the conditional fluctuations of Y_{CH_4}, Y_{CO} and Y_{H_2}

appear to be still affected by space and stratification effects, particularly at the inlet of the burner. All c_k promote similar results, suggesting that another choice of scalar is perhaps more suitable. An in-depth study investigating new scalars for the definition of c can be a topic for future work as it is considered to be out of the scope of this analysis.

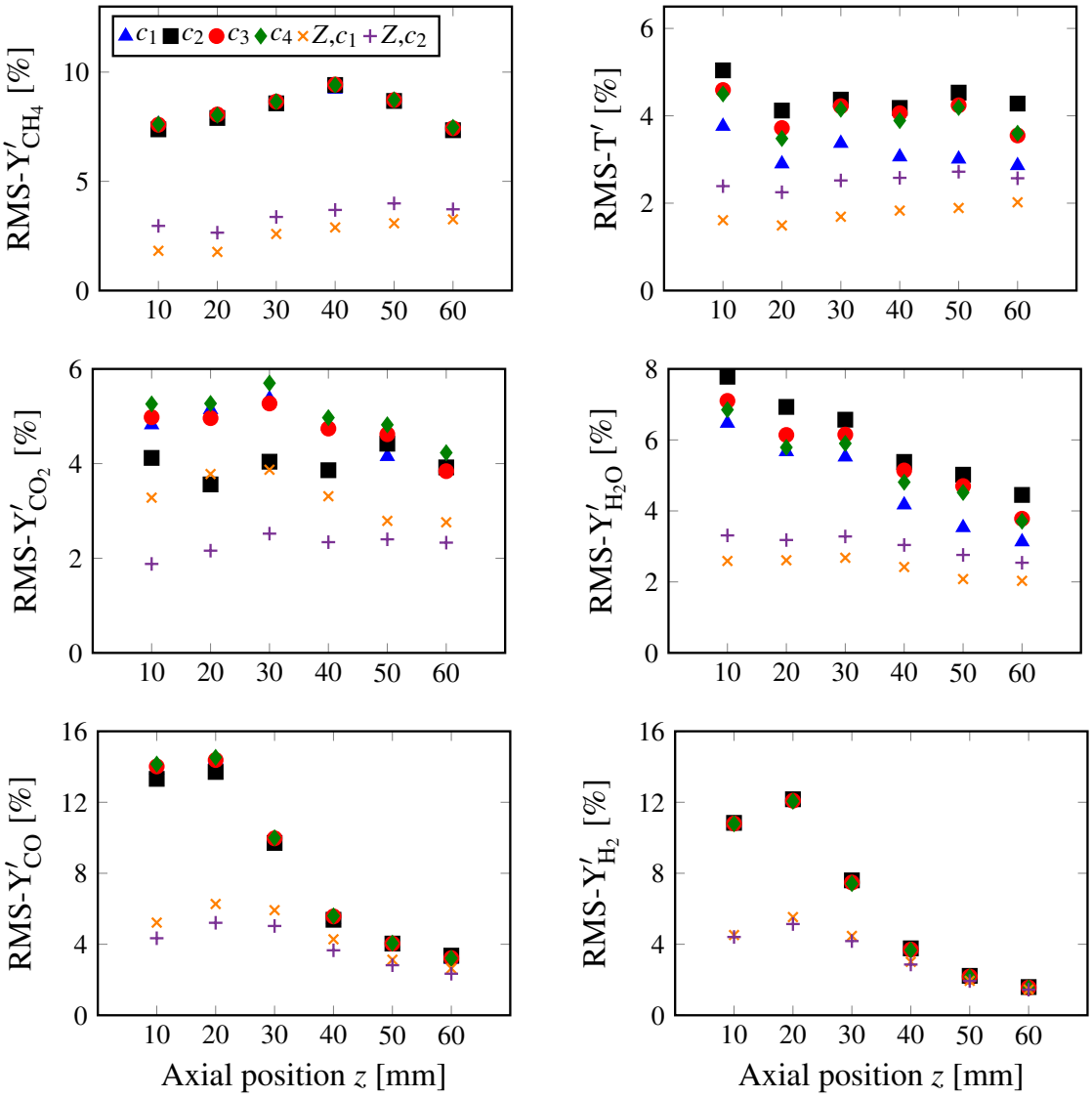

Figure 7.16: Normalised RMS of the conditional fluctuations of temperature and species mass fractions for the SwB|Hswirl database around the conditional average $\langle f|\xi = c_k\rangle(x)$ (markers) using c_k as the single conditioning variable, and around the conditional average $\langle f|\eta = Z, \xi = c_1, c_2\rangle(x)$ using the mixture fraction, and the temperature-based progress variable (crosses) or the Y_{CO_2}-based progress variable (pluses), and collecting all points at different radii together.

Just like c_2 for Y'_{CO_2}, the temperature-based progress variable provide the lowest fluctuation heights for T' and Y'_{H_2O}, with c_2 and c_3 being the worse for the considered scalars. As in the two previous databases, the local averages throughout all downstream locations are equal to zero, suggesting that the definition attributed to the progress variable is perhaps less relevant in a closure context than in an accurate representation of the chemical state. Surprisingly, Figure 7.16 shows that using a single conditioning variable for intermediate species, regardless of the definition attributed to c, equally well performs as Z,$c(T)$ and Z,$c(Y_{CO_2})$, excluding the results obtained near the inlet of the burner (i.e., $z = 10, 20$ mm) where values deviate by a factor of $\sim$2, attributed to the recirculation zone and possibly the heat exchange with the bluff body. For these axial distances, this suggests that all investigated c_k are enabling to decrease the functional dependence of conditional averages on spatial coordinates and stratification. Moreover, compared to the two other datasets, the normalised RMS of CH_4 conditional fluctuations remain below 10%, suggesting that stratification effects have perhaps less influence on conditional averages than spatial coordinates and/or swirl. Differences of magnitude between the four c_k are more pronounced for temperature and major species (excluding Y_{CH_4}), where c_1 provides the best fit for the mass fraction of H_2O, but temperature as well (as expected). As was foreseeable, the inclusion of carbon dioxide in c_2 gives the most optimal results for decreasing the RMS of Y'_{CO_2}, with no apparent differences compared to other c_k further downstream. The differences between the two combinations of doubly conditioning remain minor, with slightly better results in favour of Z,c_1, excluding the RMS of CO_2 conditional fluctuations. This suggests that the definition attributed to the progress variable can be less relevant in CMC-based approaches than in flamelet models. This perhaps relates to the fundamental basis of flamelet and conditional moment closure models, where the former focused on separating turbulence and chemistry scales. When tabulated chemistry is constructed in flamelet approaches, this involves a direct projection using control variables, whereby the stretch and individual species transport phenomena in turbulent reactive flows might be neglected, resulting in significant differences in mass burning rate predictions [274]. The implementation of flamelet models therefore might require including the projection of the source-term

and the diffusion term to make the results independent of the choice of progress variable. Conversely, in the conditional moment closure approach, one focuses on the separation of model elements which give descriptions for the moment of reactive parameters with regard to the scalar description in state-space. In that sense, the main purpose of the controlling variable is to construct a functional approximation of the conditional space where the number of control variables and their ability to capture major physical behaviour of the system (e.g., mixing) can be more relevant. This study, together with a previous study from Mousemi *et al.* [154], has demonstrated the importance of including an appropriate controlling variable to capture all physical processes where the definition of progress variable can be flexible depending on the ease of implementation potentially making the conditional moment closure type of model more attractive.

The conditional averages of temperature and mass fractions of several species around mixture fraction and the temperature progress variable are shown in Figure 7.17. The conditionally-averaged scalars around Z and c_2 are illustrated in Figure 7.18. No apparent differences can be identified among the conditional domains computed from each of the three databases (assuming the use of the same two control variables), suggesting that the conditional averaged scalars behaviour is not affected by the underlying characteristics and effects of the studied burner.

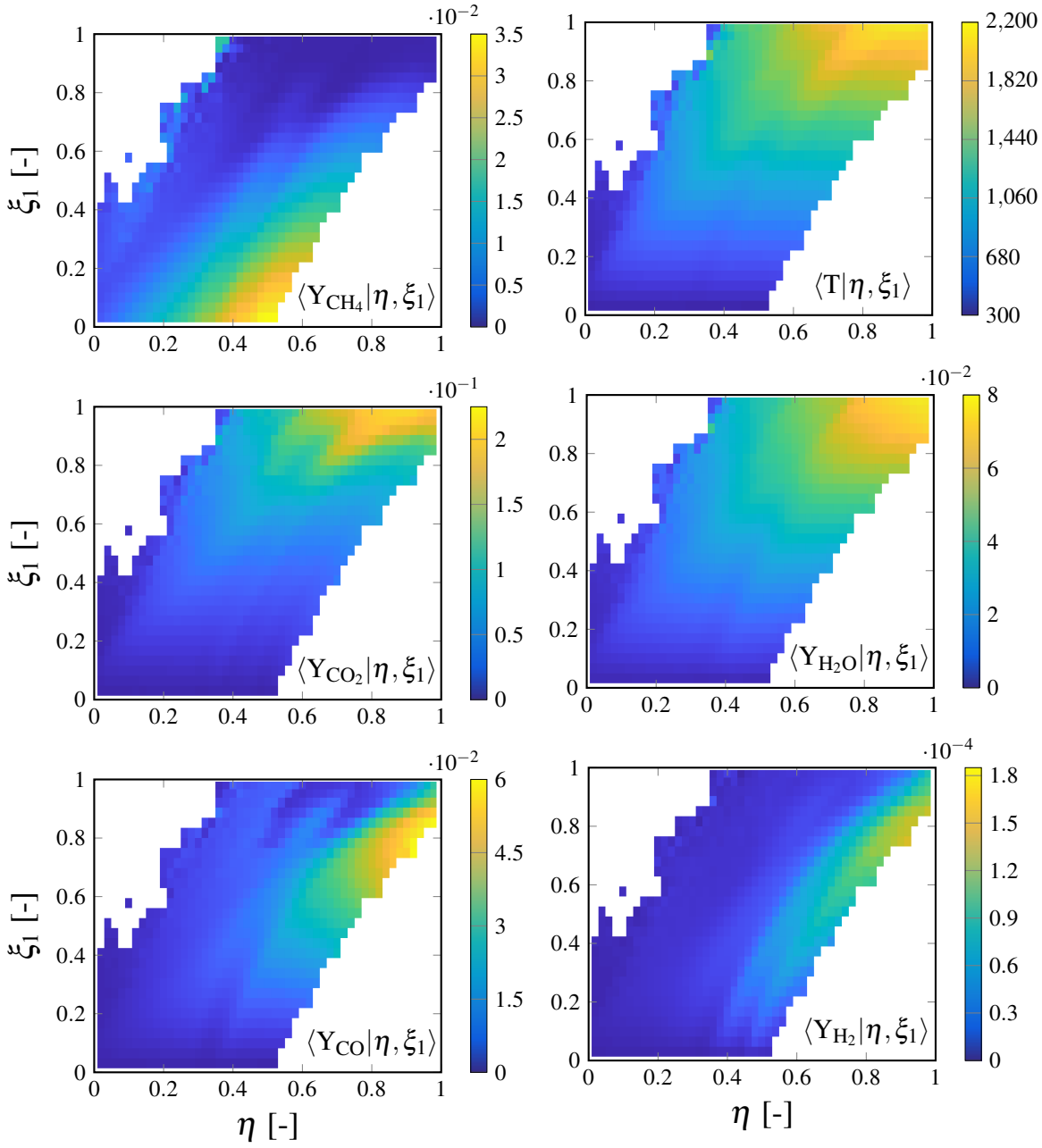

Figure 7.17: Two-condition conditionally averaged reactive scalars from SwB|Hswirl using η and ξ_1 as the sampling space variables of mixture fraction and the temperature-based progress variable c_1, respectively, and collecting data at all spatial locations (radial and axial). The temperature colourbar is expressed in Kelvin.

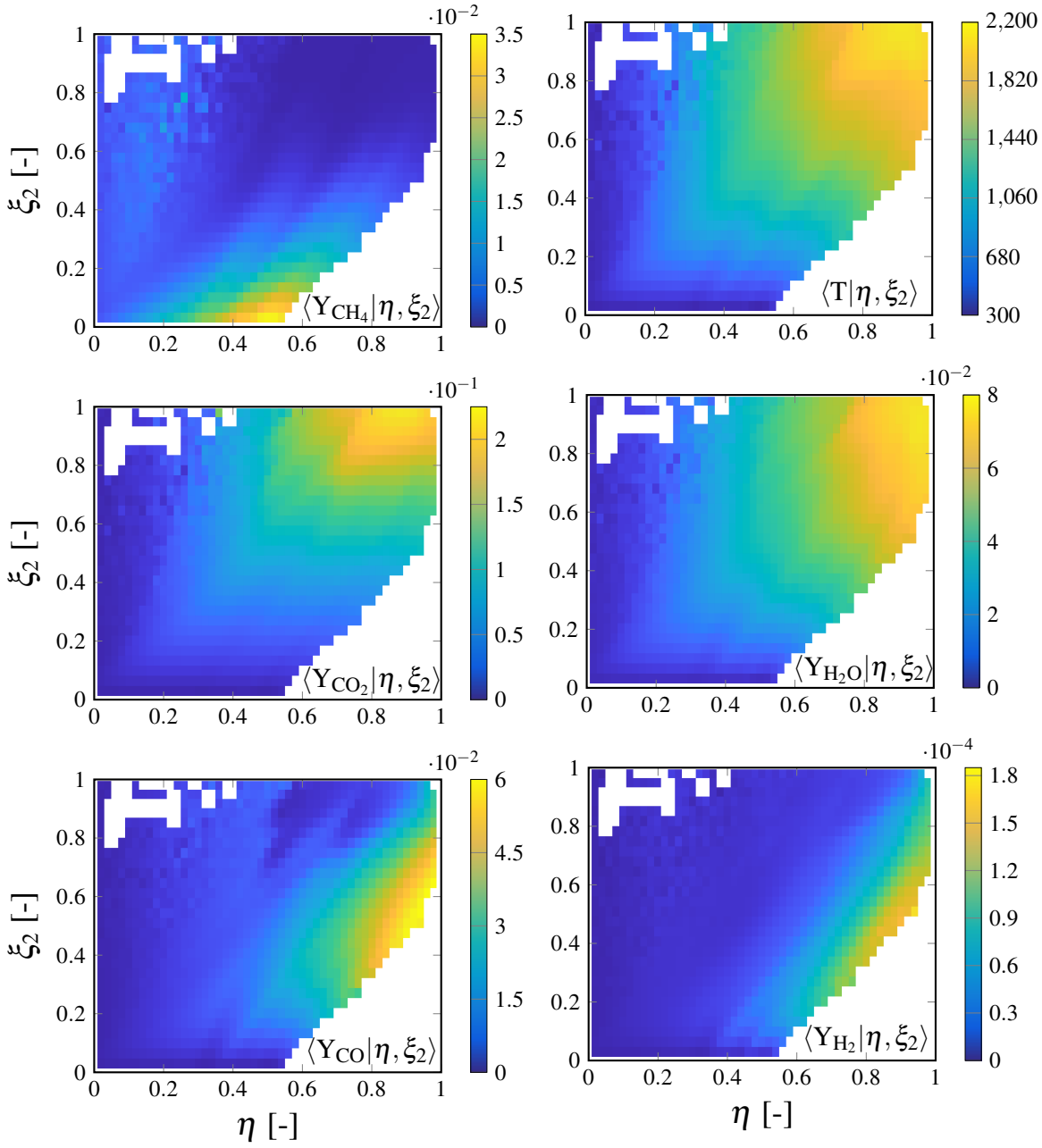

Figure 7.18: Two-condition conditionally averaged reactive scalars from SwB|Hswirl using η and ξ_2 as the sampling space variables of mixture fraction and the Y_{CO_2}-based progress variable c_2, respectively, and collecting data at all spatial locations (radial and axial). The temperature colourbar is expressed in Kelvin.

7.4.5 Sandia/TUD Burner

A complementary study was carried out to provide further evidence around the work undertaken with the previous burner. The experimental measurements of piloted methane-air

jet flames from the Sandia/TUD burner were used. Multiscalar data of four turbulent non-premixed flames (C, D, E and F) are examined with: (i) increasing velocity in the main jet and pilot, and (ii) increasing probabilities of local extinction (cf. Table 7.4). The scalar measurements include the temperature, the mixture fraction calculated using Bilger's definition and the mass fractions of CO_2, CO, H_2, CH_4, N_2, O_2, H_2O, OH and NO. Further information on the measurement techniques, the experimental setup and data pre-processing can be found in [283]. Flames C, D and (arguably) E burn as non-premixed flames, with a single reaction zone near the stoichiometric mixture fraction. As a result of the increased turbulence intensity, Flame F exhibits partially-premixed characteristics with evidence of premixed reaction flame fronts, particularly in zones of high probabilities of local extinction and re-ignition.

Table 7.4: Main flow parameters of Sandia flames C-F with $U_{j,b}$: the bulk velocity for the fuel jet, $U_{p,b}$: the bulk velocity for the pilot, T_p: the pilot temperature.

Flame	Re_{jet}	$U_{j,b}$ [m/s]	$U_{p,b}$ [m/s]	T_p [K]	Local Extinction
C	$\sim$13400	29.7	6.8	$\sim$1920	None
D	$\sim$22400	49.6	11.4	$\sim$1880	Little
E	$\sim$33600	74.4	17.1	$\sim$1880	Moderate
F	$\sim$44800	99.2	22.8	$\sim$1860	Intense

The simplicity of the flow and the existence of a fully turbulent region of the flame where the chemical kinetic effects are significant makes this burner an ideal test case for attempting to answer the two questions raised previously. It should be noted that throughout this study, mixture fractions taken from experimental measurements have been used for the current analysis (as opposed to the previous burner where Z has been calculated by the author). The reaction progress variable c was calculated for every data point in each dataset using the temperature (c_1) and the mass fraction of CO_2 (c_2). The local maximum possible CO_2 mass fraction was obtained using the mixture fraction. For the considered set of flames, the peak mass fraction $Y_{CO_{2,max}}$ was at the stoichiometric mixture fraction $Z_{st} = 0.351$ with a value of 0.151. The temperature in the burned gases was fixed to the maximal value found in the databases. The experimental measurements of all four flames were examined to take out potential outliers (e.g. $Z, c_k < 0$ and $Z, c_k > 1$), as was carried out with the Cam-

bridge/Sandia swirl database. It should be noted that for Sandia flames, c_k corresponds to either c_1 or c_2.

The conditional fluctuations of species mass fraction and temperature around one-condition (Z) conditional averages and two-condition conditional averages are calculated at each distance downstream. The conditional averages are obtained dividing each mixture fraction into 50 bins. Due to fewer point-based measurements available compared to the Cambridge/Sandia burner, the number of progress variable bins with the current database was reduced to 20.

For clarity, only the results of flames C and F will hereafter be presented. Figures with axial locations account for all data points at different radial locations. Figure 7.19 shows the normalised RMS at all six downstream locations for temperature and seven species mass fractions within the Flame C database. The normalised RMS of the conditional fluctuations using the mixture fraction remain below 10%, implying that Z is very well-suited to describe the thermo-chemical state. The normalised RMS are nearly of the same order of magnitude as both combinations of doubly conditioning, suggesting that adding a progress variable as a second control variable (regardless of c_1 and c_2) does not significantly affect the fit. This trend is expected, as for non-premixed "quasi-laminar" flames, such as Flame C, using Z as a single conditioning variable is sufficient, as premixed phenomena are not relevant in that flame. This suggests that a CSE routine adopting only the mixture fraction would probably provide good predictions of Flame C. It is worth noting that if excluding the RMS of CO_2 and temperature, both combinations of doubly conditioning equally well perform with no apparent differences. This is in good agreement with the trends observed with the Cambridge/Sandia swirl burner.

Figure 7.20 illustrates the normalised RMS of various scalars for Flame F, which is known to operate under high turbulence intensity. The RMS using single conditioning through mixture fraction appear to increase compared to the previous case. The normalised RMS of the conditional fluctuations of five scalars, namely the temperature and the mass fractions of CO_2, CO, OH and H_2O, exhibit important functional dependences on the real domain, with RMS values above the 10% limit used within this study as a guideline.

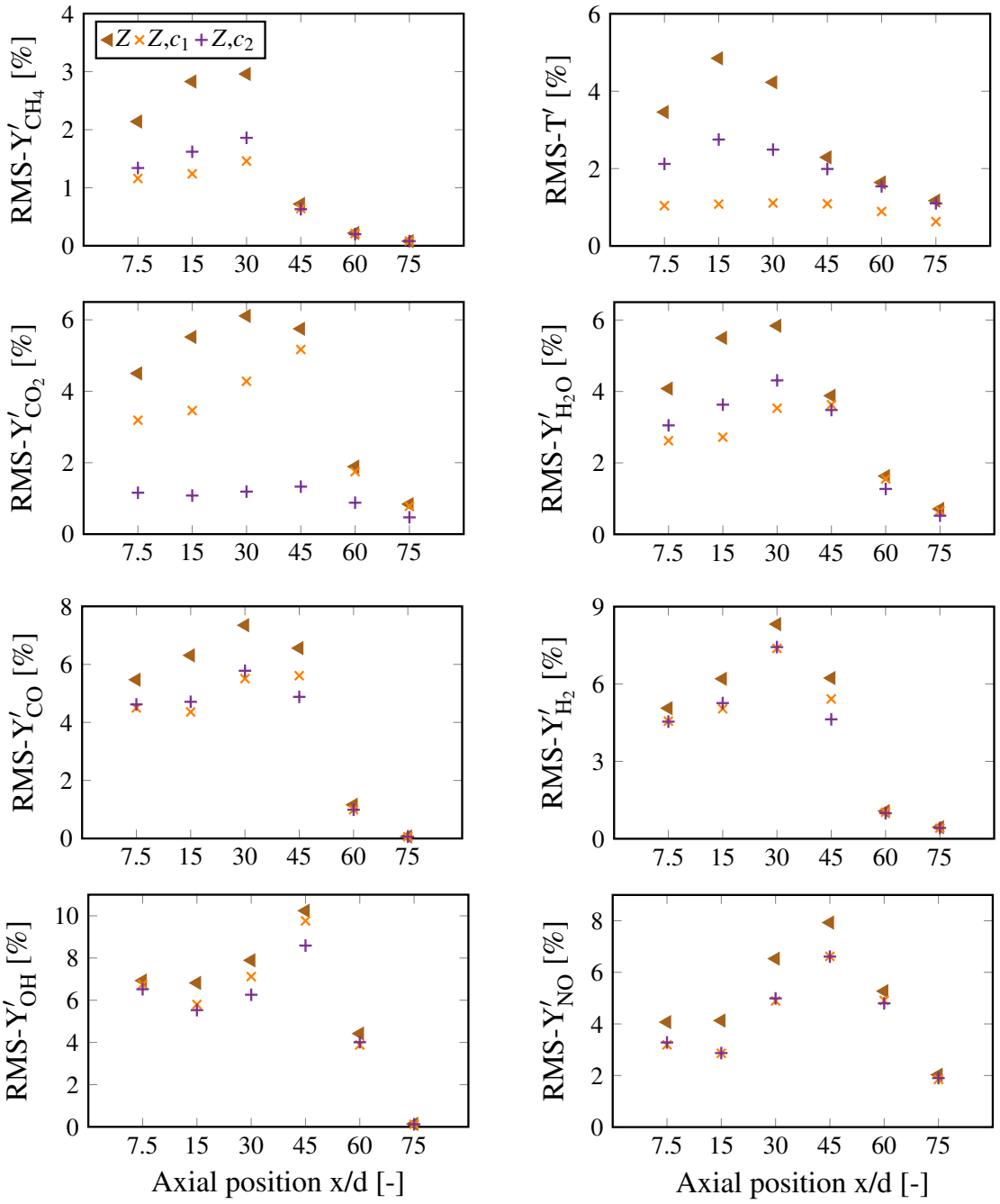

Figure 7.19: Normalised RMS of the conditional fluctuations of temperature and species mass fractions for Sandia Flame C around the conditional average $\langle f|\eta = Z\rangle(x)$ (triangles) using Z as the single conditioning variable, and around the conditional average $\langle f|\eta = Z,\xi = c_1,c_2\rangle(x)$ using the mixture fraction, and the temperature-based progress variable (crosses) or the Y_{CO_2}-based progress variable (pluses), and collecting all points at different radii together.

This trend is highlighted at axial directions corresponding to 7.5, 15 and 30, with the latter

known as the location exhibiting the most intense local extinction probabilities.

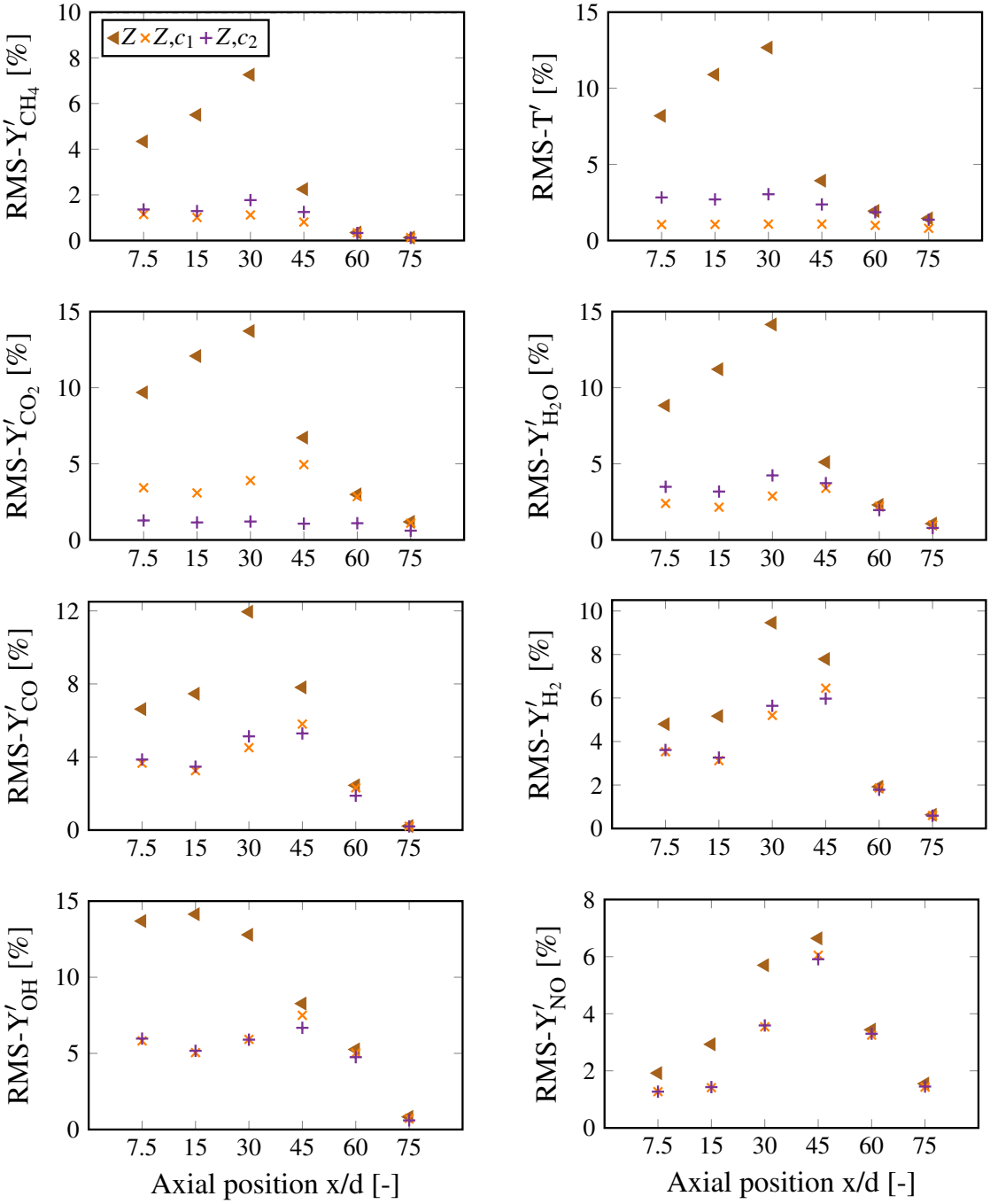

Figure 7.20: Normalised RMS of the conditional fluctuations of temperature and species mass fractions for Sandia Flame F around the conditional average $\langle f|\eta = Z\rangle(x)$ (triangles) using Z as the single conditioning variable, and around the conditional average $\langle f|\eta = Z, \xi = c_1, c_2\rangle(x)$ using the mixture fraction, and the temperature-based progress variable (crosses) or the Y_{CO_2}-based progress variable (pluses), and collecting all points at different radii together.

This suggests that a moment closure prediction of this flame will probably fail, assuming a single conditioning variable is adopted. Interestingly, the RMS of all investigated scalars around Z are of the same order of magnitude as both doubly conditioning further downstream. The same behaviour can also be depicted for Flame C in Figure 7.19. Both combinations of doubly conditioning are able to detach the thermo-chemical state-space from space and Reynolds number. Both progress variable definitions provide similar results, excluding the normalised RMS of CO_2 and temperature. Regardless of the progress variable definition selected, and assuming ensembles are defined along the axial direction, a DCSE approach using Z and c is believed to provide good predictions for the set of Sandia Flames C-F.

A thermal-based progress variable definition is believed to give a more accurate representation of the burner's chemistry for the same reasons deduced from the Cambridge/Sandia swirl burner, considering that species diffusivity is often simplified by assuming unity Lewis numbers.

7.5 Summary

Within this study, the Cambridge/Sandia swirl measurements was used in conjunction with principal component analysis (PCA) to attempt to find which set of control variables has the highest correlation with the reactive scalars. Three databases were constructed to investigate the influence of swirl, stratification and spatial coordinates. Two scaling methods for the PCA model were adopted, namely Pareto and Auto-scaling (AS). For all three datasets, and regardless of the scaling method adopted, it was found that: (i) the first principal component (PC1) accounts for the largest amount of variance, and (ii) PC1 is well-aligned with temperature.

The conditional spaces of Cambridge/Sandia flames were examined by investigating the conditional fluctuations of temperature and various species mass fractions obtained with single-conditional averages around four different progress variable definitions. While conditional fluctuations of intermediate species and methane were unchanged using the progress

variables tested, it was found that adopting a temperature-based progress variable provides minor improvements for major reactive scalars, in particular for temperature and H_2O. For all three databases, the local averages of conditional fluctuations throughout all downstream locations are anchored at zero, suggesting that the definition attributed to the progress variable is perhaps less relevant in a closure context. Regardless of the dataset, the normalised RMS of the reactive scalars indicate that a single control variable based on c is unable to detach the thermo-chemical state from spatial coordinates, swirl, or stratification, particularly for regions near the burner's tip characterised by an intense recirculation of the flow and significant heat exchanges with the bluff-body. The RMS analysis was followed by comparing the conditional averages obtained with the progress variables against doubly conditional averages using the mixture fraction and the progress variable $c(T)$. Normalised RMS around two-condition conditional averages adopting mixture fraction and a Y_{CO_2}-based progress variable were also included. Here, it was shown that the conditional fluctuations using both sets of two-condition conditional averages did not improve the dependence on the physical domain compared to a single progress variable condition further downstream the axial direction. The results were significantly improved at the burner inlet, with values not exceeding the 10% threshold used within this study as a guideline. The differences observed between both combinations of doubly conditioning were minor, suggesting that the choice of a particular progress variable definition does not seem to have an importance. Consequently, it is believed that a conditional moment closure calculation using both Z and c as two conditioning scalars might be successful, assuming that the ensemble has been divided along the axial direction. The results indicate that the success of CMC approaches does not depend on the definition attributed to the progress variable as opposed to flamelet-based architectures for which different definitions given to c will give different results.

A complementary study using the database from the Sandia/TUD burner of four non-premixed flames with various levels of turbulence intensity was also included. The conditional spaces of Sandia/TUD flames C and F were examined by investigating the conditional fluctuations of temperature and species mass fractions obtained with single-conditional

averages on Z. While adopting mixture fraction as a single conditioning scalar can more efficiently decrease the spatial dependence of the reactive scalars for Flame C, it was found that the tendencies were worse for Flame F due to enhanced turbulence intensity. The analysis was followed by comparing the conditional averages obtained with Z against both sets of two-condition conditional averages adopted for the Cambridge/Sandia burner study. Here, it was shown that the conditional fluctuations using two-condition conditional averages did not improve the dependence on the physical domain of Flame C compared to a single mixture fraction condition. The results were significantly improved for Flame F. Similar to the Cambridge/Sandia swirl burner, the differences observed between both combinations of doubly conditioning were minor, suggesting that the choice of a particular progress variable definition does not seem to have importance within a DCSE framework. Given that doubly conditioning seems to decrease the reactive scalars' dependence more effectively, it is suggested that $c(T)$ would give a more accurate representation of both burners' flames' chemistry (such as in a manifold) than a species-based progress variable, considering that species diffusivity is often simplified by assuming unity Lewis numbers. Moreover, this study demonstrates that for reactive flows exhibiting partially-premixed flame characteristics at high turbulence intensity, CSE (regardless of the chemistry tabulation method adopted) would probably fail in predicting the underlying coupling between turbulence and chemistry as conditional fluctuations around a single control variable are too large and, consequently, still depend on the real domain. This indicates that regardless of the mixture conditions, adopting a DCSE approach seems essential for modelling complex reactive flows operating under high Reynolds numbers.

Chapter 8

Original Work, Conclusions and Future Work

Anybody who has been seriously engaged in scientific work of any kind realizes that over the entrance to the gates of the temple of science are written the words: "Ye must have faith." It is a quality which the scientist cannot dispense with.

–Max Planck

Contents

8.1 Originalities

Specific originalities and novel aspects to the research work presented in this thesis include:

- The first test of an empirical laminar burning velocity (LBV) correlation for combustion of iso-octane/ethanol mixtures selected to mimic gasoline-alcohol combustion behaviour in air. The results obtained by means of a mixing rule approach were validated against previously unpublished data for iso-octane/ethanol binary fuels at elevated temperatures and pressures, both from this group and from the earlier experimental studies of Varea *et al.* (CORIA laboratory) and Broustail *et al.* (PRISME laboratory).

- The first three-dimensional spark-ignition engine simulations using the new Oxford correlation coupled with ECFM-3Z within a RANS turbulence framework. The results showed that the higher LBVs given by the Oxford correlation led to more practical combustion behaviour, especially in the ultra-lean region. The "lean-limit" of engine simulations using the Oxford correlation was further extended compared to the well-known Metghalchi & Keck correlation.

- A significant parametric study of diesel spray flames operating under engine-relevant conditions demonstrating CSE-FGM's modelling capabilities over a wide range of temperature and oxygen concentration conditions. It was shown that the inclusion of detailed chemistry and turbulence-chemistry interaction effects enabled better quantification of the complex physical and chemical phenomena occurring in low-temperature conditions.

- Point-based measurements from two of the most well-known burners in the literature were used in conjunction with a data-driven analytical tool to show that the definition attributed to the progress variable within a doubly conditional moment closure approach has no particular importance in the closure of the chemical source-term. It is recommended to use a progress variable definition based on temperature for chemistry tabulation techniques.

8.2 Summary & Conclusions

The objective of this study was to answer several questions with regard to the understanding of ultra-lean combustion involving partially-premixed flames in order to better represent these processes numerically. Key physical and chemical phenomena relevant to flows operating at high turbulence intensity were explored, in particular – the inclusion of premixed and non-premixed flames, detailed chemistry and turbulence-chemistry interaction. Figure 8.1 illustrates the scientific pathway and conclusions that guided the research activities carried out within this DPhil.

Two families of combustion models were presented which adequately account for partially-premixed flames, namely flame topologically-based models (or geometrical) and PDF methodologies. Geometrically-based combustion models have been associated with low computational costs (assuming not dealing with detailed chemistry mechanisms), relatively low implementation times, and reasonable accuracy. Despite not relying on any flame structure assumptions and combustion regimes, quite a few issues are yet to be addressed with PDF and conditional moment closure (CMC) models, such as high computational costs (in particular for the transported PDF) and low ease of integration. The flame surface density, ECFM-3Z, *G*-Equation and the flamelet/progress variable model (FPV) are among the investigated geometrical models. While historically being limited to account for a single structure of flame, over the years various studies have extended the concerned models to account for partially-premixing by adding a second control variable to describe either the mixing effects in diffusion flames or the propagation of the premixed flame front. Consequently, the applicability of geometrical model approaches under conditions investigated within this thesis was assessed. The laminar burning velocity (LBV) scalar (or turbulent flame speed in the context of the *G*-Equation model) was found to be a key parameter within these models, particularly for the closure of chemical source terms.

Chapter 1: Context/Motivation
· Facing the current environmental context, ultra-lean mixtures feasible solution
· Research needed to assess the feasibility of ultra-lean combustion in current engines
· A numerical model that accounts for turbulence-chemistry interactions (TCI), detailed chemistry, and partially-premixed flame structures is required

↓

Chapter 2: Background
· Governing equations for turbulent reacting flow modelling
· Turbulence models adopted for RANS
· Closure of averaged terms in balance equations

↓

Chapter 3: Combustion models for partially-premixed flames
· Closure of mean chemical source terms $\overline{\dot{\omega}_k}$
· Statistical models based on the PDF (presumed or transported PDF, CMC)
· Geometrical models relying on LBV scalars (*flamelets*, G-Equation)

↓

Chapter 4: Assessment of topological models
· Feasibility of adopting geometrical models by investigating the LBV scalar
· Oxford empirical correlation is validated for binary fuels, and extends the lean-limit of in-cylinder SI engine simulations compared to M&K correlation
· Unresolved issues with LBVs suggest to use another combustion model

↓

Chapter 5: Conditional Source-term Estimation (CSE)
· Combustion model adapted for RANS and LES $\rightarrow \overline{\dot{\omega}_i|\eta} \approx \dot{\omega}_i(\overline{T|\eta}, \overline{Y_i|\eta}, \overline{\rho|\eta})$
· Chemistry tabulation techniques coupled with CSE
· Possibility to adopt CSE for partially-premixed flames?

↓

Chapter 6: Assessment of a CSE-FGM approach
· RANS parametric study applied to the ECN diesel "Spray A" case
· CSE-FGM accurately captures partially-premixed structures while accounting for detailed chemistry and TCI effects under engine-like conditions
· CSE and chemistry tabulation depend on an adequate selection of control variables

↓

Chapter 7: Progress variable definition
· The definition of c is irrelevant in the context of CSE/DCSE
· A temperature-based progress variable is recommended to use
· DCSE will likely be needed for flows found in practical combustion systems

Figure 8.1: Summary of the conclusions drawn within the framework this thesis.

Following the combustion model analysis and the importance attributed to LBVs, a study based on the development of an empirical laminar burning velocity correlation for fuel blends (i.e. iso-octane and ethanol) by means of a mixing rule approach was carried out to investigate the feasibility of topologically-based combustion models in predicting flames operating under ultra-lean mixture conditions. The proposed "Oxford" empirical correlation was shown to accurately capture the burning velocity behaviours of neat fuels and iso-octane/ethanol blends in air for a wide range of pressure, temperature and equivalence ratio conditions, both within and outside the correlation's validity range. Simplified three-dimensional SI engine simulations were also performed under three lean equivalence ratios using the new Oxford correlation coupled with ECFM-3Z within a RANS turbulence framework. The simulation results obtained with the well-known Metghalchi & Keck correlation were included. The results showed that the higher LBVs given by the Oxford correlation led to more practical combustion behaviour compared to the Metghalchi & Keck correlation, especially in the ultra-lean conditions of $\phi = 0.6$. Use of the Oxford correlation with the ECFM-3Z model effectively extended the "lean-limit" of combustion simulations, below which yielded negative LBV values and unfeasible simulation results. The findings regarding the applicability of geometrical models with LBVs included:

- The equivalence ratio conditions at which LBV data points have been measured by the community have not been extended to ultra-lean mixture conditions.

- Up to this date, the experimental data of laminar burning velocities correspond to pressure and temperature conditions that are far lower than those found in real engines. Hence, the accuracy of any empirical LBV correlation or chemistry mechanism to compute flame speeds is unknown and can lead to biased simulation results.

- While the "flamelets" assumption is arguably true for many flames, at high turbulence intensity where the chemical and turbulence length scales are of the same orders of magnitude, this assumption might not be applicable as the Kolmogorov scales can become comparable or even smaller than the reaction zone and thus penetrate the inner layer of the flame. The applicability of the flame surface density, ECFM-3Z,

FPV and, more generally, flamelet models is consequently restricted to flows operating under $K_a < 1$.

The results of this work indicated that a numerical approach for ultra-lean combustion simulations involving partially-premixed flames using geometrical models could lead to misleading predictions, particularly for flows encountered in real engines where the turbulent effect can be significant. The conditional source-term estimation (CSE) is a combustion model with the same extension to higher orders such as CMC, having no constraint on flame propagation types or combustion regimes and being more computationally attractive. By adding a second conditioning variable within the chemical source-term closure, doubly CSE (DCSE) was shown suited for modelling partially-premixing through various studies. However, the inversion process used to calculate the conditional values of the thermodynamic variables (e.g. mass fractions) coupled with the current presumed shapes of the joint-PDFs have been found to be the two largest sources of error associated with DCSE [253]. Chemistry tabulation techniques offer the possibility to account for detailed chemistry while reducing computational costs. Among many others, flamelet-based chemistry manifolds have shown satisfactory modelling capabilities, including when coupled with CSE.

The CSE-FGM model developed by Fang [30] was utilised to assess the applicability of CSE coupled with the flamelet generated manifold (FGM) to account for detailed chemistry and turbulence-chemistry interaction effects. The proposed combustion approach was applied to study the Engine Combustion Network (ECN) diesel "Spray A" case within a RANS framework. The proposed test case was embedded in a turbulent spray composed of both rich partially-premixed regions and a non-premixed flame with diffusion effects mimicking diesel spray combustion. First, the efficacy of the CSE-FGM model was explored with respect to the "Spray A" autoignition and flame development characteristics for the baseline conditions and also for parametric variations of ambient temperature and oxygen concentration. The modelling results were compared with the available experimental data

and simulations performed using the well-stirred reactor (WSR) model. This included a detailed description of the trends followed by the ignition delay, the flame lift-off length, and the analysis of flame spatial contours. The newly implemented combustion model was extensively verified, showing good predictability for the transient diesel spray flame:

- The CSE-FGM approach successfully demonstrated the capability of realistically predicting the essential structure of the diesel-fueled transient spray combustion processes compared to the WSR model.
- RANS quantitatively predicted the autoignition time and flame lift-off length.
- The two-stage ignition process characteristic of n-dodecane is indeed captured by the CSE-FGM combustion model. The RANS temperature field showed reasonably good agreement with the experimental Schlieren images in terms of the location and size of the flame propagation.
- Species mass fractions of CH_2O and OH agree with the flame's underlying chemistry.
- The results showed that CSE-FGM can effectively capture partially-premixed regions while accounting for detailed chemistry and turbulence-chemistry interaction effects.
- Slight deviations under low ambient temperature conditions were noticed for ignition delay times and lift-off lengths predicted with CSE-FGM compared to experiments. The inclusion of a single control scalar based on mixture fraction is perhaps not sufficient to accurately capture the strong interactions between turbulence and chemistry.

Following the modelling capabilities of CSE-FGM, adopting DCSE, and as such including a second conditioning variable based on the progress variable, should provide a higher degree of accuracy, particularly for flows found in practical applications. Indeed, for more complex reacting flows involving high Reynolds numbers which are consequently exposed to intense turbulence, Bushe [283] highlighted that a single variable might be inadequate to describe the thermo-chemical state since conditional fluctuations are large and some scalars

exhibit a clear functional dependence on the spatial coordinate and Reynolds number. In order to take full advantage of the DCSE method, quite a few challenges were yet to be addressed (and still need to be addressed) around the definition attributed to the progress variable. Depending on the studied case and possibly the fuel involved, another definition of c would perhaps be more appropriate to accurately capture the underlying chemistry taking place. Hence, data from nine turbulent flames in the Cambridge/Sandia swirl database were combined to study how the choice of scalar variables in conditional moment closure type approaches affects the conditional spatial fluctuations of reactive scalars. In order to investigate the influence of swirl and stratification, two additional datasets were constructed. Principal component analysis (PCA) was applied to help identify the number of scalar variables and the most appropriate choices for describing the composition space. Two PCA scaling methods were adopted, namely Pareto and Auto-scaling. Four of the most common progress variable definitions for the first moment hypothesis were selected as conditioning variables to investigate the conditional fluctuations and normalised RMS of various species and temperatures from all three databases at all axial locations. The findings included:

- Regardless of the dataset investigated and the scaling method used, a single principal component correlated with temperature accounted for the largest variance.

- Two control variables based on mixture fraction, Z, and progress variable significantly reduced the conditional fluctuations of scalars compared to a single variable. Conditional averages around a single control variable exhibited an important dependence on the real domain, suggesting that a CSE calculation would probably fail in predicting the underlying chemistry.

- The selection of progress variables had minimal effects on the RMS of conditional fluctuations for all tested conditions, although a slight reduction of conditional fluctuations was found for the temperature-based progress variable.

- The success of CMC approaches does not depend on the definition attributed to the

progress variable as opposed to flamelet-based architectures, for which different definitions given to c will give different results.

- Using Z and c as two conditioning scalars enabled the detachment of the thermo-chemical state from space, swirl and stratification effects. This suggests that adopting a DCSE approach might successfully predict the considered set of flames, assuming that ensembles are divided along the axial direction.

- Given that doubly conditioning seems to decrease the reactive scalars' dependence more effectively, it is suggested that $c(T)$ could give a more accurate representation of the Cambridge/Sandia flames' chemistry (such as in a manifold) than a species-based progress variable, considering that species diffusivity is often simplified by assuming unity Lewis numbers.

- A complementary analysis using the experimental data of Sandia/TUD piloted jet flames with increasing turbulence intensity and probabilities of local extinction was also added to provide further evidence. The conclusions drawn for the Cambridge/Sandia swirl burner were in excellent agreement with the dataset of Sandia/TUD jet flames.

- DCSE will be likely needed for capturing partially-premixed flames, combustion under high levels of turbulence intensity (where the inclusion of turbulence-chemistry interaction is compulsory), and reactive flows encountered in practical combustion systems.

8.3 Future Work

The future work developed from this study should focus on further improvement of the combustion model. The present study showed that the DCSE approach is compulsory for accurately capturing and predicting key characteristics of reactive flows operating under high turbulence intensity and exhibiting partially-premixed flame structures. For the current combustion model, future work should include:

- Inversion and regularisation. The conditional averages given by the CSE/DCSE routine via an inversion operation are known to be very sensitive to the numerical process. Different inversion and regularisation methods could be used to improve both the accuracy and efficiency of the CSE/DCSE routine. Recently, Mahdipour & Salehi [269] proposed a novel form for approximating the conditional scalars in turbulent reacting flows based on the Bernstein polynomial. Using the DNS data of turbulent premixed flames, these authors showed that adopting Bernstein polynomials as the presumed functional form for the conditional scalars provides better regularisation than the conventional CSE approach. This model has been shown to improve the accuracy, reduce the computational cost and enhance the spatial localisation of the CSE model. An extension to DCSE could be considered.

- The temperature-based progress variable. Various forms of progress variable definitions for premixed and partially-premixed flames have been adopted by the community. While the monotonicity of c has been thoroughly studied for species-based progress variables, an extension of the present work to account for the monotonicity of the temperature-based progress variable could be the subject of future studies.

- Joint probability density function (joint-PDF). Up to this date, no analytical forms of the joint-PDF have been derived for the mixture fraction and progress variable. The widely adopted assumption based on their statistical independence was shown to be erroneous as correlations between conditional variables are important. One alternative approach that has aroused much interest over the past few years is to use

deep neural networks (DNN) [301, 302]. Another method worth investigating is based on Bayes's theorem, which consists of adopting a β-function for the mixture fraction PDF, and the premixed laminar flamelet-PDF for the progress variable PDF conditioned on Z. Recently, Pfitzner & Klein [134] proposed a new 1D laminar premixed flame PDF extended to large Karlovitz numbers. Preliminary work should include the extraction of the joint-PDF from various experimental measurements and should make an in-depth analysis of its shape.

- DCSE modelling capabilities. A recently developed multi-regime burner [240, 303] was designed to produce flames with partial premixing of fuel and oxidiser as well as recirculation of combustion products. Evaluating the conditional space of this burner would provide further information on which conditioning variables to select for partially-premixed flames operating under high Reynolds numbers. Finally, this burner would be an ideal test case to provide a stronger foundation on the modelling capabilities of DCSE.

References

[1] J. Heywood, *Internal Combustion Engines Fundamentals*. McGraw-Hill, 1 ed., 1988.

[2] J. A. van Oijen and L. P. H. de Goey, "A numerical study of confined triple flames using a flamelet-generated manifold," *Combustion Theory and Modelling*, vol. 8, no. 1, pp. 141–163, 2004.

[3] S. B. Pope, *Turbulent flows*. Cambridge CB: Cambridge University Press, 1 ed., 2000.

[4] O. Colin and A. Benkenida, "The 3-zones extended coherent flame model (ECFM-3Z) for computing premixed/diffusion combustion," *Oil & Gas Science and Technology*, vol. 59, no. 6, pp. 593–609, 2004.

[5] T. Poinsot and D. Veynante, *Theoretical and numerical combustion*. Philadelphia PA: RT Edwards, 2 ed., 2005.

[6] P. Dirrenberger, P. Glaude, R. Bounaceur, H. Le Gall, A. P. da Cruz, A. Konnov, and F. Battin-Leclerc, "Laminar burning velocity of gasolines with addition of ethanol," *Fuel*, vol. 115, pp. 162–169, 2014.

[7] B. Galmiche, F. Halter, and F. Foucher, "Effects of high pressure, high temperature and dilution on laminar burning velocities and Markstein lengths of iso-octane/air mixtures," *Combustion and Flame*, vol. 159, no. 11, pp. 3286–3299, 2012.

[8] Z. Meng, K. Liang, and J. Fang, "Laminar burning velocities of iso-octane, toluene, 1-hexene, ethanol and their quaternary blends at elevated temperatures and pressures," *Fuel*, vol. 237, pp. 630–636, 2019.

[9] X. Han, Z. Wang, Y. He, S. Wang, Y. Liu, and A. A. Konnov, "Temperature dependence of the laminar burning velocity for n-heptane and iso-octane/air flames," *Fuel*, vol. 276, p. 118007, 2020.

[10] R. Kumar, A. Singhal, and S. Kumar, "Laminar burning velocity measurements of iso-octane+air mixtures at higher unburnt mixture temperatures," *Fuel*, vol. 288, p. 119652, 2021.

[11] Y. Wu, P. Pal, S. Som, and T. Lu, "A skeletal chemical kinetic mechanism for gasoline and gasoline/ethanol blend surrogates for engine CFD applications," in *International Conference on Chemical Kinetics*, (Chicago, IL), may 2017.

[12] Y. Li, A. Alfazazi, B. Mohan, E. Alexandros Tingas, J. Badra, H. G. Im, and S. Mani Sarathy, "Development of a reduced four-component (toluene/n-heptane/iso-octane/ethanol) gasoline surrogate model," *Fuel*, vol. 247, pp. 164–178, 2019.

[13] J. C. G. Andrae and T. Kovács, "Evaluation of adding an olefin to mixtures of primary reference fuels and toluene to model the oxidation of a fully blended gasoline," *Energy & Fuels*, vol. 30, no. 9, pp. 7721–7730, 2016.

[14] G. Broustail, F. Halter, P. Seers, G. Moréac, and C. Mounaïm-Rousselle, "Experimental determination of laminar burning velocity for butanol/iso-octane and ethanol/iso-octane blends for different initial pressures," *Fuel*, vol. 106, pp. 310–317, 2013.

[15] L. Sileghem, V. Alekseev, J. Vancoillie, E. Nilsson, S. Verhelst, and A. Konnov, "Laminar burning velocities of primary reference fuels and simple alcohols," *Fuel*, vol. 115, pp. 32–40, 2014.

[16] T. Knorsch, A. Zackel, D. Mamaikin, L. Zigan, and M. Wensing, "Comparison of different gasoline alternative fuels in terms of laminar burning velocity at increased gas temperatures and exhaust gas recirculation rates," *Energy & Fuels*, vol. 28, no. 2, pp. 1446–1452, 2014.

[17] M. Aghsaee, D. Nativel, M. Bozkurt, M. Fikri, N. Chaumeix, and C. Schulz, "Experimental study of the kinetics of ethanol pyrolysis and oxidation behind reflected shock waves and in laminar flames," *Proceedings of the Combustion Institute*, vol. 35, no. 1, pp. 393–400, 2015.

[18] A. Katoch, A. Millán-Merino, and S. Kumar, "Measurement of laminar burning velocity of ethanol-air mixtures at elevated temperatures," *Fuel*, vol. 231, pp. 37–44, 2018.

[19] G. Kim, B. Almansour, S. Park, A. Terracciano, S. Vasu, K. Zhang, S. Wagnon, and W. Pitz, "Laminar burning velocities of high-performance fuels relevant to the co-optima initiative," *SAE International Journal of Advances and Current Practices in Mobility*, vol. 1, no. 3, pp. 1139–1147, 2019.

[20] G. Kim, A. Terracciano, S. Vasu, and B. Almansour, "High-pressure laminar burning velocity measurements of ethanol - a co-optima fuel candidate," in *WCX SAE World Congress Experience*, SAE International, 2020.

[21] Z. Wang, X. Han, Y. He, R. Zhu, Y. Zhu, Z. Zhou, and K. Cen, "Experimental and kinetic study on the laminar burning velocities of NH_3 mixing with CH_3OH and C_2H_5OH in premixed flames," *Combustion and Flame*, vol. 229, p. 111392, 2021.

[22] K. Eisazadeh-Far, A. Moghaddas, J. Al-Mulki, and H. Metghalchi, "Laminar burning speeds of ethanol/air/diluent mixtures," *Proceedings of the Combustion Institute*, vol. 33, no. 1, pp. 1021–1027, 2011.

[23] L. Sileghem, J. Vancoillie, J. Demuynck, J. Galle, and S. Verhelst, "Alternative fuels for spark-ignition engines: Mixing rules for the laminar burning velocity of gasoline–alcohol blends," *Energy & Fuels*, vol. 26, no. 8, pp. 4721–4727, 2012.

[24] G. Broustail, P. Seers, F. Halter, G. Moréac, and C. Mounaim-Rousselle, "Experimental determination of laminar burning velocity for butanol and ethanol iso-octane blends," *Fuel*, vol. 90, no. 1, pp. 1–6, 2011.

[25] E. Varea, V. Modica, B. Renou, and A. M. Boukhalfa, "Pressure effects on laminar burning velocities and Markstein lengths for isooctane–ethanol–air mixtures," *Proceedings of the Combustion Institute*, vol. 34, no. 1, pp. 735–744, 2013.

[26] N. I. D. Hinton, *Measuring laminar burning velocities using constant volume combustion vessel techniques*. PhD thesis, University of Oxford, Oxford UK, 2014.

[27] S. Jerzembeck, A. Sharma, and N. Peters, "Laminar Burning Velocities of Nitrogen Diluted Standard Gasoline-Air Mixture," in *SAE World Congress & Exhibition*, SAE International, apr 2008.

[28] A. J. Susa, A. M. Ferris, D. F. Davidson, and R. K. Hanson, "Experimental Observation of Negative Temperature Dependence in iso-Octane Burning Velocities," *AIAA Journal*, vol. 57, no. 10, pp. 4476–4481, 2019.

[29] Y.-D. Liu, M. Jia, M.-Z. Xie, and B. Pang, "Development of a New Skeletal Chemical Kinetic Model of Toluene Reference Fuel with Application to Gasoline Surrogate Fuels for Computational Fluid Dynamics Engine Simulation," *Energy & Fuels*, vol. 27, no. 8, pp. 4899–4909, 2013.

[30] X. H. Fang, *Numerical Modelling For Diesel Spray Combustion*. PhD thesis, University of Oxford, Oxford UK, 2019.

[31] M. S. Sweeney, S. Hochgreb, M. J. Dunn, and R. S. Barlow, "The structure of turbulent stratified and premixed methane/air flames I: Non-swirling flows," *Combustion and Flame*, vol. 159, no. 9, pp. 2896–2911, 2012.

[32] S. Marshall, S. Taylor, C. Stone, T. Davies, and R. Cracknell, "Laminar burning velocity measurements of liquid fuels at elevated pressures and temperatures with combustion residuals," *Combustion and Flame*, vol. 158, no. 10, pp. 1920–1932, 2011.

[33] N. Hinton, R. Stone, and R. Cracknell, "Laminar burning velocity measurements in constant volume vessels – Reconciliation of flame front imaging and pressure rise methods," *Fuel*, vol. 211, pp. 446–457, 2018.

[34] L. Pickett and G. Bruneaux, "Engine combustion network. Combustion Research Facility, Sandia National Laboratories," 2018. http://www.sandia.gov/ECN.

[35] H. Ritchie, M. Roser, and P. Rosado, "Energy," *Our World in Data*, 2020. https://ourworldindata.org/energy.

[36] BP, "BP Statistical Review of World Energy." https://www.bp.com/content/dam/bp/business-sites/en/global/corporate/pdfs/energy-economics/statistical-review/bp-stats-review-2019-full-report.pdf, 2019.

[37] ExxonMobil, "2019 Outlook for Energy: A View to 2040." https://corporate.exxonmobil.com/-/media/Global/Files/outlook-for-energy/2019-Outlook-for-Energy_v4.pdf, 2019.

[38] IEA, "Global energy review 2021," *International Energy Agency*, 2021. https://www.iea.org/reports/global-energy-review-2021.

[39] P. A. Yanguas Parra, G. Ganti, R. Brecha, B. Hare, M. Schaeffer, and U. Fuentes, "Global and regional coal phase-out requirements of the Paris Agreement: Insights from the IPCC Special Report on 1.5°C," *Climate Analytics*, 2019. https://climateanalytics.org/media/report_coal_phase_out_2019.pdf.

[40] S. Wijeyakulasuriya, J. Kim, D. Probst, K. Srivastava, P. Yang, R. Scarcelli, and P. K. Senecal, "Enabling powertrain technologies for Euro 7/VII vehicles with computational fluid dynamics," *Transportation Engineering*, vol. 9, p. 100127, 2022.

[41] R. Stone, *Introduction to internal combustion engines*. New York NY: Palgrave Macmillan, 4 ed., 2012.

[42] Y. B. Zeldovich, "The oxidation of nitrogen in combustion and explosions," *J. Acta Physicochimica*, vol. 21, pp. 577–628, 1946.

[43] I. Glassman, R. A. Yetter, and N. G. Glumac, *Combustion*. Boston MA: Academic Press, 5 ed., 2015.

[44] F. Leach, G. Kalghatgi, R. Stone, and P. Miles, "The scope for improving the efficiency and environmental impact of internal combustion engines," *Transportation Engineering*, vol. 1, p. 100005, 2020.

[45] P. Senecal and F. Leach, "Diversity in transportation: Why a mix of propulsion technologies is the way forward for the future fleet," *Results in Engineering*, vol. 4, p. 100060, 2019.

[46] D. Bradley, "2 - Fundamentals of Lean Combustion," in *Lean Combustion (Second Edition)* (D. Dunn-Rankin and P. Therkelsen, eds.), pp. 21–61, Boston: Academic Press, second edition ed., 2016.

[47] T. Poinsot, D. Veynante, and S. Candel, "Quenching processes and premixed turbulent combustion diagrams," *Journal of Fluid Mechanics*, vol. 228, p. 561–606, 1991.

[48] V. Rapp, N. Killingsworth, P. Therkelsen, and R. Evans, "4 - Lean-Burn Internal Combustion Engines," in *Lean Combustion (Second Edition)* (D. Dunn-Rankin and P. Therkelsen, eds.), pp. 111–146, Boston: Academic Press, second edition ed., 2016.

[49] S. K. Aggarwal, "Extinction of laminar partially premixed flames," *Progress in Energy and Combustion Science*, vol. 35, no. 6, pp. 528–570, 2009.

[50] B. Franzelli, E. Riber, L. Y. M. Gicquel, and T. Poinsot, "Large Eddy Simulation of combustion instabilities in a lean partially-premixed swirled flame," *Combustion and Flame*, vol. 159, no. 2, pp. 621–637, 2012.

[51] Y. Jiang, R. Gehmlich, T. Knoblinger, and K. Seshadri, "Experimental and computational investigation of partially-premixed methoxymethane flames," *Combustion and Flame*, vol. 195, no. 1, pp. 99–104, 2018.

[52] N. Peters, *Turbulent combustion*. Cambridge CB: Cambridge University Press, 1 ed., 2000.

[53] A. Masri, "Partial premixing and stratification in turbulent flames," *Proceedings of the Combustion Institute*, vol. 35, no. 2, pp. 1115–1136, 2015.

[54] A. N. Lipatnikov, "Stratified turbulent flames: Recent advances in understanding the influence of mixture inhomogeneities on premixed combustion and modeling challenges," *Progress in Energy and Combustion Science*, vol. 62, pp. 87–132, 2017.

[55] F. Ravet, G. Subramanian, and L. Vervisch, "New developments in turbulent combustion modeling for engine design: ECFM-CLEH combustion submodel," in *SAE World Congress & Exhibition*, SAE International, apr 2007.

[56] R. Bilger, S. Starner, and R. Kee, "On reduced mechanisms for methane-air combustion in nonpremixed flames," *Combustion and Flame*, vol. 80, no. 2, pp. 135 – 149, 1990.

[57] X. Wen, X. S. Bai, K. Luo, H. Wang, Y. Luo, and J. Fan, "A generalized flamelet tabulation method for partially premixed combustion," *Combustion and Flame*, vol. 198, no. 1, pp. 54–68, 2018.

[58] J. Boussinesq, *Théorie de l'écoulement tourbillonnant et tumultueux des liquides dans les lits rectilignes*. Paris IDF: Gauthier-Villars et fils, 1 ed., 1897.

[59] J. O. Hinze, *Turbulence*. New York NY: McGraw-Hill, 2 ed., 1975.

[60] C. Pérez Arroyo, J. Dombard, F. Duchaine, L. Gicquel, B. Martin, N. Odier, and G. Staffelbach, "Towards the Large-Eddy Simulation of a full engine: Integration of a 360 azimuthal degrees fan, compressor and combustion chamber. Part I: Methodology and initialisation," *Journal of the Global Power and Propulsion Society*, no. May, pp. 1–16, 2021.

[61] C. Pérez Arroyo, J. Dombard, F. Duchaine, L. Gicquel, B. Martin, N. Odier, and G. Staffelbach, "Towards the Large-Eddy Simulation of a full engine: Integration of a 360 azimuthal degrees fan, compressor and combustion chamber. Part II: Comparison against stand-alone simulations," *Journal of the Global Power and Propulsion Society*, no. May, pp. 1–16, 2021.

[62] K. Annamalai and I. K. Puri, *Combustion Science and Engineering*. Boca Raton FL: CRC Press, 1 ed., 2007.

[63] S. De, A. K. Agarwal, S. Chaudhuri, and S. Sen, *Modeling and Simulation of Turbulent Combustion*. Singapore: Springer Nature, 1 ed., 2018.

[64] D. Veynante and L. Vervisch, "Turbulent combustion modeling," *Progress in Energy and Combustion Science*, vol. 28, no. 3, pp. 193–266, 2002.

[65] A. Favre, "Statistical equations of turbulent gases," *Problems of hydrodynamics and continuum mechanics*, pp. 231–266, 1969.

[66] L. Prandtl, "Investigations on turbulent flow," *Zeitschrift fur angewandte Mathematik und Mechanik*, vol. 5, no. 2, pp. 136–139, 1925.

[67] W. P. Jones and B. E. Launder, "The prediction of laminarization with a 2-equation model of turbulence," *International Journal of Heat and Mass transfert*, vol. 15, no. 2, pp. 301–314, 1972.

[68] K. N. C. Bray, J. B. Moss, and P. A. Libby, "Flamelet crossing frequencies and mean reaction rates in premixed turbulent combustion," *Combustion Science and Technology*, vol. 41, no. 3-4, pp. 143–172, 1984.

[69] F. Gouldin, K. Bray, and J.-Y. Chen, "Chemical closure model for fractal flamelets," *Combustion and Flame*, vol. 77, no. 3, pp. 241–259, 1989.

[70] S. B. Pope, "The evolution of surfaces in turbulence," *International Journal of Engineering Science*, vol. 26, no. 5, pp. 445–469, 1988.

[71] A. Trouvé and T. Poinsot, "The evolution equation for the flame surface density in turbulent premixed combustion," *Journal of Fluid Mechanics*, vol. 278, p. 1–31, 1994.

[72] L. Vervisch, E. Bideau, K. N. C. Bray, and W. Kollmann, "Surface density function in premixed turbulent combustion modeling, similarities between probability density function and flame surface approaches," *Physics of Fluids*, vol. 7, no. 10, pp. 2496–2503, 1995.

[73] M. Boger, D. Veynante, H. Boughanem, and A. Trouve, "Direct numerical simulation analysis of flame surface density concept for large eddy simulation of turbulent premixed combustion," *Proceedings of the Combustion Institute*, vol. 27, pp. 917–925, 1998.

[74] N. Swaminathan and K. C. N. Bray, *Turbulent premixed flames*. Cambridge CA: Cambridge University Press, 1 ed., 2011.

[75] D. Veynante, "Investigation of flame surface density modeling for large eddy simulation of turbulent premixed flames by comparison with a prescribed reference solution," *Combustion and Flame*, p. 111663, 2021.

[76] P. A. Libby and F. A. Williams, *Turbulent Reacting Flows*. New York NY: Academic Press Inc., 1 ed., 1994.

[77] T. Ma, O. T. Stein, N. Chakraborty, and A. Kempf, "A posteriori testing of algebraic flame surface density models for LES," *Combustion Theory and Modelling*, vol. 17, no. 3, pp. 431–482, 2013.

[78] C. Jainski, M. Rißmann, B. Böhm, and A. Dreizler, "Experimental investigation of flame surface density and mean reaction rate during flame–wall interaction," *Proceedings of the Combustion Institute*, vol. 36, no. 2, pp. 1827–1834, 2017.

[79] R. Rasool, M. Klein, and N. Chakraborty, "Flame Surface Density based mean reaction rate closure for Reynolds averaged Navier Stokes methodology in turbulent premixed Bunsen flames with non-unity Lewis number," *Combustion and Flame*, p. 111766, 2021.

[80] J. Ren, H. Wang, K. Luo, and J. Fan, "A priori assessment of convolutional neural network and algebraic models for flame surface density of high Karlovitz premixed flames," *Physics of Fluids*, vol. 33, no. 3, p. 036111, 2021.

[81] F. Cavallo Marincola, T. Ma, and A. Kempf, "Large eddy simulations of the Darmstadt turbulent stratified flame series," *Proceedings of the Combustion Institute*, vol. 34, no. 1, pp. 1307–1315, 2013.

[82] B. Fiorina, R. Mercier, G. Kuenne, A. Ketelheun, A. Avdić, J. Janicka, D. Geyer, A. Dreizler, E. Alenius, C. Duwig, P. Trisjono, K. Kleinheinz, S. Kang, H. Pitsch, E. Proch, F. Cavallo Marincola, and A. Kempf, "Challenging modeling strategies for LES of non-adiabatic turbulent stratified combustion," *Combustion and Flame*, vol. 162, no. 11, pp. 4264–4282, 2015.

[83] O. Colin, A. Benkenida, and C. Angelberger, "3D modeling of mixing, ignition and combustion phenomena in highly stratified gasoline engines," *Oil & Gas Science and Technology - Rev. IFP*, vol. 58, no. 1, pp. 47–62, 2003.

[84] F. E. Marble and J. E. Broadwell, "The coherent flame model of non-premixed turbulent combustion," *Project Squid TRW-9-PU, Project Squid Headquarters, Chaffee Hall, Purdue University*, 1977.

[85] O. Colin, A. Pires da Cruz, and S. Jay, "Detailed chemistry-based auto-ignition model including low temperature phenomena applied to 3-D engine calculations," *Proceedings of the Combustion Institute*, vol. 30, pp. 2649–2656, 2005.

[86] R. Mobasheri, "Analysis the ECFM-3Z combustion model for simulating the combustion process and emission characteristics in a HSDI diesel engine," *International Journal of Spray and Combustion Dynamics*, vol. 7, no. 4, pp. 353–372, 2014.

[87] L. Pulga, S. Falfari, G. M. Bianchi, M. Ricci, and C. Forte, "Advanced combustion modelling of high bmep engines under water injection conditions with chemical correlations generated with detailed kinetics and machine learning algorithms," *SAE International Journal of Advances and Current Practices in Mobility*, vol. 3, pp. 77–94, sep 2020.

[88] I. Najar, B. Stengel, B. Buchholz, and E. Hassel, "Pilot injection and thermal nitrogen oxides: A numerical and experimental study," *SAE International Journal of Engines*, vol. 13, pp. 473–486, jul 2020.

[89] X. Fang, R. Ismail, M. H. Davy, and J. Camm, "Numerical studies of combustion recession on ECN diesel Spray A," *Proceedings of the ASME 2018 Internal Combustion Engine Division Fall Technical Conference*, vol. 2: Emissions Control Systems; Instrumentation, Controls, and Hybrids; Numerical Simulation; Engine Design and Mechanical Development, 11 2018. V002T06A011.

[90] X. Fang, R. Ismail, N. Sekularac, and M. Davy, "On the prediction of Spray A end of injection phenomenon using conditional source-term estimation," in *WCX SAE World Congress Experience*, SAE International, apr 2020.

[91] X. H. Fang, R. Ismail, W. K. Bushe, and M. Davy, "Simulation of ECN diesel Spray A using conditional source-term estimation," *Combustion Theory and Modelling*, vol. 24, no. 4, pp. 725–760, 2020.

[92] E. Mastorakos and T. Echekki, *Turbulent Combustion Modeling*. New York NY: Springer, 1 ed., 2011.

[93] S. Ruan, *Turbulent Partially Premixed Combustion: DNS Analysis and RANS Simulation*. PhD thesis, University of Cambridge, Cambridge CA, 2012.

[94] J. W. Labahn, I. Stanković, C. B. Devaud, and B. Merci, "Comparative study between conditional moment closure (CMC) and conditional source-term estimation (CSE) applied to piloted jet flames," *Combustion and Flame*, vol. 181, pp. 172 – 187, 2017.

[95] C. M. Müller, H. Breitbach, and N. Peters, "Partially-premixed turbulent flame propagation in jet flames," *Proceedings of the Combustion Institute*, vol. 25, pp. 1099–1106, 1994.

[96] M. Chen, M. Herrmann, and N. Peters, "Flamelet modeling of lifted turbulent methane/air and propane/air jet diffusion flames," *Proceedings of the Combustion Institute*, vol. 28, pp. 167–174, 2000.

[97] N. Peters, "The turbulent burning velocity for large-scale and small-scale turbulence," *Journal of Fluid Mechanics*, vol. 384, pp. 167–174, 1999.

[98] J. Koch, M. Schmitt, Y. M. Wright, K. Steurs, and K. Boulouchos, "LES multi-cycle analysis of the combustion process in a small SI engine," *SAE International Journal of Engines*, vol. 7, no. 1, pp. 269–285, 2014.

[99] S. Esposito, M. Mally, L. Cai, H. Pitsch, and S. Pischinger, "Validation of a RANS 3D-CFD gaseous emission model with space-, species-, and cycle-resolved measurements from an SI DI engine," *Energies*, vol. 13, no. 17, 2020.

[100] J. Kim, R. Scarcelli, S. Som, A. Shah, M. S. Biruduganti, and D. E. Longman, "Numerical investigation of a fueled pre-chamber spark-ignition natural gas engine," *International Journal of Engine Research*, vol. 0, no. 0, p. 14680874211020180, 0.

[101] S. J. Kazmouz, R. Scarcelli, J. Kim, Z. Cheng, S. Liu, M. Dai, E. Pomraning, P. K. Senecal, and S.-Y. Lee, "High-fidelity energy deposition ignition model coupled with flame propagation models at engine-like flow conditions," *Proceedings of the ASME 2021 Internal Combustion Engine Division Fall Technical Conference*, vol. ASME 2021 Internal Combustion Engine Division Fall Technical Conference, 10 2021. V001T06A002.

[102] F. A. Williams, "Recent Advances in Theoretical Descriptions of Turbulent Diffusion Flames," in *Turbulent Mixing in Nonreactive and Reactive Flows* (S. N. B. Murthy, ed.), (Boston, MA), pp. 189–208, Springer New York, 1975.

[103] N. Peters, "Laminar diffusion flamelet models in non-premixed turbulent combustion," *Progress in Energy and Combustion Science*, vol. 10, no. 3, pp. 319–339, 1984.

[104] N. Peters, "Laminar flamelet concepts in turbulent combustion," *Symposium (International) on Combustion*, vol. 21, no. 1, pp. 1231–1250, 1988.

[105] H. Pitsch and N. Peters, "A consistent flamelet formulation for non-premixed combustion considering differential diffusion effects," *Combustion and Flame*, vol. 114, no. 1, pp. 26–40, 1998.

[106] K. Claramunt, R. Cònsul, D. Carbonell, and C. Pérez-Segarra, "Analysis of the laminar flamelet concept for nonpremixed laminar flames," *Combustion and Flame*, vol. 145, no. 4, pp. 845–862, 2006.

[107] C. D. Pierce and P. Moin, "Progress-variable approach for large-eddy simulation of non-premixed turbulent combustion," *Journal of Fluid Mechanics*, vol. 504, no. 1, pp. 73–97, 2004.

[108] M. Ihme, C. M. Cha, and H. Pitsch, "Prediction of local extinction and re-ignition effects in non-premixed turbulent combustion using a flamelet/progress variable approach," *Proceedings of the Combustion Institute*, vol. 30, no. 1, pp. 793–800, 2005.

[109] K. Bray, P. Domingo, and L. Vervisch, "Role of the progress variable in models for partially premixed turbulent combustion," *Combustion and Flame*, vol. 141, no. 4, pp. 431–437, 2005.

[110] A. H. Mahdipour and M. M. Salehi, "A priori evaluation of the laminar flamelet decomposition model for turbulent premixed flames using DNS data," *Flow, Turbulence and Combustion*, vol. 108, pp. 149–180, 2022.

[111] S. B. Pope, "Small scales, many species and the manifold challenges of turbulent combustion," *Proceedings of the Combustion Institute*, vol. 34, no. 1, pp. 1–31, 2013.

[112] J. Lamouroux, M. Ihme, B. Fiorina, and O. Gicquel, "Tabulated chemistry approach for diluted combustion regimes with internal recirculation and heat losses," *Combustion and Flame*, vol. 161, no. 8, pp. 2120–2136, 2014.

[113] Y. C. See and M. Ihme, "Large eddy simulation of a partially-premixed gas turbine model combustor," *Proceedings of the Combustion Institute*, vol. 35, pp. 1225–1234, 2015.

[114] S. Popp, F. Hunger, S. Hartl, D. Messig, B. Coriton, J. H. Frank, F. Fuest, and C. Hasse, "LES flamelet-progress variable modeling and measurements of a turbulent partially-premixed dimethyl ether jet flame," *Combustion and Flame*, vol. 162, no. 8, pp. 3016–3029, 2015.

[115] Z. Gao, C. Jiang, and C.-H. Lee, "Representative interactive flamelet model and flamelet/progress variable model for supersonic combustion flows," *Proceedings of the Combustion Institute*, vol. 36, no. 2, pp. 2937–2946, 2017.

[116] F. Shan, D. Zhang, L. Hou, H. Fang, H. Zhang, and J. Zhang, "An improved flamelet/progress variable modeling for supersonic combustion," *International Journal of Hydrogen Energy*, vol. 46, no. 5, pp. 4485–4495, 2021.

[117] Z. Sun, S. Gierth, M. Pollack, C. Hasse, and A. Scholtissek, "Ignition under strained conditions: Unsteady flamelet progress variable modeling for diesel engine conditions in the transient counterflow configuration," *Combustion and Flame*, vol. 240, p. 111841, 2022.

[118] H. L. Toor, "Mass transfer in dilute turbulent and non-turbulent systems with rapid irreversible reactions and equal diffusivities," *AIChE Journal*, vol. 8, no. 1, pp. 70–78, 1962.

[119] S. Pope, "PDF methods for turbulent reactive flows," *Progress in Energy and Combustion Science*, vol. 11, no. 2, pp. 119–192, 1985.

[120] S. B. Pope, "Computations of turbulent combustion: Progress and challenges," *Symposium (International) on Combustion*, vol. 23, no. 1, pp. 591–612, 1991.

[121] F. A. Williams, *Combustion theory*. Menlo Park CA: Benjamin Cummings, 2 ed., 1985.

[122] A. W. Cook and J. J. Riley, "A subgrid model for equilibrium chemistry in turbulent flows," *Physics of Fluids*, vol. 6, no. 8, pp. 2868–2870, 1994.

[123] J. Jimenez, A. Linan, M. M. Rogers, and F. J. Higuera, "A priori testing of subgrid models for chemically reacting non-premixed turbulent shear flows," *Journal of Fluid Mechanics*, vol. 349, p. 149–171, 1997.

[124] C. Wall, B. J. Boersma, and P. Moin, "An evaluation of the assumed beta probability density function subgrid-scale model for large eddy simulation of nonpremixed, turbulent combustion with heat release," *Physics of Fluids*, vol. 12, no. 10, pp. 2522–2529, 2000.

[125] H. Pitsch and H. Steiner, "Large-eddy simulation of a turbulent piloted methane/air diffusion flame (Sandia flame D)," *Physics of Fluids*, vol. 12, no. 10, pp. 2541–2554, 2000.

[126] A. Coclite, L. Cutrone, M. Gurtner, P. De Palma, O. Haidn, and G. Pascazio, "Computing supersonic non-premixed turbulent combustion by an SMLD flamelet progress variable model," *International Journal of Hydrogen Energy*, vol. 41, no. 1, pp. 632–646, 2016.

[127] A. G. Nouri, P. Givi, and D. Livescu, "Modeling and simulation of turbulent nuclear flames in Type Ia supernovae," *Progress in Aerospace Sciences*, vol. 108, pp. 156–179, 2019.

[128] K. N. C. Bray, M. Champion, P. A. Libby, and N. Swaminathan, "Finite rate chemistry and presumed pdf models for premixed turbulent combustion," *Combustion and Flame*, vol. 146, no. 4, pp. 665–673, 2006.

[129] M. Pfitzner, "A new analytic PDF for simulations of premixed turbulent combustion," *Flow Turbulence Combustion*, vol. 106, p. 1213–1239, 2021.

[130] K. Bray and J. Moss, "A unified statistical model of the premixed turbulent flame," *Acta Astronautica*, vol. 4, no. 3, pp. 291–319, 1977.

[131] P. Domingo, L. Vervisch, S. Payet, and R. Hauguel, "DNS of a premixed turbulent V flame and LES of a ducted flame using a FSD-PDF subgrid scale closure with FPI-tabulated chemistry," *Combustion and Flame*, vol. 143, no. 4, pp. 566–586, 2005. Special Issue to Honor Professor Robert W. Bilger on the Occasion of His Seventieth Birthday.

[132] M. M. Salehi and W. K. Bushe, "Presumed PDF modeling for RANS simulation of turbulent premixed," *Combustion Theory and Modelling*, vol. 14, no. 3, pp. 381–403, 2010.

[133] M. M. Salehi, W. K. Bushe, N. Shahbazian, and C. P. T. Groth, "Modified laminar flamelet presumed probability density function for LES of premixed turbulent combustion," *Proceedings of the Combustion Institute*, vol. 34, no. 1, pp. 1203–1211, 2013.

[134] M. Pfitzner and M. Klein, "A near-exact analytic solution of progress variable and PDF for single-step Arrhenius chemistry," *Combustion and Flame*, vol. 226, pp. 380–395, 2021.

[135] A. Y. Klimenko, "Multicomponent diffusion of various admixtures in turbulent flow," *Fluid Dynamics*, vol. 25, no. 3, pp. 327–334, 1990.

[136] R. W. Bilger, "Conditional Moment Method for Turbulent Reacting Flow Using Crocco Variable Conditions," Charles Kolling Research Laboratory TN F-99, Dept. Mech. Eng., University of Sydney, 1991.

[137] R. W. Bilger, "Conditional moment closure for turbulent reacting flow," *Physics of Fluids A: Fluid Dynamics*, vol. 5, no. 2, pp. 436–444, 1993.

[138] D. Dovizio, M. M. Salehi, and C. B. Devaud, "RANS simulation of a turbulent premixed bluff body flame using conditional source-term estimation," *Combustion Theory and Modelling*, vol. 17, no. 5, pp. 935–959, 2013.

[139] A. Klimenko and R. Bilger, "Conditional moment closure for turbulent combustion," *Progress in Energy and Combustion Science*, vol. 25, no. 6, pp. 595–687, 1999.

[140] R. W. Bilger, "Conditional moment closure modeling and advanced laser measurement," *Turbulence and molecular processes in combustion (Sixth Toyota Conference)*, vol. 1, no. 1, pp. 267–85, 1993.

[141] E. E. O'Brien and T. L. Jiang, "The conditional dissipation rate of an initially binary scalar in homogeneous turbulence," *Physics of Fluids A*, vol. 3, no. 12, pp. 3121–3123, 1991.

[142] F. Salehi, M. Talei, E. R. Hawkes, *et al.*, "A comparative study of conditional moment closure modelling for ignition of iso-octane and n-heptane in thermally stratified mixtures," *Flow, Turbulence and Combustion*, vol. 95, no. 1, pp. 1–28, 2015.

[143] D. Farrace, C. Kyoungseoun, S. S. Pandurangi, *et al.*, "Unstructured LES-CMC modelling of turbulent premixed bluff body flames close to blow-off," *Proceedings of the Combustion Institute*, vol. 36, no. 2, pp. 1977–1985, 2017.

[144] D. Farrace, K. Chung, M. Bolla, Y. M. Wright, K. Boulouchos, and E. Mastorakos, "A LES-CMC formulation for premixed flames including differential diffusion," *Combustion Theory and Modelling*, vol. 22, no. 3, pp. 411–431, 2018.

[145] S. S. Patwardhan, S. De, K. N. Lakshmisha, and B. N. Raghunandan, "CMC simulations of lifted turbulent jet flame in a vitiated coflow," *Proceedings of the Combustion Institute*, vol. 32, no. 2, pp. 1705–1712, 2009.

[146] Y. M. Wright, M. Bolla, K. Boulouchos, G. Borghesi, and E. Mastorakos, "Conditional moment closure for two-phase flows – a review of recent developments and application to various spray combustion configurations," *AIP Conference Proceedings*, vol. 1642, no. 1, pp. 433–440, 2015.

[147] H. Zhang, A. Garmory, D. E. Cavaliere, and E. Mastorakos, "Large Eddy Simulation/Conditional Moment Closure modeling of swirl-stabilized non-premixed flames with local extinction," *Proceedings of the Combustion Institute*, vol. 35, no. 2, pp. 1167–1174, 2015.

[148] K. Han and K. Y. Huh, "Conditional moment closure method with tabulated chemistry in adiabatic turbulent nonpremixed jet flames," *Combustion and Flame*, vol. 234, p. 111652, 2021.

[149] A. Kronenburg and O. T. Stein, "LES-CMC of a partially premixed, turbulent dimethyl ether jet diffusion flame," *Flow, Turbulence and Combustion*, vol. 98, no. 3, pp. 803–816, 2017.

[150] A. Kronenburg, "Double conditioning of reactive scalar transport equations in turbulent nonpremixed flames," *Physics of Fluids*, vol. 16, no. 7, pp. 2640–2648, 2004.

[151] F. Salehi, M. Talei, E. R. Hawkes, *et al.*, "Doubly conditional moment closure modelling for HCCI with temperature inhomogeneities," *Proceedings of the Combustion Institute*, vol. 36, no. 3, pp. 3677–3685, 2017.

[152] M. P. Sitte and E. Mastorakos, "Modelling of spray flames with doubly conditional moment closure," *Flow, Turbulence and Combustion*, vol. 99, no. 3–4, pp. 933–954, 2017.

[153] M. P. Sitte and E. Mastorakos, "Large Eddy Simulation of a spray jet flame using Doubly Conditional Moment Closure," *Combustion and Flame*, vol. 199, pp. 309–323, 2019.

[154] A. Mousemi, W. K. Bushe, and S. Hochgreb, "Evaluation of manifold representations of chemistry in stratified, swirl-stabilized flames," *Combustion and Flame*, vol. 229, p. 111418, 2021.

[155] N. Sekularac, X. Fang, V. Shankar, S. Baker, F. Leach, and M. Davy, "Development of a laminar burning velocity empirical correlation for combustion of iso-octane/ethanol blends in air," *Fuel*, vol. 307, p. 121880, 2022.

[156] C. J. Rallis and A. M. Garforth, "The Determination of Laminar Burning Velocity," *Prog. Energy Combust. Sci.*, vol. 6, no. 4, pp. 303–329, 1980.

[157] M. Baloo, B. M. Dariani, M. Akhlaghi, and M. AghaMirsalim, "Effects of pressure and temperature on laminar burning velocity and flame instability of iso-octane/methane fuel blend," *Fuel*, vol. 170, pp. 235–244, 2016.

[158] F. Egolfopoulos, N. Hansen, Y. Ju, K. Kohse-Höinghaus, C. Law, and F. Qi, "Advances and challenges in laminar flame experiments and implications for combustion chemistry," *Progress in Energy and Combustion Science*, vol. 43, pp. 36–67, 2014.

[159] A. A. Konnov, A. Mohammad, V. R. Kishore, N. I. Kim, C. Prathap, and S. Kumar, "A comprehensive review of measurements and data analysis of laminar burning velocities for various fuel+air mixtures," *Progress in Energy and Combustion Science*, vol. 68, pp. 197–267, 2018.

[160] E. Ranzi, A. Frassoldati, R. Grana, A. Cuoci, T. Faravelli, A. Kelley, and C. Law, "Hierarchical and comparative kinetic modeling of laminar flame speeds of hydrocarbon and oxygenated fuels," *Progress in Energy and Combustion Science*, vol. 38, no. 4, pp. 468–501, 2012.

[161] J. Beeckmann, O. Röhl, and N. Peters, "Experimental and numerical investigation of iso-octane, methanol and ethanol regarding laminar burning velocity at elevated pressure and temperature," in *Powertrains, Fuels and Lubricants Meeting*, SAE International, jun 2009.

[162] J. Benajes, R. Novella, J. Gomez-Soriano, I. Barbery, C. Libert, F. Rampanarivo, and M. Dabiri, "Computational assessment towards understanding the energy conversion and combustion process of lean mixtures in passive pre-chamber ignited engines," *Applied Thermal Engineering*, vol. 178, p. 115501, 2020.

[163] Y.-D. Liu, M. Jia, M.-Z. Xie, and B. Pang, "Enhancement on a skeletal kinetic model for primary reference fuel oxidation by using a semidecoupling methodology," *Energy & Fuels*, vol. 26, no. 12, pp. 7069–7083, 2012.

[164] J. W. Turner, A. G. Lewis, S. Akehurst, C. J. Brace, S. Verhelst, J. Vancoillie, L. Sileghem, F. Leach, and P. P. Edwards, "Alcohol fuels for spark-ignition engines: Performance, efficiency, and emission effects at mid to high blend rates for ternary mixtures," *Energies*, vol. 13, no. 23, p. 6390, 2020.

[165] F. C. Leach, R. Stone, D. Richardson, J. W. Turner, A. Lewis, S. Akehurst, S. Remmert, S. Campbell, and R. Cracknell, "The effect of oxygenate fuels on PN emissions from a highly boosted GDI engine," *Fuel*, vol. 225, pp. 277–286, 2018.

[166] K. P. Shrestha, L. Seidel, T. Zeuch, and F. Mauss, "Kinetic modeling of NOx formation and consumption during methanol and ethanol oxidation," *Combustion Science and Technology*, vol. 191, no. 9, pp. 1627–1659, 2019.

[167] Y. Hua, F. Liu, H. Wu, C.-F. Lee, and Y. Li, "Effects of alcohol addition to traditional fuels on soot formation: A review," *International Journal of Engine Research*, vol. 22, no. 5, pp. 1395–1420, 2021.

[168] J. W. Turner, A. G. Lewis, S. Akehurst, C. J. Brace, S. Verhelst, J. Vancoillie, L. Sileghem, F. Leach, and P. P. Edwards, "Alcohol fuels for spark-ignition engines: Performance, efficiency and emission effects at mid to high blend rates for binary mixtures and pure components," *Proceedings of the Institution of Mechanical Engineers, Part D: Journal of Automobile Engineering*, vol. 232, no. 1, pp. 36–56, 2018.

[169] L. Zhang and Q. Qi, "A reduced mechanism for the combustion of gasoline-ethanol blend on advanced engine combustion modes," *Fuel*, vol. 300, p. 120951, 2021.

[170] Ö. L. Gülder, "Correlations of laminar combustion data for alternative S.I. engine fuels," in *West Coast International Meeting and Exposition*, SAE International, aug 1984.

[171] M. Metghalchi and J. C. Keck, "Burning velocities of mixtures of air with methanol, isooctane, and indolene at high pressure and temperature," *Combustion and Flame*, vol. 48, pp. 191–210, 1982.

[172] Ö. L. Gülder, "Burning velocities of ethanol-isooctane blends," *Combustion and Flame*, vol. 56, no. 3, pp. 261–268, 1984.

[173] M. Del Pecchia, V. Pessina, F. Berni, A. d'Adamo, and S. Fontanesi, "Gasoline-ethanol blend formulation to mimic laminar flame speed and auto-ignition quality in automotive engines," *Fuel*, vol. 264, p. 116741, 2020.

[174] M. Del Pecchia, S. Breda, A. D'Adamo, S. Fontanesi, A. Irimescu, and S. Merola, "Development of chemistry-based laminar flame speed correlation for part-load SI conditions and validation in a GDI research engine," *SAE International Journal of Engines*, vol. 11, pp. 715–741, apr 2018.

[175] F. M. Haas, M. Chaos, and F. L. Dryer, "Low and intermediate temperature oxidation of ethanol and ethanol–PRF blends: An experimental and modeling study," *Combustion and Flame*, vol. 156, no. 12, pp. 2346–2350, 2009.

[176] S. Cheng, C. Saggese, D. Kang, S. S. Goldsborough, S. W. Wagnon, G. Kukkadapu, K. Zhang, M. Mehl, and W. J. Pitz, "Autoignition and preliminary heat release of gasoline surrogates and their blends with ethanol at engine-relevant conditions: Experiments and comprehensive kinetic modeling," *Combustion and Flame*, vol. 228, pp. 57–77, 2021.

[177] R. Amirante, E. Distaso, P. Tamburrano, and R. D. Reitz, "Laminar flame speed correlations for methane, ethane, propane and their mixtures, and natural gas and gasoline for spark-ignition engine simulations," *International Journal of Engine Research*, vol. 18, no. 9, pp. 951–970, 2017.

[178] C. Pichler and E. Nilsson, "Pathway analysis of skeletal kinetic mechanisms for small alcohol fuels at engine conditions," *Fuel*, vol. 275, p. 117956, 2020.

[179] T. Hirasawa, C. Sung, A. Joshi, Z. Yang, H. Wang, and C. Law, "Determination of laminar flame speeds using digital particle image velocimetry: Binary fuel blends of ethylene, n-butane, and toluene," *Proceedings of the Combustion Institute*, vol. 29, no. 2, pp. 1427–1434, 2002.

[180] K. Saeed and C. Stone, "The modelling of premixed laminar combustion in a closed vessel," *Combustion Theory and Modelling*, vol. 8, no. 4, pp. 721–743, 2004.

[181] J. Kim and K. Min, "Modeling laminar burning velocity of gasoline using an energy fraction-based mixing rule approach," *Proceedings of the Institution of Mechanical Engineers, Part D: Journal of Automobile Engineering*, vol. 233, no. 5, pp. 1245–1258, 2019.

[182] J. Fu, B. Deng, Y. Wang, J. Yang, D. Zhang, Z. Xu, and J. Liu, "Numerical study and correlation development on laminar burning velocities of n-butanol, iso-octane and their blends: Focusing on diluent and blend ratio effects," *Fuel*, vol. 124, pp. 102–112, 2014.

[183] D. Bradley, M. Lawes, and R. Mumby, "Burning velocity and Markstein length blending laws for methane/air and hydrogen/air blends," *Fuel*, vol. 187, pp. 268–275, 2017.

[184] R. Kumar and S. Kumar, "Formulation of a three-component gasoline surrogate model using laminar burning velocity data at elevated mixture temperatures," *Fuel*, vol. 306, p. 121581, 2021.

[185] H. Le Châtelier, "Estimation of firedamp by flammability limits," *Ann. Mines*, vol. 19, no. 8, pp. 388–395, 1891.

[186] X. Zhang, C. Tang, H. Yu, Q. Li, J. Gong, and Z. Huang, "Laminar flame characteristics of iso-octane/n-butanol blend–air mixtures at elevated temperatures," *Energy & Fuels*, vol. 27, no. 4, pp. 2327–2335, 2013.

[187] H. Feng, D. Liu, X. Yang, M. An, W. Zhang, and X. Zhang, "Availability analysis of using iso-octane/n-butanol blends in spark-ignition engines," *Renewable Energy*, vol. 96, pp. 281–294, 2016.

[188] C. Ji and F. N. Egolfopoulos, "Flame propagation of mixtures of air with binary liquid fuel mixtures," *Proceedings of the Combustion Institute*, vol. 33, no. 1, pp. 955–961, 2011.

[189] K. J. Richards, P. K. Senecal, and E. Pomraning, "CONVERGE (v. 3.0) Manual," 2021.

[190] L. Cancino, M. Fikri, A. Oliveira, and C. Schulz, "Ignition delay times of ethanol-containing multi-component gasoline surrogates: Shock-tube experiments and detailed modeling," *Fuel*, vol. 90, no. 3, pp. 1238–1244, 2011.

[191] M. Mehl, W. J. Pitz, C. K. Westbrook, and H. J. Curran, "Kinetic modeling of gasoline surrogate components and mixtures under engine conditions," *Proceedings of the Combustion Institute*, vol. 33, no. 1, pp. 193–200, 2011.

[192] M. Sarathy, N. Atef, A. Alfazazi, J. Badra, Y. Zhang, T. Tzanetakis, and Y. Pei, "Reduced gasoline surrogate (toluene/n-heptane/iso-octane) chemical kinetic model for compression ignition simulations," in *WCX World Congress Experience*, SAE International, apr 2018.

[193] M. U. Alzueta, P. Glarborg, and K. Dam-Johansen, "Experimental and kinetic modeling study of the oxidation of benzene," *International Journal of Chemical Kinetics*, vol. 32, no. 8, pp. 498–522, 2000.

[194] N. Peters, G. Paczko, R. Seiser, and K. Seshadri, "Temperature cross-over and non-thermal runaway at two-stage ignition of n-heptane," *Combustion and Flame*, vol. 128, no. 1, pp. 38–59, 2002.

[195] S. Tanaka, F. Ayala, and J. C. Keck, "A reduced chemical kinetic model for HCCI combustion of primary reference fuels in a rapid compression machine," *Combustion and Flame*, vol. 133, no. 4, pp. 467–481, 2003.

[196] J. van Lipzig, E. Nilsson, L. de Goey, and A. Konnov, "Laminar burning velocities of n-heptane, iso-octane, ethanol and their binary and tertiary mixtures," *Fuel*, vol. 90, no. 8, pp. 2773–2781, 2011.

[197] F. Rau, S. Hartl, S. Voss, M. Still, C. Hasse, and D. Trimis, "Laminar burning velocity measurements using the Heat Flux method and numerical predictions of iso-octane/ethanol blends for different preheat temperatures," *Fuel*, vol. 140, pp. 10–16, 2015.

[198] N. Hinton, R. Stone, R. Cracknell, and C. Olm, "Aqueous ethanol laminar burning velocity measurements using constant volume bomb methods," *Fuel*, vol. 214, pp. 127–134, 2018.

[199] G. Cazzoli, C. Forte, G. M. Bianchi, S. Falfari, and S. Negro, "A chemical-kinetic approach to the definition of the laminar flame speed for the simulation of the combustion of spark-ignition engines," in *13th International Conference on Engines & Vehicles*, SAE International, sep 2017.

[200] S. Ratnak, J. Kusaka, Y. Daisho, K. Yoshimura, and K. Nakama, "Experiments and simulations of a lean-boost spark ignition engine for thermal efficiency improvement," *SAE Int. J. Engines*, vol. 9, no. 1, 2016.

[201] A. d'Adamo, C. Iacovano, and S. Fontanesi, "Large-Eddy simulation of lean and ultra-lean combustion using advanced ignition modelling in a transparent combustion chamber engine," *Applied Energy*, vol. 280, p. 115949, 2020.

[202] J. Zembi, F. Mariani, and M. Battistoni, "Large eddy simulation of ignition and combustion stability in a lean SI optical access engine," in *14th International Conference on Engines & Vehicles*, SAE International, sep 2019.

[203] S. P. Software, "Simcenter STAR-CCM+ (v. 2020.2)," 2020.

[204] R. I. Issa, "Solution of the implicitly discretised fluid flow equations by operator-splitting," *Journal of Computational Physics*, vol. 62, no. 1, pp. 40–65, 1986.

[205] B. E. Launder and B. I. Sharma, "Application of the energy dissipation model of turbulence to the calculation of flow near a spinning disc," *Letter in Heat and Mass Transfer*, vol. 1, no. 2, pp. 131–138, 1974.

[206] G. J. Smallwood and B. M. Deschamps, "Flame Surface Density Measurements with PLIF in an SI Engine," in *1996 SAE International Fall Fuels and Lubricants Meeting and Exhibition*, SAE International, oct 1996.

[207] S. Fontanesi, S. Paltrinieri, and G. Cantore, "LES analysis of cyclic variability in a GDI engine," in *SAE 2014 World Congress & Exhibition*, SAE International, apr 2014.

[208] P. E. Vervisch, O. Colin, J.-B. Michel, and N. Darabiha, "NO Relaxation Approach (NORA) to predict thermal NO in combustion chambers," *Combustion and Flame*, vol. 158, no. 8, pp. 1480–1490, 2011.

[209] X. Fang, N. Papaioannou, F. Leach, and M. H. Davy, "On the application of artificial neural networks for the prediction of NOx emissions from a high-speed direct injection diesel engine," *International Journal of Engine Research*, june 2020.

[210] R. Scarcelli, N. Matthias, and T. Wallner, "Numerical investigation of combustion in a lean burn gasoline engine," in *11^{th} International Conference on Engines & Vehicles*, SAE International, sep 2013.

[211] S. Wadekar, P. Janas, and M. Oevermann, "Large-eddy simulation study of combustion cyclic variation in a lean-burn spark ignition engine," *Applied Energy*, vol. 255, p. 113812, 2019.

[212] S. Kheirkhah and Ömer L. Gülder, "A revisit to the validity of flamelet assumptions in turbulent premixed combustion and implications for future research," *Combustion and Flame*, p. 111635, 2021.

[213] W. K. Bushe and H. Steiner, "Conditional moment closure for large eddy simulation of nonpremixed turbulent reacting flows," *Physics of Fluids*, vol. 11, no. 7, pp. 1896–1906, 1999.

[214] M. M. Salehi, W. K. Bushe, and K. J. Daun, "Application of the conditional source-term estimation model for turbulence-chemistry interactions in a premixed flame," *Combustion Theory and Modelling*, vol. 16, no. 2, pp. 301–320, 2012.

[215] J. W. Labahn, C. B. Devaud, T. A. Sipkens, and K. J. Daun, "Inverse analysis and regularisation in conditional source-term estimation modelling," *Combustion Theory and Modelling*, vol. 18, no. 3, pp. 474–499, 2014.

[216] P. C. Hansen, "Numerical tools for analysis and solution of Fredholm integral equations of the first kind," *Inverse Problems*, vol. 8, no. 6, pp. 849–872, 1992.

[217] R. W. Grout, W. K. Bushe, and C. Blair, "Predicting the ignition delay of turbulent methane jets using conditional source-term estimation," *Combustion Theory and Modelling*, vol. 11, no. 6, pp. 1009–1028, 2007.

[218] N. Peters and R. Kee, "The computation of stretched laminar methane-air diffusion flames using a reduced four-step mechanism," *Combustion and Flame*, vol. 68, no. 1, pp. 17–29, 1987.

[219] T. Lu and C. K. Law, "A criterion based on computational singular perturbation for the identification of quasi steady state species: A reduced mechanism for methane oxidation with NO chemistry," *Combustion and Flame*, vol. 154, no. 4, pp. 761–774, 2008.

[220] J. C. Keck and D. Gillespie, "Rate-controlled partial-equilibrium method for treating reacting gas mixtures," *Combustion and Flame*, vol. 17, no. 2, pp. 237–241, 1971.

[221] S. Elbahloul and S. Rigopoulos, "Rate-Controlled Constrained Equilibrium (RCCE) simulations of turbulent partially premixed flames (Sandia D/E/F) and comparison with detailed chemistry," *Combustion and Flame*, vol. 162, no. 5, pp. 2256–2271, 2015.

[222] U. Maas and S. B. Pope, "Simplifying chemical kinetics: Intrinsic low-dimensional manifolds in composition space," *Combustion and Flame*, vol. 88, no. 3–4, pp. 239–264, 1992.

[223] O. Gicquel, N. Darabiha, and D. Thevenin, "Laminar premixed hydrogen/air counterflow flame simulations using flame prolongation of ILDM with differential diffusion," *Proceedings of the Combustion Institute*, vol. 28, no. 2, pp. 1901–1908, 2000.

[224] B. Fiorina, R. Baron, O. Gicquel, D. Thevenin, S. Carpentier, and N. Darabiha, "Modelling non-adiabatic partially premixed flames using flame-prolongation of ILDM," *Combustion Theory and Modelling*, vol. 7, no. 3, pp. 449–470, 2003.

[225] M. Embouazza, O. Gicquel, D. Thevenin, and N. Darabiha, "Using a new kinetic reduction technique inside FLUENT to compute combustion in a domestic burner," *ASME Pressure Vessels and Piping Conference*, vol. 424, no. 1, pp. 187–198, 2001.

[226] S. B. Pope and U. Maas, "Simplifying chemical kinetics: Trajectory-generated low-dimensional manifolds," *Mechanical and Aerospace Engineering Report: FDA*, pp. 93–11, 1993.

[227] J. Huang and W. K. Bushe, "Simulation of transient turbulent methane jet ignition and combustion under engine- relevant conditions using conditional source-term estimation with detailed chemistry," *Combustion Theory and Modelling*, vol. 11, no. 6, pp. 977–1008, 2007.

[228] M. Wang, J. Huang, and W. K. Bushe, "Simulation of a turbulent non-premixed flame using conditional source-term estimation with trajectory generated low-dimensional manifold," *Proceedings of the Combustion Institute*, vol. 31, no. 2, pp. 1701–1709, 2007.

[229] R. Barlow and J. Frank, "Effects of turbulence on species mass fractions in methane/air jet flames," *Symposium (International) on Combustion*, vol. 27, no. 1, pp. 1087–1095, 1998.

[230] J. W. Labahn and C. B. Devaud, "Species and temperature predictions in a semi-industrial MILD furnace using a non-adiabatic conditional source-term estimation formulation," *Combustion Theory and Modelling*, vol. 21, no. 3, pp. 466–486, 2017.

[231] A. Hussien and C. Devaud, "Simulations of partially premixed turbulent ethanol spray flames using doubly conditional source term estimation (DCSE)," *Combustion and Flame*, p. 111651, 2021.

[232] J. V. Oijen and L. D. Goey, "Modelling of premixed laminar flames using flamelet-generated manifolds," *Combustion Science and Technology*, vol. 161, no. 1, pp. 113–137, 2000.

[233] G. Stahl and J. Warnatz, "Numerical investigation of time-dependent properties and extinction of strained methane- and propane-air flamelets," *Combustion and Flame*, vol. 85, no. 3, pp. 285–299, 1991.

[234] W. J. S. Ramaekers, *Development of flamelet generated manifolds for partially-premixed flame simulations*. PhD thesis, Eindhoven University of Technology, Eindhoven NB, 2011.

[235] J. van Oijen, A. Donini, R. Bastiaans, J. ten Thije Boonkkamp, and L. de Goey, "State-of-the-art in premixed combustion modeling using flamelet generated manifolds," *Progress in Energy and Combustion Science*, vol. 57, pp. 30–74, 2016.

[236] W. J. S. Ramaekers, J. V. Oijen, and L. D. Goey, "A priori testing of flamelet generated manifolds for turbulent partially premixed methane/air flames," *Flow, Turbulence and Combustion*, vol. 84, no. 3, pp. 439–458, 2010.

[237] W. Zhang, S. Karaca, J. Wang, Z. Huang, and J. van Oijen, "Large eddy simulation of the Cambridge/Sandia stratified flame with flamelet-generated manifolds: Effects of non-unity Lewis numbers and stretch," *Combustion and Flame*, vol. 227, pp. 106–119, 2021.

[238] E. Inanc, A. Kempf, and N. Chakraborty, "Scalar gradient and flame propagation statistics of a flame-resolved laboratory-scale turbulent stratified burner simulation," *Combustion and Flame*, vol. 238, p. 111917, 2022.

[239] S. Hartl, D. Geyer, A. Dreizler, G. Magnotti, R. S. Barlow, and C. Hasse, "Regime identification from Raman/Rayleigh line measurements in partially premixed flames," *Combustion and Flame*, vol. 189, pp. 126–141, 2018.

[240] D. Butz, S. Hartl, S. Popp, S. Walther, R. S. Barlow, C. Hasse, A. Dreizler, and D. Geyer, "Local flame structure analysis in turbulent CH_4/air flames with multi-regime characteristics," *Combustion and Flame*, vol. 210, pp. 426–438, 2019.

[241] P.-D. Nguyen, L. Vervisch, V. Subramanian, and P. Domingo, "Multidimensional flamelet-generated manifolds for partially premixed combustion," *Combustion and Flame*, vol. 157, no. 1, pp. 43–61, 2010.

[242] P. Domingo, L. Vervisch, and K. C. N. Bray, "Partially premixed flamelets in LES of nonpremixed turbulent combustion," *Combustion Theory and Modelling*, vol. 6, no. 4, pp. 529–551, 2002.

[243] P. Domingo, L. Vervisch, and J. Reveillon, "DNS analysis of partially premixed combustion in spray and gaseous turbulent flame-bases stabilized in hot air," *Combustion and Flame*, vol. 140, no. 3, pp. 172–195, 2005.

[244] C. Duwig and L. Fuchs, "Study of a gas turbine combustion chamber: Influence of the mixing on the flame dynamics," *Proceedings of the ASME Turbo Expo 2004: Power for Land, Sea, and Air*, vol. 1: Turbo Expo 2004, pp. 129–136, 06 2004.

[245] S. Ghosal and L. Vervisch, "Theoretical and numerical study of a symmetrical triple flame using the parabolic flame path approximation," *Fluid Mechanics*, vol. 415, pp. 227–260, 2000.

[246] G. R. Ruetsch, L. Vervisch, and A. Linan, "Effects of heat release on triple flames," *Physics Fluid*, vol. 6, no. 7, pp. 1447–1454, 1995.

[247] L. Wang and N. Peters, "The length-scale distribution function of the distance between extremal points in passive scalar turbulence," *Fluid Mechanics*, vol. 554, pp. 457–475, 2006.

[248] L. Wang and N. Peters, "Dissipation element analysis of turbulent scalar fields," *Physica Scripta T132*, vol. 2008, p. 014006, 2008.

[249] E. Knudsen and H. Pitsch, "A general flamelet transformation useful for distinguishing between premixed and non-premixed modes of combustion," *Combustion and Flame*, vol. 156, no. 3, pp. 678–696, 2009.

[250] E. Knudsen and H. Pitsch, "Capabilities and limitations of multi-regime flamelet combustion models," *Combustion and Flame*, vol. 159, no. 1, pp. 242–264, 2012.

[251] E. Knudsen, Shashank, and H. Pitsch, "Modeling partially premixed combustion behavior in multiphase LES," *Combustion and Flame*, vol. 162, no. 1, pp. 159–180, 2015.

[252] Y. Hu and R. Kurose, "Partially premixed flamelet in LES of acetone spray flames," *Proceedings of the Combustion Institute*, vol. 37, no. 3, pp. 3327–3334, 2019.

[253] W. K. Bushe, C. Devaud, and J. Bellan, "A priori evaluation of the Double-conditioned Conditional Source-term Estimation model for high-pressure heptane turbulent combustion using DNS data obtained with one-step chemistry," *Combustion and Flame*, vol. 217, pp. 131–151, 2020.

[254] X. Fang, N. Sekularac, and M. H. Davy, "Parametric studies of a novel combustion modelling approach for low temperature diesel spray simulation," *Proceedings of the ASME 2020 Internal Combustion Engine Division Fall Technical Conference*, vol. ASME 2020 Internal Combustion Engine Division Fall Technical Conference, 11 2020. V001T06A005.

[255] CHEM1D, "A package for the simulation of one dimensional flames," 2005.

[256] A. Wehrfritz, O. Kaario, V. Vuorinen, and B. Somers, "Large eddy simulation of n-dodecane spray flames using flamelet generated manifolds," *Combustion and Flame*, vol. 167, pp. 113 – 131, 2016.

[257] K. J. Richards, P. K. Senecal, and E. Pomraning, "CONVERGE (v. 2.4) Manual," 2017.

[258] C. M. Rhie and W. L. Chow, "Numerical study of the turbulent flow past an airfoil with trailing edge separation," *AIAA Journal*, vol. 21, pp. 1525–1532, Nov. 1983.

[259] X. Fang, R. Ismail, and M. Davy, "A study on kinetic mechanisms of diesel fuel surrogate n-dodecane for the simulation of combustion recession," in *WCX SAE World Congress Experience*, SAE International, apr 2019.

[260] T. Yao, Y. Pei, B. Zhong, S. Som, and T. Lu, "A hybrid mechanism for n-dodecane combustion with optimized low-temperature chemistry," *9th US National Combustion Meeting*, may 2015.

[261] L. M. Pickett, C. L. Genzale, G. Bruneaux, L.-M. Malbec, L. Hermant, C. Christiansen, and J. Schramm, "Comparison of diesel spray combustion in different high-temperature, high-pressure facilities," *SAE Int. J. Engines, 2010-01-2106*, vol. 3, pp. 156–181, 10, 2010.

[262] P. Kundu, M. M. Ameen, and S. Som, "Importance of turbulence-chemistry interactions at low temperature engine conditions," *Combustion and Flame*, vol. 183, pp. 283 – 298, 2017.

[263] Y. Pei, E. R. Hawkes, M. Bolla, S. Kook, G. M. Goldin, Y. Yang, S. B. Pope, and S. Som, "An analysis of the structure of an n-dodecane spray flame using TPDF modelling," *Combustion and Flame*, vol. 168, pp. 420 – 435, 2016.

[264] N. Maes, M. Meijer, N. Dam, B. Somers, H. B. Toda, G. Bruneaux, S. A. Skeen, L. M. Pickett, and J. Manin, "Characterization of Spray A flame structure for parametric variations in ECN constant-volume vessels using chemiluminescence and laser-induced fluorescence," *Combustion and Flame*, vol. 174, pp. 138–151, 2016.

[265] Z. Luo, S. Som, S. M. Sarathy, M. Plomer, W. J. Pitz, D. E. Longman, and T. Lu, "Development and validation of an n-dodecane skeletal mechanism for spray combustion applications," *Combustion Theory and Modelling*, vol. 18, no. 2, pp. 187–203, 2014.

[266] N. Wu, W. K. Bushe, and M. Davy, "On the experimental validation of combustion simulations in turbulent non-premixed jets," *Combustion Theory and Modelling*, vol. 14, no. 6, pp. 855–874, 2010.

[267] M. S. Sweeney, S. Hochgreb, M. J. Dunn, and R. S. Barlow, "The structure of turbulent stratified and premixed methane/air flames II: Swirling flows," *Combustion and Flame*, vol. 159, no. 9, pp. 2912–2929, 2012.

[268] D. Dovizio, J. W. Labahn, and C. B. Devaud, "Doubly Conditional Source-term Estimation (DCSE) applied to a series of lifted turbulent jet flames in cold air," *Combustion and Flame*, vol. 162, no. 5, pp. 1976–1986, 2015.

[269] A. H. Mahdipour and M. M. Salehi, "Localized conditional source-term estimation model for turbulent combustion," *Combustion and Flame*, p. 111715, 2021.

[270] M. Ihme, L. Shunn, and J. Zhang, "Regularization of reaction progress variable for application to flamelet-based combustion models," *Journal of Computational Physics*, vol. 231, no. 23, pp. 7715–7721, 2012.

[271] Y.-S. Niu, L. Vervisch, and P. D. Tao, "An optimization-based approach to detailed chemistry tabulation: Automated progress variable definition," *Combustion and Flame*, vol. 160, no. 4, pp. 776–785, 2013.

[272] A. Vasavan, P. de Goey, and J. van Oijen, "A novel method to automate FGM progress variable with application to igniting combustion systems," *Combustion Theory and Modelling*, vol. 24, no. 2, pp. 221–244, 2020.

[273] F. Chitgarha, F. Ommi, and M. Farshchi, "Assessment of optimal reaction progress variable characteristics for partially premixed flames," *Combustion Theory and Modelling*, vol. 0, no. 0, pp. 1–34, 2022.

[274] H. Gupta, O. J. Teerling, and J. A. van Oijen, "Effect of progress variable definition on the mass burning rate of premixed laminar flames predicted by the Flamelet Generated Manifold method," *Combustion Theory and Modelling*, vol. 25, no. 4, pp. 631–645, 2021.

[275] A. Lipatnikov and V. Sabelnikov, "Evaluation of mean species mass fractions in premixed turbulent flames: A DNS study," *Proceedings of the Combustion Institute*, vol. 38, no. 4, pp. 6413–6420, 2021.

[276] A. Lipatnikov, V. Sabelnikov, F. Hernández-Pérez, W. Song, and H. G. Im, "A priori DNS study of applicability of flamelet concept to predicting mean concentrations of species in turbulent premixed flames at various Karlovitz numbers," *Combustion and Flame*, vol. 222, pp. 370–382, 2020.

[277] A. Giusti and E. Mastorakos, "Detailed chemistry LES/CMC simulation of a swirling ethanol spray flame approaching blow-off," *Proceedings of the Combustion Institute*, vol. 36, no. 2, pp. 2625–2632, 2017.

[278] A. Varna, A. Wehrfritz, E. R. Hawkes, M. J. Cleary, T. Lucchini, G. D'Errico, S. Kook, and Q. N. Chan, "Application of a multiple mapping conditioning mixing model to ECN Spray A," *Proceedings of the Combustion Institute*, vol. 37, no. 3, pp. 3263–3270, 2019.

[279] Z. Huang, M. J. Cleary, Z. Ren, and H. Zhang, "Large eddy simulation of a supersonic lifted hydrogen flame with sparse-lagrangian multiple mapping conditioning approach," *Combustion and Flame*, p. 111756, 2021.

[280] M. Mortada and C. Devaud, "Large Eddy Simulation of lifted turbulent flame in cold air using doubly conditional source-term estimation," *Combustion and Flame*, vol. 208, pp. 420–435, 2019.

[281] D. Dovizio and C. Devaud, "Doubly Conditional Source-term Estimation (DCSE) for the modelling of turbulent stratified V-shaped flame," *Combustion and Flame*, vol. 172, pp. 79–93, 2016.

[282] C. Devaud, W. K. Bushe, and J. Bellan, "The modeling of the turbulent reaction rate under high-pressure conditions: A priori evaluation of the Conditional Source-term Estimation concept," *Combustion and Flame*, vol. 207, pp. 205–221, 2019.

[283] W. K. Bushe, "Spatial gradients of conditional averages in turbulent flames," *Combustion and Flame*, vol. 192, pp. 314–339, 2018.

[284] A. Mousemi and W. K. Bushe, "The joint probability density function of mixture fraction, reaction progress variable, and total enthalpy in a stratified, swirl-stabilized turbulent flame," *Physics of Fluids*, vol. 33, no. 3, p. 035106, 2021.

[285] J. C. Sutherland and A. Parente, "Combustion modeling using principal component analysis," *Proceedings of the Combustion Institute*, vol. 32, no. 1, pp. 1563–1570, 2009.

[286] M. Wang, J. Huang, and W. K. Bushe, "Simulation of a turbulent non-premixed flame using conditional source-term estimation with trajectory generated low-dimensional manifold," *Proceedings of the Combustion Institute*, vol. 31, no. 2, pp. 1701–1709, 2007.

[287] O. Owoyele, P. Kundu, M. M. Ameen, T. Echekki, and S. Som, "Application of deep artificial neural networks to multi-dimensional flamelet libraries and spray flames," *International Journal of Engine Research*, vol. 21, no. 1, pp. 151–168, 2020.

[288] M. Ihme, W. T. Chung, and A. A. Mishra, "Combustion machine learning: Principles, progress and prospects," *Progress in Energy and Combustion Science*, vol. 91, p. 101010, 2022.

[289] H. Mirgolbabaei and T. Echekki, "Nonlinear reduction of combustion composition space with kernel principal component analysis," *Combustion and Flame*, vol. 161, no. 1, pp. 118–126, 2014.

[290] M. R. Malik, P. Obando Vega, A. Coussement, and A. Parente, "Combustion modeling using Principal Component Analysis: A posteriori validation on Sandia flames D, E and F," *Proceedings of the Combustion Institute*, vol. 38, no. 2, pp. 2635–2643, 2021.

[291] A. Parente, J. Sutherland, L. Tognotti, and P. Smith, "Identification of low-dimensional manifolds in turbulent flames," *Proceedings of the Combustion Institute*, vol. 32, no. 1, pp. 1579–1586, 2009.

[292] J. Shlens, "A tutorial on principal component analysis," 2014.

[293] B. J. Isaac, A. Coussement, O. Gicquel, P. J. Smith, and A. Parente, "Reduced-order PCA models for chemical reacting flows," *Combustion and Flame*, vol. 161, no. 11, pp. 2785–2800, 2014.

[294] A. Biglari and J. C. Sutherland, "An a-posteriori evaluation of principal component analysis-based models for turbulent combustion simulations," *Combustion and Flame*, vol. 162, no. 10, pp. 4025–4035, 2015.

[295] B. J. Isaac, J. N. Thornock, J. Sutherland, P. J. Smith, and A. Parente, "Advanced regression methods for combustion modelling using principal components," *Combustion and Flame*, vol. 162, no. 6, pp. 2592–2601, 2015.

[296] M. R. Malik, B. J. Isaac, A. Coussement, P. J. Smith, and A. Parente, "Principal component analysis coupled with nonlinear regression for chemistry reduction," *Combustion and Flame*, vol. 187, pp. 30–41, 2018.

[297] A. Parente and J. C. Sutherland, "Principal component analysis of turbulent combustion data: Data pre-processing and manifold sensitivity," *Combustion and Flame*, vol. 160, no. 2, pp. 340–350, 2013.

[298] R. Ranade and T. Echekki, "A framework for data-based turbulent combustion closure: A priori validation," *Combustion and Flame*, vol. 206, pp. 490–505, 2019.

[299] H. Turkeri, X. Zhao, and M. Muradoglu, "Large eddy simulation/probability density function modeling of turbulent swirling stratified flame series," *Physics of Fluids*, vol. 33, no. 2, p. 025117, 2021.

[300] A. N. Lipatnikov, T. Nilsson, R. Yu, X. S. Bai, and V. A. Sabelnikov, "Assessment of a flamelet approach to evaluating mean species mass fractions in moderately and highly turbulent premixed flames," *Physics of Fluids*, vol. 33, no. 4, p. 045121, 2021.

[301] Z. X. Chen, S. Iavarone, G. Ghiasi, V. Kannan, G. D'Alessio, A. Parente, and N. Swaminathan, "Application of machine learning for filtered density function closure in mild combustion," *Combustion and Flame*, vol. 225, pp. 160–179, 2021.

[302] M. T. H. de Frahan, S. Yellapantula, R. King, M. S. Day, and R. W. Grout, "Deep learning for presumed probability density function models," *Combustion and Flame*, vol. 208, pp. 436–450, 2019.

[303] D. Butz, A. Breicher, R. Barlow, D. Geyer, and A. Dreizler, "Turbulent multi-regime methane-air flames analysed by raman/rayleigh spectroscopy and conditional velocity field measurements," *Combustion and Flame*, p. 111941, 2021.